Constraining Light Dark Vectors and Scalar Leptoquarks with Flavour Observables

Zur Erlangung des akademischen Grades eines

Doktors der Naturwissenschaften (Dr. rer. nat.)

von der Fakultät für Physik
der Technischen Universität Dortmund

vorgelegte

Dissertation

von

Jordi Folch Eguren

geboren in Barcelona

Tag der mündlichen Prüfung: 08/07/2025

Referent: Prof. Dr. Emmanuel Stamou
Korreferentin: Prof. Dr. Gudrun Hiller

Veröffentlichte und genehmigte Dissertation an der Fakultät Physik der Technischen Universität Dortmund.

Abstract

In this thesis we explore two complementary extensions of the Standard Model, corresponding to a light new physics scenario featuring a (dark) vector boson, and a heavy new physics scenario involving a scalar leptoquark. Focusing on their flavour-changing interactions and observables, which provide highly sensitive probes of physics beyond the Standard Model, we employ the framework of effective field theory to systematically analyse both setups. In the first part of this thesis, we provide an overview of the Standard Model, flavour and effective field theories. In the second part, we study the light dark vector boson model. We focus on flavour violating interactions between the new vector and the Standard Model fermions, and analyse how such interactions can arise from the Yukawa diagonalisation and the renormalisation group equations at 1-loop. Then, we use experimental data and our theory calculation from two-body decays to set constraints on the model parameters. Furthermore, we also use the tool of perturbative unitarity to set bounds on the model. In the third part, we consider scalar leptoquarks, corresponding to a heavy new physics model. Here, we compute the Wilson coefficients to order $\mathcal{O}(\alpha_s)$ for $\Delta F = 2$ processes from matching the effective and full theories, which involves the calculation of 1-loop amplitudes in the effective theory and 2-loop in the full theory. Finally, we analyse the 1-loop corrections to the effective theory for $\Delta F = 1$ processes. We focus on a particular computational procedure involving Dirac traces, which requires a careful examination of the Dirac algebra in different γ_5 schemes, and extract results in a general gauge and for different IR regulators.

Acknowledgements

This thesis has my name on it, but its completion would not have been possible without the help of many people. First of all, I would like to thank my supervisor Emmanuel Stamou, who offered me the unique opportunity to work in Dortmund. I am very grateful for the chance, as well as for his support and understanding through some intense and difficult periods. I also appreciate our physics discussions, where you gave clear explanations and objectives. I am also very thankful to Javier Virto, who was the first to introduce me into academic research and worked very closely with me all these years, giving me excellent explanations to many, many questions. Collaborators have been equally important in helping me advance and progress in my projects, and I am happy to have worked with Andreas Crivellin, Robert Ziegler and Mustafa Tabet. I must especially thank Mustafa, who not only helped me so much in my projects, but has been the best office mate I can imagine, providing unlimited sweet treats and funny moments.

I am very grateful to everyone in the Dortmund department, who welcomed me into the university and have contributed to many good memories, from playing Mario Kart, school and research stays, to memorable conversations. Thanks to the (two!) Dominiks, Kai, Lara, Daniel, Tom, Patrick, Max and Sara. I am also grateful to Gudrun Hiller and Heinrich Päs, with whom I worked in teaching several bachelor and master subjects. I also wish to thank Hector Gisbert, who was always very supportive during our shared time in Dortmund and made me not forget to speak Catalan.

After all these years in Germany I have made very good friends, and I could not be happier to have met such amazing people. I am very grateful to my first roommate Kevin, who always helped me when I needed it and welcomed me to Dortmund. I must also thank his family for their warmth, inviting me to birthday dinners and thanksgiving every year. I also have to mention my beautiful group of friends from south and north America. Thank you Victor for so many nice gym sessions, to Jesus for our interesting cultural conversations and to Guille and Dan for always preparing me food and taking care of me. Also for visiting me in Barcelona. I am so glad to have become such close and good friends with you all. I am so happy and proud to have met you all, we have formed a lovely group and I will always remember the parties and so many shared moments.

I cannot forget about my friends from Barcelona. I am thankful to Iñigo, who was my first office mate during my research at UB. We have had many special moments and continue to share time together every time I am back in Barcelona. Before my PhD, and even before my master's in Utrecht, I did my bachelor in Barcelona, and I must mention the amazing friend group that we have had for so many years. Meeting every summer and Christmas is truly something I look forward to and I enjoy more and more every year. Thank you Javi, Sergi, Albert, Marc, Flors, Rosalia, Alex, Alba and Leo. From my childhood friends, I want to thank everyone in the Buda group, particularly Quim and Marcel, who have always taken the time to visit me wherever I have been. We always have great fun and our holiday trips are always unique experiences. I also want to thank Ignasi, one of my best friends for as long as I can remember, who always takes time to meet up with me and have some fun.

Another very important group of friends are the ones who are currently in the Netherlands and the north of Europe. This includes Gastón, Leo, Robert and Chen. We met way back in the bachelor in Barcelona and I love that we have kept in contact, meeting so often and adding more and more shared moments in our lives, from Barcelona all the way to the Netherlands. I am truly grateful for these friendships, and I have no doubts that wherever we end up we will always keep seeing each other.

Undoubtedly, I must also thank Claire for her support and care. She always has her best interest for me, and her love has been a constant that has carried me through many tough moments. There is much I could say, but words cannot describe how thankful I am of her love. I also appreciate the care from her family, who always warmly welcomed me when I visited Ireland.

Finally, I must thank my parents and brother for their support during the PhD and throughout all my life. I would not be who I am without the opportunity to study in Barcelona and Utrecht, and the education I have received is what I am the most grateful for in my life. Without it, I would not be a physicist and I could have never learned so much about a topic I am passionate about. Without it, I would have never been able to live abroad, meet people from all around the world and have such incredible experiences, which have made me grow as a person and shaped me into who I am today. Ultimately, the choices that have led me to where I am today stem from my conviction that learning is life's most remarkable experience. And I will always be grateful to my parents for giving me the opportunity to learn.

This thesis has my name on it, but it is not only mine. I wish to dedicate it to my family, friends and collaborators who made it possible, because all of you made me better in some way or another, and taught me valuable lessons while also creating memories I will never forget about. Thank you all.

Contents

List of Figures

List of Tables

Chapter 1

Introduction

The Standard Model (SM) of particle physics stands as one of the most successful models of nature. From its development in the 1960s, to the discovery of the Higgs boson in 2012, the SM has been proven to be the best and most complete theory for understanding subatomic physics to date. Its success solidified the quantum field theory (QFT) framework and its predictive power, marking a triumphant achievement in the progress of science.

Despite its success, the SM is neither a "final" nor "complete" model. In the process of science, all theories and models are continuously tested, and extended, modified or developed accordingly. Of course, the SM is no exception to this process, and current evidence establishes the need for physics beyond the Standard Model (BSM). Current unexplained phenomena include Dark Matter (DM), neutrino masses and the observed matter–antimatter asymmetry, none of which can be explained within the SM. Moreover, there are puzzles in the SM itself, which are not necessarily a problem but one would hope they will be resolved. For example, in the SM there is no explanation for the notable hierarchy between the fermion masses and the elements of the quark mixing matrix. Additionally, there is the so-called strong CP puzzle, namely the unexplained reason of why the θ parameter in quantum chromodynamics (QCD) is so close to (or even exactly) zero. Of course, there is also the more broad issue of trying to reconcile the SM and gravity under a common framework.

The physics community has been and is investing much effort in researching these new physics (NP) topics, with experimental and theoretical collaborations all around the world working towards finding BSM physics. So far no direct evidence for NP has been found, but the work continues. Two complementary approaches are taken to search for NP: the direct production of new particles at high-energy colliders, and the indirect search for SM deviations in precision observables. At the high-energy frontier, experiments such as the LHC search for heavy BSM particles with masses above the electroweak (EW) scale. Meanwhile at the precision (low-energy) frontier, experiments such as BELLE-II use intense beams of particles and sensitive detectors to directly produce and study new, weakly interacting particles that lie below the EW scale.

At the precision frontier, flavour physics plays a crucial role in testing the SM and searching for BSM physics. Flavour physics is dedicated to studying the intricate interactions between the different types (flavours) of SM fermions, and how fermions change flavour in certain processes. In particular and of central importance to this work are flavour-changing neutral currents (FCNCs), processes where a quark changes its flavour (for example, from a strange quark to a down quark)

without changing its electric charge. FCNCs are highly suppressed in the SM, making them very sensitive to NP, and thus an excellent probe for BSM models. Therefore, potential contributions from NP can lead to measurable deviations of the SM predictions while also indirectly probing higher energy scales than direct searches. In this context, the appropriate framework is given by effective field theories (EFTs), since FCNCs are most prominently observed in rare, low-energy decays. Moreover, EFTs allow us to simplify and systematically study NP effects in a model independent way, that is, without committing to specific UV models. In this manner, one can link BSM effects with low energy observables, since the EFT carries imprints of NP particles.

In this thesis, we investigate two distinct BSM models: one featuring heavy NP and another involving light NP. The first model focuses on scalar leptoquarks (LQs), which are typically expected at the TeV scale, well above the EW scale. LQs are particles that directly couple to SM quark and leptons, and are motivated by their potential to explain flavour anomalies (deviations from the SM) as well as by their emergence in grand unified theories. The second model consists of light dark vectors (LDVs), with masses at the GeV scale. Recent null results in heavy NP searches have shifted some focus towards scenarios where NP is light and weakly interacting. LDVs—which encompass dark photons and Z' bosons—are compelling candidates for particle DM. Together, these two models offer complementary insights into NP effects in flavour observables, with LQs representing heavy NP, and LDVs representing light NP, each leaving distinct imprints in the EFT description.

This thesis is based on Refs. [1, 2] and organised into three main parts. In Part I, we lay the foundations by introducing the SM and discussing its essential aspects which underpin the subsequent studies of the LQ and LDV models. In particular, we focus on the SM flavour interactions and motivate how FCNCs serve as powerful probes in the search for BSM physics. Moreover, we present the EFT framework, clearly distinguishing between the scenarios in which the NP is heavy or light.

In Part II we study the LDVs. We first introduce the model under consideration, and analyse how FCNC interactions between the LDV and SM fermions can be generated (at tree-level). We then consider the FCNC of two-body decays for mesons and leptons with the LDV, and use our theoretical computation together with experimental measurements to constrain the model. We close this part with a theoretical requirement central to QFTs, namely the fact that probability is conserved and therefore, QFTs are unitary. This yields non-trivial constraints on the amplitudes of $2 \to 2$ processes, and we use such considerations to further analyse the model and deepen our understanding of the setup.

In Part III, we begin by studying the effect of LQs on meson mixing via the appropriate EFT. In the EFT, the LQs are integrated out of the theory and the mixing processes are mediated by four-fermion operators. We then compute the QCD corrections to both theories, i.e., in the full theory with LQs and the EFT, and demand both theories to be equal, which yields the relevant parameters encoding the LQ effects on the mixing processes. We later focus on the EFT for processes where the flavour quantum number changes by one unit. We compute the QCD corrections to the EFT as a function of general parameters, thereby generalising previous calculations. Finally, we close the thesis with a detailed analysis of a novel procedure to compute loop amplitudes in current–current EFT operators. This methodology can potentially simplify and speed up otherwise cumbersome and complicated calculations.

PART I

The Standard Model, Flavour and Beyond

In this first part of the thesis, the relevant concepts needed to motivate and understand Part II and Part III are introduced. Chapter 2 provides an overview of the SM, with a particular focus on flavour physics and its role as a tool to explore BSM models. Then, in Chapter 3 EFTs are introduced as the framework of the thesis, for both heavy and light BSM particles.

Chapter 2

The Standard Model

In this chapter we review the main aspects of the SM of particle physics relevant for Part II and Part III. In Section 2.1, we introduce the particle content and interactions of the SM. In Section 2.2, we discuss the Higgs mechanism for the bosonic sector, and in Section 2.3 we cover the corresponding mechanism for fermions as well as the corresponding fermion–gauge boson interactions in the EW sector. In Section 2.4, we briefly review QCD, and finally, in Section 2.5 we motivate flavour physics as an approach to study and search for NP. We use Greek indices $\mu, \nu, \alpha, \beta, \ldots$ for spacetime components, and Latin indices $i, j, k, l, \ldots$ for flavour indices. Einstein's summation convention is used throughout the thesis, i.e., repeated indices are summed over. We also use Feynman slash notation, with $\not{X} \equiv \gamma^\mu X_\mu \,, \forall X_\mu$.

2.1. Field Content

The SM is the QFT that describes all known fundamental particles and their interactions, except gravity. The interactions among SM fields are governed by symmetry principles, which determine and constraint their form. Concretely, the SM is a gauge theory with the symmetry group

$$G_{\text{SM}} = SU(3)_c \times SU(2)_L \times U(1)_Y \,. \tag{2.1}$$

The $SU(3)_c$ gauge group corresponds to QCD, and the $SU(2)_L \times U(1)_Y$ group to the EW sector. A main ingredient of the SM is the explanation for particles having mass. This is accomplished via the *Higgs mechanism*, which breaks down the EW group to $U(1)_{\text{em}}$ quantum electrodynamics (QED) according to

$$SU(3)_c \times SU(2)_L \times U(1)_Y \to SU(3)_c \times U(1)_{\text{em}} \,, \tag{2.2}$$

while $SU(3)_c$ remains unbroken. The charges of fields under the $SU(3)_c$, $SU(2)_L$ and $U(1)_Y$ groups are referred to as colour, weak isospin and hypercharge, respectively. The $U(1)_{\text{em}}$ electric charge Q of a particle is related to its weak isospin component T^3 and its hypercharge Y via the Gell-Mann–Nishijima relation

$$Q = T^3 + Y \quad \text{with} \quad T^3 = \frac{1}{2}\sigma_3 \,, \tag{2.3}$$

where T^3 is the third $SU(2)_L$ generator and σ_3 its corresponding Pauli matrix. The particle content of the SM consists of fermions with spin $1/2$ and bosons with spin 1 or 0. The fermions are

Table 2.1.: SM field content including the representation under the SM gauge group $\mathcal{G}_{SM} = U(1)_Y \times SU(2)_L \times SU(3)_C$. Different fermion flavours ($i = 1, 2, 3$) as well as the Higgs H are indicated in terms of their $SU(2)_L$ components that differ by the associated weak isospin T^3 and electric charge Q. Fermion subscripts L, R refer to left-handed (LH) and right-handed (RH) chirality, respectively.

Field	Flavours	$U(1)_Y \times SU(2)_L \times SU(3)_C$	T^3	Q
Q^i	$\begin{pmatrix} u \\ d \end{pmatrix}_L, \begin{pmatrix} c \\ s \end{pmatrix}_L, \begin{pmatrix} t \\ b \end{pmatrix}_L$	$\left(\frac{1}{6}, 2, 3\right)$	$+\frac{1}{2}$ $-\frac{1}{2}$	$+\frac{2}{3}$ $-\frac{1}{3}$
u_R^i	u_R, c_R, t_R	$\left(\frac{2}{3}, 1, 3\right)$	0	$+\frac{2}{3}$
d_R^i	d_R, s_R, b_R	$\left(-\frac{1}{3}, 1, 3\right)$	0	$-\frac{1}{3}$
L^i	$\begin{pmatrix} \nu_e \\ e \end{pmatrix}_L, \begin{pmatrix} \nu_\mu \\ \mu \end{pmatrix}_L, \begin{pmatrix} \nu_\tau \\ \tau \end{pmatrix}_L$	$\left(-\frac{1}{2}, 2, 1\right)$	$+\frac{1}{2}$ $-\frac{1}{2}$	0 -1
e_R^i	e_R, μ_R, τ_R	$(-1, 1, 1)$	0	-1
H	$\begin{pmatrix} \phi^+ \\ \phi^0 \end{pmatrix}$	$\left(\frac{1}{2}, 2, 1\right)$	$+\frac{1}{2}$ $-\frac{1}{2}$	$+1$ 0

divided into quarks and leptons, and the bosons into gauge bosons with spin 1 and the Higgs, the only spin-0 scalar particle of the SM. The gauge bosons arise from the local gauge invariance and mediate the interactions between particles. The SM fields are classified according to their charges under the SM gauge group G_{SM} of Eq. (2.1), as summarised in Table 2.1. The Higgs H is a $SU(2)_L$-doublet and QCD singlet responsible for spontaneously breaking the EW sector down to QED, as depicted in Eq. (2.2), after acquiring a non-trivial vacuum expectation value (VEV) $v \approx 246\,\text{GeV}$. The fermions are classified into colour charged quarks and colourless leptons. According to their representation under $SU(2)_L$, they are further distinguished between left-handed (LH) quark doublets Q_L and right-handed (RH) singlets d_R, u_R, as well as LH lepton doublets L_L and RH singlets e_R. Thus, LH and RH fermions carry different charges under $SU(2)_L$, rendering the SM a *chiral* theory, a very particular feature of our physical world. The upper and lower $SU(2)_L$ components of Q_L and L_L correspond to LH up- and down-type quarks u_L, d_L as well as LH neutrinos ν_L and charged leptons ℓ_L, respectively. Note that neutrinos in the SM do not have a RH counterpart, as they would be uncharged under the SM group. Notably, the SM fermion representations Q_L, u_R, u_R, L_L, e_R come in three different copies called *generations, families, or flavours* that share the same quantum numbers and only differ in their masses. The flavours are indicated by the $i = 1, 2, 3$ index in Table 2.1. *Flavour physics* [3–5] studies the properties and interactions of the different fermions, and plays a crucial role in understanding the SM and potential NP. In this thesis we study extensions of the SM with particular flavour structures not realised in the SM, and consider particular physical processes and tools to analyse such models. For now we strict the discussion to the SM and its main features. The Lagrangian of the SM is given by renormalisable operators of dimension $d \leq 4$, where eight gluons $G_\mu^a, a = 1, \ldots, 8$,

three $W^b_\mu, b = 1,2,3$ and one[1] hypercharge B_μ boson of $SU(3)_c, SU(2)_L$ and $U(1)_Y$, respectively, mediate the interactions between the SM particles given in Table 2.1. Additionally, the Higgs doublet interacts with the SM fermions through the Yukawa interaction. The Lagrangian is given by

$$\mathscr{L}_{\text{SM}} = \mathscr{L}_{\text{gauge}} + \mathscr{L}_{\text{fermion}} + \mathscr{L}_{\text{Higgs}} + \mathscr{L}_{\text{Yukawa}}\,, \tag{2.4}$$

$$\mathscr{L}_{\text{gauge}} = -\frac{1}{4}W^a_{\mu\nu}W^{a\mu\nu} - \frac{1}{4}B_{\mu\nu}B^{\mu\nu} - \frac{1}{4}G^a_{\mu\nu}G^{a\mu\nu}\,, \tag{2.5}$$

$$\mathscr{L}_{\text{fermion}} = i\bar{Q}^i \not{D} Q^i + i\bar{L}^i \not{D} L^i + i\bar{d}^i_R \not{D} d^i_R + i\bar{u}^i_R \not{D} u^i_R + i\bar{e}^i_R \not{D} e^i_R\,, \tag{2.6}$$

$$\mathscr{L}_{\text{Higgs}} = (D_\mu H)^\dagger (D^\mu H) - V(H)\,, \tag{2.7}$$

$$\mathscr{L}_{\text{Yukawa}} = -\bar{Q}^i H Y_d^{ij} d^j_R - \bar{Q}^i \tilde{H} Y_u^{ij} u^j_R - \bar{L}^i H Y_e^{ij} e^j_R + \text{h.c.} \tag{2.8}$$

where $\tilde{H} = i\sigma_2 H^\star$ and the indices i, j denote the flavour, with summation over i, j being implicit. We do not specify the Higgs potential $V(H)$ for now, which will be discussed in the next section. The first term of Eq. (2.4) contains the gauge boson kinetic terms, with

$$F^a_{\mu\nu} = \partial_\mu A^a_\nu - \partial_\nu A^a_\mu + g_G f^{abc}_G A^b_\mu A^c_\mu \quad \text{for} \quad F^a_{\mu\nu} \equiv \{W^a_{\mu\nu}, G^a_{\mu\nu}, B_{\mu\nu}\}\,. \tag{2.9}$$

In this expression, g_G is the coupling of the corresponding gauge group; with $G = \{SU(3)_c, SU(2)_L, U(1)_Y\}$ we denote $g_G = \{g_s, g, g'\}$, while f^{abc}_G are the respective group structure constants. For an Abelian group, like $U(1)_Y$, $f^{abc}_{U(1)_Y} = 0$, and thus no B_μ self-interactions are present. The second and third terms of Eq. (2.4) contain the interactions of the fermions and Higgs with the SM gauge bosons through the covariant derivative

$$D_\mu = \left(\partial_\mu - ig' Y_Q B_\mu - igT^a_{SU(2)} W^a_\mu - ig_s T^a_{SU(3)} G^a_\mu\right)\,, \tag{2.10}$$

which acts on the SM fermions and Higgs according to the charge assignments of Table 2.1. In Eq. (2.10), Y_F are the hypercharges of each family of fermions, and T^a_G the generators of the corresponding gauge group given by

$$\begin{aligned} T^a_{SU(3)} &= \frac{1}{2}\lambda_a, \quad a = 1,\ldots,8 \quad \lambda_a \equiv \text{Gell-Mann matrices}\,, \\ T^a_{SU(2)} &= \frac{1}{2}\sigma_a, \quad a = 1,2,3 \quad \sigma_a \equiv \text{Pauli matrices}\,. \end{aligned} \tag{2.11}$$

Notice the particular form of the interactions in Eq. (2.10) for each field, with the corresponding charges of Table 2.1. All fermions interact with the hypercharge boson B_μ, while only LH doublets (Q, L) interact with the W^a_μ bosons of $SU(2)_L$ (the SM is *chiral*), and only the quarks (Q, u_R, d_R) interact with the gluons G^a_μ of $SU(3)_c$, since the leptons and Higgs are colourless. Additionally, the Higgs interacts with the $SU(2)_L \times U(1)_Y$ sector. Crucially, the hypercharges $Y_f \forall f$ are the same for every generation, that is, they are *flavour universal*. This is an important feature of the SM that is not necessarily true for NP models. We will see an example of this in Chapter 5.

No explicit mass terms for gauge bosons are allowed in the SM due to gauge invariance. This is also the case for fermions since LH and RH fields transform differently under $SU(2)_L$, and thus a mass term $\sim \bar{\psi}_L \psi_R$ is forbidden. This is remedied by the Higgs mechanism, which allows for the gauge bosons to gain mass after *electroweak symmetry breaking* (EWSB) through the Higgs interactions in $\mathscr{L}_{\text{Higgs}}$ of Eq. (2.4). Likewise, the Higgs mechanism gives mass to the SM fermions through the Yukawa interaction $\mathscr{L}_{\text{Yukawa}}$ after EWSB. In the next two sections we focus on the $\mathscr{L}_{\text{Higgs}}$ and $\mathscr{L}_{\text{Yukawa}}$ respectively, and explain the relevant elements of the Higgs mechanism for the bosons and fermions, where flavour plays a central role.

[1] The number of gauge bosons equals the dimensionality of their corresponding gauge group, given by $\dim SU(N) = N^2 - 1$ and $\dim U(N) = N^2$.

2.2. Electroweak Symmetry Breaking

In the SM, the masses of the EW bosons, as well as the fermions, are generated through EWSB. This occurs when the EW gauge symmetry spontaneously breaks down to electromagnetism:

$$SU(2)_L \times U(1)_Y \to U(1)_{\text{em}} \,. \tag{2.12}$$

The Higgs–gauge Lagrangian before EWSB reads

$$\begin{aligned} \mathscr{L}_H &= -\frac{1}{4}\left(W^a_{\mu\nu}\right)^2 - \frac{1}{4}B^2_{\mu\nu} + \left(D_\mu H\right)^\dagger \left(D^\mu H\right) - V(H)\,, \\ V(H) &= -m^2 H^\dagger H + \lambda\left(H^\dagger H\right)^2 \,. \end{aligned} \tag{2.13}$$

For $m > 0, \lambda > 0$, the potential $V(H)$ is minimised at

$$\langle H^\dagger H\rangle = \frac{m^2}{2\lambda} = \frac{v^2}{2} \quad \text{with} \quad v = m/\sqrt{\lambda} = 246\,\text{GeV}\,. \tag{2.14}$$

Then, the Higgs field acquires a nonzero VEV $\langle H\rangle = 1/\sqrt{2}(0, v)^T$. This vacuum state "breaks" three of the generators of $SU(2)_L \times U(1)_Y$, corresponding to T^1, T^2, and the orthogonal combination of T^3 and Y. The unbroken generator is given by $Q = T^3 + Y$, which we identify as the electric charge associated with $U(1)_{\text{em}}$. According to Goldstone's theorem, EWSB results in three massless scalar fields, π^a ($a = 1, 2, 3$), known as the Goldstone bosons. Due to the $SU(2)_L$ symmetry, they can be rotated away, and in *unitary gauge*, these Goldstone modes are absorbed by the gauge fields, providing them with mass. Meanwhile, the gauge boson associated with $U(1)_{\text{em}}$ remains massless and is identified with the photon A_μ. Let us parametrise the Higgs field in unitary gauge as follows:

$$H = \begin{pmatrix} 0 \\ \dfrac{v}{\sqrt{2}} + \dfrac{h}{\sqrt{2}} \end{pmatrix} \,, \tag{2.15}$$

where the neutral real scalar field h is the physical Higgs boson. The masses of the gauge bosons arise from the $\left(D_\mu H\right)^\dagger \left(D^\mu H\right)$ term[1] of the Lagrangian in Eq. (2.13). The covariant derivative acting on the Higgs reads

$$D_\mu H = \partial_\mu H - igW^a_\mu T^a H - \frac{i}{2}g' B_\mu H \,. \tag{2.16}$$

With the parametrisation of Eq. (2.15) (and ignoring h terms), we find the following quadratic gauge boson terms

$$\left(D_\mu H\right)^\dagger \left(D^\mu H\right) \supset \frac{g^2 v^2}{8}\left[\left(W^1_\mu\right)^2 + \left(W^2_\mu\right)^2 + \left(\frac{g'}{g}B_\mu - W^3_\mu\right)^2\right] . \tag{2.17}$$

To diagonalise the mixed terms, the $\{B_\mu, W^3_\mu\}$ bosons are rotated to the mass eigenstate basis $\{A_\mu, Z_\mu\}$ according to the Weinberg rotation

$$\begin{pmatrix} B_\mu \\ W^3_\mu \end{pmatrix} = \begin{pmatrix} \cos\theta_W & -\sin\theta_W \\ \sin\theta_W & \cos\theta_W \end{pmatrix} \begin{pmatrix} A_\mu \\ Z_\mu \end{pmatrix} \quad \text{with} \quad \tan\theta_W = \frac{g'}{g}\,, \tag{2.18}$$

[1] The Higgs h gets a mass term from the potential, $V(H) = \frac{1}{2}m_h^2 h^2 + \lambda v h^3 + \frac{\lambda}{4}h^4 - \frac{\lambda}{4}v^4$, with $m_h = \sqrt{2\lambda}v = 125$ GeV.

where $\theta_{\rm W}$ is the Weinberg angle. On the other hand, the charged bosons are identified with $W_\mu^\pm = 1/\sqrt{2}\left(W_\mu^1 \mp i W_\mu^2\right)$, and the following mass spectrum is obtained

$$m_Z = \frac{gv}{2\cos\theta_{\rm W}}, \quad m_W = \frac{gv}{2}, \quad m_A = 0\,. \tag{2.19}$$

Therefore, the $Z_\mu, W_\mu^\pm$ bosons have acquired a mass while the photon A_μ remains massless. In the broken phase, the covariant derivative $D_\mu = \partial_\mu - igT^a W_\mu^a - ig'YB_\mu$ reads

$$\begin{aligned} D_\mu &= \partial_\mu - i\frac{g}{\sqrt{2}}\left(W_\mu^+ T^+ + W_\mu^- T^-\right) - i\frac{1}{\sqrt{g^2+g'^2}}\left(g^2 T^3 - g'^2 Y\right) Z_\mu - i\frac{gg'}{\sqrt{g^2+g'^2}}\left(T^3+Y\right) A_\mu \\ &= \partial_\mu - i\frac{g}{\sqrt{2}}\left(W_\mu^+ T^+ + W_\mu^- T^-\right) - i\frac{g}{\cos\theta_{\rm W}}\left(T^3 - Q\sin^2\theta_{\rm W}\right) Z_\mu - ieQA_\mu\,, \end{aligned} \tag{2.20}$$

with $T^\pm = \frac{1}{2}\left(\sigma^1 \pm i\sigma^2\right)$. The electromagnetic coupling e and charge Q have been identified with A_μ according to

$$\begin{aligned} e &= \frac{gg'}{\sqrt{g^2+g'^2}} = g\sin\theta_{\rm W} = g'\cos\theta_{\rm W}\,, \\ Q &= T^3 + Y\,. \end{aligned} \tag{2.21}$$

It is instructive to count the degrees of freedom (DOF) before and after EWSB. Prior to the mechanism, the theory contains massless W_μ^a, B_μ bosons, each with two physical polarisation states, giving $2\times 4 = 8$ DOF. Including the four real scalar fields from the Higgs, the total number of DOF is 12. After EWSB, the three Goldstone bosons arising from the Higgs field are "eaten" by the gauge bosons, which then acquire a longitudinal polarisation. Consequently, the gauge sector now contains $3\times 3 = 9$ DOF from the massive bosons together with 2 DOF from the (massless) photon, plus the Higgs boson h, preserving the total 12 DOF.

At energies much higher than the electroweak scale ($E \gg m_W, m_Z$), the *Goldstone Boson Equivalence Theorem (GBET)* [6–8] asserts that the scattering amplitudes involving longitudinally polarised electroweak gauge bosons ($W_L^\pm, Z_L$) are equivalent to those involving the corresponding Goldstone bosons ($\pi^\pm, \pi^0$), up to corrections of order $\mathcal{O}(m_W/E)$. This equivalence arises because, in the high-energy limit, the dominant contribution to the longitudinal polarisation of massive gauge bosons behaves as if it were provided by the Goldstone bosons that are "eaten" during EWSB. At high energies, the longitudinal W polarisation can be approximated by [9] $\epsilon_L^\mu(p) \sim p^\mu/m_W$ and the corresponding amplitude can be found scattering the Goldstone boson via replacing $W_L^\mu \to -\partial^\mu\pi/m_W$, so that $\mathcal{M}(W_L W_L \to X) \simeq \mathcal{M}(\pi\pi \to X)$, which considerably simplifies high-energy calculations. In Section 5.2 we will see an explicit example of the GBET for an abelian massive vector. Importantly, scattering processes with longitudinal bosons might (and do) grow with the energy (since $\epsilon_L^\mu(p) \sim p^\mu/m_W$). This leads to a violation of unitarity. Unitarity requires that the S matrix satisfies $SS^\dagger = \mathbb{I}$, which in turn imposes that scattering amplitudes must not grow uncontrollably with energy; otherwise, cross sections would increase without bound, leading to a violation of probability conservation. For instance, processes such as $W_L^+W_L^- \to W_L^+W_L^-$ would violate unitarity if the energy–growing terms were not precisely canceled by the corresponding Higgs contributions. Indeed, the Higgs interactions that generate the gauge boson masses also cancel the otherwise problematic energy–growing terms in scattering amplitudes. In fact, unitarity arguments impose an upper bound on the Higgs boson mass of roughly $m_h \lesssim 1\,\text{TeV}$ [10] to ensure perturbative consistency, which nowadays we know to be in agreement with the observed value $m_h = 125\,\text{GeV}$. In Chapter 7, we will further explore the implications of unitarity for a particular BSM setup.

2.3. Fermion Masses and Interactions

The SM Lagrangian of Eq. (2.4) contains the $SU(2)_L \times U(1)_Y$ invariant Yukawa interaction

$$\mathscr{L}_{\text{Yukawa}} = -\bar{Q}^i H Y_d^{ij} d_R^j - \bar{Q}^i \tilde{H} Y_u^{ij} u_R^j - \bar{L}^i H Y_e^{ij} e_R^j + \text{h.c.} \tag{2.22}$$

where the Higgs couples to LH doublets and RH $SU(2)_L$ singlets through the 3×3 Yukawa couplings Y_f^{ij}. The Yukawa interactions are responsible for generating fermion masses after EWSB[1]. After symmetry breaking and using the Higgs parametrisation of Eq. (2.15), we find

$$\mathscr{L}_{\text{Yukawa}} = -\frac{v}{\sqrt{2}} \left(\bar{d}_L^i Y_d^{ij} d_R^j + \bar{u}_L^i Y_u^{ij} u_R^j + \bar{e}_L^i Y_e^{ij} e_R^j \right) \left(1 + \frac{h}{v} \right) + \text{h.c.} \tag{2.23}$$

The interaction in Eq. (2.23) can be diagonalised according to the singular value decomposition, such that $Y_f = U_f \hat{Y}_f K_f^\dagger$, where U_f, K_f are unitary matrices and $\hat{Y}_f$ is diagonal. Afterwards, we perform the following field redefinitions[2]

$$\begin{aligned} u_L &\to U_u u_L\,, \quad d_L \to U_d d_L\,, \quad e_L \to U_e e_L\,, \\ u_R &\to K_u u_R\,, \quad d_R \to K_d d_R\,, \quad e_R \to K_e e_R\,, \end{aligned} \tag{2.24}$$

under which the Yukawa terms reduce to the fermion mass terms and fermion–Higgs interaction[3]

$$\begin{aligned} \mathscr{L}_{\text{Yukawa}} =& - \left(m_d^i \bar{d}_L^i d_R^i + m_u^i \bar{u}_L^i u_R^i + m_e^i \bar{e}_L^i e_R^i \right) \left(1 + \frac{h}{v} \right) + \text{h.c.}\,, \\ m_u =& \frac{v}{\sqrt{2}} \hat{Y}_u = \text{diag}\left(m_u, m_c, m_t \right)\,, \\ m_d =& \frac{v}{\sqrt{2}} \hat{Y}_d = \text{diag}\left(m_d, m_s, m_b \right)\,, \\ m_e =& \frac{v}{\sqrt{2}} \hat{Y}_e = \text{diag}\left(m_e, m_\mu, m_\tau \right)\,. \end{aligned} \tag{2.25}$$

We observe that the Higgs mechanism results in the fermions acquiring masses and flavour diagonal interactions to h. Thus, EWSB allows for the gauge bosons and fermions to acquire mass terms, which are not (explicitly) allowed in the unbroken phase of Eq. (2.4). In the case of the gauge sector (see Section 2.2), the diagonalisation is accomplished via the Weinberg rotation to the $\{Z_\mu, A_\mu\}$ mass eigenstates. On the other hand, the Yukawa diagonalisation is implemented by the singular value decomposition, and via the rotations of Eq. (2.24). This rotation transforms the Lagrangian from the *flavour basis* (FB) to the *mass basis* (MB). In the FB, the quarks and leptons are described in terms of their weak interactions and the Yukawa interactions are non-diagonal. In the MB, on the other hand, they are described in terms of their physical states, where the Yukawa interactions are diagonalised as given by Eq. (2.25).

Until now, we have considered the gauge–Higgs sector (in Section 2.2) and the Yukawa interactions. Crucially, the Weinberg rotation and the "MB rotation" of Eq. (2.24) must also be applied to the fermion–gauge boson interactions of the SM Lagrangian of Eq. (2.4). *Before* rotating to the

[1] Neutrino masses can be implemented via a Yukawa interaction $\sim \bar{L}_i Y_\nu \tilde{H} \nu_R + \text{h.c.}$, but in the SM $m_\nu = 0$ and thus such a term is not considered.

[2] Notice that neutrinos do not have to be rotated since they do not appear in the Yukawa interaction.

[3] Since $\hat{Y}_f$ are diagonal the Lagrangian is flavour diagonal.

MB, the interactions of the SM fermions in the FB of Eq. (2.4) are given by (omitting the $SU(3)_c$ interactions, which we discuss in Section 2.4)

$$\begin{aligned}\mathscr{L}_{\text{FB}} \supset\ & \bar{u}_L^i \left(Y_Q g' \not{B} + \frac{g}{2}\not{W}^3\right) u_L^i + \bar{d}_L^i \left(Y_Q g' \not{B} - \frac{g}{2}\not{W}^3\right) d_L^i + \bar{u}_R^i \left(Y_u g' \not{B}\right) u_R^i + \bar{d}_R^i \left(Y_d g' \not{B}\right) d_R^i \\ & + \bar{e}_L^i \left(Y_L g' \not{B} + \frac{g}{2}\not{W}^3\right) e_L^i + \bar{\nu}_L^i \left(Y_L g' \not{B} - \frac{g}{2}\not{W}^3\right) \nu_L^i + \bar{e}_R^i \left(Y_e g' \not{B}\right) e_R^i \\ & + \frac{g}{\sqrt{2}} \bar{u}_L^i \not{W}^+ d_L^i + \frac{g}{\sqrt{2}} \bar{d}_L^i \not{W}^- u_L^i + \frac{g}{\sqrt{2}} \bar{\nu}_L^i \not{W}^+ e_L^i + \frac{g}{\sqrt{2}} \bar{e}_L^i \not{W}^- \nu_L^i \\ & - \frac{v}{\sqrt{2}} Y_d^{ij} \bar{d}_L^i d_R^j - \frac{v}{\sqrt{2}} Y_u^{ij} \bar{u}_L^i u_R^j - \frac{v}{\sqrt{2}} Y_e^{ij} \bar{e}_L^i e_R^j + \text{h.c.}\end{aligned} \tag{2.26}$$

The first two lines correspond to the B_μ, W_μ^3 neutral currents (NCs) of quarks and leptons, respectively. The charged currents (CCs) of quarks and leptons in the third line are already expressed in terms of the $W_\mu^\pm = 1/\sqrt{2}\left(W_\mu^1 \mp i W_\mu^2\right)$ bosons. The last terms correspond to the Yukawa interactions after EWSB. In the FB, the interactions of the fermions with the gauge bosons are flavour diagonal, but the Yukawa terms are non-diagonal. In order to go to the MB, the diagonal Yukawa matrices are introduced according to $Y_f = U_f \hat{Y}_f K_f^\dagger$ together with the rotations of Eq. (2.24). The effect of this rotation on the neutral currents is as follows[1]

$$\begin{aligned}\mathscr{L}_{\text{NC}} &\supset \bar{d}_L^i Y_Q \not{B} d_L^i \to \bar{d}_L^i \left(U_d^\dagger Y_Q U_d\right)^{ij} \not{B} d_L^j = \bar{d}_L^i Y_Q \not{B} d_L^i\,, \\ \mathscr{L}_{\text{NC}} &\supset \bar{d}_R^i Y_d \not{B} d_R^i \to \bar{d}_R^i \left(K_d^\dagger Y_d K_d\right)^{ij} \not{B} d_R^j = \bar{d}_R^i Y_d \not{B} d_R^i\,, \\ \mathscr{L}_{\text{NC}} &\supset \bar{d}_L^i \not{W}^3 d_L^i \to \bar{d}_L^i \left(U_d^\dagger U_d\right)^{ij} \not{W}^3 d_L^j = \bar{d}_L^i \not{W}^3 d_L^i\,,\end{aligned} \tag{2.27}$$

where we have considered the down quarks, with the analogous results for the up quarks and leptons. We see that the neutral interactions are unaffected by the rotations of Eq. (2.24) and remain flavour diagonal in the MB. While the W_μ^3 interactions (last line of Eq. (2.27)) are trivially unaffected by the rotation, for the B_μ interactions (first two lines of Eq. (2.27)) this is a consequence from the fact that the SM hypercharges Y_f are *flavour universal*, that is, the same for each of the three generations of each fermion family[2]. Mathematically, and with explicit flavour indices, this means

$$Y_f^{ij}|_{\text{hypercharge}} = Y_f \mathbb{I}_{3\times 3} \quad \forall f = Q, u, d, L, e\,, \tag{2.28}$$

where the subscript hypercharge is to clarify that we are refering to the SM hypercharges and not to the Yukawa matrices. Therefore, the rotation matrices U_f, K_f commute with the hypercharges and the NCs remain flavour diagonal in the MB. As a result, *flavour-changing neutral currents* (FCNCs) are forbidden in the SM. FCNCs are processes in which a quark changes its flavour without altering its electric charge, mediated by neutral particles such as the Z_μ. We just showed that in the SM such processes are not possible (at tree-level), due to the flavour universality of the hypercharges. This is not necessarily the case for NP models, and in Part II of this thesis we will consider a BSM model in which the new charges are not flavour universal, which allows for tree-level FCNC interactions. For the quark CCs, the rotation to the MB modifies the Lagrangian according to

$$\mathscr{L}_{\text{CC}} \supset \frac{g}{\sqrt{2}} \not{W}^+ \bar{u}_L^i V_{\text{CKM}}^{ij} d_L^j + \frac{g}{\sqrt{2}} \not{W}^- \bar{d}_L^i (V_{\text{CKM}}^\dagger)^{ij} u_L^j\,, \tag{2.29}$$

[1] Kinetic terms are invariant under the rotations of Eq. (2.24).
[2] If this were not the case, the SM would be anomalous.

where $V_{\text{CKM}} \equiv U_u^\dagger U_d$ is the Cabibbo–Kobayashi–Maskawa (CKM) matrix. Unlike for the NCs, the charged interactions exchange up and down quarks of distinct flavour with [11]

$$|V_{\text{CKM}}| = \begin{pmatrix} |V_{ud}| & |V_{us}| & |V_{ub}| \\ |V_{cd}| & |V_{cs}| & |V_{cb}| \\ |V_{td}| & |V_{ts}| & |V_{tb}| \end{pmatrix} = \begin{pmatrix} 0.97435 & 0.22500 & 0.00369 \\ 0.22486 & 0.97349 & 0.04182 \\ 0.00857 & 0.04110 & 0.99911 \end{pmatrix} . \tag{2.30}$$

Note that the matrix is close to unity in the diagonal entries $V_{ii} \sim 1$, while $V_{i\neq j} \ll 1$. It is instructive to write the CKM matrix in the Wolfenstein parametrisation [11]

$$V_{\text{CKM}} = \begin{pmatrix} 1 - \frac{\lambda^2}{2} & \lambda & A\lambda^3(\rho - i\eta) \\ -\lambda & 1 - \frac{\lambda^2}{2} & A\lambda^2 \\ A\lambda^3(1 - \rho - i\eta) & -A\lambda^2 & 1 \end{pmatrix} + \mathcal{O}(\lambda^4) \tag{2.31}$$

with $\lambda = 0.22453 \pm 0.00044, A = 0.836 \pm 0.015, \rho = 0.122^{+0.018}_{-0.017}, \eta = 0.355^{+0.012}_{-0.011}$. This parametrisation elegantly reveals the hierarchical structure of the CKM matrix: its diagonal elements are of order one, while the smallest off-diagonal entries appear in the upper right and bottom left corners. Thus, unlike FCNCs, flavour-changing charged currents (FCCCs) are possible in the SM, with the CKM controlling their strength. Crucially, the parameter η, corresponding to the CKM matrix complex phase, is the source of CP-violation in the SM. Finally, the quark–gauge boson interactions and quark masses in the MB read

$$\begin{aligned} \mathscr{L}_{\text{MB}} =& \frac{e}{\sin\theta_{\text{W}}} Z_\mu J^{Z\mu} + eA_\mu J^\mu_{\text{em}} - \left(m_d \bar{d}_L d_R + m_u \bar{u}_L u_R + L \leftrightarrow R\right) \\ &+ \frac{e}{\sqrt{2}\sin\theta_{\text{W}}} \left[W^+_\mu \bar{u}^i_L \gamma^\mu V^{ij} d^j_L + W^-_\mu \bar{d}^i_L \gamma^\mu \left(V^{ij}\right)^\dagger u^j_L\right] , \end{aligned} \tag{2.32}$$

where we have introduced the Z_μ, A_μ bosons with the Weinberg rotation of Eq. (2.18), and the flavour diagonal NCs are given as follows

$$\begin{aligned} J^\mu_{\text{em}} &= Q_i \left(\bar{Q}^i \gamma^\mu Q^i + \bar{u}^i_R \gamma^\mu u^i_R + \bar{d}^i_R \gamma^\mu d^i_R\right) = J^Y_\mu + J^3_\mu \\ J^Z_\mu &= \cos\theta_{\text{W}} J^3_\mu - \frac{\sin^2\theta_{\text{W}}}{\cos\theta_{\text{W}}} J^Y_\mu \\ J^3_\mu &= \bar{Q}^i \gamma^\mu T^3 Q^i = \frac{1}{2}\bar{u}^i_L \gamma^\mu u^i_L - \frac{1}{2}\bar{d}^i_L \gamma^\mu d^i_L , \\ J^Y_\mu &= \bar{Q}^i Y_Q \gamma^\mu Q^i + \bar{u}^i_R Y_u \gamma^\mu u^i_R + \bar{d}^i_R Y_u \gamma^\mu d^i_R . \end{aligned} \tag{2.33}$$

In the lepton sector, the situation is similar but the key differences are that there is only one Yukawa term and that no RH neutrinos are present in the SM. As we have seen, after rotating to the MB according to Eq. (2.24) the NCs remain flavour diagonal, since the lepton hypercharges are also flavour universal. But for the charged interactions

$$\mathscr{L}_{\text{CC}} \supset \frac{g}{\sqrt{2}} \bar{\nu}^i_L W^+ U^{ij} e^j_L + \frac{g}{\sqrt{2}} \bar{e}^i_L W^- (U^\dagger)^{ij} \nu^j_L , \tag{2.34}$$

where $U_{\text{PMNS}} \equiv U_\nu^\dagger U_e$ is the Pontecorvo–Maki–Nakagawa–Sakata (PMNS) matrix, which arises after rotating e_L according to Eq. (2.24) and $\nu_L \to U_\nu \nu_L$. The PMNS matrix is the leptonic analogous to the CKM matrix in the quark sector. But since no neutrino mass term is present in the SM, the U_ν matrix can be freely taken to be $U_\nu = U_e$ such that $U_{\text{PMNS}} = \mathbb{I}$. Therefore, in the

SM no PMNS matrix arises because there is no neutrino mass matrix to diagonalise, and there is no mismatch between the neutrino flavour and mass basis. Consequently, flavour-changing processes in the lepton sector are not induced, and the lepton–gauge boson interactions and fermion masses

$$\begin{aligned}\mathscr{L}_{\text{MB}} =& \frac{e}{\sin\theta_{\text{W}}} Z_\mu J^{Z\mu} + eA_\mu J^\mu_{\text{em}} - (m_e \bar{e}_L e_R + L \leftrightarrow R) \\ &+ \frac{e}{\sqrt{2}\sin\theta_{\text{W}}} \left[W^+_\mu \bar{\nu}^i_L \gamma^\mu e^i_L + W^-_\mu \bar{e}^i_L \gamma^\mu \nu^i_L \right] .\end{aligned} \tag{2.35}$$

Despite this, the observation of neutrino oscillations [12] indicates that neutrinos must possess small masses, with $\sum m_\nu \leq 0.12$ eV on the total neutrino mass [13]. Neutrino masses can be generated through a Yukawa term upon including a RH neutrino in the SM, but to generate a neutrino mass $m_\nu \sim 0.1$ eV a tiny Yukawa coupling is needed, with $Y_\nu \sim 10^{-12}$. This is unnaturally small compared to the Yukawa couplings of other leptons like the electron, with $Y_e \sim 10^{-6}$. This brings up the possibility that a different mechanism generates the neutrino masses. If the neutrinos are Majorana particles, i.e., their own antiparticle, a new mass term can be written in the Yukawa sector

$$\mathscr{L}^\nu_{\text{Yukawa}} = \bar{L}^i Y^{ij}_\nu \tilde{H} \nu^j_R - \frac{1}{2} M^{ij}_R \bar{\nu}^{ic}_R \nu^j_R + \text{h.c.} \tag{2.36}$$

where $\nu^c_R = C\bar{\nu}^T_R$, with C being the charge conjugation matrix. After EWSB, the corresponding mass matrix is diagonalised for $M_R \gg m = Y_\nu v/\sqrt{2}$, which results in heavy $m_H \sim M_R$ and light eigenstates $m_L \sim m^2/M_R$. This process is known as the seesaw mechanism, and explains the smallness of the neutrino masses by assuming heavy RH neutrinos. The need for neutrino masses implies the existence of BSM physics, with the possibility of having RH neutrinos and mass generation mechanisms that differ from the SM Higgs mechanism. In this thesis we do not focus on neutrino physics, but we note that it is a relevant topic for BSM physics, and we refer the interested reader to Refs. [14, 15] for further details on the topic.

2.4. Quantum Chromodynamics

QCD is the theory of strong interactions, corresponding to the $SU(3)_c$ gauge group of the SM symmetry group of Eq. (2.1). The strong force is what binds quarks together to form protons, neutrons, and other hadrons. It is the strongest of the fundamental forces, but only operates at very short distances (on the scale of atomic nuclei). QCD contains eight gluons $G^a_\mu, a = 1, \ldots, 8$ which mediate quark interactions, as given in Eq. (2.10). The leptons and Higgs are uncharged under QCD and thus do not participate in its interactions.

In QCD, quarks and gluons have a quantum number called *colour*. Quarks transform under the fundamental representation of $SU(3)_c$ and come in one of three colours (red, blue or green), and are represented as q_α, where $\alpha = 1, 2, 3$ is the colour index. Meanwhile, gluons carry a combination of colour and anti-colour and transform under the adjoint representation of $SU(3)_c$, with eight possible combinations of colour and anti-colour. In sections Sec 2.2 and Sec 2.3 we have seen that EWSB results in the gauge bosons and fermions acquiring mass, and discussed the flavour interactions in the FB and MB. We learned that FCNCs are not present in the SM, while FCCCs are possible through the CKM and PMNS matrices (if neutrinos are massive). While quarks come in different flavours, gluons are massless particles with *flavour blind* interactions. The QCD Lagrangian reads

$$\mathscr{L}_{\text{QCD}} = -\frac{1}{4} G^{A\mu\nu} G^A_{\mu\nu} + \bar{q}_\alpha (i\not{\partial}) q_\beta \delta_{\alpha\beta} - m_q \bar{q}_\alpha q_\alpha + g_s \bar{q}_\alpha \not{G}^A q_\beta T^A_{\alpha\beta} , \tag{2.37}$$

where α, β are colour indices and $T_{\alpha\beta}$ are the $SU(3)_c$ generators, as given in Eq. (2.11). No flavour indices i, j are explicitly written for QCD because the interactions are flavour independent and thus the interactions are flavour diagonal. Notice that we have written an explicit mass term for the quarks in Eq. (2.37), which corresponds to the mass term generated after EWSB, as discussed in Sec 2.3. Moreover, the QCD Lagrangian is readily in the MB, as it is trivially invariant under the rotations of Eq. (2.24).

QCD exhibits a particular property known as *confinement*. In nature, quarks and gluons are never found in isolation, and are always confined in hadrons. This is because the strong force becomes stronger as quarks move farther apart, making it energetically unfavorable for quarks to separate. Additionally, QCD is *asymptotically free*, meaning that the theory becomes strongly coupled at low energies, and weakly coupled at high energies. The reason for this behaviour is that the $\beta(g_s)$ function of QCD, which encodes the change of the strong coupling g_s with energy, is negative. Indeed, at 1-loop

$$\beta(g_s) = \frac{dg_s}{d\log\mu} = -\frac{g_s^3}{(4\pi)^2}\left(\frac{11}{3}N_c - \frac{2}{3}N_f\right), \tag{2.38}$$

where N_c is the number colours, N_f the number of flavours and μ is the energy scale. Since in the SM $N_c = 3, N_f = 6$, the beta function is negative $\beta(g_s) < 0$ and g_s grows (decreases) at low (high) energies. Asymptotic freedom renders perturbation methods viable for describing high energy scattering, while low energy effects are non-perturbative and encapsulated in quantities such as parton distribution functions (PDFs) and hadronic matrix elements. The factorisation of high and low energy contributions in QCD amplitudes is a cornerstone of the theoretical framework underpinning hadronic processes, which provides the foundation for precision predictions in high-energy experiments.

In Part III of this thesis we are going to extend the SM with a new heavy scalar particle, the LQ. This NP setup mediates quark–lepton interactions, which are not present in the SM. We will consider the LQ to be charged under $SU(3)_c$ so that it interacts with quarks and gluons. Therefore, the SM QCD Lagrangian of Eq. (2.37) will be modified accordingly and we will consider the QCD corrections for a specific process. These QCD corrections are essential for ensuring precision in theoretical predictions [16]. At the heart of many BSM models, including those involving scalar LQs, are processes that are sensitive to strong interactions. In such models, the associated QCD corrections modify the observables of these processes. Without these corrections, predictions could be off by significant margins, undermining comparisons between theory and experiment. For instance, at particle colliders, where high energy interactions between protons or heavy ions occur, accurate theoretical models that include QCD corrections are critical for extracting meaningful experimental results, particularly when looking for deviations from SM predictions that could indicate the presence of NP.

2.5. Flavour as a Guide for New Physics

In the previous sections we have established that FCNCs do not occur in the SM. On the other hand, FCCCs arise in the quark sector via the CKM matrix, as dictated by the interactions in Eq. (2.32). While FCNC processes are forbidden at tree level, they can still occur at loop level through interactions involving the $W_\mu^\pm$ bosons. Loop amplitudes are suppressed by a factor of $1/(4\pi)^2$, making them much rarer than tree-level amplitudes. Furthermore, the CKM matrix provides an additional suppression: the off-diagonal elements that connect different quark flavours are typically small, particularly for transitions involving quarks from the 1-3 generations. This

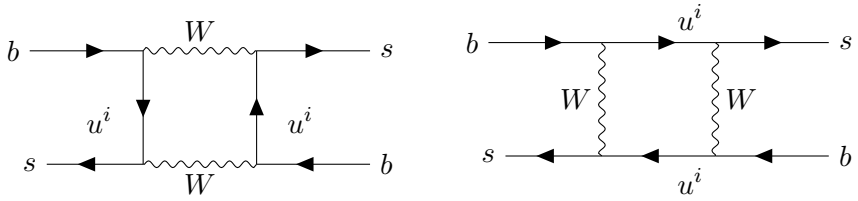

Figure 2.1.: Feynman diagram depicting the SM contributions to the B_s mixing.

is evident from the values of the CKM matrix elements, as seen in Eq. (2.30). Another important source of suppression comes from the Glashow–Iliopoulos–Maiani (GIM) mechanism [17], which stems from the fact that FCNC amplitudes are proportional to the differences in the quark masses involved in the loop $\sim (m_q^2 - m_{q'}^2)/m_W^2$. This is because if all quarks in a given sector were degenerate, then there would be no flavour changing $W_\mu^\pm$ interactions[1]. Concretely, FCNCs in the down (up) sector are proportional to mass-squared differences between the quarks of the up (down) sector. Consequently, the GIM mechanism fails for down sector transitions whenever contributions of the top quark dominate in the loops because $m_t > m_W$, while it further suppresses up-type FCNCs because $m_{d,s,b} \ll m_W$. Schematically, an amplitude for a FCNC process in the SM scales as

$$\mathcal{A}_{\text{FCNC}}^{\text{SM}} \sim \text{loop suppression} \times \text{CKM suppression} \times \frac{m_q^2 - m_{q'}^2}{m_W^2} \quad \text{GIM mechanism}\,, \tag{2.39}$$

where $m_q, m_{q'}$ are the masses of the quarks in the loop. As an example of the FCNC suppression in the SM we consider B_s mixing, which we will study in Part III in the context of scalar LQs. B_s mixing is the process in which a neutral B_s meson (composed of b, s quarks and written as $B_s = \bar{b}s$) oscillates between two different states: a B_s meson and its antimeson $\bar{B}_s$. This is a FCNC process in which the b and s quarks change flavour, and thus in the SM the process occurs via 1-loop box diagrams with four CKM insertions, as shown Figure 2.1. The B_s mixing amplitude in the SM reads (assuming $m_u = 0$) [18–20]

$$\mathcal{A}_{B_s-\bar{B}_s}^{\text{SM}} \propto \frac{g^4}{64\pi^2 m_W^2}\Big((V_{tb}^\star V_{ts})^2\, S(x_t) + 2V_{tb}^\star V_{ts} V_{cb}^\star V_{cs} S(x_c, x_t) + (V_{cb}^\star V_{cs})^2\, S(x_c)\Big)\langle\mathcal{O}\rangle\,, \tag{2.40}$$

where $\langle\mathcal{O}\rangle$ is the tree-level matrix element of $\mathcal{O} = (\bar{b}_\alpha \gamma_\mu P_L s_\alpha)(\bar{b}_\beta \gamma^\mu P_L s_\beta)$, and $S(x_i), S(x_i, x_j)$ are the Inami–Lim functions [21] with $x_i \equiv m_i^2/m_W^2$, and the unitarity of the CKM matrix has been used to substitute $V_{ub}^\star V_{us} = -V_{tb}^\star V_{ts} - V_{cb}^\star V_{cs}$. The CKM factors in Eq. (2.40) all scale as λ^4 in terms of the Wolfenstein parameter, see Eq. (2.31). Therefore, since $S(x_t) \gg S(x_c, x_t) > S(x_c)$ we can approximate

$$\mathcal{A}_{B_s-\bar{B}_s}^{\text{SM}} \propto \frac{g^4}{64\pi^2 m_W^2}\,(V_{tb}^\star V_{ts})^2\, S(x_t)\langle\mathcal{O}\rangle\,, \tag{2.41}$$

rendering the top quark as the leading contribution, for which no GIM mechanism occurs because $x_t \sim 4$. Of course, the amplitude is still loop and CKM suppressed, with $V_{tb}^\star V_{ts} \sim \lambda^2$. This behaviour is found among all FCNC processes in the SM. For example, the $D^0 = c\bar{u}$ meson mixing is dominated by the strange quark according to $(V_{us}V_{cs}^\star)^2 x_s \sim \lambda^2 x_s$. Notice that although $m_b \gg m_s$, this is not enough to compensate the smallness of the V_{ub}, V_{cb} CKM elements. As another example, the $K^0 = \bar{s}d$ mixing is dominated by the charm quark with $(V_{cd}V_{cs}^\star)^2 x_c \sim \lambda^2 x_c$. In general, the CKM factors in any FCNC amplitude appear as

$$\mathcal{A}_{\text{FCNC}}^{\text{SM}} \propto \sum_{i=u,c,t} \kappa_i F(x_i) \quad \text{or} \quad \mathcal{A}_{\text{FCNC}}^{\text{SM}} \propto \sum_{i,j=u,c,t} \kappa_i \kappa_j F(x_i, x_j)\,, \tag{2.42}$$

[1] Indeed, for degenerate masses the rotation U_d, U_u matrices of Eq. (2.24) that diagonalise the Yukawas can be freely chosen so that the CKM reduces to the identity, $V_{\text{CKM}} = \mathbb{I}$.

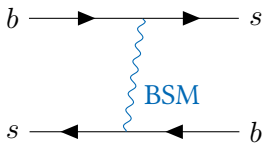

Figure 2.2.: Feynman diagram depicting the BSM contribution to the B_s mixing, with the NP field depicted in blue.

where κ_i are the corresponding CKM contributions ($\kappa_i = V_{ib}^\star V_{is}$ for B_s mixing, see Eq. (2.40)). The first (left) possibility of Eq. (2.42) corresponds to two CKM insertions; this is the case for processes such as the penguin mediated $b \to s\gamma$, which scales as $V_{ts}^\star V_{tb} x_t \sim \lambda^2 x_t$. The second option, with four CKM insertions, is precisely the one of meson mixing. From Eq. (2.42), we conclude that if the quarks are degenerate, the unitarity of the CKM matrix $\kappa_u + \kappa_c + \kappa_t = 0$ implies the vanishing of FCNC processes, and the GIM mechanism is *exact*. In summary, in the SM FCNC processes are suppressed due to the specific flavour interactions (forcing loop amplitudes), the quark masses ($m_q \ll m_W, q \neq t$) and the smallness of the CKM elements. These features are particular to the SM, and do not necessarily hold in NP models. Let us assume a NP model with tree level down-type FCNCs. In this scenario, B_s mixing is given by the diagram in Figure 2.2, where the blue line indicates the new BSM field coupling to b, s quarks at tree level. Under this assumption, the B_s mixing is not loop suppressed nor CKM suppressed. Therefore, $\mathcal{A}^{\text{BSM}}_{B_s-\bar{B}_s}$ can compete with the SM contribution $\mathcal{A}^{\text{SM}}_{B_s-\bar{B}_s}$. In other words, FCNC processes are *sensitive* to NP, and are a mechanism to study and potentially discover BSM physics.

Historically, flavour physics has proven its success in developing the SM. The GIM mechanism explained the suppression of FCNCs and predicted the existence of the charm quark—which was experimentally validated at Stanford Linear Accelerator Center (SLAC) and the Brookhaven National Laboratory during the so-called November Revolution of the early 1970s. Subsequently, the observation of CP violation in the Kaon system posed a significant challenge to the existing framework of weak interactions. Initially, flavour mixing was described by the Cabibbo angle, which accounted for transitions between the down and strange quarks in a two generation model. However, the presence of CP violation indicated that a two generation SM could not accommodate the necessary complex phase that would allow for CP violation in the decay processes. This was solved by extending the SM to include a third generation, with the formulation of the CKM matrix. This framework was later corroborated by the discoveries of the bottom and top quarks.

One of the main topics in BSM physics is that of DM [22]. DM being a new particle not present in the SM is one of the most widely discussed possibilities, with many proposed candidates such as axions, dark photons and sterile neutrinos. These models typically assume a weakly interacting particle coupled to the SM, rendering DM elusive and difficult to detect in its nature. In Part II of this thesis we are going to study a generic model encompassing dark photons and Z' models [23–25], and we will show that flavour physics sets very stringent constraints on the model. Another promising NP model are scalar LQs, which we consider in Part III. LQs [26] are attractive candidates for BSM because they provide a direct connection between the quark and lepton sectors–two areas that are otherwise treated as fundamentally separate in the SM. As hypothetical particles carrying both baryon and lepton quantum numbers, LQs naturally arise in various unified theories such as Grand Unified Theories (GUTs) [27–29]. One of the most compelling motivations for considering LQs is their potential to account for anomalies observed in flavour physics experiments. For instance, deviations from lepton flavor universality in rare B meson decays [30], as reported by experiments like LHCb and Belle, suggest the presence of NP that

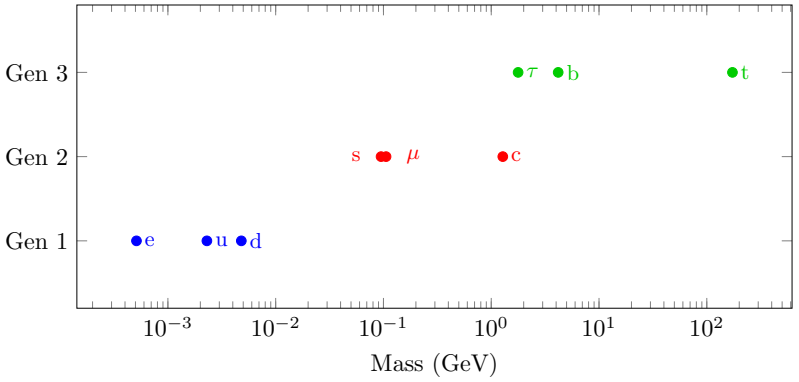

Figure 2.3.: SM masses for quarks and charged leptons. The first matter generation (1) is lighter than the second one (2), which in turn is lighter than the third generation (3).

could be mediated by LQs. Additionally, LQs have been proposed as a possible explanation for the discrepancies observed in the muon anomalous magnetic moment [31].

Other open problems in the SM and beyond include the observed imbalance between matter and antimatter in the universe, known as baryon asymmetry, incorporating gravity into the framework and the strong CP problem. For the former, the (three) Sakharov conditions [**?**] must be fulfilled, and while the SM does include mechanisms that satisfy these conditions to some extent, they are insufficient to account for the observed baryon asymmetry and thus require BSM physics. There are other issues within the SM itself, such as the *flavour puzzle* [32], which is not a problem per se but an inquiry which might serve as a clue for the nature of the yet unknown BSM physics. In the SM the fermion masses exhibit a clear hierarchical structure, in which the first generation is lighter than the second one, and the latter is lighter than the third generation. See Figure 2.3 for a representation of this structure. Moreover, the CKM matrix also presents a hierarchical structure among generations, see Eq. 2.30. Since the masses and CKM matrix come from the Yukawa interactions, why is there a hierarchical structure on the Yukawa couplings when they all couple to the Higgs in the same manner? Notice that the Yukawa matrices are independent of each other, and yet they show a similar hierarchical structure. This is certainly not assumed to be arbitrary, and an explanation is expected.

Until now the discussion has focused on the quark sector, as it plays a central role in this thesis. But leptons also offer the possibility to test the SM and explore NP models. As discussed in Section 2.3, charged lepton flavour violation (CLFV) is not present in the SM because neutrinos are massless. But since the observation of neutrino oscillations (corresponding to neutral lepton flavour violation), it is known that neutrinos must possess (tiny) masses, and therefore a U_{PMNS} matrix allows for CLFV processes such as $\mu \to e\gamma$, which arise equivalently to the SM process $b \to s\gamma$ with neutrinos in the loop and U_{PMNS} vertices. CLFV is therefore expected to occur but it is yet to be observed, with current theory estimates of $\text{Br}(\mu \to e\gamma) = 10^{-54}$, which lies beyond any foreseeable experimental reach, with the current limit at $\text{Br}(\mu \to e\gamma) < 10^{-13}$. The nature of the mechanism giving mass to the neutrinos is of much importance in this research area (as briefly discussed in Section 2.3), with BSM models typically allowing for CLFV. See Ref. [33] for a review on CLFV.

There is no doubt that the SM is incomplete, and BSM physics can be studied and searched for with flavour physics. Additionally, flavour allows to deepen our understanding of the SM itself, with highly accurate measurements and predictions. It is the hope of the community that through theoretical, phenomenological and experimental research, NP will be discovered and understood in connection to the SM.

Chapter 3

Effective Field Theories

In this chapter we present a comprehensive review of the foundational aspects of EFTs in particle physics. We begin with a broad overview in Section 3.1 that lays the groundwork for the subsequent discussions. In Section 3.2, we introduce the weak effective theory (WET) framework employed in Part III to address heavy new physics, whereas Section 3.3 is devoted to the EFT approach applied in Part II for light new physics scenarios. For additional context and deeper insights, we refer the reader to Refs. [19, 34–36].

3.1. Overview of EFTs in Particle Physics

An EFT is a framework in which physical phenomena is described by its relevant DOF at a certain scale, without the need to know all the details of the potentially unknown fundamental theory. For example, although special relativity is a more fundamental description of reality than Newtonian mechanics, slow moving objects follow to great precision Newton's law. This is because Newtonian mechanics is the $v \ll 1$ limit of special relativity. As another example, the vibration of the atoms in a macroscopic object is too fast to affect at all the movement of the object, and the movement of the object is too slow to affect at all the vibration of its atoms, so both physical processes can be studied independently. Therefore, the key element to EFTs is the the role of distinct scales, where different physical phenomena are mostly independent of one another because they operate at completely different scales. It is interesting to note that scale separation is very natural and *real* in the physical world, for instance, engineers designing bridges rely on Newtonian mechanics without delving into QFT because quantum effects are negligible at macroscopic scales. It is therefore most convenient to only work with the DOF that are relevant at a particular scale, otherwise the problem becomes more (and unnecessarily) complex.

In particle physics, an EFT is defined by distance or energy scales, with the dynamics at low energies not depending on the details of the dynamics at high energies. This is guaranteed by the decoupling theorem of Appelquist–Carazzone [37], which states that the heavy DOF decouple at energy scales much lower than their mass. By decoupling, it is meant that the contributions of these heavy DOF are suppressed by inverse powers of the heavy scale (up to logarithmic corrections). In essence, in the EFT approach any interaction respecting the symmetries of the theory is included in the Lagrangian, which is given by a tower of operators where higher dimensional $d > 4$ operators are suppressed by the large scale Λ

$$\mathscr{L}_{\text{EFT}} = \mathscr{L}_{\text{UV}} + \sum_{d>4} \sum_{i} \frac{1}{\Lambda^{d-4}} C_i \mathcal{O}_i^d \,. \tag{3.1}$$

Here, $\mathscr{L}_{\text{UV}}$ denotes the renormalisable part of the Lagrangian, with operators of dimension $d \leq 4$. On the other hand, $\mathcal{O}_i^d$ denotes a local operator of dimension $d > 4$, composed of the dynamical DOF at energies below Λ, and the index i runs over all possible operators of dimension d. The couplings C_i are the Wilson coefficients (WCs) and contain the short-distance contributions, that is, the physics above Λ. The Lagrangian of Eq. (3.1) contains a series of effective vertices multiplied by the effective coupling constants C_i. This series is known as the operator product expansion (OPE), and allows to separate the long-distance and short-distance contributions through the operators and WCs, respectively. The $\mathcal{O}_i^d$ operators are not renormalisable in the traditional sense, meaning that the theory requires an infinite number of counterterms to cancel the divergences from loop amplitudes. However, in the EFT framework this is not problematic because higher-dimensional operators are increasingly suppressed by inverse powers of the large scale Λ, which serves as the expansion parameter. Consequently, these operators are included in the relevant Green's functions only to the extent necessary for calculations to a specific order in the $1/\Lambda$ series. According to this line of reasoning, *above* the EW scale the SM Lagrangian of Eq. (2.4) can be extended to the Standard Model Effective Field Theory (SMEFT) [38]

$$\mathscr{L}_{\text{SMEFT}} = \mathscr{L}_{\text{SM}} + \sum_{d>4} \sum_i \frac{1}{\Lambda_{\text{NP}}^{d-4}} C_i \mathcal{O}_i^d \,, \tag{3.2}$$

where $\mathscr{L}_{\text{SM}}$ is the (renormalisable) SM Lagrangian, extended with higher dimensional operators of $d > 4$. In the SMEFT no further field content than the one of the SM (specified in Table 2.1) is considered, and thus the $\mathcal{O}_i^d$ operators are built out of SM fields. In this scenario, Λ_{NP} is the high energy scale at which BSM physics kicks in, which is still unknown but expected to be around the TeV scale. This EFT approach allows for a controlled study of contributions from NP above the EW scale, where lower-dimensional operators contribute more significantly at energies accessible in current experiments, and higher-dimensional operators contribute with smaller corrections. In this manner, SM deviations are systematically studied in a $1/\Lambda_{\text{NP}}$ expansion. On the other hand, for processes *below* the EW scale, the W_μ, Z_μ, h bosons and the top quark are integrated out of the SM. Then, the SM Lagrangian is reduced to the low–energy effective field theory (LEFT)

$$\mathscr{L}_{\text{LEFT}} = \mathscr{L}_{\text{QED+QCD}} + \mathscr{L}_{\text{WET}} \,, \tag{3.3}$$

where $\mathscr{L}_{\text{WET}}$ is the weak effective field theory (WET) describing processes below the EW scale that are purely or predominantly weak, as it is the case for FCNCs. The WET Lagrangian is given by

$$\mathscr{L}_{\text{WET}} = -\sum_i C_i \mathcal{O}_i \,, \tag{3.4}$$

where it is understood that $\mathcal{O}_i$ are higher dimensional operators, in agreement with the second term in Eq. (3.1). In this case, C_i are dimensionful, as we have not factored out the high scale. For practical purposes there is no loss in precision in using the WET for flavour physics rather than the full SM, and it is computationally simpler. Therefore, even if the underlying theory of a certain phenomena is known, EFTs can still be used and be helpful. The 'bottom-up' usage of EFTs is for situations where the fundamental theory is unknown, such as the SMEFT. The 'top-down' approach applies when the fundamental theory is known, and EFT is used to simplify calculations or make them possible in the first place. A frequent and significant example of the WET is given by the Fermi theory, which applies to energies well below the EW scale. Consider the amplitude for the beta decay $d \to \bar{\nu}_e + e + u$, which according to the EW theory reads

$$\mathcal{A}_{\text{full}} = \left(\frac{ig}{\sqrt{2}}\right)^2 V_{ud} \left(\bar{u}\gamma_\alpha P_L d\right) \left(\bar{e}\gamma_\beta P_L \nu_e\right) \frac{-ig_{\alpha\beta}}{q^2 - m_W^2} \,, \tag{3.5}$$

which we label as full because in this example the EW theory is the fundamental/underlying model. The momentum transfer satisfies $q^2 \ll m_W^2 \to q^2/m_W^2 \ll 1$ due to the small masses of the fermions. Therefore, the W propagator can be expanded according to

$$\frac{1}{q^2 - m_W^2} = -\frac{1}{m_W^2} - \frac{q^2}{m_W^4} + \mathcal{O}(q^2/m_W^2)\,. \tag{3.6}$$

Keeping the first order term, the amplitude of Eq. (3.5) reads

$$\mathcal{A}_{\text{full}} = \frac{i}{m_W^2}\left(\frac{ig}{\sqrt{2}}\right)^2 V_{ud}\,(\bar{u}\gamma_\alpha P_L d)\,(\bar{e}\gamma^\alpha P_L \nu_e) + \mathcal{O}(q^2/m_W^2)\,. \tag{3.7}$$

This amplitude can be reproduced with the following effective Lagrangian

$$\mathscr{L}_{\text{Fermi}} = -\frac{4G_{\text{F}}}{\sqrt{2}} V_{ud}\,(\bar{u}\gamma_\alpha P_L d)\,(\bar{e}\gamma^\alpha P_L \nu_e)\ , \tag{3.8}$$

where G_{F} is the Fermi constant (the WC for this EFT), and gives rise to the following amplitude for $d \to \bar{\nu}_e + e + u$

$$\mathcal{A}_{\text{Fermi}} = -i\frac{4G_{\text{F}}}{\sqrt{2}} V_{ud}\,(\bar{u}\gamma_\alpha P_L d)\,(\bar{e}\gamma^\alpha P_L \nu_e)\ . \tag{3.9}$$

In order for this amplitude to reproduce the full amplitude $\mathcal{A}_{\text{full}}$, the G_{F} constant is identified with the EW parameters g, m_W via the *matching* of the full and EFT amplitudes

$$\mathcal{A}_{\text{full}} = \mathcal{A}_{\text{Fermi}} + \mathcal{O}(q^2/m_W^2) \iff G_{\text{F}} = \frac{\sqrt{2}g^2}{8m_W^2} = \frac{1}{\sqrt{2}v^2}\,. \tag{3.10}$$

Notice that the Fermi theory of Eq. (3.8) does not contain the W boson as a dynamical DOF, i.e., it has been integrated out. This process is depicted in Figure 3.1, and shows that the process in the Fermi theory corresponds to a contact interaction with no propagating W. The Fermi Lagrangian in Eq. (3.8) precisely looks like the WET one of Eq. (3.4), where $\mathscr{L}_{\text{Fermi}}$ contains a four-quark operator of dimension $d = 6$

$$\mathcal{O}^6_{\text{Fermi}} = (\bar{u}\gamma_\alpha P_L d)\,(\bar{e}\gamma^\alpha P_L \nu_e)\ . \tag{3.11}$$

This operator contains the relevant DOF at scales $q^2 \ll m_W^2$, while the coefficient $G_{\text{F}} \sim 1/m_W^2$ depends on the W mass and encodes the high energy effects. Notice that taking into account higher order terms in the W propagator expansion of Eq. (3.6), a tower of dimensionally increasing operators is generated, which are further suppressed by powers of the high scale m_W. Indeed, at second order dimension-eight operators arise, which are suppressed by $1/m_W^4$. Thus, increasing the precision of the EFT comes at the price of an increasing number of operators that have to be considered.

In this example[1] we have followed a top-down approach: starting with the EW theory we have built the Fermi theory. While the Fermi theory is not strictly necessary—since the underlying EW theory is already known—this example illustrates how working within the EFT framework simplifies calculations while remaining valid for $q^2 \ll m_W^2$. Historically, the development proceeded in the opposite direction: the Fermi theory was formulated before the SM and served as a bottom-up approach to weak interactions. In this scenario, once the WCs are measured (i.e., the G_{F}), the EFT can be tested by checking its predictions over a range of observables. On the

[1] The B_s mixing process considered in Section 2.5, given by Eq. (2.41), can be recovered with the EFT $\mathscr{L}_{B_s\text{mixing}} = -G_{\text{G}}^2/2\pi^2\,(V_{tb}^\star V_{ts})^2\,C\mathcal{O}$ where $\mathcal{O} = (\bar{b}_\alpha\gamma_\mu P_L s_\alpha)(\bar{b}_\beta\gamma^\mu P_L s_\beta)$ and via matching $C = m_W^2 S(x_t)$. Thus, as in the Fermi theory, for the B_s mixing the EFT (at first order) is described by dim-6 operators.

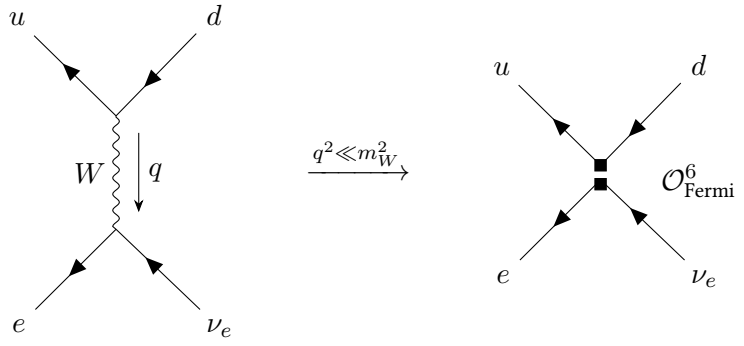

Figure 3.1.: Feynman diagrams for the $d \to \bar{\nu}_e + e + u$ process in the EW (left) and Fermi (right) theory. At $q^2 \ll m_W^2$ the W boson is integrated out and the process is given by a contact operator $\mathcal{O}^6_{\text{Fermi}}$ in the Fermi EFT.

other hand, if the underlying theory is known (or assumed), the parameters of the UV theory are explicitly contained in the WCs. This latter situation is precisely the one of the Fermi theory example. Since G_{F} is matched to the EW parameters, and concretely to the mass of the W, by measuring G_{F} one can infer the mass of the W to be at the GeV scale. Of course, this was later successfully proven to be the case. Therefore, while EFTs do not contain the heavy DOF as dynamical fields (that is, not partaking in the $\mathcal{O}_i$ operators), the WCs depend on the parameters of the heavy states and thus the EFT carries "imprints" of the UV theory.

3.2. The Weak Effective Field Theory and Heavy New Physics

Below the EW scale the SM is broken down to the $SU(3)_c \times U(1)_{\text{em}}$ group. At such scales the EW bosons and the top quark are not dyamical DOF, and are integrated out of the theory. As previously stated, the EFT describing processes below the EW scale is the LEFT, which contains QCD, QED and the WET. For the latter, its dynamics are described by the effective Lagrangian

$$\mathscr{L}_{\text{WET}} = -\sum_i C_i(\mu)\mathcal{O}_i \,. \tag{3.12}$$

In this Lagrangian, the WCs contain the high scale suppression according to $C_i \sim 1/\Lambda^{d-4}$, where Λ is typically a function of the masses and couplings of the heavy states (m_W, g in the previous Fermi theory example). Crucially, the WCs depend on the energy scale μ at which the EFT is applied since distinct particles are integrated out at different energy scales, and the WCs contain the physics contributions from energy scales higher than μ. The μ scale corresponds to the renormalisation scale, as it is through the renormalisation procedure (whih we discuss in the next paragraphs) that the μ dependence of the theory is studied. Therefore, an amplitude for a $i \to f$ process is given by

$$\mathcal{A}(i \to f) = \sum_i C_i(\mu) \left\langle f \right| \mathcal{O}_i \left| i \right\rangle |_\mu \,. \tag{3.13}$$

In this manner, the OPE allows to separate the short distance contributions, corresponding to $C_i(\mu)$, from the long distance contributions corresponding to the hadronic matrix elements $\langle f| \mathcal{O}_i |i\rangle$. The matrix elements also depend on the energy scale μ, as they contain the physics below the μ scale. The WCs are computed perturbatively, for as long as μ is not too small QCD can be treated perturbatively due to asymptotic freedom. On the other hand, matrix elements are non-perturbative and other techniques must be used. Of particular significance are lattice

QCD calculations and sum rules. While these methods are not explicitly employed in this work, several hadronic matrix elements used in this thesis are taken from various collaborations that rely on these techniques. Crucially, the amplitude $\mathcal{A}$ computed within the EFT framework must be independent of the renormalisation scale μ. This requires the μ-dependence of the WCs to exactly cancel the μ-dependence of the hadronic matrix elements.

The μ dependence of the EFT is studied through the renormalisation of the theory. This method absorbs ultraviolet (UV) divergences from loop diagrams into the unrenormalised parameters (couplings, masses, etc) of the theory, known as bare parameters, through the renormalisation factors (Z). This procedure ensures that physical observables remain finite and well defined. In carrying out this technique, the parameters obtain a μ dependence and the evolution of the parameters as a function of μ (called *running*) is given by the renormalisation group equations (RGEs), which encapsulate the quantum corrections across different scales. Additionally, the running enables for the resummation of large logarithms[1] such as $\ln(\mu/\Lambda)$, which arise when there is a significant scale separation between μ and the high-energy scale Λ. As an example of a RGE, in Section 2.4 we discussed the beta function $\beta(g_s)$ of the strong coupling, which dictates its μ dependence. For the WCs, the μ dependence is captured by a RGE governed by the *anomalous dimension matrix* (ADM). In order to define the ADM, we introduce the operator renormalisation according to

$$\mathcal{O}_i^0 = Z_{ij}\mathcal{O}_j\,, \tag{3.14}$$

where the superscript 0 indicates the bare operator, and Z_{ij} is the renormalisation factor, which is a matrix in operator space[2]. Note that Z_{ij} is independent of the high energy theory, as it is a genuine factor belonging to the EFT. Thus, once Z_{ij} is computed, it can be used for any underlying theory which is described by the EFT under consideration. The ADM is found from the renormalisation factor according to (in matrix notation)

$$\gamma = Z^{-1}\frac{dZ}{d\log\mu} = \frac{\alpha_s}{4\pi}\gamma^{(0)} + \left(\frac{\alpha_s}{4\pi}\right)^2\gamma^{(1)} + \dots\,, \tag{3.15}$$

where $\gamma^{(0)}$ is the 1-loop ADM, $\gamma^{(1)}$ is the 2-loop ADM and so on. There is some arbitrariness in the definition of the Z factors, which are fixed by the choice of a renormalisation scheme. In this thesis we consider the minimal subtraction scheme (MS), in which only the poles ($\sim 1/\epsilon$) are subtracted. Expanding the Z factor of Eq. (3.14) in the strong coupling and using Eq. (3.15), we find

$$Z_{ij} = \delta_{ij} + \frac{\alpha_s}{4\pi}\frac{1}{\epsilon}\delta Z_{ij} + \mathcal{O}(\alpha_s^2) \to \gamma_{ij}^{(0)} = -2\delta Z_{ij}\,, \tag{3.16}$$

where we have used the QCD beta function $d\alpha_s/d\log\mu = -2\epsilon\alpha_s + \mathcal{O}(\alpha_s^2)$. Crucially, the Z factor contains the quark field renormalisation as well as the vertex corrections to the EFT operators. For four-quark operators (such as the operator of Eq. (3.11) in the Fermi theory), $Z = Z_q^2 Z'$ where Z_q is the quark field renormalisation ($q^0 = \sqrt{Z_q}q$) and Z' is the genuine EFT renormalisation factor. After expanding Z_q, Z' in the strong coupling we find

$$\gamma_{ij}^{(0)} = -2\delta Z_{ij} = -2\left(2\delta Z_q\delta_{ij} + \delta Z'_{ij}\right) \quad \text{with} \quad \delta Z_q = -\xi C_F\,, \tag{3.17}$$

where ξ is the R_ξ gauge parameter. The ADM dictates the running of the WCs[3] through the RGE

$$\mu\frac{dC_i}{d\mu} = \gamma_{ji}C_j\,. \tag{3.18}$$

[1] Specifically, the logarithms that appear from QCD radiative corrections are of the form $\alpha_s^n(\log\Lambda/\mu)^m$ with $m \le n = 0, 1, 2, \dots$ The leading log (LL) resummation takes care of the $m = n$ logarithms, while the next to leading log (NLL) takes care of the $\alpha_s(\alpha_s\log\Lambda/\mu)^n$ terms.

[2] This means that loop amplitudes from the insertion of a $\mathcal{O}_i$ operator are proportional to other operators $\mathcal{O}_j$ with $i \neq j$, i.e., there is operator mixing. In Section 9.1.1 we will explicitly see this.

[3] The WCs are renormalised according to $C_i^0 = Z_{ji}^{-1}C_j$, so that the bare and renormalised Lagrangian are equal.

Initially, the EFT is constructed by integrating out heavy DOF at a high energy scale μ_H, and the WCs are determined through a *matching* calculation, where the amplitudes of the full theory and the EFT are equated (recall the Fermi example). The WCs are then evolved using the RGE of Eq. (3.18), which governs the running from the high-energy scale down to lower scales through the ADM. In some cases, when new DOF become relevant at intermediate scales, the theory must be *re-matched* by integrating out additional heavy particles, and the WCs are recalculated at this new scale. This procedure of successive matching and running allows the EFT to remain valid at lower energies, ultimately leading to the determination of WCs at the relevant low-energy scale, where physical observables can be computed. Through this approach, EFT provides a systematic way to connect high-energy physics with low-energy observables, ensuring that quantum corrections and operator mixing are properly accounted for across different scales. At leading order (LO) the differential equation Eq. (3.18) is solved with

$$C(\mu) = \left(\frac{\alpha_s(\Lambda)}{\alpha_s(\mu)}\right)^{\frac{\gamma^{(0)T}}{2\beta^0}} C(\Lambda) \quad \text{with} \quad \beta_0 = 11 - \frac{2}{3}N_F\,, \tag{3.19}$$

where we have used the definition of the QCD beta function to first order, $\beta(\alpha_s) = -2\alpha_s^2\beta_0/4\pi$. Generally, the evolution of the WCs is given by

$$C(\mu) = U\left(\Lambda, \mu\right) C(\Lambda)\,, \tag{3.20}$$

where the evolution matrix $U\left(\Lambda, \mu\right)$ takes a more complicated form [19, 39, 40]. In Part III of this thesis we employ the WET framework to describe the B_s mixing process, which was introduced in Section 2.5 within the context of the SM. Due to the low energy scale at which neutral meson mixing occurs, the SM EW particles (W, Z, Higgs, and top quark) are treated as non-dynamical DOF and integrated out from the action. We will consider a full (fundamental) theory consisting of scalar LQs, which mediate the B_s-mixing through box diagrams as in the SM, but with LQs in the loop instead of W bosons. Crucially, the LQs are taken to be *heavy* new physics (HNP) states above the EW scale, and are also integrated out from the theory. FCNCs are then mediated by four-quark WET operators of dimension six or higher (see, e.g. [41]), where the dynamical DOFs are SM quarks (excluding the top).

3.3. Effective Field Theory for Light New Physics

In the previous sections we have discussed EFTs with the notion that NP and/or the underlying theory is composed of heavy states which are integrated out in the EFT. This is the case for the SMEFT, as the Λ_{NP} scale is above the EW scale where BSM physics is expected, and the dynamical DOF are the SM fields. The WET follows the same concept since the underlying theory, the EW sector of the SM, is composed of particles with masses above the typical scale for FCNCs. Additionally, if considering *heavy* BSM modes such as scalar LQs, these particles are also integrated out of the EFT at $E \ll m_W$. Therefore, no BSM particles have been considered as dynamical DOF because they lie at or above the EW scale.

Another possibility is that NP particles are *light* and weakly coupled to the SM. This scenario is of particular interest because so far no new particles have been found above the EW scale, and they arise in distinct situations. Examples include sterile neutrinos and axions, which naturally appear in the SM. They are attractive models for DM and albeit weakly coupled, the models are tested in precision experiments for processes such as meson decays, where small deviations from SM predictions can provide evidence of NP. The LDV, which we study in Part II, is a model in which the SM is extended with a new boson V'_μ, taken to have a mass below the EW scale $m_{V'} \sim \mathcal{O}(1)$ GeV.

Under these assumptions and unlike for heavy states (e.g. LQs), new light particles (e.g. LDVs) are dynamical DOF and thus part of the EFT operators $\mathcal{O}_i^d$. The EFT approach is no different than discussed before, but unlike the previous EFTs where new (heavy) particles are integrated out, low energy EFTs may include new light states that are not part of the SM and can directly contribute to physical observables. Just as before, EFTs provide a framework to study the low energy effects of NP without requiring detailed knowledge of the UV complete theory, as it is understood that certain parameters, such as the masses of the new particles, can be generated from an unknown high energy theory. The EFT Lagrangian for light new physics (LNP) includes both (the relevant) SM operators and new operators involving the BSM light states, organised in a power series suppressed by a high-energy scale Λ

$$\mathscr{L}_{\text{LNP}} = \mathscr{L}_{\text{SM}} + \mathscr{L}_{\text{new}} + \sum_{d>4} \sum_i \frac{1}{\Lambda^{d-4}} C_i \mathcal{O}_i^d \,, \tag{3.21}$$

where $\mathscr{L}_{\text{new}}$ includes the kinetic terms and interactions of the new particles, and $\mathcal{O}_i^d$ are the operators containing the interactions of SM and BSM fields while respecting the symmetries of the model. With this approach, EFT provides a framework that captures the physics of a wide range of UV complete theories in a model independent way, offering a systematic way to explore NP at low energies.

Chapter 4

Conclusion

In this first part of the thesis we have reviewed the key elements of the SM to motivate and understand the upcoming two parts. We have explained the specific flavour structure of the SM, which implies that FCNCs are suppressed and serve as probes for potential NP. In Part II we will consider a BSM setup consisting of a LNP vector boson, the LDV, with a mass well below the EW scale. Therefore, the theory is given by an EFT with the NP field being a dynamical DOF coupled to SM fermions, as discussed in Section 3.3. It will be of special importance to recall the discussion of Section 2.3, where the rotation of the SM interactions to the mass basis is accomplished according to the field redefinitions of Eq. (2.24). Unlike for the SM, we will see that such a rotation can potentially generate tree-level FCNCs between the LDV and SM fermions. The model will be constrained using the phenomenology of two-body decays, where experimental bounds are taken from distinct experimental collaborations while the theory calculation necessitates non-perturbative hadronic matrix elements. Additionally, we will study how the RGEs of the couplings can generate FCNC interactions via running from the high to the low scale. Finally, we will consider the unitarity bounds which historically were applied to the SM, as we briefly discussed at the end of Section 2.2.

In Part III we will consider a HNP model consisting of scalar LQs. We will study the B_s mixing process, which we introduced in Section 2.5 in the context of the SM. Since we assume the LQs to have masses above the EW scale, the processes is described by the WET through dimension-six four-quark operators, discussed in Section 3.2. We will compute the ADM and perform the next-to-leaing order matching in α_s between the EFT (corresponding to a 1-loop calculation) and full theory (corresponding to a 2-loop computation). We conclude the thesis with an exhaustive analysis of 1-loop calculations for four-quark operators, where we employ and examine a method that requires particular care of the Dirac algebra.

Therefore, in this thesis we study both a LNP (the LDV) and a HNP model (e.g., LQs). Figure 4.1 illustrates how NP can be organised in the mass–coupling plane. Traditionally, much of the effort in collider physics has focused on the upper-right region of this plane, where NHP with sizable couplings are expected. Past experimental findings and theoretical expectations motivated searches for BSM physics in the hundreds of GeV to multi-TeV range, where large couplings would yield prominent signals. However, many portions of this parameter space have since been excluded by high-energy experiments such as those conducted at the LHC. In contrast, the lower-left region, which corresponds to LNP with feeble couplings, has only recently attracted significant attention. Often referred to as the “intensity frontier” or the “dark sector”, this region

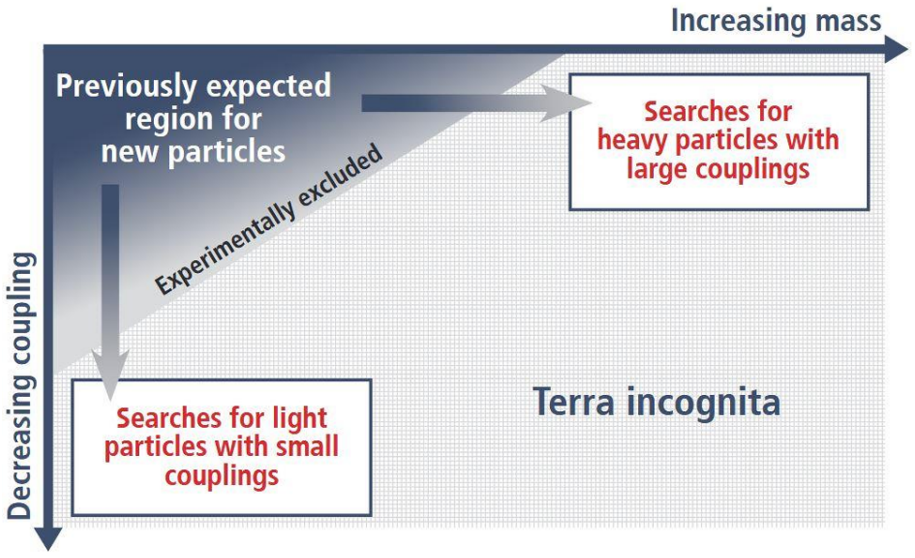

Figure 4.1.: Parameter space of couplings and masses for BSM models, where it highlights HNP (top right) and LNP (bottom left). Figure taken from [42].

remained largely unexplored by traditional colliders that were optimized for heavy resonances. As a result, novel experimental approaches—including beam-dump experiments, fixed-target setups, and precision measurements—are now being developed to probe this largely uncharted territory. Together, these two extremes define the modern frontier in searches for BSM physics. It is the aim of this thesis to study two models belonging to the two different regions in Figure 4.1, and illustrate the current progress and challenges in the search for NP.

PART II

Light New Physics

In this second part of the thesis we study light NP. Concretely, the model under consideration is that of a LDV, i.e., a massive neutral boson V'_μ added to the SM with a mass well below the EW. In Chapter 5, we use the low-energy EFT approach as discussed in Chapter 3, and introduce two types of FCNC interactions between the LDV and SM fermions. In Chapter 6, we constrain the FCNC couplings of the model by comparing the experimental data with the theory prediction for the rates of two-body meson, baryon and lepton decays. In Chapter 7, we use the theoretical tool of perturbative unitarity for $2 \to 2$ processes and further analyse the model by distinguishing amplitudes that grow with energy, leading to a unitarity bound, from those that do not, which instead give a perturbativity bound.

Chapter 5

Light Dark Vectors

In recent years, light new particles interacting very weakly with the SM have gained increased interest. The so far negative results on searches for heavy particles above the EW scale at the LHC and high-intensity experiments have increased the interest in less explored scenarios, with additional DOF beyond the SM with masses at sub-GeV scales. Such particles can be motivated by dynamics addressing the Strong CP Problem (in case of the QCD axion) or the origin of neutrino masses (in case of sterile neutrinos), but probably the main motivation is the possibility that such light particles could be connected to the origin of particle DM [22, 43].

In this context a popular scenario is the dark photon [23, 44], which is either itself DM or is the only mediator ("Vector Portal") between the SM and a hidden "dark sector", which contains one or several DM particles [45, 46], see Ref. [24] for a review. The term "dark photon" usually refers to a light vector particle coupled to the SM only via kinetic mixing or dipole operators and that is often taken as the only new DOF. Instead, the term Z' is typically reserved for the vast model space of theories of gauged $U(1)'$ extensions of the SM, where also a complete Higgs sector for $U(1)'$ breaking is explicitly present, besides additional matter needed for anomaly cancellation, see, e.g., Ref. [47] for a classification. While the Z' vector boson is often taken to be heavy, with a mass much above the EW scale, this particle can also be much lighter. The resulting coupling patterns are often related to the underlying UV symmetries, see, e.g., Refs. [48–51], and can leave imprints in low-energy phenomenology/anomalies in current data, e.g., in $(g-2)_\mu$ [52] or in low-energy QCD [53]. Beyond perturbative models, light vector particles can also be in the spectrum of light resonances of low-energy, dark strongly coupled sectors, see, e.g., Ref. [54]. To encompass all these cases, we employ the term "light dark vector" (LDV), which is a massive vector boson with mass much below the EW scale, with sufficiently suppressed couplings to SM particles such that it is stable on collider scales.

In this first chapter of Part II, we introduce and motivate the LDV model that we study later in Chapter 6 and Chapter 7. In Section 5.1 we introduce the kinetic mixing, that is, the interaction that acts as the "portal" between the visible (SM) and dark sector (DS). In Section 5.2, we explore the connection between the Stueckelberg and Higgs mechanisms, which can generate the LDV mass. In Section 5.3 and 5.4 we introduce the interactions between the LDV and the SM fermions, motivating the generation of tree level FCNC couplings between the LDV and the SM fermions. In Section 5.5, we focus on some possible UV models that motivate the low-energy (renormalisable) interactions. Finally, in Section 5.6, we discuss the possibility that FCNC interactions between the

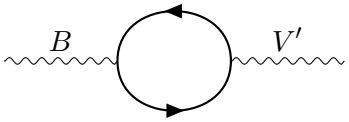

Figure 5.1.: Feynman diagram depicting the generation of kinetic mixing between the B boson and LDV V' via a fermion loop.

LDV and the SM fermions are generated from the 1-loop RGEs via the running of the couplings from the high to the low scale.

5.1. Light Dark Vectors with Kinetic Mixing

Consider two gauge bosons B_μ and V'_μ associated to two gauge groups $U(1)$ and $U(1)'$, respectively. The corresponding kinetic Lagrangian takes the form

$$\mathscr{L}_{\text{kinetic}} = -\frac{1}{4}B_{\mu\nu}B^{\mu\nu} - \frac{1}{4}V'_{\mu\nu}V'^{\mu\nu} - \frac{\epsilon}{2}B_{\mu\nu}F'^{\mu\nu}\,, \tag{5.1}$$

where the last term is the kinetic mixing (KM) [23] between the field strength of B_μ and V'_μ

$$\mathscr{L}_{\text{KM}} = -\frac{\epsilon}{2}B_{\mu\nu}V'^{\mu\nu}\,. \tag{5.2}$$

Notice that this is a renormalisable dimension-four operator which respects the symmetries of the theory. Phenomenological constraints on the KM parameter ϵ dictate that it remains extremely small over a broad range of mass scales [24, 55]. In particular, astrophysical observations—such as limits from stellar energy loss and supernova cooling—as well as cosmological data impose upper bounds on ϵ that can be as stringent as $\epsilon \lesssim 10^{-12}$ for very light V'. In the MeV–GeV mass window, where LDVs are often probed via beam-dump experiments, rare meson decays, and fixed-target searches, ϵ is typically restricted to values on the order of 10^{-3}–10^{-4}. For heavier LDVs, EW precision measurements and collider experiments further limit ϵ to be at most a few percent, with many models favoring values near 10^{-3}–10^{-2}. These small values of ϵ naturally emerge if one considers the KM to be a loop induced effect, inherently suppressed by a factor of $1/(16\pi^2)$. This is exemplified in Figure 5.1, where a heavy fermion charged under both $U(1)$ and $U(1)'$ generates the KM at 1-loop as given by [56, 57]

$$\epsilon = \frac{g g_D}{16\pi^2}\sum_i q_i q'_i \log\frac{m_i^2}{\mu^2}\,, \tag{5.3}$$

where g, g_D are the $U(1), U(1)'$ couplings and q_i, q'_i the charges of the fermion under $U(1)$ and $U(1)'$, respectively. Some other relevant examples for the generation of the KM include string theory and supersymmetric theories [58–60]; see [61] for a review with different models. In this work we do not specify the origin of the KM, for our purposes it suffices to notice that the KM is a dimension four operator respecting the symmetries of the model and thus allowed in the theory, and we simply consider it as given in Eq. (5.2) without loss of generality in our low energy approach.

The importance of the setup lies on the fact that it is a relatively simple model with potential implications for DM and BSM models [62], typically referred as dark photons or hidden photon models. The KM acts as a *vector portal* connecting fields charged under different gauge groups, connecting a "visible sector", composed of SM fields and neutral under $U(1)'$, and a NP *dark sector* charged under $U(1)'$ but neutral under the SM.

Let us consider the scenario in which the neutral vector V'_μ is added to the SM[1]. Before EWSB, the EW gauge sector Lagrangian for $SU(2)_L \times U(1)_Y \times U(1)'$ reads (see Section 2.2)

$$\begin{aligned}\mathscr{L} = &-\frac{1}{4}W^a_{\mu\nu}W^{a\mu\nu} - \frac{1}{4}B_{\mu\nu}B^{\mu\nu} - \frac{1}{4}V'_{\mu\nu}V'^{\mu\nu} + \frac{m^2_{V'}}{2}V'^{\mu}V'_{\mu} + \mathscr{L}_{\text{KM}} \\ &+ (D_\mu H)^\dagger (D^\mu H) + m^2 H^\dagger H - \lambda\left(H^\dagger H\right)^2 ,\end{aligned} \tag{5.4}$$

where the first line includes the kinetic terms of the W^a_μ, B_μ and V'_μ bosons, as well as the KM between the hypercharge boson B_μ and V'_μ, as given in Eq. (5.2). Notice that we have included a mass term for V'_μ (with $m_{V'} \ll v_{\text{EW}}$), which can be generated from the breaking of $U(1)'$ with a dark Higgs or from the Stueckelberg mechanism [65–68], and is decoupled from the SM Higgs sector. We discuss the V'_μ mass in the next Section 5.2. The KM in the Lagrangian of Eq. (5.4) is diagonalised by the following rotation

$$\begin{pmatrix} V'_\mu \\ B_\mu \end{pmatrix} \to \begin{pmatrix} t & 0 \\ -\epsilon t & 1 \end{pmatrix} \begin{pmatrix} V'_\mu \\ B_\mu \end{pmatrix} \quad \text{with} \quad t \equiv \frac{1}{\sqrt{1-\epsilon^2}} , \tag{5.5}$$

which reduces to the shift $B_\mu \to B_\mu - \epsilon V'_\mu$ at $\mathcal{O}(\epsilon)$[2]. We must now take into account the EWSB of the SM group $SU(2)_L \times U(1)_Y$ which generates the masses of the EW bosons, as described in Section 2.2. After diagonalising the KM, the covariant derivative of H takes the form

$$D_\mu H = \partial_\mu H - igW^a_\mu \tau^a H - \frac{i}{2}g'\left(B_\mu - \epsilon t V'_\mu\right) H , \tag{5.6}$$

which is shifted in the last term with respect to the SM one, see Eq. (2.16). After the Higgs acquires a VEV and is parametrised in the unitary gauge according to Eq. (2.15), the gauge boson quadratic terms in $(D_\mu H)^\dagger (D^\mu H)$ read

$$(D_\mu H)^\dagger (D^\mu H) \supset \frac{g^2 v^2}{8}\left[\left(W^1_\mu\right)^2 + \left(W^2_\mu\right)^2 + \left(\frac{g'}{g}B_\mu - W^3_\mu - \frac{\epsilon t g'}{g}A'_\mu\right)^2\right] . \tag{5.7}$$

Compared to the SM case of Eq. (2.17), the neutral B, W^3 sector changes due to the KM. Therefore, when we rotate to the mass basis of the charged $W^\pm_\mu$ and neutral Z_μ, A_μ, V'_μ bosons, the former shall have the same masses as in the SM, while the masses of the neutral bosons change, but A_μ must remain massless because $U(1)_{\text{em}}$ is unbroken. This is expected because the KM occurs solely between the field strengths of $U(1)_Y$ and $U(1)'$, thereby affecting only the neutral bosons. The mass matrix of the three neutral bosons B_μ, W^3_μ, V'_μ reads as follows

$$M^2 = \frac{v^2}{4}\begin{pmatrix} g'^2 & -g'g & -g'^2 t\epsilon \\ -g'g & g^2 & g'gt\epsilon \\ -g'^2 t\epsilon & g'gt\epsilon & \frac{4m^2_{V'}}{v^2}t^2 + g'^2\epsilon^2 t^2 \end{pmatrix} , \tag{5.8}$$

and is diagonalised via the following rotation

$$\begin{pmatrix} B_\mu \\ W^3_\mu \\ V'_\mu \end{pmatrix} \to \begin{pmatrix} \cos\theta_W & -\sin\theta_W \cos\xi & \sin\theta_W \sin\xi \\ \sin\theta_W & \cos\theta_W \cos\xi & -\cos\theta_W \sin\xi \\ 0 & \sin\xi & \cos\xi \end{pmatrix} \begin{pmatrix} A_\mu \\ Z_\mu \\ V'_\mu \end{pmatrix} . \tag{5.9}$$

[1] Relevant references for the upcoming discussion are Refs. [51, 63, 64].

[2] The KM can also be diagonalised with the shift $V'_\mu \to V'_\mu - \epsilon B_\mu$, known as the milli-charged scenario [69, 70]. Of course, physical observables are independent on the diagonalisation and thus on the gauge basis.

Here, θ_W is the Weinberg angle and ξ is given by

$$\tan 2\xi = -\frac{2\eta \sin\theta_W}{1-\eta^2 \sin^2\theta_W - \delta} \quad \text{with} \quad \eta = \epsilon t, \delta \equiv m_{V'}^2/m_Z^2 \,. \tag{5.10}$$

The masses of the neutral gauge bosons are given by, up to $\mathcal{O}(\epsilon)$,

$$\begin{aligned} m_A &= 0\,, \\ m_Z^2 &\equiv m_Z^2 \left(1 + \frac{\epsilon^2 \sin^2\theta_W}{1-\delta}\right)\,, \\ m_{V'}^2 &\equiv m_{V'}^2 \left(1 + \epsilon^2 \frac{\delta - 1 + \sin^2\theta_W}{\delta - 1}\right)\,. \end{aligned} \tag{5.11}$$

We see that the photon indeed remains massless. Notice that for $\epsilon = 0$, that is, for no KM, the rotation of Eq. (5.9) reduces to the SM Weinberg rotation of Eq. (2.18). We observe that the mass of the Z boson gets an $\mathcal{O}(\epsilon)$ shift respect its SM value. However, precision EW measurements of the Z mass, such as those performed at LEP and SLD (with $m_Z = 91.1876 \pm 0.0021$ GeV [11]), constrain any NP contributions to be extremely small. Consequently, while the theoretical framework permits modifications to m_Z that could be significant, the experimental data requires the KM parameter ϵ to be very small to ensure that any deviation from the SM prediction remains within the narrow experimental uncertainty [71].

5.2. Massive Light Dark Vector, Proca and Stueckelberg

We now discuss the origin of the LDV mass $m_{V'}$, concretely in the context of the Stueckelberg mechanism and in relation to the Proca theory. The free Lagrangian of the LDV in Eq. (5.4) corresponds to the Proca theory of a massive vector

$$\mathscr{L}_{\text{Proca}} = -\frac{1}{4} V'_{\mu\nu} V'^{\mu\nu} + \frac{m_{V'}^2}{2} V'_\mu V'^\mu \,, \tag{5.12}$$

which is not (explicitly) gauge invariant. The Stueckelberg trick introduces a scalar π, the Stueckelberg field, into Eq. (5.12) via the field redefinition [65–68]

$$V'_\mu \to V'_\mu - \frac{\partial_\mu \pi}{m_{V'}} \Rightarrow \mathscr{L}_{\text{St}} = -\frac{1}{4} V'_{\mu\nu} V^{\mu\nu\prime} + \frac{m_{V'}^2}{2} \left(V'_\mu - \frac{\partial_\mu \pi}{m_{V'}}\right)^2 \,. \tag{5.13}$$

The Stueckelberg Lagrangian $\mathscr{L}_{\text{St}}$ is now manifestly $U(1)'$ gauge invariant under

$$\begin{aligned} V'_\mu &\to V'_\mu + \partial_\mu \alpha(x)\,, \\ \pi &\to \pi + m_{V'} \alpha(x)\,. \end{aligned} \tag{5.14}$$

The theories of Eq. (5.12) and Eq. (5.13) are physically equivalent, leading to the same S-matrix [72]. The Stueckelberg transformation of Eq. (5.13) decomposes a massive vector field into the (two) transverse and (one) longitudinal DOF corresponding to a (transverse) vector and a scalar field, respectively. To be precise, the longitudinal mode of the massive vector is identified with the Stueckelberg field as follows

$$\left(V'_\mu\right)_{\text{long}} \equiv -\frac{\partial_\mu \pi}{m_{V'}} \,. \tag{5.15}$$

The physical equivalence between the Proca and Stueckelberg theories stems from the fact that the Proca theory can be viewed as a gauge fixed abelian $U(1)'$ theory after spontaneous symmetry breaking. The theory of a $U(1)'$ vector field V'_μ coupled to a complex scalar field S is given by

$$\mathscr{L} = -\frac{1}{4} V'_{\mu\nu} V'^{\mu\nu} + \left(D_\mu S\right)^\dagger \left(D^\mu S\right) - V(S)\,, \tag{5.16}$$

with $D_\mu = \partial_\mu - ig'V'_\mu$ and $V(S) = -m^2|S|^2 + \lambda/4|S|^4$. This theory is $U(1)'$ gauge invariant under

$$\begin{aligned} S &\to e^{ig'\alpha(x)}S\,, \\ V'_\mu &\to V'_\mu + \partial_\mu\alpha(x)\,. \end{aligned} \tag{5.17}$$

After symmetry breaking, S acquires a VEV $v' = \sqrt{4m^2/\lambda}$. Using the polar parametrisation

$$S = \frac{1}{\sqrt{2}}\left(v' + h\right)e^{-i\pi/v'}\,, \tag{5.18}$$

the Lagrangian of Eq. (5.16) reads

$$\begin{aligned} \mathscr{L} =& -\frac{1}{4}V'_{\mu\nu}V'^{\mu\nu} + \frac{g'^2}{2}V'_\mu V'^\mu\left(h+v'\right)^2 - \frac{g'}{v'}V'_\mu\left(h+v'\right)^2\partial^\mu\pi \\ &+ \frac{1}{2}\partial_\mu h\partial^\mu h + \frac{\left(v'+h\right)^2}{2v'^2}\partial_\mu\pi\partial^\mu\pi - V(\phi)\,, \\ V(\phi) =& m^2h^2 + \frac{\sqrt{\lambda}m}{2}h^3 + \frac{\lambda}{16}h^4\,. \end{aligned} \tag{5.19}$$

We observe the following mass spectrum in the theory

$$m_{V'} = g'v', \quad m_h = \sqrt{2}m, \quad m_\pi = 0\,. \tag{5.20}$$

The gauge field V'_μ and scalar h have acquired mass while π is massles, i.e., π is the Goldstone boson. In the decoupling limit $\lambda \to \infty$ and $m \to \infty$ (while keeping v fixed), the radial mode h decouples from the theory and the Lagrangian reads

$$\mathscr{L} = -\frac{1}{4}V'_{\mu\nu}V'^{\mu\nu} + \frac{m^2_{V'}}{2}\left(V'_\mu - \frac{\partial_\mu\pi}{m_{V'}}\right)^2\,, \tag{5.21}$$

which is precisely the Stueckelberg theory of Eq. (5.13). Therefore, the Stueckelberg theory corresponds to a broken $U(1)'$ theory in which the radial mode h has been decoupled. Moreover, due to gauge invariance, given by Eq. (5.14), we can fix a gauge; choosing the unitary gauge $\pi = 0$, Eq. (5.21) reduces to

$$\mathscr{L} = -\frac{1}{4}V'_{\mu\nu}V'^{\mu\nu} + \frac{m^2_{V'}}{2}V'_\mu V'^\mu\,, \tag{5.22}$$

which is the Proca Lagrangian of Eq. (5.12). Thus, starting with a $U(1)'$ gauge theory with symmetry breaking and taking the decoupling limit, we obtain the Stueckelberg theory. If we further fix the unitary gauge such that the Goldstone π vanishes, we find the Proca theory. This sheds light into the hidden gauge symmetry of the Proca theory; since a gauge is fixed, gauge invariance is explicitly lost and only through the Stueckelberg transformation does it become manifest.

In order to find the propagators of the Stueckelberg theory of Eq. (5.13), we apply the gauge fixing R_ξ procedure. Then, the theory reads[1]

$$\mathscr{L}_{\text{St}} = -\frac{1}{4}V'_{\mu\nu}V'^{\mu\nu} + \frac{m^2_{V'}}{2}\left(V'_\mu - \frac{\partial_\mu\pi}{m_{V'}}\right)^2 - \frac{1}{2\xi}\left(\partial_\mu V'^\mu + \xi m_{V'}\pi\right)^2\,, \tag{5.23}$$

[1] For an Abelian theory the ghost field trivially decouples, i.e., is a free field with no interaction with V' nor π. Therefore, we do not include it in this discussion.

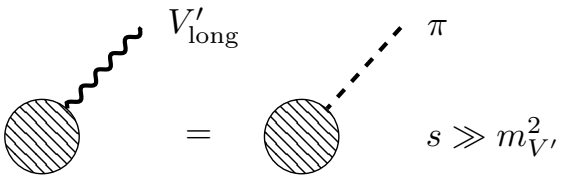

Figure 5.2.: Representation of the GBET: at high energies, the scattering of a longitudinal massive vector is equivalent to scattering the Goldstone boson.

such that the crossed $V'_\mu \partial^\mu \pi$ terms conveniently vanish. Then, the propagators are given by

$$\begin{aligned} \Delta^{\mu\nu}_{V'}|_{\text{St}} &= \frac{-i}{k^2 - m^2_{V'}} \left(g^{\mu\nu} - \frac{k^\mu k^\nu}{k^2 - \xi m^2_{V'}} (1 - \xi) \right) , \\ \Delta_\pi &= \frac{i}{k^2 - \xi m^2_{V'}} . \end{aligned} \tag{5.24}$$

On the other hand, the propagator for the Proca field of Eq. (5.12) is given by

$$\Delta^{\mu\nu}_{V'}|_{\text{Proca}} = \frac{-i}{k^2 - m^2_{V'}} \left(g^{\mu\nu} - \frac{k^\mu k^\nu}{m^2_{V'}} \right) . \tag{5.25}$$

This propagator can be obtained from the propagators of Eq. (5.24) through the Stueckelberg relation $V'_\mu \to V'_\mu - \partial_\mu \pi / m_{V'}$ in momentum space, i.e.,

$$\Delta^{\mu\nu}_{V'}|_{\text{Proca}} = \Delta^{\mu\nu}_{V'}|_{\text{St}} + \frac{k^\mu k^\nu}{m^2_{V'}} \Delta_\pi . \tag{5.26}$$

The ξ dependence on the right hand side of Eq. (5.26) drops automatically, as it should because the Proca theory has three physical DOF without (explicit) gauge invariance. We now turn our attention to the GBET for the Stueckelberg theory. In an unbroken abelian theory such as QED, amplitudes with an external vector boson ($\mathcal{M}^\mu$) satisfy the Ward identity $k_\mu \mathcal{M}^\mu = 0$, which decouples the longitudinal modes and ensures the good high energy behaviour of the theory. In the case of a spontaneously broken theory, longitudinal modes become physical. In that case, an amplitude with an external vector boson of mass $m_{V'}$ satisfes

$$k^\mu \mathcal{M}_\mu = m_{V'} \mathcal{M}(\pi) , \tag{5.27}$$

where $\mathcal{M}(\pi)$ is the amplitude where the external vector boson has been replaced by the Goldstone π. Considering the high energy limit $k \gg m_{V'}$ and taking the leading contribution of the longitudinal ϵ_L polarisation of a massive vector, Eq. (5.27) reads

$$\epsilon^\mu_L = \frac{k^\mu}{m_V} + \mathcal{O}\left(m_V / E\right) \Rightarrow \epsilon^\mu_L \mathcal{M}_\mu = \mathcal{M}(\pi) . \tag{5.28}$$

This is the GBET [72]: in the high energy regime, amplitudes with longitudinally polarised vector bosons are equivalent to amplitudes where (all) the vectors have been replaced by the Goldstone boson. Analogously, for the Stueckelberg theory of Eq. (5.21) with the propagators of Eq (5.24), by choosing the Landau gauge[1] $\xi = 0$ the vector boson becomes purely transverse, and the longitudinal polarisation of V' is fully captured by π as in Eq. (5.15).

[1] In unitary gauge $\xi \to \infty$, π decouples since $m_\pi = \xi m_{V'} \to \infty$ and $\Delta^{\mu\nu}_{V'}|_{\text{St}} = \Delta^{\mu\nu}_{V'}|_{\text{Proca}}$. Therefore, $\xi \to \infty$ is equivalent to the gauge fixing $\pi = 0$ used to obtain Eq. (5.22).

5.3. Light Dark Vector Coupled to SM Fermions

In Section 5.1 we focused on the gauge sector of the EW SM with KM to the LDV. We are now interested in the gauge–fermion interactions, particularly in the scenario in which the LDV couples to SM matter. The relevant Lagrangian is given by

$$\begin{aligned}\mathscr{L} =& -\frac{1}{4}W^a_{\mu\nu}W^{a\mu\nu} - \frac{1}{4}B_{\mu\nu}B^{\mu\nu} - \frac{1}{4}V'_{\mu\nu}V'^{\mu\nu} - \frac{\epsilon}{2}B^{\mu\nu}V'_{\mu\nu} + \frac{m^2_{V'}}{2}V'^{\mu}V'_{\mu} \\ &+ g' J^\mu_Y B_\mu + g J^\mu_3 W^3_\mu + \mathscr{L}_{\text{Yukawa}} + \mathscr{L}_H \\ &+ J^\mu_D V'_\mu + J^\mu V'_\mu + \frac{1}{\Lambda^2_6}V'_{\mu\nu}J^{\mu\nu}\,.\end{aligned} \tag{5.29}$$

The first line corresponds to the gauge sector terms, with the kinetic terms for the EW and $U(1)'$ gauge bosons, the KM between the $U(1)_Y, U(1)'$ and the LDV mass term. The second line contains the neutral SM interactions[1], with the currents given in Eq. (2.33), as well as the Yukawa and Higgs interactions of Eq. (2.22) and Eq. (2.13), respectively. The last line contains the interactions[2] of the LDV with the $U(1)'$ dark sector matter J^μ_D, and with SM matter through J^μ, $J^{\mu\nu}$. We do not specify the DS current J^μ_D since we are interested in the J^μ, $J^{\mu\nu}$ interactions of the LDV with the SM matter. In this thesis, we consider the following interactions

$$\begin{aligned}J^\mu &= \bar{Q}^i C^{\text{V}}_Q \gamma^\mu Q^j + \bar{u}^i_R C^{\text{V}}_u \gamma^\mu u^j_R + \bar{d}^i_R C^{\text{V}}_d \gamma^\mu d^j_R + \bar{L}^i C^{\text{V}}_L \gamma^\mu L^j + \bar{e}^i_R C^{\text{V}}_e \gamma^\mu e^j_R\,, \\ J^{\mu\nu} &= \bar{Q}^i \tilde{H} C^{\text{D}}_u \sigma^{\mu\nu} u^j_R + \bar{Q}^i H C^{\text{D}}_d \sigma^{\mu\nu} d^j_R + \bar{L}^i H C^{\text{D}}_e \sigma^{\mu\nu} e^j_R + \text{h.c}\,.\end{aligned} \tag{5.30}$$

As discussed in Section 3.3, we adopt the low-energy EFT approach such that these are effective interactions coming from an unspecified UV theory. Therefore, such interactions are treated phenomenologically and we do not detail how the $U(1)'$ symmetry is realised, and the charges and couplings $C^{\text{V}}_f, C^{\text{D}}_f$ are treated as general free parameters. Then, the interactions of the LDV with the SM are given by the most general operators that respect the unbroken part of the SM gauge group, $SU(3)_c \times U(1)_{\text{em}}$. The interaction $J^\mu V'_\mu$ is a dimension-4 interaction with vectorial Dirac structure (γ_μ), and we thus refer to it as the *vector interaction*. On the other hand, $J^{\mu\nu}V'_{\mu\nu}$ is a Yukawa-like dimension-6 operator (and thus suppressed by the high scale as $1/\Lambda^2_6$) with dipole structure ($\sigma_{\mu\nu}$), so we refer to it as the *dipole interaction*.

The aim of this section is to analyse the effect of the EWSB and Yukawa diagonalisation on the vector and dipole interactions, together with the KM diagonalisation. After EWSB, it was argued in Section 2.3 that the Yukawa interactions are diagonalised via the field redefinitions of Eq. (2.24). The SM neutral currents J^μ_Y, J^μ_3 are unaffected by these rotations because the $U(1)_Y$ hypercharges are flavour universal. But this is not necessarily true for the $C^{\text{V}}_f, C^{\text{V}}_F$ couplings of the vector interaction. Let us examine the LH up quark interaction of J^μ; under the rotations of Eq. (2.24) we have

$$\bar{u}^i_L \gamma^\mu \left(C^{\text{V}}_Q\right)^{ij} u^j_L A'_\mu \to \bar{u}^i_L \gamma^\mu \left(U^\dagger_u C^{\text{V}}_Q U_u\right)^{ij} u^j_L A'_\mu\,. \tag{5.31}$$

Therefore, if C^{V}_Q is not flavour universal the U_u rotation matrices do not commute with C^{V}_Q and FCNC couplings between the LDV and SM matter are generated. Analogously, FCNC interactions

[1] Charged interactions are as in the SM, given by Eq. (2.29), since the LDV couples to neutral bosons and interactions.
[2] Interactions between the LDV and SM matter are possible through the mixing of the SM and dark Higgs, known as Higgs portal. This generates Yukawa-like interactions between the LDV and SM fermions. Here, we assume that the dark Higgs and SM Higgs are decoupled and thus such interactions are not present.

are generated for the LH down quarks, RH quarks and leptons. Subsequently, we define the following FCNC couplings for the vector interaction

$$\mathbb{C}^{\mathrm{VL}}_{ij} = \left(U_f^\dagger C_F^{\mathrm{V}} U_f\right)^{ij}, \quad \mathbb{C}^{\mathrm{VR}}_{ij} = \left(K_f^\dagger C_f^{\mathrm{V}} K_f\right)^{ij}, \quad f = u, d, e, \quad F = Q, L. \tag{5.32}$$

Notice that we drop the F and f indices in the couplings. This is because while $i, j = 1, 2, 3$, one can also understand the flavour indices as running through the fermions, that is, $i, j = u, c, t$ for up-quarks, $i, j = d, s, b$ for the down-quarks and $i, j = e, \mu, \tau$ for leptons. This is the convention that we adopt from now on. For the $J^{\mu\nu}$ dipole interaction, FCNCs are also generated via the rotations of Eq. (2.24). Let us examine the following down quark interaction under the rotations to the mass basis

$$\frac{v}{\sqrt{2}} \bar{d}^i_L C^{\mathrm{D}}_d \sigma^{\mu\nu} d^j_R \to \frac{v}{\sqrt{2}} \bar{d}^i_L \left(U_d^\dagger C_d^{\mathrm{D}} K_d\right)^{ij} \sigma^{\mu\nu} d^j_R \,. \tag{5.33}$$

In this case, FCNC couplings are generated as long as the couplings C^{D}_f are not aligned with the SM Yukawas, since $U_f^\dagger Y_f K_f = \hat{Y}_f$. The FCNC dipole couplings read

$$\mathbb{C}^{\mathrm{DR}}_{ij} = \left(U_f^\dagger C_f^{\mathrm{D}} K_f\right)^{ij}, \quad \mathbb{C}^{\mathrm{DL}}_{ij} = \left(\mathbb{C}^{\mathrm{DR}}_{ij}\right)^\dagger, \quad f = u, d, e \,. \tag{5.34}$$

Therefore, unlike in the SM, we have a setup in which tree-level FCNCs between the LDV and SM fermions are possible. After the Yukawa diagonalisation, the LDV–SM interactions read[1]

$$\begin{aligned} J^\mu &= \bar{f}^i_L \gamma^\mu \mathbb{C}^{\mathrm{VL}}_{ij} f^j_L + \bar{f}^i_R \gamma^\mu \mathbb{C}^{\mathrm{VR}}_{ij} f^j_R \,, \\ J^{\mu\nu} &= \frac{v}{\sqrt{2}} \bar{f}^i_L \mathbb{C}^{\mathrm{DR}}_{ij} \sigma^{\mu\nu} f^j_R + \frac{v}{\sqrt{2}} \bar{f}^i_R \mathbb{C}^{\mathrm{DL}}_{ij} \sigma^{\mu\nu} f^i_L \,. \end{aligned} \tag{5.35}$$

After the Yukawa diagonalisation, the KM and gauge diagonalisation is accomplished as described in Section 5.1. The resulting interaction Lagrangian is given by

$$\begin{aligned} \mathscr{L}_{\mathrm{int}} =& e J^\mu_{\mathrm{em}} A^\mu \\ &+ Z^\mu \left(e \frac{\cos\xi}{\sin\theta_{\mathrm{W}}} J'^Z_\mu + \sin\xi \left(J^D_\mu + J_\mu\right) \right) + \frac{1}{\Lambda_6^2} \sin\xi Z_{\mu\nu} J^{\mu\nu} \\ &+ V'_\mu \left(e \frac{\sin\xi}{\sin\theta_{\mathrm{W}}} J^{V'}_\mu + \cos\xi \left(J^D_\mu + J_\mu\right) \right) + \frac{1}{\Lambda_6^2} \cos\xi F'_{\mu\nu} J^{\mu\nu} \,, \end{aligned} \tag{5.36}$$

with the following currents solely composed of SM matter

$$\begin{aligned} J'^Z_\mu =& \cos\theta_{\mathrm{W}} J^3_\mu - \tan\theta_{\mathrm{W}} J^Y_\mu \left(\sin\theta_{\mathrm{W}} + \eta \tan\xi\right) \\ =& \frac{J^3_\mu}{\cos\theta_{\mathrm{W}}} \left(1 + \eta \sin\theta_{\mathrm{W}} \tan\xi\right) - \tan\theta_{\mathrm{W}} J_{\mathrm{em}\mu} \left(\sin\theta_{\mathrm{W}} + \eta \tan\xi\right) \,, \\ J^{V'}_\mu =& J^Y_\mu \tan\theta_{\mathrm{W}} \left(\sin\theta_{\mathrm{W}} - \eta \frac{\cos\xi}{\sin\xi}\right) - J^3_\mu \cos\theta_{\mathrm{W}} \\ =& J_{\mathrm{em}\mu} \tan\theta_{\mathrm{W}} \left(\sin\theta_{\mathrm{W}} - \eta \frac{\cos\xi}{\sin\xi}\right) - J^3_\mu \tan\theta_{\mathrm{W}} \left(\frac{1}{\sin\theta_{\mathrm{W}}} - \eta \frac{\cos\xi}{\sin\xi}\right) \,, \end{aligned} \tag{5.37}$$

where $J^\mu_{\mathrm{em}}, J^3_\mu, J^\mu_Y$ are given in Eq. (2.33). The angle ξ is given in Eq. (5.10), and $\eta = t\epsilon$. The first line in the Lagrangian of Eq. (5.36) corresponds to the SM QED interaction, while the second one corresponds to the Z boson interaction and the last one to the LDV interactions. Notice that the

[1] Notice that after EWSB, the dipole interaction becomes a dimension-five operator due to the Higgs VEV $\langle H \rangle \sim (0, v)^T$.

electromagnetic interaction remains as in the SM, since $U(1)_{\rm em}$ is unbroken. On the other hand, the Z couples to the DS matter and to the vector and dipole interactions due to the KM. But these interactions are suppressed by the KM parameter according to $\sin\xi \sim \xi \ll 1$. In the limit of $\epsilon \ll 1$ the Lagrangian reads

$$\begin{aligned}\mathscr{L}_{\rm int} =& e J^{\mu}_{\rm em} A_{\mu} \\ &+ Z^{\mu}\left(\frac{e}{\sin\theta_{\rm W}} J'^{Z}_{\mu} + \epsilon\left(J^{D}_{\mu} + J_{\mu}\right)\right) + \frac{\epsilon}{\Lambda_6^2} Z_{\mu\nu} J^{\mu\nu} \\ &+ V'^{\mu}\left(\frac{e\epsilon}{\sin\theta_{\rm W}} J^{V'}_{\mu} + J^{D}_{\mu} + J_{\mu}\right) + \frac{1}{\Lambda_6^2} F'_{\mu\nu} J^{\mu\nu} + \mathcal{O}(\epsilon^2)\,,\end{aligned} \tag{5.38}$$

with the corresponding currents

$$\begin{aligned} J'^{Z}_{\mu} =& \cos\theta_{\rm W} J^{3}_{\mu} - \tan\theta_{\rm W}\sin\theta_{\rm W} J^{Y}_{\mu} = J^{Z}_{\mu}\,, \\ J^{V'}_{\mu} =& J^{Y}_{\mu}\tan\theta_{\rm W}\left(\sin\theta_{\rm W} - 1\right) - J^{3}_{\mu}\cos\theta_{\rm W}\,. \end{aligned} \tag{5.39}$$

Here, we see that J'^{Z}_{μ} reduces to the SM current J^{Z}_{μ} of Eq. (2.33). For no KM ($\epsilon \to 0$) the SM decouples from the $J^{\mu}_{D}, J^{\mu}, J^{\mu\nu}$ currents and the A, Z interactions correspond to the SM ones, while the LDV couples to the DS matter and the vector and dipole interactions. Indeed,

$$\begin{aligned}\lim_{\epsilon\to 0}\mathscr{L}_{\rm int} =& e J^{\rm em}_{\mu} A^{\mu} + \frac{e}{\sin\theta_{\rm W}} J^{Z}_{\mu} Z^{\mu} \\ &+ V'_{\mu} J^{\mu}_{D} + V'_{\mu} J^{\mu} + \frac{1}{\Lambda_6^2} F'_{\mu\nu} J^{\mu\nu}\,,\end{aligned} \tag{5.40}$$

where the first line corresponds to the SM interactions. In this section we have seen a mechanism in which FCNCs between the LDV and SM are generated (in Section 5.6 we will discuss another possible source of FCNCs). Unlike in the SM, the Yukawa diagonalisation potentially allows for flavour violation for the vector and dipole interactions, as long as their corresponding couplings are not universal and not aligned to the SM Yukawas, respectively. Notice that the KM does not generate any FCNCs—it merely shifts the boson fields, enabling interactions between distinct sectors. Indeed, the interaction $V'^{\mu} J^{V'}_{\mu}$ of Eq. (5.36) does not contain any FCNCs since $J^{V'}_{\mu}$ is composed of the SM neutral currents J^{Y}_{μ}, J^{3}_{μ}. Therefore, in the upcoming analysis we do not explicitly consider KM, as it only leads to a shift in the flavour-diagonal couplings after going to the gauge mass basis, and can thus be understood as being absorbed in the diagonal couplings. By working in this basis, our results also apply to models with KM, upon re-defining the flavour-universal couplings. Therefore, the scope of this work is to go beyond KM and study FCNCs between V'_{μ} and SM fermions.

5.4. Setup

After the previous sections we are now in position to introduce the specific model that we are going to study. As previously stated, we extend the SM by a new, neutral, massive vector boson V'_{μ} with a small mass $m_{V'}$, which arises either by spontaneous symmetry breaking of, e.g., a $U(1)'$ gauge symmetry or by the Stueckelberg mechanism [65, 73, 74] as discussed in Section 5.2. We focus on the vector and dipole FCNC interactions written in the fermion mass basis, and we further assume that a possible KM has been diagonalised such that V'_{μ} is also in the mass-eigenstate basis. In the previous section we saw how FCNCs can be generated via rotating to the Yukawa mass basis, with the vector and dipole currents of Eq. (5.35). Without loss of generality, we can write the dipole and vector interactions as follows

$$\begin{aligned}\mathscr{L}_{\rm D} &= \frac{1}{\Lambda} V'_{\mu\nu}\,\overline{f}_i \sigma^{\mu\nu}\left(\mathbb{C}^{\rm DL}_{ij} P_L + \mathbb{C}^{\rm DR}_{ij} P_R\right) f_j\,, \\ \mathscr{L}_{\rm V} &= \frac{m_{V'}}{\Lambda} V'_{\mu}\,\bar{f}_i \gamma^{\mu}\left(\mathbb{C}^{\rm VL}_{ij} P_L + \mathbb{C}^{\rm VR}_{ij} P_R\right) f_j\,,\end{aligned} \tag{5.41}$$

where f denotes a fermion, i, j are flavour indices and the couplings satisfy the hermicity relations $\mathbb{C}^{\rm DL}_{ij} = (\mathbb{C}^{\rm DR}_{ji})^*$, $\mathbb{C}^{\rm VL}_{ij} = (\mathbb{C}^{\rm VL}_{ji})^*$, $\mathbb{C}^{\rm VR}_{ij} = (\mathbb{C}^{\rm VR}_{ji})^*$. Notice that in Eq. (5.41) the dipole interaction is already written as a dimension-five operator below the EW scale. In order to match it to the corresponding interaction of Eq. (5.35) above the EW scale, we find $\Lambda_6^2 = v\Lambda/\sqrt{2}$. The interactions of Eq. (5.41) are in the "L/R" basis but can also be written in a different basis ("V/A") in which γ_5 is explicit

$$\begin{aligned} \mathscr{L}_{\rm D} &= \frac{1}{\Lambda} V'_{\mu\nu}\, \overline{f}_i \sigma^{\mu\nu} \left(\mathbb{C}^{\rm D}_{ij} + i\mathbb{C}^{\rm D5}_{ij}\gamma_5\right) f_j \,, \\ \mathscr{L}_{\rm V} &= \frac{m_{V'}}{\Lambda} V'_{\mu}\, \overline{f}_i \gamma^{\mu} \left(\mathbb{C}^{\rm V}_{ij} + \mathbb{C}^{\rm V5}_{ij}\gamma_5\right) f_j \,, \end{aligned} \tag{5.42}$$

with $\left(\mathbb{C}^{\rm D}_{ij}\right)^* = \mathbb{C}^{\rm D}_{ji}$, $\left(\mathbb{C}^{\rm D5}_{ij}\right)^* = \mathbb{C}^{\rm D5}_{ji}$, $\left(\mathbb{C}^{\rm V}_{ij}\right)^* = \mathbb{C}^{\rm V}_{ji}$ and $\left(\mathbb{C}^{\rm V5}_{ij}\right)^* = \mathbb{C}^{\rm V5}_{ji}$. The relations between the "V/A" and the "L/R" bases are

$$\mathbb{C}^{\rm D}_{ij} = \frac{1}{2}\left(\mathbb{C}^{\rm DL}_{ij} + \mathbb{C}^{\rm DR}_{ij}\right) = \frac{1}{2}\left(\left(\mathbb{C}^{\rm DR}_{ji}\right)^* + \mathbb{C}^{\rm DR}_{ij}\right) , \qquad \mathbb{C}^{\rm V}_{ij} = \frac{1}{2}\left(\mathbb{C}^{\rm VL}_{ij} + \mathbb{C}^{\rm VR}_{ij}\right) , \tag{5.43}$$

$$\mathbb{C}^{\rm D5}_{ij} = \frac{i}{2}\left(\mathbb{C}^{\rm DL}_{ij} - \mathbb{C}^{\rm DR}_{ij}\right) = \frac{i}{2}\left(\left(\mathbb{C}^{\rm DR}_{ji}\right)^* - \mathbb{C}^{\rm DR}_{ij}\right) , \qquad \mathbb{C}^{\rm V5}_{ij} = \frac{1}{2}\left(\mathbb{C}^{\rm VR}_{ij} - \mathbb{C}^{\rm VL}_{ij}\right) . \tag{5.44}$$

Notice the $m_{V'}/\Lambda$ prefactor in $\mathscr{L}_{\rm V}$, which we did not include in Eq. (5.35) of the previous section. Naively the vector interactions are dimension-four below the EW scale. However, such flavour-violating couplings violate $U(1)'$ gauge invariance (flavour-violating currents are not conserved), and thus must be proportional to some power of the $U(1)'$-breaking order parameter, which we take as the VEV in the dark sector. Therefore, the flavour-violating vector couplings are actually dimension-five or higher, depending on the underlying UV model. In perturbative UV completions the lowest possible scaling is proportional to a single power of the dark VEV, which upon including the dark gauge coupling becomes the LDV mass $m_{V'}$. By choosing a scaling that is (at least) linear in $m_{V'}/\Lambda$, we ensure that the growth of amplitudes with longitudinally polarised LDVs in initial and/or final states $\propto E/m_{V'}$ as $m_{V'} \to 0$ is cancelled by the $m_{V'}$ dependence in the interaction. This leads to finite amplitudes in the $m_{V'} \to 0$ limit (see Refs. [75–79] for related discussions), which are just the amplitudes with the corresponding Goldstone bosons as initial/final states. An explicit example for a UV model that provides this linear scaling is provided by Froggatt–Nielsen type models [80], discussed in Section 5.5. However, the linear scaling with $m_{V'}$ is only one possibility. For example, in UV models in which SM fermions do not carry $U(1)'$ charges the scaling can be quadratic in the dark VEV, as the coefficients involve additional powers of the $U(1)'$ breaking scale v', $\propto m_{V'}v'/\Lambda^2$. An explicit realisation of this scenario is also discussed in Section 5.5. We emphasise that above the EW scale, the operators must be expressed in a manifestly $SU(2)_{\rm L} \times U(1)_Y$ invariant manner. For $\mathscr{L}_{\rm V}$ this is directly the case after embedding the LH and RH fermions in the corresponding $SU(2)_{\rm L}$ doublets and singlets, respectively. Instead, the dipole operators in $\mathscr{L}_{\rm D}$ require an additional Higgs insertion as written in Section 5.3,

$$\mathscr{L}_{\rm D6} = \frac{1}{\Lambda_6^2} V'_{\mu\nu} \left(\overline{F}_i H \mathbb{C}^{\rm D}_{ij} \sigma^{\mu\nu} P_R f_j + \text{h.c.}\right) , \tag{5.45}$$

with F_i and f_j denoting here $SU(2)_{\rm L}$ doublets and singlets, respectively.

5.5. UV Motivation of Vector Couplings

In this section we motivate the scaling behavior of the flavour-violating vector coupling in the Lagrangian of Eq. (5.42), both by EFT considerations and explicit UV-complete models. In perturbative UV completions, the scaling is at least linear in the dark $U(1)'$ breaking scale, and we will provide two example scenarios: one that gives linear and one that gives quadratic scaling. We begin with the EFT discussion of the latter.

5.5.1. EFT Discussion for Quadratic Scaling

For the EFT approach it is convenient to consider the coupling to the Goldstone boson π, rather than the coupling of the dark vector V'_μ itself. They are related by the GBET as given in Eq. (5.15), which states that at sufficiently high energies, the LDV coupling is dominated by its longitudinal polarisation, and given by the scattering of the the Goldstone boson. Thus one can work out the couplings of the Goldstone boson and recover the relevant LDV couplings by replacing $\partial_\mu \pi \to -m_{V'} V'_\mu$ in the interaction Lagrangian.

We, therefore, consider the case where the dark $U(1)'$ gauge group is spontaneously broken by some (SM singlet) scalar field S with charge $+1$ under the $U(1)'$. We take the gauge-less limit, so that π is a true Goldstone boson, contained in S according to

$$S = \frac{v'}{\sqrt{2}} \exp\left(i\pi/v'\right) , \tag{5.46}$$

where $v'/\sqrt{2}$ is the (real) VEV that breaks $U(1)'$, connected to the dark vector mass by $m_{V'} = g'v'$, and we have ignored the radial mode that obtains its mass around v'. This mode, together with all UV fields are taken to be much heavier than the EW scale, so that in the IR there is only the SM and the Goldstone boson $G \supset S$, which is formally invariant under global $U(1)'$ transformations treating S as a spurion with charge $+1$. Writing down the general EFT for this setup, it is clear that if SM fields are not charged under $U(1)'$, the possible couplings of the Goldstone to SM fields must involve the same powers of $S^\dagger$ and S. The first such bilinear that gives a non-trivial combination containing the Goldstone is then $S^\dagger \overset{\leftrightarrow}{\partial}_\mu S \supset iv'\partial_\mu G$. This implies that, e.g., RH down quarks can only couple to the Goldstone at the level of dimension-six operators

$$\mathscr{L}^{\text{EFT}}_{\text{quadratic}} \supset \frac{c_{ij}}{\Lambda^2}(iS^\dagger \overset{\leftrightarrow}{\partial}_\mu S)\left(\overline{d}^i_R \gamma^\mu d^j_R\right) = -\frac{c_{ij}}{\Lambda^2} v' \partial_\mu \pi \left(\overline{d}^i_R \gamma^\mu d^j_R\right) , \tag{5.47}$$

where Λ is the UV scale and in general there is flavour violation in the (hermitian) EFT coefficients, $c_{i\neq j} \neq 0$. The coupling of the dark vector V'_μ in this setup is then recovered by $\partial_\mu \pi \to -m_{V'} V'_\mu$, so is given by

$$\mathscr{L}^{\text{EFT}}_{\text{quadratic}} \supset c_{ij} \frac{v' m'_V}{\Lambda^2} V'_\mu \left(\overline{d}^i_R \gamma^\mu d^j_R\right) . \tag{5.48}$$

This analysis demonstrates that the interactions of dark vectors with SM fields that are neutral under the $U(1)'$ scale at least as $m'_V/\Lambda \times v'/\Lambda$. In particular, they involve an additional factor of the $U(1)'$ breaking scale as compared to Eq. (5.42). In Section 5.5.3 we will confirm this expectation in an explicit UV model.

5.5.2. EFT Discussion for Linear Scaling

In order to have LDV couplings with a linear scaling in the $U(1)'$ breaking scale, one necessarily has to charge SM fields under $U(1)'$. In this case the vector boson couples directly to the charged fields via the dimension-four operator, e.g., for RH down quarks

$$\mathscr{L}_{\text{linear}} \supset g' V'_\mu \left(\overline{d}_R \gamma^\mu X_d d_R\right) . \tag{5.49}$$

where X_d is the diagonal $U(1)'$ charge matrix. To see how off-diagonal entries are generated, one has to rotate to the mass basis, which is governed by the Yukawa couplings. From the discussion in Section 5.3, it is clear that there is no flavour violation if X_d is universal. If instead charges are non-universal, the mass matrix cannot be generic at the renormalisable level, i.e., it does not

yield realistic fermion masses without breaking $U(1)'$. Therefore, insertions of S or $S^\dagger$ have to be considered to obtain realistic fermion masses.

Restricting for simplicity to two generations, and charging only d_R^1 with charge $+1$, i.e., $X_d = \mathrm{Diag}(1,0)$, $X_Q = X_H = 0$, the full Yukawa matrix requires higher-dimensional operators to have full rank

$$\mathscr{L}^{\text{EFT}}_{\text{linear}} \supset -y_i \overline{Q}_i H d_R^2 - z_i \frac{S^\dagger}{\Lambda} \overline{Q}_i H d_R^1 + \text{h.c.} \tag{5.50}$$

Thus the down-quark Yukawa matrix is given by

$$Y_d = \begin{pmatrix} z_1\epsilon & y_1 \\ z_2\epsilon & y_2 \end{pmatrix} \quad \text{with} \quad \epsilon = \frac{v'}{\sqrt{2}\Lambda}\,. \tag{5.51}$$

We can ignore here the Goldstone in S, since we already have the coupling of the gauge field in Eq. (5.49), which leads to flavour-violating couplings with V' after rotating to the mass basis. Nevertheless, we can also reproduce this coupling with the same arguments as above: in the gauge-less limit, we rescale $d_R^1 \to d_R^1 e^{i\pi/v'}$, which removes π from the Yukawa sectors. Ignoring chiral anomalies, this rescaling only affects the kinetic terms, as it is a *local* $U(1)'$ transformation

$$\mathscr{L}^{\text{EFT}}_{\text{linear}} \supset i\overline{d}_R^1 \not{\partial} d_R^1 \to -\frac{\partial_\mu \pi}{v'} \overline{d}_R^1 \gamma^\mu d_R^1\,, \tag{5.52}$$

which reproduces Eq. (5.49) upon $\partial_\mu \pi \to -m_{V'} V_\mu = -g' v' V_\mu$.

We are left to diagonalise the Yukawa matrix Y_d in Eq. (5.51), or rather $Y_d^\dagger Y_d$, in order to find the mixing matrix V_d of RH down quarks, defined as $U_d^\dagger Y_d K_d = \hat{Y}_d$. In the limit when $\epsilon \ll 1$, one has

$$K_d \approx \begin{pmatrix} 1 & z_2/y_2\epsilon \\ -z_2/y_2\epsilon & 1 \end{pmatrix}\,, \tag{5.53}$$

where we have set $y_1 = 0$ without loss of generality. Rotating the dark-vector couplings in Eq. (5.49) to the mass basis defined by $d_R \to K_d d_R$ gives finally

$$\mathscr{L}_{\text{linear}} \supset g' V'_\mu \left(\overline{d}_R \gamma^\mu K_d^\dagger X_d K_d d_R\right) = g' V'_\mu (K_d^*)_{1i} (K_d)_{1j} \left(\overline{d}_R^i \gamma^\mu d_R^j\right)\,, \tag{5.54}$$

so that indeed off-diagonal couplings are generated proportional to $g'(K_d^*)_{11}(K_d)_{12} \sim g'\epsilon \sim m'_V/\Lambda$.

To summarise, we have demonstrated that vector interactions of dark vectors can indeed be proportional to a single power of the $U(1)'$ breaking, and thus scale with the dark-vector mass as in Eq. (5.49), if SM fermions have non-universal $U(1)'$ charges. This situation is quite generic in models where SM Yukawa hierarchies are explained by non-anomalous abelian flavour symmetries, for example simple $U(1)_F$ Froggatt-Nielsen models [80], see e.g. Refs. [47] for examples of such models without extra heavy fermions to cancel anomalies. It is well-known how to build UV completions for such models [81,82], and below in Section 5.5.4 we will present an illustrative example.

	Q_i	d_R^i	H	S	ψ_L^i	ψ_R^i
$SU(2)_L$	2	1	2	1	1	1
$U(1)_Y$	1/6	−1/3	1/2	0	−1/3	−1/3
$U(1)'$	0	0	0	1	−1	−1

Table 5.1.: Field content of a renormalizable model featuring quadratic scaling. We restrict the discussion to the down-quark sector with two generations for SM quarks and heavy vector-like fermions ψ_L^i, ψ_R^i, with $i = 1, 2$ carrying $U(1)'$ charges in addition to the scalar S.

5.5.3. Explicit UV Model for Quadratic Scaling

We first construct an explicit renormalisable model for the scaling of vector interactions in Eq. (5.42) quadratic in the dark $U(1)'$ breaking scale. We restrict the discussion for simplicity to the down-quark sector with two generations. The field content is summarised in Table 5.1, which is anomaly-free. The Lagrangian reads

$$\mathscr{L} = \mathscr{L}_{\text{kinetic}} + \mathscr{L}_{\text{Yukawa}} + \mathscr{L}_{\text{scalar}} + \mathscr{L}_{\text{int-}V'} \,, \tag{5.55}$$

with standard kinetic terms for all fields and

$$\mathscr{L}_{\text{Yukawa}} = -Y_{ij}^d \overline{Q}^i H d_R^j - m_\psi \overline{\psi}_L^i \psi_R^i - \alpha_{ij} \overline{\psi}_L^i d_R^j S^\dagger + \text{h.c.} \tag{5.56}$$

$$\mathscr{L}_{\text{int-}V'} = -g' V'_\mu \left(\overline{\psi}_L^i \gamma^\mu \psi_L^i + \overline{\psi}_R^i \gamma^\mu \psi_R^i \right) \,, \tag{5.57}$$

$$\mathscr{L}_{\text{scalar}} = m_H^2 |H|^2 + m_S^2 |S|^2 - \lambda_H |H|^4 - \lambda_S |S|^4 - \lambda_{HS} |H|^2 |S|^2 \,. \tag{5.58}$$

For a suitable choice of parameters, the last part in $\mathscr{L}_{\text{scalar}}$ gives a vacuum expectation value to S, $\langle S \rangle = v'/\sqrt{2}$, which sets the mass of the dark vector boson to

$$m_{V'} = v' g' \,, \tag{5.59}$$

and induces a mixing between chiral quarks, d_{R}, and vector-like fermions, ψ, from the mixing term in $\mathscr{L}_{\text{Yukawa}}$. In the limit of $m_\psi \gg v' \gg v$ we can integrate out the vector-like fermions using their equations of motion neglecting their kinetic terms

$$\psi_R^i = -\frac{\alpha_{ij}}{m_\psi} d_R^j S^\dagger \,, \qquad\qquad \psi_R^i = 0 \,. \tag{5.60}$$

Plugging this back into kinetic terms and $\mathscr{L}_{\text{int}}$ leads to the EFT

$$\mathscr{L}_{\text{int}} \supset -g' V'_\mu \frac{S^\dagger S}{m_\psi^2} C_{ij} \left(\overline{d}_R^i \gamma^\mu d_R^j \right) + \frac{S^\dagger S}{m_\psi^2} C_{ij} \left(i \overline{d}_R^i \not{\partial} d_R^j \right) + \frac{S i \partial_\mu S^\dagger}{m_\psi^2} C_{ij} \left(\overline{d}_R^i \gamma^\mu d_R^j \right) \,, \tag{5.61}$$

where $C_{ij} = (\alpha^\dagger \alpha)_{ij}$. Next we integrate out the radial mode by substituting S with the Goldstone parametrization in Eq. (5.46) and use the definition of the dark-vector mass to find

$$\mathscr{L}_{\text{int}} \supset -V'_\mu \frac{m_{V'} v'}{2 m_\psi^2} C_{ij} \left(\overline{d}_R^i \gamma^\mu d_R^j \right) + \frac{(v')^2}{2 m_\psi^2} C_{ij} \left(i \overline{d}_R^i \not{\partial} d_R^j \right) + \partial_\mu \pi \frac{v'}{2 m_\psi^2} C_{ij} \left(\overline{d}_R^i \gamma^\mu d_R^j \right) \,, \tag{5.62}$$

recovering the gauge-invariant[1] combination $V'_\mu - \partial_\mu \pi / m'_V$. Without loss of generality we can assume that Y_{ij}^d is diagonal, so that we are already in the mass basis. Nevertheless, we do need

[1] In our conventions $V'_\mu \to V'_\mu + \partial_\mu \beta / g'$, $S \to \exp(i\beta) S$, $G \to G + \beta v'$, $\psi \to \exp(-i\beta)\psi$.

	Q_i	d^1_R	d^2_R	H	S	ψ_L	ψ_R
$SU(2)_L$	2	1	1	2	1	1	1
$U(1)_Y$	1/6	$-1/3$	$-1/3$	1/2	0	$-1/3$	$-1/3$
$U(1)'$	0	1	0	0	1	0	0

Table 5.2.: Field content of a renormalizable model featuring linear scaling. We restrict the discussion to the down-quark sector with two generations for SM quarks and one family of heavy vector-like fermions ψ_L, ψ_R uncharged under $U(1)'$.

to re-diagonalise the kinetic terms due to the second term in Eq. (5.62) induced in the EFT. In the limit of $v' \ll m_\psi$ this is readily achieved by the rescaling $d^i_R \to d^i_R - (v')^2/(4m^2_\psi)C_{ij}d^j_R$. This leads to additional small corrections of $\mathcal{O}(1/m^4_\psi)$ to the final dark-vector couplings, which can be neglected, such that the leading couplings from the first term in Eq. (5.62) remain

$$\mathscr{L}_{\text{quadratic}} = -\frac{m_{V'}v'}{2m^2_\psi}C_{ij}V'_\mu\left(\overline{d}^i_R\gamma^\mu d^j_R\right) . \tag{5.63}$$

These couplings are indeed quadratic in v' and are in general flavour violating, $C_{i\neq j} \neq 0$. This matches to the EFT term in Eq. (5.48) upon identifying $C_{ij}/m^2_\psi = -2c_{ij}/\Lambda^2$.

5.5.4. Explicit UV Model for Linear Scaling

We now construct an explicit renormalisable model for the minimal scaling of vector interactions in Eq. (5.42) proportional to a single power of the dark-vector mass. We restrict the discussion for simplicity to the down-quark sector with two generations. The field content is summarised in Table 5.2, and is *not* anomaly-free. However, we can always introduce further suitably charged chiral fermions in the RH up- and charged-lepton sector in order to cancel colour and electromagnetic anomalies, respectively. Note that ψ_R and d^2_R carry the same quantum numbers.

The Lagrangian reads

$$\mathscr{L} = \mathscr{L}_{\text{kinetic}} + \mathscr{L}_{\text{Yukawa}} + \mathscr{L}_{\text{scalar}} + \mathscr{L}_{\text{int-}V'} , \tag{5.64}$$

with standard kinetic terms for all fields and

$$\mathscr{L}_{\text{Yukawa}} = -y_i\overline{Q}_i H d^2_R - z_i\overline{Q}_i H\psi_R - m_\psi\overline{\psi}_L\psi_R - \alpha\overline{\psi}_L d^1_R S^\dagger + \text{h.c.} \tag{5.65}$$

$$\mathscr{L}_{\text{int-}V'} = g'V'_\mu\overline{d}^1_R\gamma^\mu d^1_R , \tag{5.66}$$

$$\mathscr{L}_{\text{scalar}} = m^2_H|H|^2 + m^2_S|S|^2 - \lambda_H|H|^4 - \lambda_S|S|^4 - \lambda_{HS}|H|^2|S|^2 , \tag{5.67}$$

where we have simply defined ψ_R to be that field having a mass term with ψ_L. This already gives Eq. (5.49) and the first term in Eq. (5.50) from the EFT discussion, so it only remains to show that integrating out ψ_L, ψ_R induces the second term in Eq. (5.50). The equations of motion for the heavy fermions read, neglecting kinetic terms

$$\overline{\psi}_L = -\frac{z_i}{m_\psi}\overline{Q}_i H , \qquad \psi_R = -\frac{\alpha}{m_\psi}d^1_R S^\dagger , \tag{5.68}$$

and, therefore, the resulting EFT Lagrangian term is

$$\mathscr{L}_{\text{linear}} \supset \frac{z_i\alpha}{m_\psi}\overline{Q}_i H d^1_R S^\dagger . \tag{5.69}$$

This indeed reproduces Eq. (5.50) with the identification of the UV scale as $\Lambda = -m_\psi/\alpha$. The remaining calculation follows the EFT discussion, which shows that in these type of UV models the flavour violating couplings to V' scale indeed linearly with $m_{V'}/\Lambda$.

5.6. Renormalization Group Equations

In Section 5.3, we demonstrated how FCNCs between the LDV and SM fermions can arise due to the rotation to the Yukawa mass basis. Here, we explore an alternative scenario, where FCNCs are induced via the running of the couplings as dictated by their RGEs. We assume a flavour-universal UV theory, such that flavour-violating couplings emerge solely from the running between the high and low scale. Starting just below the UV scale Λ—assumed to be well above the EW scale—we consider $SU(2)_L \times U(1)_Y$-invariant vector and dipole interactions of V' with the SM. The vector interactions follow the straightforward $SU(2)_L \times U(1)_Y$ generalization of Eq. (5.41), while the dipole interactions are given in Eq. (5.45). To align new sources of flavour violation with those in the SM, we impose flavour universality on the vector couplings, making them proportional to the identity matrix in flavour space. Likewise, we take the dipole couplings to be proportional to the SM Yukawa matrices, ensuring that both remain flavour-diagonal in the mass basis (see Section 5.3). Consequently, FCNCs involving V' are induced solely by RGE evolution down to the EW scale and remain proportional to the CKM matrix. Thus, in the IR, flavour-violating couplings follow the paradigm of minimal flavour violation (MFV) [83]. The relevant terms in the Lagrangian—comprising the SM Yukawa interaction, dipole, and vector interactions with the LDV—are given by (omitting flavour indices):

$$\begin{aligned}
\mathscr{L}_{\text{Yukawa}} &= -\overline{Q}\, Y_u \widetilde{H} u_R - \overline{Q}\, Y_d H d_R + \text{h.c.}\,, \\
\mathscr{L}_{\text{Dipole}} &= \frac{1}{\Lambda_6^2} V'_{\mu\nu} \left(\overline{Q} C_u^{\text{D}} \sigma^{\mu\nu} \widetilde{H} u_R + \overline{Q} C_d^{\text{D}} \sigma^{\mu\nu} H d_R + \text{h.c.} \right)\,, \\
\mathscr{L}_{\text{Vector}} &= V'_\mu \left(\overline{Q} C_Q^V \gamma^\mu Q + \overline{u}_R C_u^V \gamma^\mu u_R + \overline{d}_R C_d^V \gamma^\mu d_R \right)\,,
\end{aligned} \tag{5.70}$$

with the SM Yukawa matrices $Y_f, f = u, d$ and 3×3 matrices $C_f^{\text{D}}, C_f^{\text{V}}$. We do not consider the lepton interactions because the running of the corresponding RGE does not induce flavour violation. The reason is that while there are two SM Yukawa coupligns Y_u, Y_d in the quark sector, there is only one Yukawa coupling Y_e in the SM lepton sector. Therefore, the Y_e combinations that appear in the lepton RGE are trivially diagonalised after going to the mass basis, and no flavour violation is induced. The one-loop RGE of the vector couplings proportional to the SM Yukawas reads [84]

$$\begin{aligned}
16\pi^2 \frac{\mathrm{d}C_Q^{\text{V}}}{\mathrm{d}\ln\mu} &= -Y_u C_u^{\text{V}} Y_u^\dagger - Y_d C_d^{\text{V}} Y_d^\dagger + \frac{1}{2}\left(Y_u Y_u^\dagger + Y_d Y_d^\dagger \right) C_Q^{\text{V}} + \frac{1}{2} C_Q^{\text{V}} \left(Y_u Y_u^\dagger + Y_d Y_d^\dagger \right)\,, \\
16\pi^2 \frac{\mathrm{d}C_u^{\text{V}}}{\mathrm{d}\ln\mu} &= -2 Y_u^\dagger C_Q^{\text{V}} Y_u + Y_u^\dagger Y_u C_u^{\text{V}} + C_u^{\text{V}} Y_u^\dagger Y_u\,, \\
16\pi^2 \frac{\mathrm{d}C_d^{\text{V}}}{\mathrm{d}\ln\mu} &= -2 Y_d^\dagger C_Q^{\text{V}} Y_d + Y_d^\dagger Y_d C_d^{\text{V}} + C_d^{\text{V}} Y_d^\dagger Y_d\,.
\end{aligned} \tag{5.71}$$

For the one-loop RGE of the dipole couplings proportional to the SM Yukawas [84], we find

$$\begin{aligned}
16\pi^2 \frac{\mathrm{d}C_u^{\text{D}}}{\mathrm{d}\ln\mu} &= \frac{5}{2} Y_u Y_u^\dagger C_u^{\text{D}} - \frac{3}{2} Y_d Y_d^\dagger C_u^{\text{D}} - C_d^{\text{D}} Y_d^\dagger Y_u + 2 C_u^{\text{D}} Y_u^\dagger Y_u \\
&\quad + n_c \text{Tr}\left[Y_u Y_u^\dagger + Y_d Y_d^\dagger \right] C_u^{\text{D}}\,, \\
16\pi^2 \frac{\mathrm{d}C_d^{\text{D}}}{\mathrm{d}\ln\mu} &= \frac{5}{2} Y_d Y_d^\dagger C_d^{\text{D}} - \frac{3}{2} Y_u Y_u^\dagger C_d^{\text{D}} - C_u^{\text{D}} Y_u^\dagger Y_d + 2 C_d^{\text{D}} Y_d^\dagger Y_d \\
&\quad + n_c \text{Tr}\left[Y_u Y_u^\dagger + Y_d Y_d^\dagger \right] C_d^{\text{D}}\,.
\end{aligned} \tag{5.72}$$

with $n_c = 3$ denoting the number of colors. The one-loop running of the Yukawas is relevant for the dipole analysis[1] because the RG-evolved Yukawas contribute to the flavour-violating couplings upon rotating to the quark mass-eigenstates at the EW scale [85]. The one-loop RGEs for Yukawa running read [84]

$$\begin{aligned} 16\pi^2 \frac{\mathrm{d}Y_u}{\mathrm{d}\ln\mu} &= \frac{3}{2}\left(Y_u Y_u^\dagger Y_u - Y_d Y_d^\dagger Y_u\right) + n_c \mathrm{Tr}\left[Y_u Y_u^\dagger + Y_d Y_d^\dagger\right] Y_u \,, \\ 16\pi^2 \frac{\mathrm{d}Y_d}{\mathrm{d}\ln\mu} &= \frac{3}{2}\left(Y_d Y_d^\dagger Y_d - Y_u Y_u^\dagger Y_d\right) + n_c \mathrm{Tr}\left[Y_u Y_u^\dagger + Y_d Y_d^\dagger\right] Y_d \,, \end{aligned} \tag{5.73}$$

5.6.1. Vector Interaction

We now focus on the vector interaction $\mathscr{L}_{\text{Vector}}$ of Eq. (5.70), and solve the corresponding RGEs for the couplings C_f^{V}. The RGEs of Eq. (5.71) are solved at leading logarithm, with the following initial conditions at the high scale Λ

$$C_Q^{\mathrm{V}}(\Lambda) = c_Q^{\mathrm{V}}\, \mathbb{1}_3 \,, \qquad C_u^{\mathrm{V}}(\Lambda) = c_u^{\mathrm{V}}\, \mathbb{1}_3 \,, \qquad C_d^{\mathrm{V}}(\Lambda) = c_d^{\mathrm{V}}\, \mathbb{1}_3 \,, \tag{5.74}$$

with $c_f^{\mathrm{V}} \in \mathbb{R}$, such that the interactions are flavour diagonal at Λ (in the mass basis, see Section 5.3). Once the RGEs are solved for each coupling, the rotations of Eq. (2.24) are applied accordingly to go to the mass basis. Finally, a matching is performed with the vector interaction of Eq. (5.41) in the "L/R" basis. Following this procedure, the couplings at the low scale μ read

$$\begin{aligned} \left(\frac{m_{V'}}{\Lambda}\right) \mathbb{C}_u^{\mathrm{VL}}(\mu) &= c_Q^{\mathrm{V}} \mathbb{1}_3 - \frac{1}{16\pi^2}\left(\left(c_Q^{\mathrm{V}} - c_u^{\mathrm{V}}\right) \hat{Y}_u \hat{Y}_u^\dagger + \left(c_Q^{\mathrm{V}} - c_d^{\mathrm{V}}\right) V_{\mathrm{CKM}} \hat{Y}_d \hat{Y}_d^\dagger V_{\mathrm{CKM}}^\dagger\right) \log(\Lambda/\mu) \,, \\ \left(\frac{m_{V'}}{\Lambda}\right) \mathbb{C}_d^{\mathrm{VL}}(\mu) &= c_Q^{\mathrm{V}} \mathbb{1}_3 - \frac{1}{16\pi^2}\left(\left(c_Q^{\mathrm{V}} - c_u^{\mathrm{V}}\right) V_{\mathrm{CKM}}^\dagger \hat{Y}_u \hat{Y}_u^\dagger V_{\mathrm{CKM}} + \left(c_Q^{\mathrm{V}} - c_d^{\mathrm{V}}\right) \hat{Y}_d \hat{Y}_d^\dagger\right) \log(\Lambda/\mu) \,, \\ \left(\frac{m_{V'}}{\Lambda}\right) \mathbb{C}_u^{\mathrm{VR}}(\mu) &= c_u^{\mathrm{V}} \mathbb{1}_3 - \frac{1}{8\pi^2}\left(c_u^{\mathrm{V}} - c_Q^{\mathrm{V}}\right) \hat{Y}_u^\dagger \hat{Y}_u \log(\Lambda/\mu) \,, \\ \left(\frac{m_{V'}}{\Lambda}\right) \mathbb{C}_d^{\mathrm{VR}}(\mu) &= c_d^{\mathrm{V}} \mathbb{1}_3 - \frac{1}{8\pi^2}\left(c_d^{\mathrm{V}} - c_Q^{\mathrm{V}}\right) \hat{Y}_d^\dagger \hat{Y}_d \log(\Lambda/\mu) \,. \end{aligned} \tag{5.75}$$

We see that through the RGEs flavour violating couplings are induced in both the up and down LH quark sector, while the couplings of RH interactions $\mathbb{C}_u^{\mathrm{VR}}, \mathbb{C}_d^{\mathrm{VR}}$ are flavour diagonal. The flavour violation in the LH sector is proportional to $c_Q^{\mathrm{V}} - c_u^{\mathrm{V}}$ and $c_Q^{\mathrm{V}} - c_d^{\mathrm{V}}$. Therefore, if the UV couplings are also universal among the different sectors, i.e., $c_Q^{\mathrm{V}} = c_u^{\mathrm{V}} = c_d^{\mathrm{V}}$, there is no flavour violation in the IR at one-loop, as in this case the LDV actually couples to the baryon-number current, which is conserved at tree-level inducing flavour violation only at two-loop level [86].

We now discuss this fact in more detail. One can rewrite the vector interactions in Eq. (5.70) for the case of flavour-universal UV boundary conditions in Eq. (5.74) in terms of the tree-level conserved (but anomalous) $U(1)_B$ current $J_B^\mu = \sum_i \left(\bar{Q}^i \gamma^\mu Q^i + \bar{u}_{\mathrm{R}}^i \gamma^\mu u_{\mathrm{R}}^i + \bar{d}_{\mathrm{R}}^i \gamma^\mu d_{\mathrm{R}}^i\right)$, and the two non-conserved currents $J_{Nd}^\mu = \sum_i \bar{d}_{\mathrm{R}}^i \gamma^\mu d_{\mathrm{R}}^i$, and $J_{Nu}^\mu = \sum_i \bar{u}_{\mathrm{R}}^i \gamma^\mu u_{\mathrm{R}}^i$. As all currents are not conserved beyond tree-level, we take their coefficients to be proportional to the LDV mass

$$\mathscr{L}_{\mathrm{int}} \supset -\left(\overline{Q}\, Y_u \widetilde{H} u_{\mathrm{R}} + \overline{Q}\, Y_d H d_{\mathrm{R}} + \mathrm{h.c.}\right) + \frac{m_{V'}}{\Lambda} V'_\mu \left[C_B^{\mathrm{V}} J_B^\mu + C_{Nd}^{\mathrm{V}} J_{Nd}^\mu + C_{Nu}^{\mathrm{V}} J_{Nu}^\mu\right] , \tag{5.76}$$

Matching to Eqs. (5.70) and (5.74) gives

$$\frac{m_{V'}}{\Lambda} c_B^{\mathrm{V}} = c_Q^{\mathrm{V}} \,, \qquad \frac{m_{V'}}{\Lambda} c_{Nd}^{\mathrm{V}} = c_d^{\mathrm{V}} - c_Q^{\mathrm{V}} \,, \qquad \frac{m_{V'}}{\Lambda} c_{Nu}^{\mathrm{V}} = c_u^{\mathrm{V}} - c_Q^{\mathrm{V}} \,. \tag{5.77}$$

[1] For the vector interaction, Yukawa corrections appear at the two-loop level, and thus we neglect these contributions.

At the one-loop level there is no flavour violation proportional to $C_B^{\rm V}$. However, flavour violation does arise due to the non-conserved currents and is thus proportional to the difference of couplings $c_Q^{\rm V} - c_u^{\rm V}$ and $c_Q^{\rm V} - c_d^{\rm V}$. Rewriting Eq. (5.75) in terms of the UV coefficients $c_B^{\rm V}, c_{Nd}^{\rm V}, c_{Nu}^{\rm V}$ with the proper LDV mass scaling gives

$$\begin{aligned}
\left(\frac{m_{V'}}{\Lambda}\right)\mathbb{C}_u^{\rm VL}(\mu) &= \frac{m_{V'}}{\Lambda}\left[c_B^{\rm V}\mathbb{1}_3 + \frac{1}{16\pi^2}\left(c_{Nu}^{\rm V}\hat{Y}_u\hat{Y}_u^\dagger + c_{Nd}^{\rm V}V_{\rm CKM}\hat{Y}_d\hat{Y}_d^\dagger V_{\rm CKM}^\dagger\right)\log(\Lambda/\mu)\right] ,\\
\left(\frac{m_{V'}}{\Lambda}\right)\mathbb{C}_d^{\rm VL}(\mu) &= \frac{m_{V'}}{\Lambda}\left[c_B^{\rm V}\mathbb{1}_3 + \frac{1}{16\pi^2}\left(c_{Nu}^{\rm V}V_{\rm CKM}^\dagger\hat{Y}_u\hat{Y}_u^\dagger V_{\rm CKM} + c_{Nd}^{\rm V}\hat{Y}_d\hat{Y}_d^\dagger\right)\log(\Lambda/\mu)\right] ,\\
\left(\frac{m_{V'}}{\Lambda}\right)\mathbb{C}_u^{\rm VR}(\mu) &= \frac{m_{V'}}{\Lambda}\left[\left(c_B^{\rm V} + c_{Nu}^{\rm V}\right)\mathbb{1}_3 - \frac{1}{8\pi^2}c_{Nu}^{\rm V}\hat{Y}_u^\dagger\hat{Y}_u\log(\Lambda/\mu)\right] ,\\
\left(\frac{m_{V'}}{\Lambda}\right)\mathbb{C}_d^{\rm VR}(\mu) &= \frac{m_{V'}}{\Lambda}\left[\left(c_B^{\rm V} + c_{Nd}^{\rm V}\right)\mathbb{1}_3 - \frac{1}{8\pi^2}c_{Nd}^{\rm V}\hat{Y}_d^\dagger\hat{Y}_d\log(\Lambda/\mu)\right] ,
\end{aligned} \tag{5.78}$$

and thus we see that flavour violation is proportional to the non-conserved currents. In Table 5.3 the leading flavour violation transitions are parametrised in terms of the Wolfenstein parameter λ (see Eq. (2.31)) and Yukawa couplings, were we observe that bottom (top) contributions dominate for the up (down) transitions.

$i-j$	$2-1$	$3-2$	$3-1$
$(\mathbb{C}_u^{\rm VL})_{i\neq j}$	$\lambda^5 y_b^2$	$\lambda^2 y_b^2$	$\lambda^3 y_b^2$
$(\mathbb{C}_d^{\rm VL})_{i\neq j}$	$\lambda^5 y_t^2$	$\lambda^2 y_t^2$	$\lambda^3 y_t^2$

Table 5.3.: Parametric size of leading flavour-violating contributions to the low-energy vector couplings of V' in the UV universal scenario, cf. Eq. (5.75). Here $\lambda \approx 0.23$ denotes the Wolfenstein parameter. Up-quark transitions (first line) are proportional to the high-scale coupling $c_u^{\rm V} - c_Q^{\rm V} = c_{Nu}^{\rm V}$, down-quark transitions (second line) are proportional to the high-scale coupling $c_d^{\rm V} - c_Q^{\rm V} = c_{Nd}^{\rm V}$, and all entries are multiplied by $\log(\Lambda/\mu)/(16\pi^2)$.

5.6.2. Dipole Interaction

We now follow the same procedure for the dipole interaction of Eq. (5.70), for which the RGEs are given in Eq. (5.72). For the UV universal setup that we consider, the initial conditions at the UV scale Λ_6 are

$$C_d^{\rm D}\big|_{\mu=\Lambda_6} = c_d^{\rm D}\, Y_d\big|_{\mu=\Lambda_6} , \qquad C_u^{\rm D}\big|_{\mu=\Lambda_6} = c_u^{\rm D}\, Y_u\big|_{\mu=\Lambda_6} , \tag{5.79}$$

with $c_f^{\rm D} \in \mathbb{C}$. By solving the RGE at leading-logarithmic accuracy and subsequently rotating to the mass basis, we find the low-energy dipole couplings in the L/R notation of Eq. (5.41) with $f = u, d$ to be[1]

$$\begin{aligned}
\frac{1}{\Lambda}\mathbb{C}_u^{\rm DR}(\mu) &= \frac{v}{\sqrt{2}\Lambda_6^2}\left(c_u^{\rm D}\hat{Y}_u - \frac{1}{16\pi^2}\left(3c_u^{\rm D}\hat{Y}_u\hat{Y}_u^\dagger\hat{Y}_u - c_d^{\rm D}V_{\rm CKM}\hat{Y}_d\hat{Y}_d^\dagger V_{\rm CKM}^\dagger\hat{Y}_u\right)\log(\Lambda_6/\mu)\right) ,\\
\frac{1}{\Lambda}\mathbb{C}_d^{\rm DR}(\mu) &= \frac{v}{\sqrt{2}\Lambda_6^2}\left(c_d^{\rm D}\hat{Y}_d - \frac{1}{16\pi^2}\left(3c_d^{\rm D}\hat{Y}_d\hat{Y}_d^\dagger\hat{Y}_d - c_u^{\rm D}V_{\rm CKM}^\dagger\hat{Y}_u\hat{Y}_u^\dagger V_{\rm CKM}\hat{Y}_d\right)\log(\Lambda_6/\mu)\right) ,
\end{aligned} \tag{5.80}$$

[1] Since the couplings at the UV scale Λ_6 are aligned to the SM Yukawa matrices, a correction from the Yukawa RGE of Eq. (5.73) is taken into account.

where $V_{\rm CKM}$ is the CKM matrix, and $\hat{Y}_f = m_f/v$ are the diagonal SM Yukawas. The LH couplings $\mathbb{C}_f^{\rm DL}$ are related to the ones in Eq. (5.80) by hermitian conjugation, $\mathbb{C}_f^{\rm DL} = (\mathbb{C}_f^{\rm DR})^\dagger$. Note that flavour off-diagonal entries are generated in both the up- and the down-quark sector at one-loop. They are proportional to the CKM matrix and the UV coupling of the other sector, i.e., $\mathbb{C}_u^{\rm DR} \propto c_d^D$ and $\mathbb{C}_d^{\rm DR} \propto c_u^D$. Carrying out the matrix multiplications, one can identify the numerically leading contribution to a given flavour transition. We show these leading contributions in Table 5.4 for both sectors.

$i-j$	$2-1$	$1-2$	$2-3$	$3-2$	$1-3$	$3-1$
$(\mathbb{C}_u^{\rm DR})_{i\neq j}/\Lambda$	$\lambda^5 y_b^2 y_c$	$\lambda^5 y_b^2 y_c$	$\lambda^2 y_b^2 y_t$	$\lambda^2 y_b^2 y_t$	$\lambda^3 y_b^2 y_t$	$\lambda^3 y_b^2 y_t$
$(\mathbb{C}_d^{\rm DR})_{i\neq j}/\Lambda$	$\lambda^5 y_t^2 y_s$	$\lambda^5 y_t^2 y_s$	$\lambda^2 y_t^2 y_b$	$\lambda^2 y_t^2 y_b$	$\lambda^3 y_t^2 y_b$	$\lambda^3 y_t^2 y_b$

Table 5.4.: Parametric size of leading flavour-violating contributions at low-energy in the UV universal scenario for dipole couplings, cf. Eq. (5.80). Here $\lambda \approx 0.23$ denotes the Wolfenstein parameter and $y_f = m_f/v$ are SM Yukawas couplings. Up-quark transitions (first line) are proportional to the high-scale coupling $c_d^{\rm D}$, down-quark transitions (second line) are proportional to the high-scale coupling $c_u^{\rm D}$, and all entries are multiplied by $v/\Lambda_6^2 \log(\Lambda_6/\mu)/(16\pi^2)$.

Chapter 6

Phenomenology of Two-Body Decays

6.1. Motivation and Searches

While constraints on light particles have been extensively studied in the context of colliders, beam-dump experiments, astrophysics, and cosmology, their phenomenology at precision flavour experiments has so far received less attention (see Ref. [75, 87] for early studies). Even if flavour-violating couplings may be considered more model-dependent than flavour-diagonal couplings, they can provide for an efficient production of light invisible particles from decays of SM leptons, mesons or baryons. Interestingly, direct searches at laboratory experiments for such two-body decays with missing energy have the potential to probe enormously large scales, as the relevant Lagrangian interactions can be dimension-five, instead of dimension-six as in the case of heavy NP. For example, in models with sufficiently light invisible bosons like the QCD axion, precision experiments are sensitive to scales as large as $10^{12}\,\mathrm{GeV}$ from $K \to \pi + \text{invis.}$ searches at NA62 [88], $10^{10}\,\mathrm{GeV}$ from $\mu \to e + \text{invis.}$ searches at MEG-II [89, 90], Mu3e [91], Mu2e or COMET [92], and $10^{8}\,\mathrm{GeV}$ for $b \to d/s$ transitions at Belle II [93].[1]

The aim of this chapter is to systematically study the flavour phenomenology of LDVs, both in the quark and lepton sectors. We restrict the discussion to invisible particles, since after all the main (only) motivation for these particles is the observed DM abundance, and we have in mind scenarios where either the LDV is itself stable on cosmological scales or promptly decays to stable DM particles. This analysis includes scenarios where the LDVs are just sufficiently long-lived to appear as missing energy. This is particularly justified for vector particles lighter than the electron, as their decay into two photons is forbidden by the Landau–Yang theorem [98, 99]. As we shall discuss, the resulting limits on flavour-violating interactions can be as strong as in the axion case, which is not unexpected due to the GBET. In light of past and ongoing experimental searches, it is thus important to systematically study the phenomenological differences between light dark scalars and vectors originating from their distinct helicity and coupling structure.

Earlier works have focused on the case of flavour-violating dipole couplings of a massless dark photon in $\mu \to e$, $s \to d$ and $c \to u$ transitions [24, 100–105], or considered general interactions and masses, but using only the available experimental limits on three-body decays to neutrinos to study limits from $s \to d$ and $b \to s$ transitions [75, 106]. Here instead we consider the case of a light vector particle, the LDV, with generic mass and either dipole or minimal couplings to

[1] For the flavour phenomenology of the QCD axion and light invisible axion-like particles see Refs. [75, 89, 93–97].

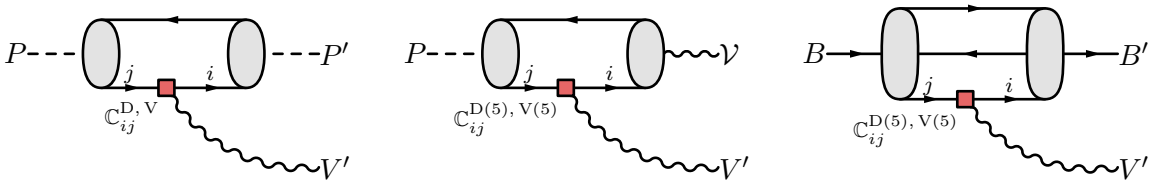

Figure 6.1.: Illustrative Feynman diagrams with a flavour-violating $q_j \to q_i$ transition in two-body decays of type $P \to P' + V'$, $P \to \mathcal{V} + V'$, and $B \to B' + V'$, in the left, middle, and right panel, respectively.

SM fermions as discussed in Section 5.4, and recast available experimental data for two-body kinematics in the case of hadron decays. For the case of minimal couplings to a light invisible vector particle, lepton flavour-violating (LFV) decays have been studied in Refs. [107, 108], here we also discuss dipole couplings and include lepton polarisation, which plays an important role in separating signal from SM background. We derive bounds in the general parameter plane of light-vector mass and the appropriate flavour-changing coupling by comparing theoretical predictions for the decay rates to the experimental bounds from various flavour factories, such as NA62 [109, 110], BaBar [111, 112], CLEO [113], Belle II [114, 115], BES III [116], and TWIST [117]. Whenever not available (as in the case of, e.g., $B \to K/K^*/\pi + \text{invis.}$ or $D \to \pi + \text{invis.}$ decays), we derive model-independent limits on the two-body decay rate as a function of the invisible particle mass by recasting experimental data on the three-body decay with two invisible neutrinos. Finally, we also analyse the scenario discussed in Section 5.6, in which FCNC couplings are induced through the running of the RGEs. We use our results to convert limits on the flavour-changing interactions into limits on flavour-diagonal UV couplings.

6.2. Quark Phenomenology of Light Dark Vectors

In this section we derive bounds on the flavour-violating couplings $\mathbb{C}_{ij}^{\mathrm{D(5)}}$ and $\mathbb{C}_{ij}^{\mathrm{V(5)}}$ in Eq. (5.42) for the quark-flavour transitions: $s \to d$, $b \to s$, $b \to d$, and $c \to u$. We employ the following three types of two-body decays containing the LDV as an invisible final state[1]

- $P \to P' + V'$: pseudoscalar meson to pseudoscalar meson and LDV,
- $P \to \mathcal{V} + V'$: pseudoscalar meson to vector meson and LDV,
- $B \to B' + V'$: baryon to baryon and LDV.

Figure 6.1 shows representative Feynman diagrams for the three types of decays. Appendix C contains the analytical expressions for the corresponding decays rates (including the dependence on $m_{V'}$); the relevant form factors are collected in Appendix C.1. Comparing the decay rates to the experimental upper limits on the branching ratios, we set upper bounds on the couplings in the V/A basis[2] of Eq. (5.42), i.e. on the set $\{\mathbb{C}_{ij}^{\mathrm{D}}, \mathbb{C}_{ij}^{\mathrm{D5}}, \mathbb{C}_{ij}^{\mathrm{V}}, \mathbb{C}_{ij}^{\mathrm{V5}}\}$. The limits are determined as a function of the LDV mass, with range $0 \leq m_{V'}^2 \leq (m_{\mathrm{I}} - m_{\mathrm{F}})^2 \equiv m_{V'\mathrm{max}}^2$ depending on the masses of the initial (m_{I}) and final (m_{F}) states of the decay at hand. Crucially, the form factors depend on the LDV mass and it is, therefore, essential to consider the full form-factor parametrisation for an accurate analysis.

The available theoretical and experimental information is summarized in Table 6.1, where we collect the references for the form factors and relevant experimental limits. Often the experimental

[1] Three-body decays and neutral meson mixing typically give weaker constraints, e.g., for example LHCb constraints on $B_{(s)} \to \mu\mu a$ cannot compete with Belle II limits [118].
[2] In Appendix B we show the bounds in the L/R basis.

collaborations do not provide limits on two-body decays with missing energy. Yet, in some cases there is enough information to extract this bound from available data. We indicate this case by a subindex "r" in the last column of the table, and either use existing recasts in the literature or perform our own recast, e.g., to find a bound on $B \to \pi/K/K^* + \text{invis.}$ from BaBar data on the corresponding three-body decays [111, 112], see Appendix A for details.

Concretely we use our recast for $B \to K^{(*)} + \text{invis.}$ only for LDV masses above 3 GeV. Note that we can recast only the experimental results of the BaBar collaboration and cannot use the newer Belle measurements, since the Belle collaboration does not provide the event count as a (binned) function of the missing-momentum distribution. We use existing recasts for $B \to \rho + \text{invis.}$ decays from LEP [119, 120], $B \to K + \text{invis.}$ decays from Belle II [115, 121] (this recast is limited to masses below $m_{V'} = 3\,\text{GeV}$), $B \to K^* + \text{invis.}$ decays from BaBar [112, 121] (below $m_{V'} = 3\,\text{GeV}$). For invisible baryon decays for which there is no analysis, we derive limits using the total lifetime from the PDG [122] after subtracting all observed channels as in Ref. [93].

For the bound based on $D \to \pi + \text{invis.}$ decays we use the result of Ref. [93] for $m_{V'} \approx 0$, obtained from recasting CLEO data on $D \to (\tau \to \pi\nu)\nu$ [113]. We also perform a recast of these data for LDV masses up to $m_{V'} \approx 0.5\,\text{GeV}$ (which is the upper range of the CLEO data set), assuming the efficiency in all bins to be the same as for $m_{V'} \approx 0$. Note that recasting BES III data [123] on $D \to \pi\nu\overline{\nu}$ gives weaker constraints [93], although this result does not use the full experimental information. It would be interesting if BES III would provide an explicit two-body recast of their full data set. The collaboration actually does this for the case of two-body hyperon decays $\Lambda_c \to p + \text{invis.}$, albeit only for "massless" invisible particles. Their signal region in fact covers invisible masses up to 316 MeV, and leads to limits that are much stronger than the ones obtained by saturating the total Λ_c lifetime [93]. As a conservative limit, to be replaced by a dedicated experimental analysis, we multiply their limit for the massless case by a factor 1/2 (since close to the endpoint of the signal region half of the signal events are lost due to energy resolution). We use the resulting bound $\text{BR}(\Lambda_c \to pV') < 1.6 \times 10^{-4}$ for LDV masses up to 316 MeV, and take lifetime limits above 316 MeV. We notice that a search for the decay $D \to \pi + X$ would not suffer from two-body SM backgrounds in contrast to hyperon decays, where $\Lambda_c \to p + \gamma$ contributes to the signal of a massless X, if the photon is missed.

To set constraints on the couplings $\{\mathbb{C}^{\text{D}}_{ij}, \mathbb{C}^{\text{D5}}_{ij}, \mathbb{C}^{\text{V}}_{ij}, \mathbb{C}^{\text{V5}}_{ij}\}$ we consider dipole ($\mathscr{L}_{\text{D}}$) and vector interactions ($\mathscr{L}_{\text{V}}$) separately, and turn on a single coupling at a time. We use the theory predictions of Appendix C together with the form factors in Table 6.1 (see also Appendix C.1) to calculate the decay rates as a function of the couplings and the LDV mass. The rates are then compared to the experimental limits to obtain the bounds in the mass–coupling plane. We include statistical and systematic uncertainties as follows. For the theory predictions we only use the systematic uncertainties associated with hadronic form factors (these are the most relevant ones), while the treatment of uncertainties of experimental limits depend on their nature: for decays where the experimental collaborations provide two-body interpretations (or a theory recast exists), we add the experimental and form-factor uncertainties in quadrature. In the case where we performed our own two-body recast (as described in Appendix A), we treat theory uncertainties as Gaussian uncertainties smearing the expectation values of the underlying Poisson probability distribution functions.

Our results are summarized in Figures 6.2 and 6.3 in which we show the lower bounds on the effective inverse coupling $\Lambda/\mathbb{C}_{ij}$ for given LDV mass $m_{V'}$. The plots are organized according to the underlying flavour transition, i.e, $s \to d$, $b \to s$, $b \to d$, and $c \to u$ and we separate dipole $\{\mathbb{C}^{\text{D}}_{ij}, \mathbb{C}^{\text{D5}}_{ij}\}$ (Figure 6.2) and vector couplings $\{\mathbb{C}^{\text{V}}_{ij}, \mathbb{C}^{\text{V5}}_{ij}\}$ (Figure 6.3). Each plot shows the bound on a single coupling for a given quark-flavour transition, with each line corresponding to a particular hadronic decay, excluding the region below. Note that $P \to P' + V'$ decays are

Quark Transition	Hadronic Process	Form Factors	Experimental Limit
$s \to d$	$K^+ \to \pi^+ + V'$	[124, 125]	NA62 [88, 109, 110]
	$\Sigma^+ \to p + V'$	[105, 126–128]	BES III [129], Lifetime$_r$ [93, 122]
	$\Xi^- \to \Sigma^- + V'$	[105, 126–128]	Lifetime$_r$ [93, 122]
	$\Xi^0 \to \Sigma^0 + V'$	[105, 126–128]	Lifetime$_r$ [93, 122]
	$\Xi^0 \to \Lambda + V'$	[105, 126–128]	Lifetime$_r$ [93, 122]
	$\Lambda \to n + V'$	[105, 126–128]	Lifetime$_r$ [93, 122]
$b \to s$	$B^+ \to K^+ + V'$	[130, 130]	BaBar$_r$ [112], Belle II$_r$ [115, 121]
	$B \to K^* + V'$	[130, 130]	BaBar$_r$ [112, 121]
	$\Lambda_b \to \Lambda + V'$	[131, 131]	Lifetime$_r$ [93, 122]
$b \to d$	$B^+ \to \pi^+ + V'$	[130, 132]	BaBar$_r$ [111]
	$B \to \rho + V'$	[130, 130]	LEP$_r$ [119, 120]
	$\Lambda_b \to n + V'$	[131, 133]	Lifetime$_r$ [93, 122]
$c \to u$	$D^+ \to \pi^+ + V'$	[134, 135]	CLEO$_r$ [93, 113]
	$\Lambda_c \to p + V'$	[136, 136]	BES III [116], Lifetime$_r$ [93, 122]

Table 6.1.: Overview of considered hadron decays with invisibles in the final state. The first column shows the underlying quark-flavour transition, the second the specific hadronic process. The relevant vector and dipole form factors are taken from the references in the third column. The last column contains the references for the experimental upper limits on the respective branching ratios. A subindex "r" indicates that a recast of experimental data was needed, see text and Appendix A for details.

only sensitive to $\{\mathbb{C}^{\mathrm{D}}_{ij}$ and $\mathbb{C}^{\mathrm{V}}_{ij}\}$ couplings, which follows from parity conservation of the strong interactions and the Lorentz structure of the form factors (see Appendix C.1). Also note that dipole operators are dimension-six above the electroweak scale, so in fact the actual UV scale probed is $\Lambda_6 = \sqrt{v\Lambda}/2^{1/4}$ in all transitions.

6.2.1. Dark Dipole Interactions

$s \to d$ Transitions

The bounds on the dipole couplings $\{\mathbb{C}^{\mathrm{D}}_{sd}, \mathbb{C}^{\mathrm{D5}}_{sd}\}$ are set by $K \to \pi + \text{invis.}$ and hyperon decays, cf. Table 6.1 and Figure 6.2. For the two-body decay $K \to \pi + \text{invis.}$ we use the bound provided by the NA62 collaboration [110]. For baryon decays there is an upper limit from BES III [129] on the decay $\Sigma^+ \to p + \text{invis.}$ with a massless invisible. We estimate the potential reach for this search by extending it to larger invisible masses by assuming that the same experimental limit

is valid for the whole kinematic range. This is indicated by a dashed orange line. For all other baryon searches, we set upper limits on branching ratios indirectly as in Ref. [93] by subtracting the measured branching fractions for all relevant hyperon decay channels from unity. Due to this rather weak limit, $K \to \pi$ sets a much more stringent constraint than hyperon decays, limiting the UV scale $\Lambda/\mathbb{C}^{\mathrm{D}}_{ij}$ to be at least of the order 10^{11} GeV. Note however that the search for $\Sigma^+ \to p + \text{invis.}$ strenghtens the upper limit by two orders of magnitude compared to the conservative limit estimated with the total lifetime, and thus, out of all baryon decays, it yields the strongest limit of order 10^7 GeV on the scale $\Lambda/\mathbb{C}^{\mathrm{D}}_{ij}$.

Nevertheless baryon decays with missing energy are important for two reasons. The decays to pseudoscalar, such as $K \to \pi$, are only sensitive to the $\{\mathbb{C}^{\mathrm{D}}_{ij}, \mathbb{C}^{\mathrm{V}}_{ij}\}$ couplings. Thus baryon decays are crucial to constrain the axial coupling $\Lambda/\mathbb{C}^{\mathrm{D5}}_{ij}$ (of the order of a few $\times 10^7$ GeV), as there are no two-body decays to vector particles in $s \to d$ transitions. Moreover, the decay rates of pseudoscalar processes are proportional to the LDV mass for the dipole interaction $\mathscr{L}_{\mathrm{D}}$ (cf. Eq. (C.14)), and thus only baryon decays can constrain $\mathbb{C}^{\mathrm{D}}_{ij}$ for small LDV masses. This can be see in Figure 6.2 (upper left panel), where the bounds on $\mathbb{C}^{\mathrm{D}}_{sd}$ from hyperon decays dominate for LDV masses of $m_{V'} \approx 0$ yielding a limit of $\mathcal{O}(10^7\ \mathrm{GeV})$ on the axial coupling $\Lambda/\mathbb{C}^{\mathrm{D5}}_{ij}$. This provides a strong motivation for explicit direct searches targeting baryon decays with invisible final states.

$b \to s$ Transitions

The limits on the dipole couplings $\{\mathbb{C}^{\mathrm{D}}_{bs}, \mathbb{C}^{\mathrm{D5}}_{bs}\}$ are set by B-meson decays $B \to K/K^* + \text{invis.}$ and baryon decays $\Lambda_b \to \Lambda + \text{invis.}$ The limits from the B-meson decays are obtained from our own recast of BaBar data (cf. Appendix A), except for $B^+ \to K^+ + \text{invis.}$ for LDV masses $m_{V'} < 3\,\mathrm{GeV}$ where we use the recast in Ref. [121] of the recent Belle II measurement of $B^+ \to K^+\overline{\nu}\nu$ [115]. We also use the recast in Ref. [121] of the BaBar measurement of $B \to K^*\overline{\nu}\nu$ [112] below LDV masses of 3 GeV. The limit on unobserved Λ_b decays such as $\Lambda_b \to \Lambda + \text{invis.}$ is obtained by comparing the SM prediction for the total lifetime with the experimental one inferred from all observed channels, ascribing the difference to the allowed value for the two-body invisible decay [93]. As for $s \to d$ transitions, decays to pseudoscalar mesons such as $B^+ \to K^+$ can neither constrain the axial coupling $\mathbb{C}^{\mathrm{D5}}_{bs}$, nor $\mathbb{C}^{\mathrm{D}}_{bs}$ for very small LDV masses. Otherwise, however, they do dominate over the constraint from $\Lambda_b \to \Lambda$.

In contrast to $s \to d$ transitions, there is also a decay with vector mesons in the final-state, $B \to K^*$, which constrains both the $\mathbb{C}^{\mathrm{D}}_{bs}$ and the $\mathbb{C}^{\mathrm{D5}}_{bs}$ couplings in the entire LDV mass range, if kinematically allowed. Hence, $B \to K^*$ decays are complementary to $B \to K$ decays in constraining $\Lambda/\mathbb{C}^{\mathrm{D}}_{bs}$, setting limits on the UV scale of the order 10^8 GeV, and also dominate the bounds on $\Lambda/\mathbb{C}^{\mathrm{D5}}_{bs}$ of similar size, up to a small region where this channel is kinematically closed and $\Lambda_b \to \Lambda$ decays set the strongest limit, of the order 10^7 GeV. Note that there is an *upper* limit of order 10^8 GeV on $\Lambda/\mathbb{C}^{\mathrm{D}}_{bs}$ at around $m_{V'} \approx 2\,\mathrm{GeV}$ coming from $B \to K + V'$ decays [121], due to a $2.8\,\sigma$ excess in the latest Belle II measurement of $B^+ \to K^+\nu\overline{\nu}$ [115].

$b \to d$ Transitions

The bounds on the dipole couplings $\{\mathbb{C}^{\mathrm{D}}_{bd}, \mathbb{C}^{\mathrm{D5}}_{bd}\}$ are obtained from B-meson decays $B \to \pi/\rho + \text{invis.}$ and baryon decays $\Lambda_b \to n + \text{invis.}$ The limit on $B \to \pi$ decays is obtained from our recast of BaBar data (cf. Appendix A), while a limit on $B \to \rho$ decays from LEP data [119] has been derived in Ref. [120]. Analogously to $b \to s$ transitions, the pseudoscalar decay $B \to \pi$ does neither constrain the axial coupling $\mathbb{C}^{\mathrm{D5}}_{bd}$ nor $\mathbb{C}^{\mathrm{D}}_{bd}$ for small LDV masses, while the decay to vector mesons $B \to \rho$ does. Thus the two meson decays are complementary in setting limits on $\Lambda/\mathbb{C}^{\mathrm{D}}_{bd}$, of the order of 10^8 GeV, while $B \to \rho$ dominates the bounds on the limits on $\Lambda/\mathbb{C}^{\mathrm{D5}}_{bd}$ of

similar size, except for LDV masses above the kinematic threshold where $\Lambda_b \to n$ decays take over, constraining UV scales up to $10^7\,\mathrm{GeV}$.

$c \to u$ Transitions

Finally, the constraints on the dipole couplings $\{\mathbb{C}^{\mathrm{D}}_{cu}, \mathbb{C}^{\mathrm{D5}}_{cu}\}$ are set by $D \to \pi + \text{invis.}$ and the baryonic process $\Lambda_c \to p + \text{invis.}$ For $D \to \pi$ and LDV masses $m_{V'} \lesssim 0.5\,\mathrm{GeV}$, we performed a recast of the CLEO data set (analogous to the B-decay recasts in Appendix A). The result is shown as a solid, blue line in the bottom panel of Figure 6.2. CLEO has only collected data up to masses of $m_{V'} \approx 0.5\,\mathrm{GeV}$, but we also show the potential bound that could be obtained above this mass by extrapolating the bound for massless invisible particles [93] to the whole kinematic range, which we indicate by a dashed blue line.

For $\Lambda_c \to p$ we show two limits in the bottom panel of Figure 6.2: solid, orange lines denote the bound obtained from simply saturating the total Λ_c lifetime, i.e., $\mathrm{BR}(\Lambda_c \to p + V') < 1$, while the green line indicates the 95% CL bound obtained from the BES III [116] result for "massless" invisible particles, $\mathrm{BR}(\Lambda_c \to p + V) < 8.0 \times 10^{-5}$ at 90% CL, which in fact covers invisible masses up to $316\,\mathrm{MeV}$ and are multiplied by a factor 1/2, see the discussion in the beginning of this section. We estimate the potential reach for a search extending to larger invisible masses by assuming that the same experimental limit below $316\,\mathrm{MeV}$ is also valid above, and indicate this extrapolation by a dashed, green line. We observe that the strongest limits on $\Lambda/\mathbb{C}^{\mathrm{D}}_{cu}$ are set by the BES III search for a "massless" LDV in $\Lambda_c \to p$ decays, which are valid for $m_{V'} \lesssim 316\,\mathrm{MeV}$ and are of the order of $10^7\,\mathrm{GeV}$. Between $316\,\mathrm{MeV} \lesssim m_{V'} \lesssim 500\,\mathrm{MeV}$ a limit of similar size is obtained from $D \to \pi$ decays, recasting CLEO data on $D \to (\tau \to \pi\nu)\nu$. The only available limit on LDV masses above $0.5\,\mathrm{GeV}$ arises from the total Λ_c lifetime, which sets limits of order $10^5\,\mathrm{GeV}$. Naively extrapolating the limits from CLEO on $D \to \pi$ and BES III on $\Lambda_c \to p$ decays to higher LDV masses instead suggests that present bounds could be strengthened by two orders of magnitude, if BES III would either analyze the available searches for $\Lambda_c \to p$ decays with extended signal regions, or use available data on $D \to \pi\nu\overline{\nu}$ to set a limit on the two-body decay.

Currently only $\Lambda_c \to p$ decays are capable to set constraints on the axial coupling $\Lambda/\mathbb{C}^{\mathrm{D5}}_{cu}$, of the order of $10^5\,\mathrm{GeV}$ and $10^7\,\mathrm{GeV}$ for LDV masses above and below $316\,\mathrm{MeV}$, respectively. Besides extending the search for $\Lambda_c \to p + V'$ to higher LDV masses, this also motivates dedicated searches for other processes such as $D \to \rho + \text{invis.}$ or $D_s \to K^* + \text{invis.}$ at current or future experiments.

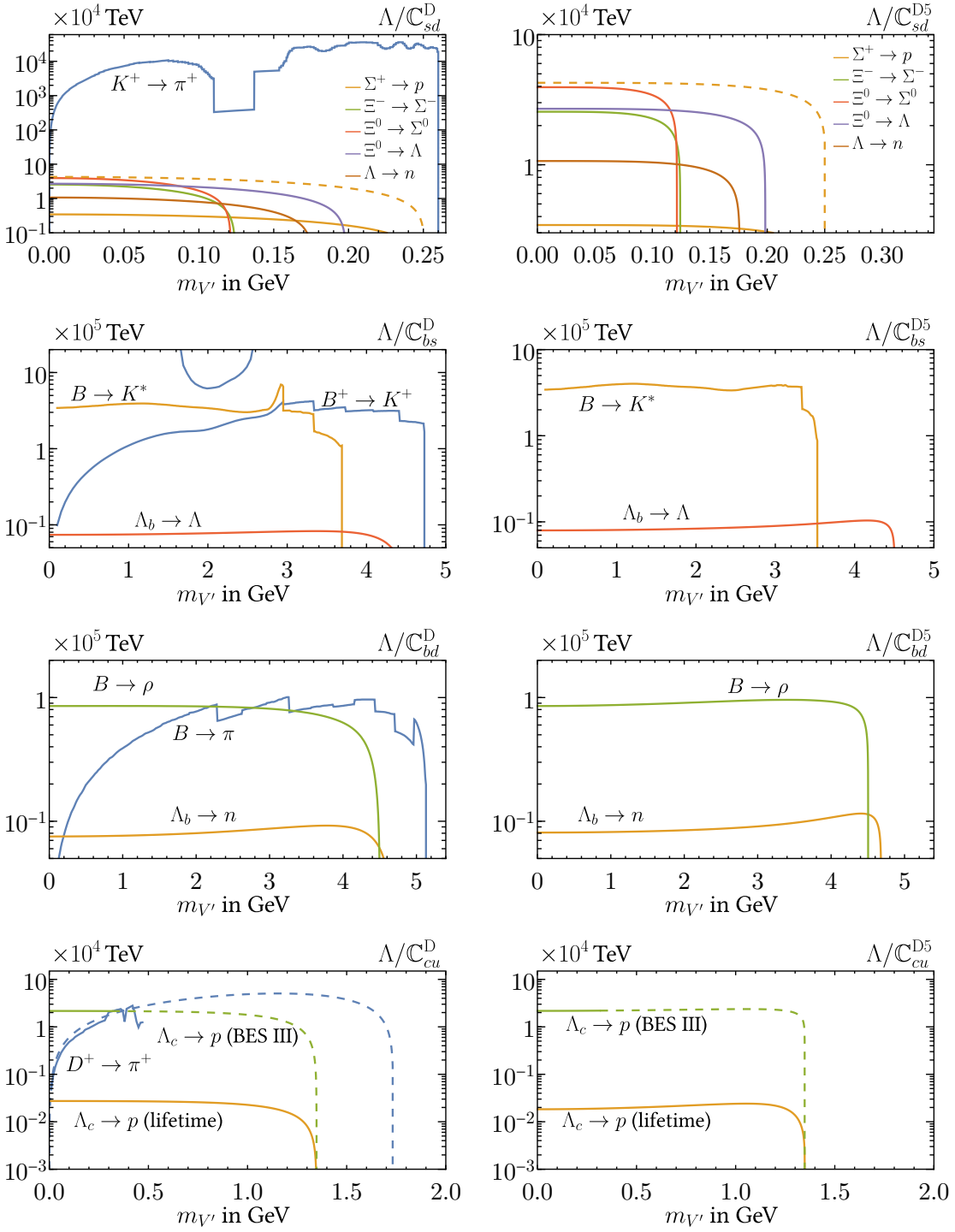

Figure 6.2.: Lower limits on quark-flavour violating dipole couplings $\Lambda/|\mathbb{C}^{\mathrm{D}}_{ij}|$ (left column) and $\Lambda/|\mathbb{C}^{\mathrm{D5}}_{ij}|$ (right column) of the LDV for $s \to d, b \to s, b \to d, c \to u$ transitions @95% $\mathrm{CL}_{(\mathrm{s})}$. See text for details.

6.2.2. Dark Vector Interactions

$s \to d$ Transitions

The limits on the vector couplings $\{\mathbb{C}^{\mathrm{V}}_{sd}, \mathbb{C}^{\mathrm{V5}}_{sd}\}$ are shown in Figure 6.3. As for dipole couplings, the relevant constraints arise from $K \to \pi$ and hyperon decays, see Table 6.1. Analogous to the dipole case, the limit from BES III on the decay $\Sigma^+ \to p + \text{invis.}$ for a massless invisible is tentatively assumed to be valid for the whole kinematic range. The limit on the scale is indicated by a dashed orange line. $K \to \pi$ decays dominate the limits on $\Lambda/\mathbb{C}^{\mathrm{V}}_{sd}$, restricting UV scales up to $10^{12}\,\mathrm{GeV}$, but cannot constrain the axial coupling $\Lambda/\mathbb{C}^{\mathrm{V5}}_{sd}$, where hyperon decays set the only available bounds of the order of $10^7\,\mathrm{GeV}$. All limits are non-vanishing when the LDV mass is taken to zero, which is due to the choice of the prefactor in $\mathscr{L}_{\mathrm{V}}$ linear in the LDV mass, see Eq. (5.42). This corresponds to the gauge-less limit where the longitudinal polarization of the LDV is essentially a Goldstone boson. With this scaling the flavour-violating decay is similar to the SM decay $t \to Wb$, which also remains finite in the gauge-less $g \to 0$ limit, since the top quark dominantly decays to the charged Goldstone Higgs, which couples only via Yukawas to the quarks. Different choices for the prefactor, corresponding to specific UV completions, would result in bounds that would vanish in the limit of massless LDVs, with a LDV mass dependence that can obtained by rescaling the limits presented here.

$b \to s$ Transitions

The constraints on the vector couplings $\mathbb{C}^{\mathrm{V}}_{bs}$, $\mathbb{C}^{\mathrm{V5}}_{bs}$ are obtained from B-meson decays $B \to K/K^* + \text{invis.}$ and the baryonic decays $\Lambda_b \to \Lambda + \text{invis.}$ $B^+ \to K^+$ sets the strongest constraint on $\Lambda/\mathbb{C}^{\mathrm{V}}_{bs}$ of the order of $10^8\,\mathrm{GeV}$, but cannot constrain the axial coupling $\Lambda/\mathbb{C}^{\mathrm{V5}}_{bs}$. Here the dominant constraints are set by $B \to K^*$ decays, also of the order of $10^8\,\mathrm{GeV}$, apart from the region where this channel is kinematically closed and $\Lambda_b \to \Lambda$ takes over and sets limits on the UV scales up to $10^6\,\mathrm{GeV}$. Again there is an *upper* limit of order $10^{12}\,\mathrm{GeV}$ on $\Lambda/\mathbb{C}^{\mathrm{V}}_{bs}$ at around $m_{V'} \approx 2\,\mathrm{GeV}$ coming from $B \to K + V'$ decays [121], due to a $2.8\,\sigma$ excess from the latest Belle II measurement of $B^+ \to K^+ \nu\overline{\nu}$ [115].

$b \to d$ Transitions

The bounds on the vector couplings $\mathbb{C}^{\mathrm{V}}_{bd}$, $\mathbb{C}^{\mathrm{V5}}_{bd}$ arise from B-meson decays $B \to \pi/\rho + \text{invis.}$ and the baryonic decays $\Lambda_b \to n + \text{invis.}$. Analogously to $b \to s$ transitions $B \to \pi$ decay sets the strongest constraint on $\Lambda/\mathbb{C}^{\mathrm{V}}_{bd}$ of the order of $10^8\,\mathrm{GeV}$, while $\Lambda/\mathbb{C}^{\mathrm{V5}}_{bd}$ is limited to about the same values by $B \to \rho$ decays, up to LDV masses at the kinematic threshold where $\Lambda_b \to n$ decays dominate the bound of order $10^6\,\mathrm{GeV}$.

$c \to u$ Transitions

Finally, the bounds on the vector couplings $\mathbb{C}^{\mathrm{V}}_{cu}$, $\mathbb{C}^{\mathrm{V5}}_{cu}$ are set by the decays $D \to \pi + \text{invis.}$ and $\Lambda_c \to p + \text{invis.}$ Meson decays $D \to \pi$ dominate the bound on $\Lambda/\mathbb{C}^{\mathrm{V}}_{cu}$ of order $10^8\,\mathrm{GeV}$, while only baryon decays $\Lambda_c \to p$ can constrain the axial coupling $\Lambda/\mathbb{C}^{\mathrm{V5}}_{cu}$ at order 10^5 and $10^7\,\mathrm{GeV}$, using the total lifetime and the extrapolation of the BES III measurement, respectively, analogous to the dipole case. Again, it would be interesting if BES III could extend their search for $\Lambda_c \to p + V'$ to higher invisible masses, as this is expected to strengthen the present bound on the UV scale by two orders of magnitude.

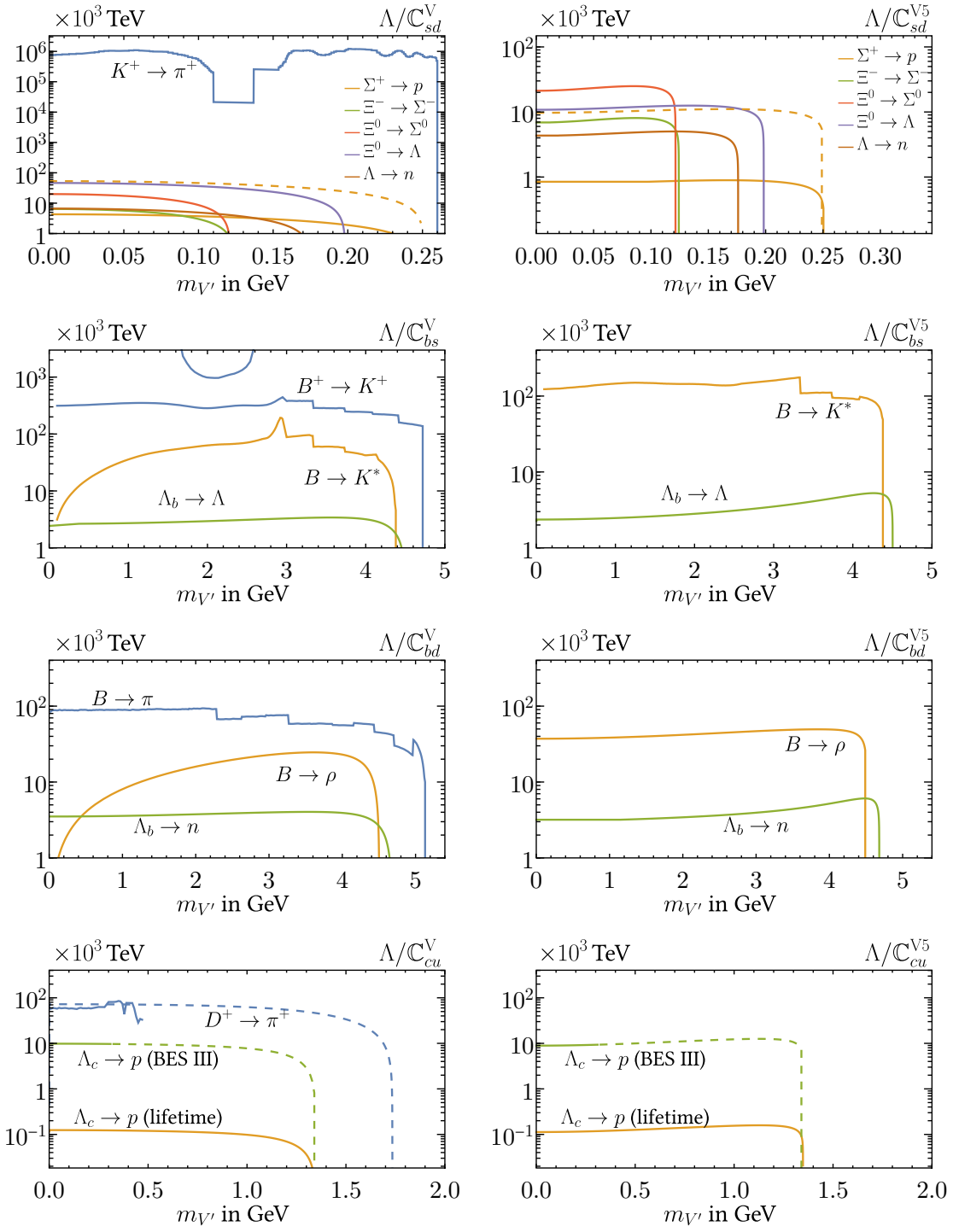

Figure 6.3.: Lower limits on quark-flavour violating vector couplings $\Lambda/|\mathbb{C}^{\rm V}_{ij}|$ (left column) and $\Lambda/|\mathbb{C}^{\rm V5}_{ij}|$ (right column) of the LDV for $s \to d, b \to s, b \to d, c \to u$ transitions @95% $\text{CL}_{(\text{s})}$. See text for details.

6.3. Lepton Phenomenology of Light Dark Vectors

In this section we present the bounds on the flavour-violating couplings in Eq. (5.42) from LFV decays $\ell \to \ell' + V'$ for the lepton-flavour transitions $\mu \to e$, $\tau \to e$, and $\tau \to \mu$. There are three main differences to the quark-sector analysis: *i)* there is no hadronic input required, *ii)*

LFV Transition	Experimental Limit
$\mu \to e$	TWIST [117], Jodidio$_r$ [89, 137]
$\tau \to e$	Belle II [114]
$\tau \to \mu$	Belle II [114]

Table 6.2.: The LFV transitions relevant for the two-body decays $\ell \to \ell' + V'$ and the corresponding relevant experimental measurements. The subindex "r" indicates that a recast of experimental data was needed.

the total decay rates only depend on the combination $|\mathbb{C}^{\rm D}_{ij}|^2 + |\mathbb{C}^{\rm D5}_{ij}|^2$ and $|\mathbb{C}^{\rm V}_{ij}|^2 + |\mathbb{C}^{\rm V5}_{ij}|^2$, and *iii)* for the case of $\mu \to e$ transitions one can profit from polarisation in order to suppress SM background from Michel decays. This allows us to distinguish between $\mathbb{C}^{\rm V}_{ij}$ and $\mathbb{C}^{\rm V5}_{ij}$ using the angular distribution of the outgoing electron.

Concretely, for $\mu \to e$ we restrict the discussion to three benchmark scenarios, depending on the angular dependence of the differential two-body LFV decay rate in the limit of $m_e = m_{V'} = 0$

$$\frac{d\Gamma(\mu \to e + V')}{d\cos\theta} \propto (1 + A\cos\theta)\,, \tag{6.1}$$

where θ is the angle between the outgoing electron momentum and the muon polarisation. We distinguish three benchmark cases: isotropic decays ($A = 0$), "V − A" structure $A = -1$, and "V + A" structure $A = +1$. Clearly polarisation does not help to distinguish a LFV signal from the SM background for the SM case $A = -1$. Thus one can only rely on the monochromatic electron as the signal, which leads to weaker bounds than in the other cases $A = 0, +1$ [89]. Interestingly, many proposals have been put forward to look for this decay at present and future high-luminosity muon facilities [89–92], which are sensitive also to invisible LDVs. We take present constraints on LFV transitions from the references indicated in Table 6.2, and compare them to the predictions for (polarised) lepton decay rates calculated in Appendix C.5.

$\mu \to e$ Transitions

The bounds from $\mu \to e +$ invis. decays on dipole and vector couplings are shown in Figure 6.4. We derive them employing constraints from experiments conducted at TRIUMF, both by the TWIST collaboration [117] in 2015 (left panel) and Jodidio et al. [137] in 1986 (right panel). For the latter, we use the recast of Ref. [89]. The three curves in Figure 6.4 show the bounds for the three benchmark scenarios for chiral structures, corresponding to $\mathbb{C}^{\rm D}_{e\mu} = 0$ or $\mathbb{C}^{\rm D5}_{e\mu} = 0$ for $A = 0$, and $\mathbb{C}^{\rm D}_{e\mu} = \pm i\mathbb{C}^{\rm D5}_{e\mu}$ for $A \approx \pm 1$ in the upper panel, while in the lower panel they correspond to $\mathbb{C}^{\rm V}_{e\mu} = 0$ or $\mathbb{C}^{\rm V5}_{e\mu} = 0$ for $A = 0$, and $\mathbb{C}^{\rm V}_{e\mu} = \pm\mathbb{C}^{\rm V5}_{e\mu}$ for $A \approx \pm 1$. For couplings that are not aligned to the SM, i.e., not "V − A", the dominant constraints on LDVs lighter than about 5 MeV are set by the Jodidio experiment, which limits UV scales of the order of 10^{10} GeV. Heavier LDVs are constrained only by TWIST, setting limits of the order of few $\times 10^9$ GeV. LDVs with "V − A" couplings are constrained by TWIST with bounds of the same order, exceeding the corresponding Jodidio limits also in the light-mass regime.

$\tau \to \mu/e$ Transitions

The limits from Belle II on $\tau \to \mu/e +$ invis. decays constrain $\tau \to e$ and $\tau \to \mu$ transitions according to Figure 6.5, where we shows the bounds on the dipole $\Lambda/\mathbb{C}^{\rm D}_{\tau\ell}$ (left panel) and vector

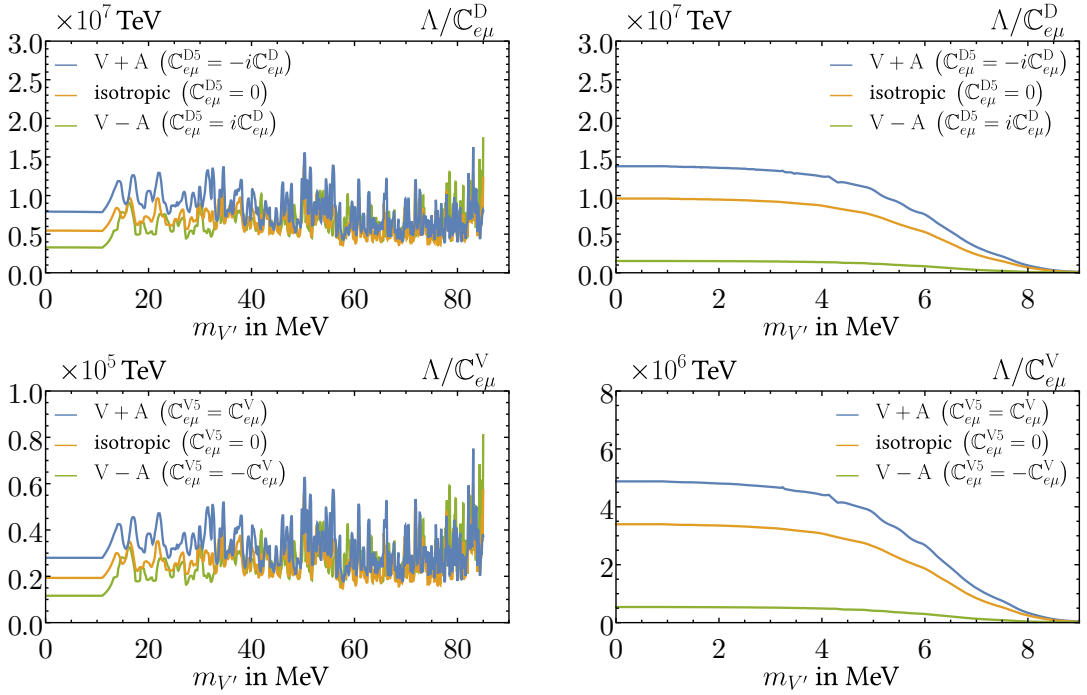

Figure 6.4.: *Upper panel:* Lower limits on the dipole coupling for $\mu \to e$ transitions $\Lambda/|\mathbb{C}^{\rm D}_{e\mu}|$ from TWIST [117] (left panel) and Jodidio et al. [89,137] (right panel). The bounds are shown for three different choices for $\mathbb{C}^{\rm D5}_{e\mu}$, corresponding to different angular distributions of the electron momentum, cf. Eq. (6.1): isotropic decay ($A = 0$), alignment to SM decay "$V-A$" ($A = -1$) and "$V+A$" ($A = +1$). *Lower panel:* Same for the vector coupling $\Lambda/|\mathbb{C}^{\rm V}_{e\mu}|$. See text for details.

couplings $\Lambda/\mathbb{C}^{\rm V}_{\tau\ell}$ (right panel). Constraints on the axial couplings $\Lambda/\mathbb{C}^{\rm D5}_{\tau\ell}$ and $\Lambda/\mathbb{C}^{\rm V5}_{\tau\ell}$ are at the same level, as the difference is suppressed by m_ℓ/m_τ, cf. Appendix C.5. Bounds for $\tau \to e$ and $\tau \to \mu$ transitions are comparable, limiting UV scales of the order of few $\times 10^7$ GeV for dipole couplings, and few $\times 10^6$ GeV for vector couplings.

6.4. Flavour-Violating LDVs from the Renormalization Group

In this section we study the phenomenologically interesting scenario in which flavour violation is induced via the RGEs as discussed in Section 5.6, and set bounds on the UV couplings from the previous flavour-violating decays. We discuss separately the case of dipole and vector couplings in Section 6.4.1 and 6.4.2, respectively.

6.4.1. Dipole Interactions

We determine the experimental limits on the high-scale couplings $c^{\rm D}_d$ and $c^{\rm D}_u$ in Eq. (5.79) from the limits on two-body meson decays discussed in Section 6.2. Note that the renormalisation scale μ is set to the EW scale, since below there is no Yukawa running. As expected from the high-level of flavour suppression inherent to the setup (see Table 5.4), the resulting bounds are very mild and often weaker than the constraints from perturbative unitarity. For this reason we only display in Figure 6.6 (left panel) the strongest bounds, which come from $B \to K^*$ and require $\Lambda_6 \sim$ TeV for $c^{\rm D}_u = 1$ (for $c^{\rm D}_d = 1$ the limit on Λ_6 is far below the EW scale and is therefore not shown).

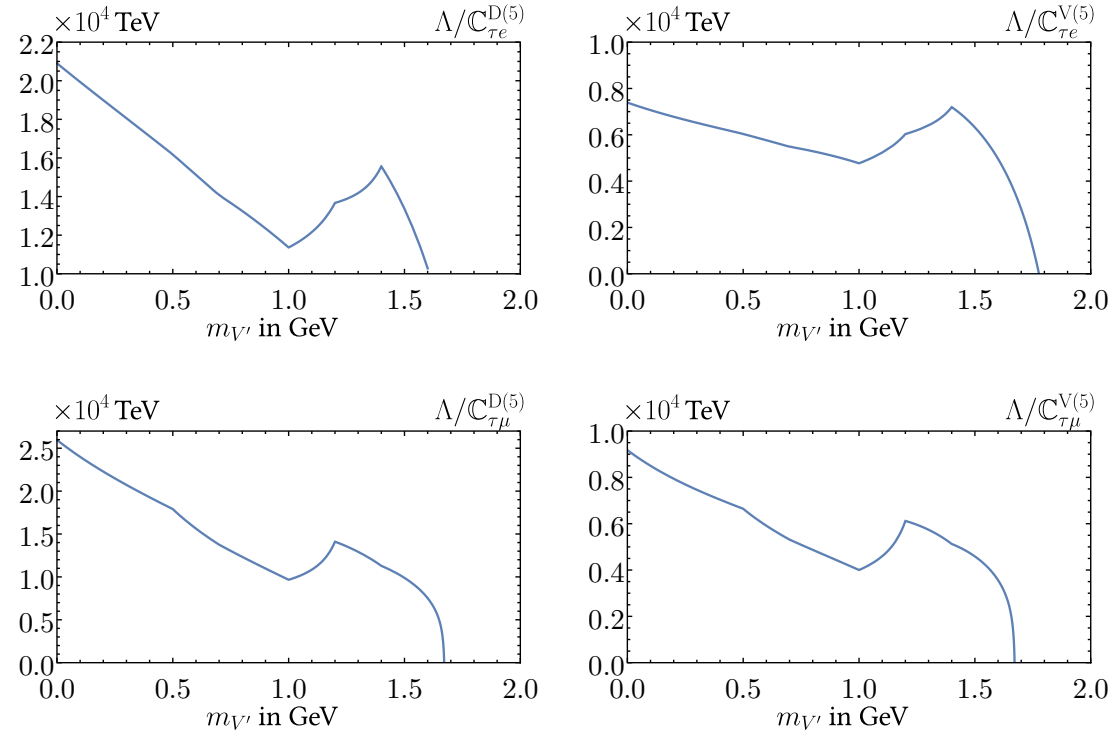

Figure 6.5.: *Upper panel:* Lower limits on the dipole (left panel) and vector (right panel) couplings for $\tau \to e$ transitions $\Lambda/|\mathbb{C}^{\mathrm{D}}_{\tau e}|$, $\Lambda/|\mathbb{C}^{\mathrm{V}}_{\tau e}|$ from Belle II [114] *Lower panel:*same for $\tau \to \mu$ transitions $\Lambda/|\mathbb{C}^{\mathrm{D}}_{\tau \mu}|$, $\Lambda/|\mathbb{C}^{\mathrm{V}}_{\tau \mu}|$. Constraints on the axial couplings $\Lambda/|\mathbb{C}^{\mathrm{D5}}_{\tau \ell}|$ and $\Lambda/|\mathbb{C}^{\mathrm{V5}}_{\tau \ell}|$ are essentially of the same size, as the difference is suppressed by m_ℓ/m_τ, cf. Appendix C.5.

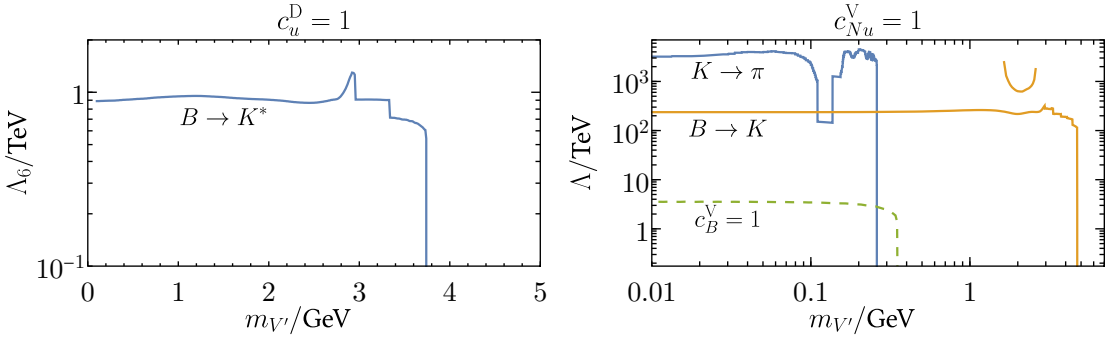

Figure 6.6.: Lower limits on the UV scale in the UV universal scenario for dipole (left panel) and vector couplings (right panel), only showing the strongest constraints. See text for details.

6.4.2. Vector Interaction

The numerically leading contributions to a given (hermitian) flavour transition in LH interactions are shown in Table 5.3 for both sectors. We display the resulting bounds on Λ in the right panel of Figure 6.6 for $c^{\mathrm{V}}_{Nu} = 1$ (there is no constraint from c^{V}_{Nd} at one-loop), which are of order $\Lambda \geq 10^3\,\mathrm{TeV}$ for $K \to \pi$ transitions. These limits are weakened by about an order of magnitude for LDV masses above $m_K - m_\pi$, where the dominant constraint comes from $B \to K$ transitions. In dashed green, we also show the limits coming from the flavour-violating contribution that is induced at the two-loop level by the coupling of the LDV to the anomalous baryon current J^μ_B. The corresponding limit on the scale Λ has been obtained by rescaling the result for $K \to \pi$ of Figure (1) from Ref. [86], giving $\Lambda \geq 3.5\,\mathrm{TeV}$ for $c^{\mathrm{V}}_B = 1$ and $c^{\mathrm{V}}_{Nu} = c^{\mathrm{V}}_{Nd} = 0$. This is about three orders of magnitude weaker than the limit one obtains if the LDV also couples to currents that are not conserved at tree-level, i.e., taking $c^{V}_{Nu} = c^{V}_{Nd} = 1$.

Chapter 7

Unitarity and Perturbativity

Constraints on light particles have been extensively studied in the context of colliders, beam-dump experiments, astrophysics, and cosmology, as well as their phenomenology at precision flavour experiments [1, 88, 93, 105]. Complementary, bounds from theoretical considerations are also possible. In this context, we consider constraints from the unitarity of the S matrix, which allows to set limits on the parameters of the theory. Early work can be traced back to the Froissart–Martin bound [138, 139], the application of unitarity to the Fermi theory [140], and to the introduction of the *tree unitarity* concept [72]. The technique was later pioneered by Lee, Quigg and Thacker (LQT) [10], who set an upper bound of 1 TeV on the Higgs boson mass from $2 \to 2$ boson scattering via partial waves [141]. The LQT bound was later improved and extended by including fermion scattering [142–144]. Since then, the unitarity tool has been extensively used to constrain NP models, such as supersymmetry [145–147], two Higgs doublet models [148–150], DM models [151–154], BSM models tackling the $g-2$ anomaly [155, 156], and others [157–164]. For recent studies, see Refs. [165–167]. Moreover, partial wave analysis is a tool that goes beyond unitarity, see Ref. [168], where anomalous dimensions are extracted from partial waves.

In this chapter we set bounds from perturbative unitarity on flavour interactions between SM fermions mediated by LDVs through the dipole and vector interactions, presented in Section 5.4. For completeness we give the Lagrangian of the model again. Below the EW scale the lowest dimensional interactions of the LDV are described by two classes of operators: dipole and vector interactions. The Lagrangian of the theory is given by

$$\begin{aligned}
\mathscr{L} &= \mathscr{L}_{\text{kin}} + \mathscr{L}_{\text{V}} + \mathscr{L}_{\text{D}}\,, \\
\mathscr{L}_{\text{kin}} &= -\frac{1}{4} V'_{\mu\nu} V'^{\mu\nu} + \frac{m^2_{V'}}{2} V'_{\mu} V'^{\mu}\,, \\
\mathscr{L}_{\text{V}} &= \frac{m_{V'}}{\Lambda} V'_{\mu}\, \overline{f}_i \gamma^{\mu} \left(\mathbb{C}^{V}_{ij} + \mathbb{C}^{V5}_{ij}\gamma_5\right) f_j\,, \\
\mathscr{L}_{\text{D}} &= \frac{1}{\Lambda} V'_{\mu\nu}\, \overline{f}_i \sigma^{\mu\nu} \left(\mathbb{C}^{D}_{ij} + i\mathbb{C}^{D5}_{ij}\gamma_5\right) f_j\,,
\end{aligned} \tag{7.1}$$

where $V'_{\mu\nu} = \partial_\mu V'_\nu - \partial_\nu V'_\mu$ is the LDV field strength, $\sigma^{\mu\nu} = \frac{i}{2}[\gamma^\nu, \gamma^\nu]$, $i \neq j$ denote SM quark or lepton flavours, and the couplings are hermitian matrices in flavour space, $\left(\mathbb{C}^{\text{D(V)}}_{ij}\right)^* = \mathbb{C}^{\text{D(V)}}_{ji}$ and $\left(\mathbb{C}^{\text{D5(V5)}}_{ij}\right)^* = \mathbb{C}^{\text{D5(V5)}}_{ji}$.

We shall consider the flavour and helicity structure of $2 \to 2$ processes. We keep non-zero fermion masses, and take into account the tranverse and longitudinal polarisations for the massive LDV. We set bounds on the size of quark and lepton flavour violating transitions, and on diagonal couplings. We also provide the analytical expressions for the energy growing partial waves in the high energy regime, where $s \gg m_{V'}^2, m_f^2$. While the non-perturbative amplitudes of the renormalisable (UV complete) theory must satisfy the unitarity condition, the amplitudes on a perturbative theory do not necessarily have to. Large couplings can lead to a violation of unitarity, and this signals the breakdown of the perturbative expansion. On the other hand, for non-renormalisable or effective models, such as the SM wihout the Higgs or the Fermi theory, the violation of unitarity signals the presence of NP. At the unitarity violation energy scale new DOF become relevant and restore the unitarity of the theory.

7.1. Partial Wave Unitarity

In order to study the unitarity via partial waves, we consider the helicity amplitudes of a $2 \to 2$ process at tree-level with initial (final) two-particle states $i = i_1 i_2$ ($f = f_1 f_2$). We label the helicity of each particle λ_i, so that the process reads

$$i_1(\lambda_{i_1}) + i_2(\lambda_{i_2}) \to f_1(\lambda_{f_1}) + f_2(\lambda_{f_2})\,. \tag{7.2}$$

The corresponding helicity amplitude is denoted by $\mathcal{T}_{fi}\,(s, \cos\theta)$, where θ is the scattering angle and $\sqrt{s}$ the center of mass energy. The *partial amplitude/wave* is defined as the projection [141, 145]

$$\mathcal{T}^j_{fi}(s) = \frac{\beta_i^{1/4}\beta_f^{1/4}}{32\pi s}\int_0^\pi d\theta \sin\theta\, d^j_{\lambda_i\lambda_f}(\theta)\mathcal{T}_{fi}(s,\theta)\,, \tag{7.3}$$

with fixed angular momentum j. The function $d^j_{\lambda_i\lambda_f}(\theta)$ is the d-Wigner function, see Appendix F, and λ_i, λ_f denote the difference in the helicities of the initial and final state particles, respectively, i.e. $\lambda_i = \lambda_{i_1} - \lambda_{i_2}$ and $\lambda_f = \lambda_i|_{i\leftrightarrow f}$. Further, β_i denotes the Källén function

$$\beta_i = \left(m_{i_1}^2 - \left(\sqrt{s} + m_{i_2}\right)^2\right)\left(m_{i_1}^2 - \left(\sqrt{s} - m_{i_2}\right)^2\right)\,, \quad \beta_f = \beta_i|_{i\leftrightarrow f}\,. \tag{7.4}$$

The unitarity of the S-matrix implies, for each of the partial amplitudes,

$$\frac{1}{2i}\left(\mathcal{T}^j_{fi} - \mathcal{T}^{j*}_{if}\right) = \sum_k \mathcal{T}^{j*}_{kf}\mathcal{T}^j_{ki}\,, \tag{7.5}$$

with k running over intermediate states, see Appendix E for further details. Considering the same initial and final states, $i = f$, and restricting the sum to two-particle states, yields

$$\mathrm{Im}\mathcal{T}^j_{ii} = \sum_k |\mathcal{T}^j_{ki}|^2 \geq |\mathcal{T}^j_{ii}|^2\,. \tag{7.6}$$

Since $\mathrm{Im}\mathcal{T}^j_{ii} \leq |\mathcal{T}^j_{ii}|$, Eq. (7.6) implies

$$|\mathcal{T}^j_{ii}| \leq 1\,. \tag{7.7}$$

This unitarity condition defines the Argand circle [145, 147] in the complex plane, in which all partial waves have to lie in order to ensure the unitarity of the S-matrix. With such a condition, the value of the energy at which the j-th partial wave crosses the unitarity limit, i.e., $|\mathcal{T}^j_{ii}| = 1$, defines the unitarity violation scale, at which NP is expected to be relevant. The physical matrix $\mathcal{T}^j_{fi}$ can be diagonalised, and the bound of Eq. (7.7) applies to its eigenvalues according to

$$|\lambda_{\max}| \leq 1\,, \tag{7.8}$$

where λ_{max} corresponds to the largest eigenvalue, giving the strongest constraint. Using Eq. (7.8), we set bounds on the couplings $\{\mathbb{C}_{ij}^{V}, \mathbb{C}_{ij}^{V5}, \mathbb{C}_{ij}^{D}, \mathbb{C}_{ij}^{D5}\}$ of the Lagrangian in Eq. (7.1). In this work we consider three types of processes:

$$ff \to ff \qquad V'f \to V'f \qquad V'V' \to \bar{f}f \tag{7.9}$$

where V' is the LDV and f the SM fermions. We take into account the flavour and helicity structure of these processes, keep the full fermion mass dependences and consider the longitudinal polarisation of the LDV. Details on the calculation are illustrated in the next section. Regarding the values of j in the partial amplitudes of Eq. (7.3), for $ff \to ff$ and $V'V' \to \bar{f}f$, j takes integer values $j = 0, 1, \ldots$, while for $V'f \to V'f$ it takes half integer values $j = 1/2, 3/2, \ldots$ and typically, the lower j the stronger the bound that is obtained. Moreover, amplitudes that grow with the energy $\propto (\sqrt{s})^{\alpha}$ with $\alpha > 0$ yield a genuine unitarity bound, while amplitudes that do not grow with the energy yield a *perturbativity* bound. Therefore, we consider these two situations separately, and set unitarity bounds in Section 7.4 and perturbativity bounds in Section 7.5, from the three types of processes in Eq. (7.9).

7.2. Partial Wave Decomposition in Flavour and Helicity Space

In this section we outline the details of the calculation of the partial amplitudes defined in Eq. (7.3). Following the discussion in Section 7.1, we consider the following $2 \to 2$ scattering processes at tree level

$$ff \to ff\,, \qquad V'V' \to \bar{f}f\,, \qquad V'f \to V'f\,, \tag{7.10}$$

and their conjugated combinations. For now we consider *only* flavour-violating processes with two flavours i, j with $i \neq j$, and at the end of the section we discuss the flavour-diagonal case. Therefore, the amplitudes are proportional to c_{ij}^2, where c_{ij} denotes any of the couplings in Eq. (7.1), i.e., $c_{ij} \equiv \{\mathbb{C}_{ij}^{V}, \mathbb{C}_{ij}^{V5}, \mathbb{C}_{ij}^{D}, \mathbb{C}_{ij}^{D5}\}$. The relevant set of two-particle states is given by

$$\{f_i f_j, \bar{f}_i f_j, f_i \bar{f}_j, \bar{f}_i \bar{f}_j, \bar{f}_i f_i, \bar{f}_j f_j, V' f_i, V' f_j, V' \bar{f}_i, V' \bar{f}_j\}\,, \tag{7.11}$$

for fixed flavour indices i, j with $i \neq j$. Considering solely flavour violating transitions, the three types of decays, cf. Eq. (7.10), factorise in flavour space and each of these sectors is to be considered separately. The contributing channels to every process are given in Table 7.1, and the scattering amplitudes in flavour space are given as shown in Table 7.2. Notice that for some processes, some channels do not contribute to probing flavour violating couplings (c_{ij}) and are instead only proportional to flavour diagonal couplings (c_{ii}).

In the scattering matrix of Table 7.2, the colour of each block/sector is selected to enhance visual clarity; for example, when we write $ff \to ff$, we mean the whole green transition matrix in Table 7.2 with the corresponding flavour and helicity structure. The non-empty entries in Table 7.2 are specified by the size of their matrix amplitude in helicity space. The helicity of a spin-1/2 fermion can take values $\lambda_f = \{\pm 1/2\}$, while the helicity of a massive spin-1 vector, like the LDV, can take the values $\lambda_{V'} = \{\pm 1, 0\}$, where ± 1 are the transverse modes and 0 the longitudinal mode. Thus, the full transition amplitude given by Table 7.2 is a 57×57 block matrix in helicity space, with sub-matrices from three distinct sectors: $ff \to ff$ (green), $V'f \to V'f$

Table 7.1.: Processes and channels considered. Not all channels in a certain process contribute to probing flavour-violating couplings $c_{ij}, i \neq j$, as some channels have exclusively diagonal flavour structure c_{ii}.

Process	Channels	c_{ij}^2	c_{ii}^2
$f_i f_j \to f_i f_j$	t, u	u	t, u
$\bar{f}_i \bar{f}_j \to \bar{f}_i \bar{f}_j$	t, u	u	t, u
$\bar{f}_i f_j \to \bar{f}_i f_j$	s, t	s	s, t
$\bar{f}_i f_j \to f_i \bar{f}_j$	s, u	s, u	s, u
$V' f_i \to V' f_i$	s, u	s, u	s, u
$V' \bar{f}_i \to V' \bar{f}_i$	s, u	s, u	s, u
$V' V' \to \bar{f}_i f_i$	t, u	t, u	t, u

Table 7.2.: Flavour violating transitions ($i \neq j$) corresponding to the processes in Eq. (7.10). Non-zero entries are specified by the size of the matrix amplitude in helicity space. Every sector is assigned a colour for clarity, i.e., $ff \to ff$ (green), $V'f \to V'f$ (blue) and $V'V' \to f\bar{f}$ (orange).

	$f_i f_j$	$\bar{f}_i f_j$	$f_i \bar{f}_j$	$\bar{f}_i \bar{f}_j$	$\bar{f}_i f_i$	$\bar{f}_j f_j$	$V'V'$	$V'f_i$	$V'f_j$	$V'\bar{f}_i$	$V'\bar{f}_j$
$f_i f_j$	4×4										
$\bar{f}_i f_j$		4×4	4×4								
$f_i \bar{f}_j$		4×4	4×4								
$\bar{f}_i \bar{f}_j$				4×4							
$\bar{f}_i f_i$							4×9				
$\bar{f}_j f_j$							4×9				
$V'V'$					9×4	9×4					
$V'f_i$								6×6			
$V'f_j$									6×6		
$V'\bar{f}_i$										6×6	
$V'\bar{f}_j$											6×6

Table 7.3.: Flavour diagonal transitions ($i = j$). Non-empty entries are specified by the size of the matrix amplitude in helicity space, while empty entries are zero. Every sector is assigned a colour for clarity, i.e., $ff \to ff, V'V' \to \bar{f}f$ (yellow) and $V'f \to V'f$ (blue).

	f_if_i	$\bar{f}_if_i$	$\bar{f}_i\bar{f}_i$	$V'V'$	$V'f_i$	$V'\bar{f}_i$
f_if_i	4×4					
$\bar{f}_if_i$		4×4		4×9		
$\bar{f}_i\bar{f}_i$			4×4			
$V'V'$		9×4				
$V'f_i$					6×6	
$V'\bar{f}_i$						6×6

(blue) and $V'V' \to \bar{f}f$ (orange). The corresponding helicity amplitudes for each of the three types of processes at hand take the following form (independently of the flavour structure)[1]

$$\mathcal{T}^{\lambda_3\lambda_4}_{\lambda_1\lambda_2}(ff \to ff) = \begin{pmatrix} \mathcal{T}^{++}_{++} & \mathcal{T}^{+-}_{++} & \mathcal{T}^{-+}_{++} & \mathcal{T}^{--}_{++} \\ \mathcal{T}^{++}_{+-} & \mathcal{T}^{+-}_{+-} & \mathcal{T}^{-+}_{+-} & \mathcal{T}^{--}_{+-} \\ \mathcal{T}^{++}_{-+} & \mathcal{T}^{+-}_{-+} & \mathcal{T}^{-+}_{-+} & \mathcal{T}^{--}_{-+} \\ \mathcal{T}^{++}_{--} & \mathcal{T}^{+-}_{--} & \mathcal{T}^{-+}_{--} & \mathcal{T}^{--}_{--} \end{pmatrix}, \tag{7.12}$$

$$\mathcal{T}^{\lambda_3\lambda_4}_{\lambda_1\lambda_2}(V'f \to V'f) = \begin{pmatrix} \mathcal{T}^{0+}_{0+} & \mathcal{T}^{0-}_{0+} & \mathcal{T}^{++}_{0+} & \mathcal{T}^{+-}_{0+} & \mathcal{T}^{-+}_{0+} & \mathcal{T}^{--}_{0+} \\ \mathcal{T}^{0+}_{0-} & \mathcal{T}^{0-}_{0-} & \mathcal{T}^{++}_{0-} & \mathcal{T}^{+-}_{0-} & \mathcal{T}^{-+}_{0-} & \mathcal{T}^{--}_{0-} \\ \mathcal{T}^{0+}_{++} & \mathcal{T}^{0-}_{++} & \mathcal{T}^{++}_{++} & \mathcal{T}^{+-}_{++} & \mathcal{T}^{-+}_{++} & \mathcal{T}^{--}_{++} \\ \mathcal{T}^{0+}_{+-} & \mathcal{T}^{0-}_{+-} & \mathcal{T}^{++}_{+-} & \mathcal{T}^{+-}_{+-} & \mathcal{T}^{-+}_{+-} & \mathcal{T}^{--}_{+-} \\ \mathcal{T}^{0+}_{-+} & \mathcal{T}^{0-}_{-+} & \mathcal{T}^{++}_{-+} & \mathcal{T}^{+-}_{-+} & \mathcal{T}^{-+}_{-+} & \mathcal{T}^{--}_{-+} \\ \mathcal{T}^{0+}_{--} & \mathcal{T}^{0-}_{--} & \mathcal{T}^{++}_{--} & \mathcal{T}^{+-}_{--} & \mathcal{T}^{-+}_{--} & \mathcal{T}^{--}_{--} \end{pmatrix}, \tag{7.13}$$

[1] The number of all possible helicity amplitudes for a process $\lambda_1 + \lambda_2 \to \lambda_3 + \lambda_4$ is given by $(2s_1+1)(2s_2+1)(2s_3+1)(2s_4+1)$, where s_i is the spin of the corresponding particle.

$$\mathcal{T}^{\lambda_3\lambda_4}_{\lambda_1\lambda_2}\left(V'V' \to \bar{f}f\right) = \begin{pmatrix} \mathcal{T}^{++}_{00} & \mathcal{T}^{+-}_{00} & \mathcal{T}^{-+}_{00} & \mathcal{T}^{--}_{00} \\ \mathcal{T}^{++}_{+0} & \mathcal{T}^{+-}_{+0} & \mathcal{T}^{-+}_{+0} & \mathcal{T}^{--}_{+0} \\ \mathcal{T}^{++}_{-0} & \mathcal{T}^{+-}_{-0} & \mathcal{T}^{-+}_{-0} & \mathcal{T}^{--}_{-0} \\ \mathcal{T}^{++}_{0+} & \mathcal{T}^{+-}_{0+} & \mathcal{T}^{-+}_{0+} & \mathcal{T}^{--}_{0+} \\ \mathcal{T}^{++}_{0-} & \mathcal{T}^{+-}_{0-} & \mathcal{T}^{-+}_{0-} & \mathcal{T}^{--}_{0-} \\ \mathcal{T}^{++}_{++} & \mathcal{T}^{+-}_{++} & \mathcal{T}^{-+}_{++} & \mathcal{T}^{--}_{++} \\ \mathcal{T}^{++}_{+-} & \mathcal{T}^{+-}_{+-} & \mathcal{T}^{-+}_{+-} & \mathcal{T}^{--}_{+-} \\ \mathcal{T}^{++}_{-+} & \mathcal{T}^{+-}_{-+} & \mathcal{T}^{-+}_{-+} & \mathcal{T}^{--}_{-+} \\ \mathcal{T}^{++}_{--} & \mathcal{T}^{+-}_{--} & \mathcal{T}^{-+}_{--} & \mathcal{T}^{--}_{--} \end{pmatrix} . \tag{7.14}$$

The notation is such that the lower (upper) indices indicate the initial (final) state, with the identification $\lambda_{V'} = \{\pm 1, 0\} \equiv \{\pm, 0\}, \lambda_A = \{\pm 1\} \equiv \{\pm\}$ for the vector boson polarisations and $\lambda_f = \{\pm 1/2\} \equiv \{\pm\}$ for the fermion helicities. While with this notation many amplitudes have the same labeling for different processes, in the coming discussion it should be clear to which process we are referring each time. Regarding the colours for processes with external LDVs, we distinguish between three cases: both bosons have longitudinal polarisation (LL, blue), both have transverse polarisation (TT, gray), and one is transverse while the other one is longitudinal (TL, green). Such distinctions will be relevant for the coming discussion.

For flavour-diagonal interactions, corresponding to $i = j$, the situation is slightly different to the flavour violating case. For *only* diagonal interactions of Eq. (7.1), the set of two-particle states is given by

$$\{f_i f_i, \bar{f}_i f_i, \bar{f}_i \bar{f}_i, V' f_i, V' \bar{f}_i\} , \tag{7.15}$$

for a fixed flavour index i. The corresponding matrix amplitude in flavour space is given in Table 7.3, with the non-empty entries of the table specified by the size of the corresponding matrix in helicity space, see Eq. (7.13). Unlike in the flavour-violating case, $ff \to ff$ and $V'V' \to \bar{f}f$ mix in the transition matrix of Table 7.3. For flavour violating insertions, see Table 7.2, they are separated because we only consider insertions with $i \neq j$, and thus $V'V' \to \bar{f}_i f_i$ and $\bar{f}_i f_j \to \bar{f}_i f_j$ (and all other conjugated combinations) contribute to different sectors. For $i = j$, it is clear that they combine.

With such a setup, the first task corresponds to computing the helicity amplitudes $\mathcal{T}_{fi}(s, \theta)$ for a process $i_1(\lambda_{i_1}) + i_2(\lambda_{i_2}) \to f_1(\lambda_{f_1}) + f_2(\lambda_{f_2})$. Details of the calculation can be found in Appendix D. Once the helicity amplitudes are obtained, the partial amplitudes are computed according to Eq. (7.3). Then, following Section 7.1, the transition matrices of Table 7.2 and Table 7.3 must be diagonalised in the flavour violating and diagonal case, respectively. Each sector (process) yields eigenvalues, and the strongest bound on the corresponding coupling is found from the largest eigenvalue λ_{max} by demanding

$$|\lambda_{\text{max}}| \leq 1 . \tag{7.16}$$

7.3. Energy Growth and Infrared Divergences

As discussed in the previous section, in our analysis we consider the following processes with SM fermions f and the LDV V'

$$ff \to ff , \qquad V'f \to V'f , \qquad V'V' \to \bar{f}f , \tag{7.17}$$

as well as their conjugated ones. For the purpose of clarity in the coming discussion, we simply consider the processes in Eq. (7.17), since the following argument holds independently of conjugation, flavour and helicity.

We wish to elucidate which processes grow with energy, meaning that their amplitude $\propto (\sqrt{s})^\alpha$ with $\alpha > 0$ at high energies. For such processes the unitarity Eq. (7.7) is violated above a certain scale, as in the high energy regime amplitudes grow uncontrollably. In this scenario, a radial Higgs-like mode would be needed in order to restore the unitarity of the theory, just as in the EW sector of the SM [10]. On the other hand, processes which do not grow with energy can also violate Eq. (7.7), e.g., for large couplings. In this case the interactions are strongly coupled and perturbation theory breaks down. In the first scenario, the amplitudes yield a unitarity bound, while in the second scenario they set a perturbativity bound.

In order to identify which processes in Eq. (7.17) have energy growing amplitudes (and thus set a unitarity bound), we can use the sum rules derived from the Slavnov–Taylor identities (STI). These relate the couplings of the interactions among each other to ensure the unitarity of the theory when certain processes grow with the energy. We follow the analysis of Ref. [169], and introduce a radial Higgs mode h coupled to the fermions and the LDV V'

$$\mathscr{L} = \sum_\sigma Y^\sigma_{hff} h \bar{f} P_\sigma f + \sum_\sigma \mathbb{C}^{V\sigma}_{V'ff} V'_\mu \bar{f} \gamma^\mu P_\sigma f + \frac{1}{2} g_{V'V'h} V'_\mu V'^\mu h \,, \tag{7.18}$$

where the second term corresponds to the interaction $\mathscr{L}_{\rm V}$ of Eq. (5.41) in the L/R basis (up to the $m_{V'}/\Lambda$ prefactor) for a fixed fermion flavour, $i = j$. The index σ denotes the chirality, $\sigma = {\rm L/R}$, while the subindices in the couplings are introduced to illustrate their corresponding interaction. We consider one single fermion with mass m for simplicity and stress that the discussion also applies to a more general scenario with more fermion flavours. From the STI, the following sum rule is obtained

$$g_{V'V'h} Y^\sigma_{hff} = -2m \left(\mathbb{C}^{V\sigma}_{V'ff}\right)^2 - 2m \left(\mathbb{C}^{V\bar{\sigma}}_{V'ff}\right)^2 + 4m \left(\mathbb{C}^{V\sigma}_{V'ff} \mathbb{C}^{V\bar{\sigma}}_{V'ff}\right) \,, \tag{7.19}$$

where $\bar{\sigma} = \sigma|_{\rm L\leftrightarrow R}$. Recall that Eq. (7.19) is a relation among couplings that guarantees the cancellation of energy growing amplitudes, rendering the theory unitary at high energies. Tree-level amplitudes from the processes $ff \to ff, V'f \to V'f, V'V' \to \bar{f}f$ are precisely of order $\mathcal{O}((\mathbb{C}^{V\sigma}_{V'ff})^2)$, with the couplings at such order being on the RHS of Eq. (7.19). According to Eq. (7.19), energy growing amplitudes from the processes $ff \to ff, V'f \to V'f, V'V' \to \bar{f}f$ are canceled by amplitudes of order $\mathcal{O}(g_{V'V'h} Y^\sigma_{hff})$, as dictated by the LHS of Eq. (7.19). Therefore, $ff \to ff$ processes cannot grow with energy, because if that were the case such amplitudes could not be canceled by amplitudes with $g_{V'V'h}, Y^\sigma_{hff}$ vertices. Following this line of reasoning, it is clear that the processes growing with energy are the ones with two external LDVs, $V'f \to V'f$ and $V'V' \to \bar{f}f$, which are taken care of by amplitudes with $g_{V'V'h}, Y^\sigma_{hff}$ vertices where h is propagating[1]. Therefore, in the high energy regime $V'f \to V'f$ and $V'V' \to \bar{f}f$ contain energy growing amplitudes that allow to set a unitarity bound, while $ff \to ff$ sets a perturbativity bound. For the $\mathscr{L}_{\rm D}$ interaction we cannot follow these arguments as it is a dim-5 operator in the EFT and the STI do not apply to non-renormalisable interactions. By using a naive power counting we expect all processes with $\mathscr{L}_{\rm D}$ insertions to grow with energy $\propto (s/\Lambda^2)^\alpha$ with $\alpha > 0$.

An interesting observation can be made from the sum rule of Eq. (7.19). Amplitudes with two $\mathscr{L}_{\rm V}$ vertices and two external V' grow with energy proportionally to the fermion mass, that is, their amplitudes scale as $\propto m(\sqrt{s})^\alpha$ with $\alpha > 0$. Therefore, considering massive fermions is

[1] We will see in Section 7.4 that the amplitudes growing with the energy are the ones with longitudinally polarised V', the sum rules do not specify which helicity amplitudes grow with the energy.

necessary in order to account for the amplitudes that grow with energy. In our calculation we indeed find such a behavior, albeit in a more complicated manner since we consider FCNCs. We will discuss this finding in more detail, for the time being we are content to note which processes grow with energy without the need to explicitly compute any amplitudes.

We have seen that $ff \to ff$ processes with $\mathscr{L}_{\rm V}$ insertions cannot grow with the energy. But infrared (IR) divergences can arise for such type of processes, which can manifest as energy growing amplitudes, in contradiction with the sum rule Eq. (7.19). Concretely, for scattering angles $\theta = 0$ and $\theta = \pi$, t, u channels in the high energy regime diverge respectively according to[1]

$$\mathcal{T}_t \sim \frac{1}{t} \sim \frac{1}{s\,(1-\cos\theta)}\,, \quad \mathcal{T}_u \sim \frac{1}{u} \sim \frac{1}{s\,(1+\cos\theta)}\,. \tag{7.20}$$

The behaviour of Eq. (7.20) typically manifests as a logarithmic term [157, 168] in the partial wave, akin to the Bhabha and Moller scattetring in QED. As an example, we consider the t-channel helicity amplitude of $\bar{f}f \to \bar{f}f$ with $\lambda_f = 1/2$, two vertices of $\mathscr{L}_{\rm V}$ and a propagating LDV. The Proca propagator for the massive V' reads

$$\Delta^{\mu\nu}_{V'} = \frac{-i}{k^2 - m^2_{V'}}\left(g^{\mu\nu} - \frac{k^\mu k^\nu}{m^2_{V'}}\right)\,. \tag{7.21}$$

Let us consider the high energy regime and take the fermions and LDV to be massless. Computing the $j = 0$ partial wave according to Eq. (7.3) (for which $d^0_{00} = 1$) we find

$$\mathcal{T}^0 \sim 2\log\left(\sin\frac{\theta}{2}\right)\Big|^{\theta=\pi}_{\theta=0}\,, \tag{7.22}$$

which diverges at $\theta = 0$. This singularity comes exclusively from the $g^{\mu\nu}$ piece in Eq. (7.21). The $k^\mu k^\nu$ piece is proportional to the fermion masses, and thus vanishes for massless fermions. But even for massive fermions the divergence of Eq. (7.22) is present. Indeed, the divergence comes from the singularity in the t-channel as illustrated in Eq. (7.20), where the LDV mass is set to zero. If we consider keeping the LDV mass, the θ integration poses no issues and we obtain the corresponding partial amplitude, which is found to have the following behaviour

$$\mathcal{T}^0 \sim \log\left(\frac{s}{m^2_{V'}}\right)\,. \tag{7.23}$$

According to Eq. (7.23), the process $\bar{f}f \to \bar{f}f$ grows with energy $\propto \log s$. The reason Eq. (7.23) has this form is because $m_{V'}$ acts as a regulator of the θ divergence in Eq. (7.22), so the divergence moved from $\theta = 0$ to $m_{V'} = 0$. But we argued that $ff \to ff$ processes cannot have such a behaviour, so the scaling with energy of Eq. (7.23) cannot be considered a unitarity problem, and at high energies one should not extract unitarity constraints from amplitudes with the form of Eq. (7.23). Since the singularity comes from the $g^{\mu\nu}$ term of the LDV propagator in Eq. (7.21), we drop this term and consider only the $k^\mu k^\nu$ term of the propagator [144, 153]. We are therefore forced to keep non-zero fermion masses for the $ff \to ff$ amplitudes to not vanish. This discussion is equivalent for the u-channel for which the divergence is at $\theta = \pi$, and also for all other processes with external fermions and a propagating LDV. We stress that this is what we do in the case of unitarity in Section 7.4.1, in which only the corresponding energy growing amplitudes of the $V'V' \to \bar{f}f, V'f \to V'f$ processes are considered, while in the case of perturbativity, Section 7.5, we actually do the inverse procedure and keep only the $g^{\mu\nu}$ piece of the LDV propagator, and consider only transverse modes of V' for the $V'V' \to \bar{f}f, V'f \to V'f$ processes. This is because energy growing amplitudes are directly linked to longitudinally polarised V', and thus, we

[1] See Appendix D for the kinematics of $2 \to 2$ processes.

Table 7.4.: We indicate which of the three sectors $ff \to ff, V'V' \to \bar{f}f, V'f \to V'f$ yield unitarity and perturbativity bounds for the vector and dipole interactions.

Interaction	Perturbativity	Unitarity
$\mathscr{L}_{\rm V}$	All	$V'V' \to \bar{f}f, V'f \to V'f$
$\mathscr{L}_{\rm D}$	$\times$	All

shall not consider these modes in our perturbativity analysis. In this scenario, even if amplitudes of the form of Eq. (7.23) arise, we understand that these amplitudes are not to be taken as energy growing amplitudes, i.e., they are not valid for $\sqrt{s} \to \infty$. Notice that for the $\mathscr{L}_{\rm D}$ interaction of Eq. (7.1), the $k^\mu k^\nu$ piece of the LDV propagator does not contribute due to the Dirac structure, $\mathscr{L}_{\rm D} \propto \sigma^{\mu\nu}$. For the dipole interaction we keep the $g^{\mu\nu}$ piece of the LDV propagator, which yields no issues because the interaction is dim-5 in the EFT and all amplitudes genuinely grow with energy for all processes. We must remark that when we say that $V'V' \to \bar{f}f, V'f \to V'f$ processes grow with the energy, we mean that some of the corresponding helicity amplitudes of Eq. (7.13) grow with energy, but not all do. This is indeed what we find in our calculation, and therefore (for $\mathscr{L}_{\rm V}$) only some helicity amplitudes of the $V'V' \to \bar{f}f, V'f \to V'f$ processes yield a unitarity bound, but all three sectors yield a perturbativity bound since all contain helicity amplitudes that do not grow with energy. In the coming discussion we point out which helicity amplitudes yield unitarity bounds. On the other hand, all amplitudes for all processes grow with the energy for the $\mathscr{L}_{\rm D}$ interaction. See Table 7.4, where we specify which processes yield unitarity bounds and which yield perturbativity for each interaction.

7.4. Unitarity

In this section we show the analytical expressions for the partial amplitudes of each sector that grow with the energy, and set bounds on the corresponding couplings of the model in Eq. (7.1). The expressions are given in the high energy regime $s \gg m_{V'}^2, m_i^2, m_j^2$, and thus in powers of $\sqrt{s}$.

7.4.1. Vector Interaction

We start discussing the unitarity amplitudes in the context of the interaction $\mathscr{L}_{\rm V}$ from Eq. (7.1). From the discussion in Section 7.3, we expect that $ff \to ff$ processes do not grow with the energy, and thus, do not yield a unitarity bound. This is confirmed by our calculation in which we find the $ff \to ff$ amplitudes to scale according to $\propto (\sqrt{s})^\alpha$ with $\alpha < 0$ in the high energy regime. On the other hand, the processes $V'f \to V'f, V'V' \to \bar{f}f$ with LDVs have energy growing amplitudes $\propto (\sqrt{s})^\alpha$ with $\alpha > 0$. For these two processes, we have the colour assignments LL, TL or TT depending on the helicities of the LDVs, see Eq. (7.13). We find that the LL sector with two longitudinally polarised LDVs gives energy growing amplitudes. This can be understood from the fact that longitudinal modes are enhanced in the high energy, that is, for $s \gg m_{V'}^2 \to \epsilon_{\rm L}(k) \sim k/m_{V'}$. In order to find the energy growing amplitudes we consider the amplitude matrix of Table 7.2 and expand all amplitudes in the limit $s \gg m_{V'}^2, m_i^2, m_j^2$. The corresponding energy growing partial amplitudes are given as follows

- $V'V' \to \bar{f}f$:

$$\left(\mathcal{T}_{00}^{++}\right)^{j=0} = \left(\mathcal{T}_{00}^{--}\right)^{j=0} = \frac{\sqrt{s}}{8\sqrt{2}\pi\Lambda^2}\sqrt{(m_i-m_j)^2\left|\mathbb{C}_{ij}^{V}\right|^4+(m_i+m_j)^2\left|\mathbb{C}_{ij}^{V5}\right|^4+2|\mathbb{C}_{ij}^{V}|^2|\mathbb{C}_{ij}^{V5}|^2\left(m_i^2-m_j^2\cos 2\left(\phi_1-\phi_5\right)\right)}\,. \tag{7.24}$$

- $V'f \to V'f$:

$$\left(\mathcal{T}_{0+}^{0-}\right)^{j=1/2} = \left(\mathcal{T}_{0-}^{0+}\right)^{j=1/2} = \frac{\sqrt{s}}{16\pi\Lambda^2}\sqrt{(m_i-m_j)^2\left|\mathbb{C}_{ij}^{V}\right|^4+(m_i+m_j)^2\left|\mathbb{C}_{ij}^{V5}\right|^4+2|\mathbb{C}_{ij}^{V}|^2|\mathbb{C}_{ij}^{V5}|^2\left(m_i^2-m_j^2\cos 2\left(\phi_1-\phi_5\right)\right)}\,. \tag{7.25}$$

We observe that the amplitudes of Eq. (7.24)–(7.25) are proportional to the fermion masses, appearing as the difference (sum) for $\mathbb{C}_{ij}^{V}(\mathbb{C}_{ij}^{V5})$. Therefore, if we neglect the fermion masses (i.e., setting $m_i = 0 \forall i$) no energy growing amplitudes are obtained and no unitarity bounds can be set for the vector interaction. Moreover, for $m_i = m_j$ the $\mathbb{C}_{ij}^{V}$ contributions vanish. This highlights the importance of taking into account the distinct fermion masses in the amplitudes for the flavour violating transitions. From these amplitudes we can infer the corresponding amplitudes for the diagonal case by setting $m_i = m_j$[1]. The leading amplitudes for the axial coupling $\mathbb{C}_{ii}^{V5}$ correspond to the ones in Eq. (7.24)–(7.25), since they have a proportionality factor $(m_i+m_j) = 2m_i$ for $m_i = m_j$. Recall that in the diagonal scenario the $ff \to ff$ and $V'V' \to \bar{f}f$ processes mix, see Table 7.3 (yellow block), but since $ff \to ff$ processes do not yield unitarity issues, the relevant amplitude in this mixing sector comes from the energy growing $V'V' \to \bar{f}f$ process, given in Eq. (7.24), with $m_i = m_j$. On the other hand, the $\mathbb{C}_{ii}^{V}$ terms of the leading amplitudes Eq. (7.24)–(7.25) vanish for $m_i = m_j$ as they have a prefactor $(m_i - m_j)$. In this case, there are no energy growing amplitudes in the high energy regime for $\mathbb{C}_{ii}^{V}$, and setting $m_i = m_j$ is effectively equivalent to considering massless fermions.

We wish to set unitarity bounds on the Λ/coupling combination. To this end and as discussed in Section 7.2, the corresponding matrices of Table 7.2 have to be diagonalised and the strongest bound is found from the largest eigenvalue according to Eq. (7.16). The largest eigenvalue of the matrix amplitude corresponds to the $V'V' \to \bar{f}f$ sector's largest eigenvalue. Notice from the amplitudes of Eq. (7.24)–(7.25) that the $V'V' \to \bar{f}f$ amplitude is larger than the one of $V'f \to V'f$. We find the largest eigenvalue to be

$$|\lambda_{\text{max}}| = 2\left|\left(\mathcal{T}_{00}^{++}\right)^{j=0}\right| = 2\left|\left(\mathcal{T}_{00}^{--}\right)^{j=0}\right|\,. \tag{7.26}$$

To extract a unitarity bound, we consider one coupling $(\mathbb{C}_{ij}^{V}, \mathbb{C}_{ij}^{V5})$ at a time. Then, we apply the unitarity condition $|\lambda_{\text{max}}| \leq 1$ discussed in Section 7.2, and we fix the value of $\sqrt{s}$ so that we demand the theory to be unitary up to the considered $\sqrt{s}$ value. Therefore, the unitarity bound on each coupling for a general flavour violating ij transition is given by

$$\begin{aligned}\left|\frac{\Lambda}{\mathbb{C}_{ij}^{V}}\right| &\geq \left(\frac{s}{2}\right)^{1/4}\sqrt{\frac{m_i-m_j}{4\pi}}\,,\\ \left|\frac{\Lambda}{\mathbb{C}_{ij}^{V5}}\right| &\geq \left(\frac{s}{2}\right)^{1/4}\sqrt{\frac{m_i+m_j}{4\pi}}\,,\end{aligned} \tag{7.27}$$

[1] We have of course checked that setting $m_i = m_j$ yields the correct diagonal amplitudes by direct calculation of the diagonal processes in Table 7.3.

Table 7.5.: Lower unitarity bounds on $\Lambda/\text{coupling}$ for the flavour violating vector interaction at fixed $\sqrt{s} = 1$ TeV and $\sqrt{s} = 10$ TeV.

	$\sqrt{s} = 1$ TeV		$\sqrt{s} = 10$ TeV	
Sector	$\Lambda/\mathbb{C}_{ij}^{V}$/GeV	$\Lambda/\mathbb{C}_{ij}^{V5}$/GeV	$\Lambda/\mathbb{C}_{ij}^{V}$/GeV	$\Lambda/\mathbb{C}_{ij}^{V5}$/GeV
bs	15.16	15.51	47.95	49.04
bd	15.33	15.35	48.47	48.53
sd	2.23	2.35	7.07	7.43
cu	8.44	8.46	26.71	26.76

while for flavour diagonal transitions ($m_i = m_j$) we have the following unitarity bound on the axial coupling $\mathbb{C}_{ii}^{V5}$

$$\left|\frac{\Lambda}{\mathbb{C}_{ii}^{V5}}\right| \geq \left(\frac{s}{2}\right)^{1/4} \sqrt{\frac{m_i}{2\pi}}\,, \tag{7.28}$$

and no unitarity bound can be set for the diagonal $\mathbb{C}_{ii}^{V}$ couplings. From the expressions in Eq. (7.27) and Eq. (7.28) we set numerical bounds for different flavour-violating and diagonal transitions $bd, bs, cu, sd, bb, ss, dd, cc, uu$, see Table 7.5 and Table 7.6, respectively, for the explicit numerical bounds at fixed $\sqrt{s} = 1$ TeV and $\sqrt{s} = 10$ TeV. In Figure 7.1 we show the bounds on the couplings for different flavour violating transitions, and in Figure 7.2 we show the bounds on the flavour diagonal coupling $\mathbb{C}_{ii}^{V5}$. The plots are such that the region below the curves are excluded by unitarity. As given by Eq. (7.27) and Eq. (7.28), the bounds are more stringent for transitions with heavier quarks, i.e., bs (bb) gets a more constraining bound than sd (ss)in the flavour-violating (diagonal) case. Moreover, since $m_b \gg m_{d,s}$, for the bs and bd transitions the bounds are practically identical (see the corresponding numerical bounds in Table 7.5). More generally, notice that the bounds on $\mathbb{C}_{ij}^{V}$, $\mathbb{C}_{ij}^{V5}$ shown in Figure 7.1 and with the numerical values in Table 7.5, are practically the same, since in every flavour-violating transition ij one quark is considerably heavier than the other, and thus $m_i - m_j \approx m_i + m_j$, rendering the bounds of Eq. (7.27) equivalent for a fixed flavour transition. Crucially, the energy growing amplitudes of Eq. (7.24)–(7.25), and thus, the unitarity bounds Eq. (7.27)–(7.28) are independent of the mass of the LDV $m_{V'}$. Therefore, the bounds derived here are valid for any value of the LDV mass (of course, with $m_{V'} \ll \sqrt{s}$) and solely controlled by the value of $\sqrt{s}$, with the fermion masses fixed to their corresponding values for each transition. While the bounds from unitarity are much weaker compared to the bounds from two body decays, discussed in Chapter 6, the unitarity bounds are valid for all the range of $m_{V'}$, as they do not have a kinematical endpoint unlike the two body decays, as can seen in the plots of Section 6.2. Moreover, the unitarity analysis employs a theoretical bound, and therefore no experimental input is needed to extract unitarity constraints.

7.4.2. Dipole Interaction

For the dipole couplings of Eq. (7.1) all processes yield energy growing amplitudes since the operator is of dimension five. The corresponding amplitudes are the same for every flavour transition and coupling ($\mathbb{C}_{ij}^{D}$, $\mathbb{C}_{ij}^{D5}$) in the high energy limit, that is, independent of the fermion masses. Of the three sectors LL, TL, TT, see Eq. (7.13), the leading amplitudes for $V'f \to V'f, V'V' \to \bar{f}f$

Table 7.6.: Lower unitarity bounds on $\Lambda/\mathbb{C}_{ii}^{V5}$ for diagonal flavour transitions at fixed $\sqrt{s} = 1$ TeV and $\sqrt{s} = 10$ TeV.

	$\sqrt{s} = 1$ TeV	$\sqrt{s} = 10$ TeV
Sector	$\Lambda/\mathbb{C}_{ii}^{V5}$/ GeV	$\Lambda/\mathbb{C}_{ii}^{V5}$/ GeV
bb	21.69	68.59
ss	3.24	10.25
dd	0.72	2.29
cc	11.96	37.81
uu	0.49	1.56

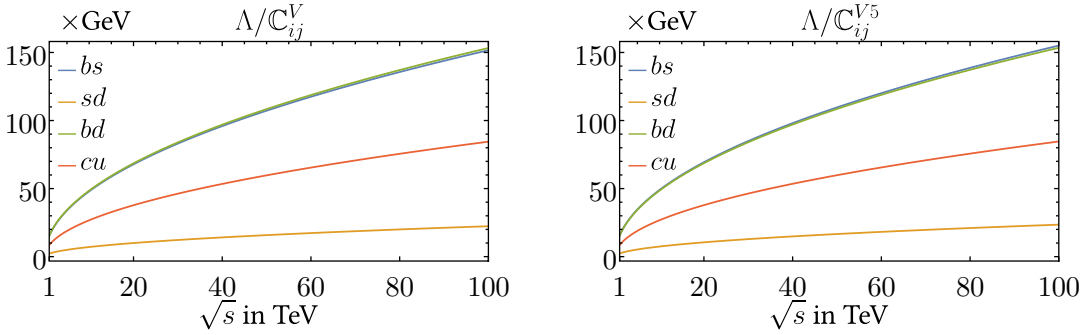

Figure 7.1.: Unitarity bounds on the vector couplings $\mathbb{C}_{ij}^{V}, \mathbb{C}_{ij}^{V5}$ as a function of $\sqrt{s}$ for different flavour-violating quark transitions.

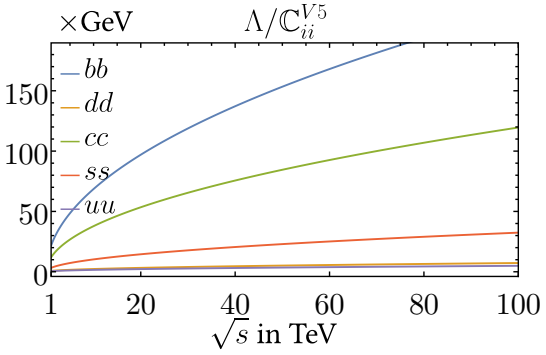

Figure 7.2.: Unitarity bounds on the vector couplings $\mathbb{C}_{ii}^{V5}$ as a function of $\sqrt{s}$ for different flavour-diagonal quark transitions.

correspond to the TT sector. This can be understood from the fact that longitudinal vector boson polarisations are proportional to the LDV momenta at $s \gg m_{V'}^2 \to \epsilon_{\mathrm{L}}(k) \sim k/m_{V'}$, and thus LL, TL amplitudes are suppressed by the dirac structure $\sigma^{\mu\nu}$ of the interaction $\mathscr{L}_{\mathrm{D}}$. Just as in the case of the vector interaction, we expand the matrix amplitudes of Table 7.2 in the limit $s \gg m_{V'}^2, m_i^2, m_j^2$. The corresponding energy growing amplitudes are given as follows

- $V'V' \to \bar{f}f$:

$$\left(\mathcal{T}^{+-}_{++}\right)^{j=1} = \left(\mathcal{T}^{-+}_{++}\right)^{j=1} = \left(\mathcal{T}^{+-}_{--}\right)^{j=1} = \left(\mathcal{T}^{-+}_{--}\right)^{j=1} = \frac{s}{12\pi\Lambda^2}\sqrt{|\mathbb{C}^{D}_{ij}|^4 + |\mathbb{C}^{D5}_{ij}|^4 + 2|\mathbb{C}^{D}_{ij}|^2|\mathbb{C}^{D5}_{ij}|^2 \sin\left(\phi_{1D} - \phi_{5D}\right)}\,, \tag{7.29}$$

- $V'f \to V'f$:

$$\left(\mathcal{T}^{++}_{++}\right)^{j=1/2} = \left(\mathcal{T}^{--}_{--}\right)^{j=1/2} = \frac{s}{4\pi\Lambda^2}\sqrt{|\mathbb{C}^{D}_{ij}|^4 + |\mathbb{C}^{D5}_{ij}|^4 + 2|\mathbb{C}^{D}_{ij}|^2|\mathbb{C}^{D5}_{ij}|^2 \sin\left(\phi_{1D} - \phi_{5D}\right)}\,, \tag{7.30}$$

- $ff \to ff$:

For this sector there are two distinct leading amplitudes corresponding to distinct conjugated processes, which are of the same order in the expansion, i.e. $\propto s$. The leading amplitudes read

$$\left(\mathcal{T}^{--}_{++}\right)^{j=0}_{ff\to ff} = \left(\mathcal{T}^{++}_{--}\right)^{j=0}_{ff\to ff} = \left(\mathcal{T}^{--}_{++}\right)^{j=0}_{f\bar{f}\to\bar{f}f} = \left(\mathcal{T}^{++}_{--}\right)^{j=0}_{f\bar{f}\to\bar{f}f} = \frac{3s}{8\pi\Lambda^2}\sqrt{|\mathbb{C}^{D}_{ij}|^4 + |\mathbb{C}^{D5}_{ij}|^4 + 2|\mathbb{C}^{D}_{ij}|^2|\mathbb{C}^{D5}_{ij}|^2 \cos 2\left(\phi_{1D} - \phi_{5D}\right)}\,, \tag{7.31}$$

while there is also the following partial amplitudes

$$\begin{aligned}&\left(\mathcal{T}^{++}_{++}\right)^{j=0}_{\bar{f}f\to\bar{f}f} = \left(\mathcal{T}^{--}_{--}\right)^{j=0}_{\bar{f}f\to\bar{f}f} = \left(\mathcal{T}^{--}_{++}\right)^{j=0}_{\bar{f}f\to\bar{f}f} = \\ &\left(\mathcal{T}^{++}_{--}\right)^{j=0}_{\bar{f}f\to\bar{f}f} = \left(\mathcal{T}^{++}_{++}\right)^{j=0}_{\bar{f}f\to f\bar{f}} = \left(\mathcal{T}^{--}_{--}\right)^{j=0}_{\bar{f}f\to f\bar{f}} = \\ &\frac{s}{8\pi\Lambda^2}\sqrt{|\mathbb{C}^{D}_{ij}|^4 + |\mathbb{C}^{D5}_{ij}|^4 + 2|\mathbb{C}^{D}_{ij}|^2|\mathbb{C}^{D5}_{ij}|^2 \cos 2\left(\phi_{1D} - \phi_{5D}\right)}\,,\end{aligned} \tag{7.32}$$

We observe that the leading amplitudes in every sector and process are independent of the fermion masses and the LDV mass $m_{V'}$. Therefore, unlike for the vector interaction $\mathscr{L}_{\rm V}$, see Eq. (7.24)–(7.25), for $\mathscr{L}_{\rm D}$ one can set the fermion masses to zero to find the unitarity bounds. Therefore, for the diagonal $m_i = m_j$ case the amplitudes are the same, except that now $V'V' \to \bar{f}f$ and $ff \to ff$ processes mix as shown in Table 7.3. The leading amplitude for these mixing processes corresponds to the $ff \to ff$ one given in Eq. (7.31). The largest eigenvalue among the three sectors of Table 7.2 comes from $ff \to ff$ processes, which we find to be

$$|\lambda_{\rm max}| = 2\left|\left(\mathcal{T}^{--}_{++}\right)^{j=0}_{ff\to ff}\right|\,. \tag{7.33}$$

Considering a coupling $(\mathbb{C}^{D}_{ij}, \mathbb{C}^{D5}_{ij})$ at a time and applying the unitarity condition $|\lambda_{\rm max}| \leq 1$, we find the unitarity bound on the Λ/coupling combination to be

$$\left|\frac{\Lambda}{\mathbb{C}^{D(5)}_{ij}}\right| \geq \left(\frac{3s}{4\pi}\right)^{1/2} \approx \frac{\sqrt{s}}{2}\,, \tag{7.34}$$

for both couplings and all flavour violating and diagonal transitions. Therefore, for the dipole interaction the unitarity bound takes a very simple form and is totally controlled by the value of $\sqrt{s}$, with no fermion mass dependence. In Table 7.7 we give the numerical bound on the size of Λ/coupling for $\sqrt{s} = 1$ TeV and $\sqrt{s} = 10$ TeV. In Figure 7.3 we plot the bound as a function of $\sqrt{s}$, where the region below the curve is excluded. As in the case of the vector interaction, the unitarity bound of Eq. (7.34) is independent of the $m_{V'}$ mass, and thus, equal for all $m_{V'}$ values (with $m_{V'} \ll \sqrt{s}$).

Table 7.7.: Lower unitarity bounds on $\Lambda/$coupling of the dipole interaction for $\sqrt{s} = 1$ TeV and $\sqrt{s} = 10$ TeV for any ij flavour violating and diagonal transition.

$\sqrt{s}$/ TeV	$\Lambda/\mathbb{C}_{ij}^{D(5)}$/ TeV
1	0.49
10	4.89

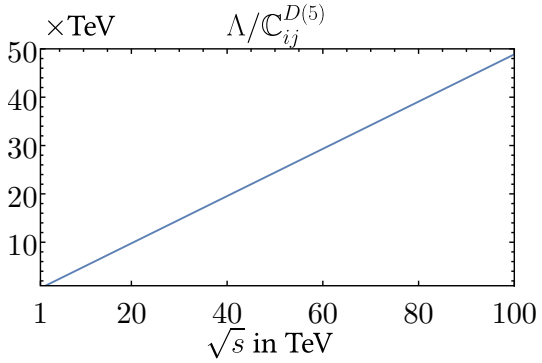

Figure 7.3.: Unitarity bounds on the dipole couplings $\mathbb{C}_{ij}^{D}, \mathbb{C}_{ij}^{D5}$ as a function of $\sqrt{s}$. This bound is valid for any flavour violating and flavour diagonal transition, as the corresponding bound is independent of the fermion masses, see Eq. (7.34).

7.5. Perturbativity

In this section we discuss the perturbativity amplitudes and bounds, that is, partial amplitudes that do not grow with the energy. In this scenario, we only have to consider the vector interaction $\mathscr{L}_{\rm V}$, since for the dipole interaction $\mathscr{L}_{\rm D}$ all amplitudes grow with the energy. Of the three processes under consideration, all of the them yield perturbativity bounds, with $ff \to ff$ only giving perturbaitivity and no unitarity bounds, because as discussed in Section 7.3, this sector has no amplitudes that grow with the energy. Indeed, in the unitarity Section 7.4.1 we did not consider $ff \to ff$ processes. In this section we consider *only* transverse modes of the LDV, and therefore for the $V'f \to V'f, V'V' \to \bar{f}f$ processes we only take into account the TT helicity modes, see Eq. (7.13). For $ff \to ff$, we keep the $g^{\mu\nu}$ piece from the LDV propagator, and drop the $k^\mu k^\nu/m_{V'}^2$ piece corresponding to the longitudinal polarisation of V', see the discussion of Section 7.3. This implies that some partial waves grow with $\propto \log s$, but since now we focus on perturbativity and not in the high energy regime, we are safe to do this as long as we understand the analysis of $ff \to ff$ to be valid up to some energy, i.e., not valid for $\sqrt{s} \to \infty$. Crucially, singularities appear for $m_{V'} = 0$ in $ff \to ff$, and thus we shall avoid considering a massless LDV. Moreover, for each of the processes $V'f \to V'f$, $V'V' \to \bar{f}f$, and $ff \to ff$, t and u channels, see Table 7.1, exhibit kinematical singularities in the partial waves arising from the θ integration. We circumvent these singularities by deriving the conditions on the masses and energy values that define a range free of such singular behavior. In the following, we give the conditions for every sector, in both the flavour-violating and diagonal case:

- $\boldsymbol{ff \to ff}$:

$$\frac{s\left(s + m_{V'}^2 - 2m_i^2 - 2m_j^2\right)}{\left(m_i^2 - m_j^2\right)^2 - m_{V'}^2 s} < 0\,, \quad m_{V'} > 0 \quad \text{for } i \neq j. \tag{7.35}$$

$$s > 4m^2 - m_{V'}^2\,, \quad m_{V'} > 0 \quad \text{for } i = j\,. \tag{7.36}$$

- $\boldsymbol{V'f \to V'f}$:

$$-1 > \frac{\left(m_i^2 - m_{V'}^2\right)^2 + 2s\left(m_{V'}^2 + m_i^2 - m_j^2\right) - s^2}{m_i^4 - 2m_i^2\left(m_{V'}^2 + s\right) + \left(m_{V'}^2 - s\right)^2} > 1\,, \quad \text{for } i \neq j. \tag{7.37}$$

$$-1 > \frac{2m_{V'}^2 s + \left(m^2 - m_{V'}^2\right)^2 - s^2}{m^4 - 2m^2\left(m_{V'}^2 + s\right) + \left(m_{V'}^2 - s\right)^2} > 1 \quad \text{for } i = j\,, \tag{7.38}$$

and the equivalent condition for $i \neq j$ with $m_i \leftrightarrow m_j$.

- $\boldsymbol{V'V' \to \bar{f}f}$:

$$-1 > -\frac{m_i^4 - 2\left(m_{V'}^2 - s\right)m_i^2 + m_{V'}^4 + 2m_{V'}^2 s - s\left(2m_j^2 + s\right)}{\left(4m_i^2 - s\right)\left(s - 4m_{V'}^2\right)} > 1\,, \quad \text{for } i \neq j. \tag{7.39}$$

$$-1 > \frac{2m_{V'}^2 s + \left(m_i^2 - m_{V'}^2\right)^2 - s^2}{m^4 - 2\left(m_{V'}^2 + s\right)m^2 + \left(m_{V'}^2 - s\right)^2} > 1\,, \quad \text{for } i = j\,, \tag{7.40}$$

and the equivalent condition for $i \neq j$ with $m_i \leftrightarrow m_j$.

Additionally, s channel diagrams in the $ff \to ff$ sector present poles when the LDV mass is on-shell, i.e., $m_{V'}^2 = s$. To regulate these divergences, we follow the approach of Ref. [159] and discard the s channel amplitudes if the condition

$$\left|1 - \frac{1}{x}\right| > \frac{1}{4} \to 0.8 > x > 1.33 \quad \text{with} \quad x = \frac{m_{V'}^2}{s}\,, \tag{7.41}$$

is violated[1]. In that scenario, a bound can still be set from t and u channels. In our analysis, the fermion masses are fixed according to the specific transition under consideration. Consequently, singularities are avoided by choosing appropriate values of $m_{V'}$ and s (with $m_{V'} \ll \sqrt{s}$) so that the required conditions of Eq. (7.35)–Eq. (7.41) are met. We now focus on the case of massless fermions, i.e., $m_i = m_j = 0$. In this case, the amplitudes can be fully parametrised in terms of the single variable $x \equiv m_{V'}^2/s$, and the previous conditions reduce to

- $x > 0$ for $ff \to ff$,
- $\frac{1}{2} < x < 1$ for $V'f \to V'f$,
- $x < \frac{1}{4}$ for $V'V' \to \bar{f}f$.

Note that for zero LDV mass (corresponding to $x = 0$) we cannot set a bound because of the prefactor in the vector interaction, see Eq. (5.42), from which the partial amplitudes scale as $\mathcal{T}^l \sim m_{V'}^2 \text{coupling}^2/\Lambda^2$. Since we consider only transverse modes, all amplitudes vanish in the limit $m_{V'} \to 0$. Taking $m_i = 0\ \forall i$, we set bounds on the combination $\Lambda/\text{coupling} \times m_{V'}$ (where the $m_{V'}$ factor accounts for the vector interaction prefactor) for both the off-diagonal and diagonal couplings as a function of x. Our analysis shows that the strongest bound arises from the $ff \to ff$ sector[2]; hence, we present the bound from this sector in Figure 7.4, where the left (right) plot corresponds to the bound on the off-diagonal (diagonal) coupling. As discussed in Section 7.2, in the diagonal case the processes $ff \to ff$ and $V'V' \to \bar{f}f$ mix; however, since the

[1] See Refs. [145, 165] for an alternative treatment of s channel poles.

[2] For massless fermions the $j = 0$ partial amplitudes of $V'V' \to ff$ vanish, so $j = 1$ is the lowest admissible value.

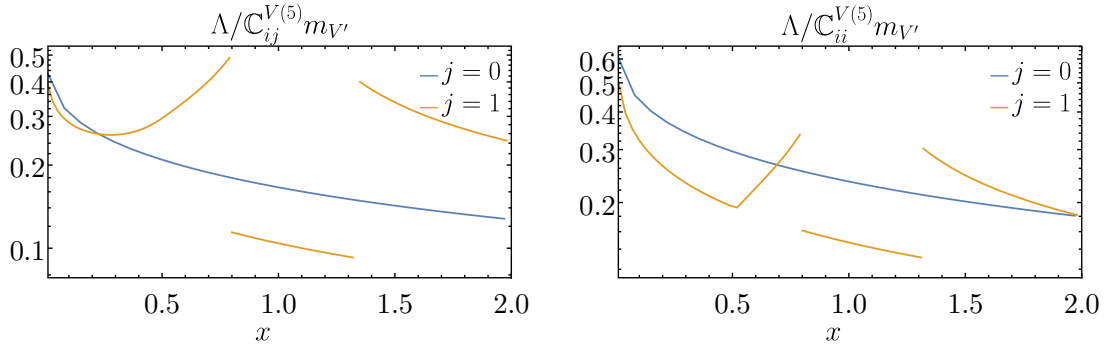

Figure 7.4.: Bound on the vector couplings $\mathbb{C}_{ij}^{V(5)}(\mathbb{C}_{ii}^{V(5)})$ on the left (right) as a function of $x \equiv m_{V'}^2/s$ from $ff \to ff$. We show the bound from the $j = 0$ and $j = 1$ partial waves, corresponding to the blue and orange lines, respectively.

Table 7.8.: Lower unitarity bounds on $\Lambda/\mathbb{C}_{ij}^{V(5)}$ for the flavour violating vector interaction at fixed $\sqrt{s} = 100$ GeV, $\sqrt{s} = 1$ TeV, and $\sqrt{s} = 10$ TeV. The bound at $\sqrt{s} = 100$ GeV for $m_{V'} = 0.1$ GeV is not applicable to the bd, bs sectors because the conditions needed to avoid singularities are not satisfied.

	$\sqrt{s} = 100$ GeV			$\sqrt{s} = 1$ TeV			$\sqrt{s} = 10$ TeV		
$m_{V'}$/ GeV	0.1	1	10	0.1	1	10	0.1	1	10
ij	0.074	0.61	4.29	0.085	0.74	6.05	0.096	0.86	7.41

dominant bound is set by $ff \to ff$ (and $V'V' \to \bar{f}f$ is relevant only for $x < 1/4$), we consider solely the $ff \to ff$ amplitudes to extract the bound[1].

In Figure 7.4 the bounds from the $j = 0$ (blue) and $j = 1$ (orange) partial waves are displayed. In the case of $j = 0$, no s channels contribute to the amplitudes, and thus the cut of Eq. (7.41) is not needed. On the other hand, for $j = 1$ the s channels contribute and the cuts are implemented. This can be seen in the plots, where the orange line (bound) jumps from 0.8 to 1.33, as within this range s channel amplitudes are not considered. For the general flavour-violating scenario with $m_i \neq m_j$, we fix $\sqrt{s} = \{0.1, 1, 10\}$ TeV and choose values of $m_{V'} = \{0.1, 1, 10\}$ GeV, for which the conditions needed to avoid singularities are satisfied, except for the bd, bs sectors for $m_{V'} = 0.1$ GeV, $\sqrt{s} = 100$ GeV. Just as in the previous case with massless fermions, we find that the strongest bound comes from $ff \to ff$. This is because we are only considering transverse modes, and the longitudinal modes for the $V'V' \to \bar{f}f, V'f \to V'f$ contribute the most to the bound.

[1] We have verified that including the $V'V' \to \bar{f}f$ channel does not significantly affect the bound. In particular, for $j = 0$ the partial amplitudes cancel and do not contribute, while for $j = 1$ they yield considerably weaker bounds than those from $ff \to ff$.

7.6. High Energy Amplitudes from the Stueckelberg Mechanism

As discussed in Section 5.2, the LDV V'_μ can acquire mass through the Stueckelberg mechanism [65, 66]. By virtue of the GBET, in the high energy regime the longitudinal mode of V' is identified with the scalar field π according to

$$\left(V'_\mu\right)_{\text{long}} \equiv -\frac{\partial_\mu \pi}{m_{V'}} \,. \tag{7.42}$$

Plugging in this relation into the interaction Lagrangian of Eq. (7.1), integrating by parts and using the fermion equations of motion we find

$$\begin{aligned} \left(\mathscr{L}_{\text{V}}\right)_{\text{long}} &= \frac{i\pi}{\Lambda} \bar{f}_i \left(\mathbb{C}^V_{ij} \left(m_i - m_j\right) + \gamma_5 \mathbb{C}^{V5}_{ij} \left(m_i + m_j\right)\right) f_j \,, \\ \left(\mathscr{L}_{\text{D}}\right)_{\text{long}} &= 0 \,. \end{aligned} \tag{7.43}$$

This Lagrangian reproduces the order $\mathcal{O}(\pi)$ amplitudes (such as $Af \to V'f$) but not $\mathcal{O}(\pi^2)$ amplitudes (such as $V'f \to V'f$), since using the classical EOM only reproduces the theory to linear order in the Goldstone [170, 171]. Using the classical EOM imposes on-shell conditions that accurately capture only the leading linear contributions, while higher-order, non-linear effects are systematically neglected. This procedure, akin to a field redefinition, preserves physical observables order by order, but omits terms beyond the first order. Consequently, to work out the form of the Lagrangian to second order one must perform the appropriate field redefiniton, given by

$$f_i \to \left(e^{\frac{i\pi}{m_{V'}}\left(\mathbb{C}^V_{ij} - \mathbb{C}^{V5}_{ij}\right)} P_L + e^{\frac{i\pi}{m_{V'}}\left(\mathbb{C}^V_{ij} + \mathbb{C}^{V5}_{ij}\right)} P_R \right) f_j \,, \tag{7.44}$$

after which we find, additionally to the order $\mathcal{O}(\pi)$ interactions in Eq. (7.43), the $\mathcal{O}(\pi^2)$ terms

$$\begin{aligned} \left(\mathscr{L}_{\text{V}}\right)_{\text{long}} = &- \frac{\pi^2}{2\Lambda m_{V'}} \bar{f}_i \left(\left(m_i - m_j\right) \gamma_5 \left(\mathbb{C}^{V5}_{ik} \mathbb{C}^V_{kj} + \mathbb{C}^V_{ik} \mathbb{C}^{V5}_{kj}\right) \right. \\ &\left. + \left(m_i + m_j\right) \left(\mathbb{C}^V_{ik} \mathbb{C}^V_{kj} + \mathbb{C}^{V5}_{ik} \mathbb{C}^{V5}_{kj}\right) \right) f_j \,, \\ &- \frac{\pi^2}{\Lambda m_{V'}} \bar{f}_i \left(\mathbb{C}^V_{ik} - \mathbb{C}^{V5}_{ik}\right) m_k \left(\mathbb{C}^V_{kj} + \mathbb{C}^{V5}_{kj}\right) f_j \,, \end{aligned} \tag{7.45}$$

corresponding to the vector interaction, since the field redefinition does not generate dipole-like interactions. The Lagrangian of Eq. (7.43) and Eq. (7.45) reproduce the leading partial amplitudes given in Section 7.4. For $\mathscr{L}_{\text{D}}$ the leading amplitudes of Eq. (7.29)–(7.32) are instead for transverse polarisations of the LDV, as longitudinal modes vanish in the high energy regime due to the Dirac structure of the interaction, i.e, $\mathscr{L}_{\text{D}} \propto \sigma^{\mu\nu}$, and hence the result in Eq. (7.43). Therefore, using the Stueckelberg trick leads to the correct leading amplitudes for $\mathscr{L}_{\text{V}}$ (corresponding to LL), but not for $\mathscr{L}_{\text{D}}$ (corresponding to TT).

We emphasize that while the scattering of π interacting with the SM fermions as in Eq. (7.43) and Eq. (7.45) must lead to the same contributions as the scattering of longitudinal LDVs in the high energy, we computed all amplitudes with the theory of Eq. (7.1) corresponding to a massive Proca vector, and did not consider the high energy regime except when extracting the analytical form of the leading amplitudes in Section 7.4. We have computed the *full* amplitudes, and only when needed we have taken certain limits of the amplitudes, such as the high energy limit to extract the energy growing amplitudes in Section 7.4.1. In the case of perturbativity, we have taken the complete amplitudes and numerically extracted the bound by diagonalising the matrices of Table 7.2 and Table 7.3. The Stueckelberg mechanism and subsequent Eq. (7.43) serves as a check of the calculation in the high energy regime, leading to the same amplitudes as for longitudinal

V' in $\mathscr{L}_{\rm V}$. Moreover, we have verified that for the dipole TL, LL amplitudes vanish in the high energy regime in agreement with Eq. (7.43).

The result of Eq. (7.43) for $\mathscr{L}_{\rm V}$ can also be obtained via the STI sum rules, in a similar way to the analysis of Section 7.3. Consider the following interactions of the Goldstone π and V' with SM fermions in the L/R basis of $\mathscr{L}_{\rm V}$ in Eq. (5.41)

$$\mathscr{L} = \sum_{\sigma} Y^{\sigma}_{\pi ij} \pi \bar{f}_i P_\sigma f_j + \sum_{\sigma} \mathbb{C}^{V\sigma}_{ij} V'_\mu \bar{f}_i \gamma^\mu P_\sigma f_j \,, \tag{7.46}$$

with several fermion species i, j, and $\sigma = {\rm L}, {\rm R}$. The sum rule for the coupling of the Goldstone boson to two fermions reads [169]

$$Y^{\sigma}_{\pi ij} = -\frac{i}{m_{V'}} \left(m_i \mathbb{C}^{V'\sigma}_{ij} - m_j \mathbb{C}^{V'\bar{\sigma}}_{ij} \right) \,, \tag{7.47}$$

while Eq. (7.43) in the L/R basis reads

$$(\mathscr{L}_{\rm V})_{\rm long.} = \frac{i\pi}{\Lambda} \bar{f}_i \left(P_L \left(m_i \mathbb{C}^{V'L}_{ij} - m_j \mathbb{C}^{V'R}_{ij} \right) + P_R \left(m_i \mathbb{C}^{V'R}_{ij} - m_j \mathbb{C}^{V'L}_{ij} \right) \right) f_j \,. \tag{7.48}$$

The couplings of Eq. (7.47) and Eq. (7.48) coincide up to the $m_{V'}/\Lambda$ prefactor in $\mathscr{L}_{\rm V}$ and up to a minus sign coming from demanding the cancellation of energy growing amplitudes. The sum rule of Eq. (7.47) reproduces Eq. (7.48) because energy growing amplitudes correspond to longitudinally polarised V' for $\mathscr{L}_{\rm V}$, which are identified as in Eq. (7.42).

Chapter 8

Conclusion

In this second part of the thesis we have considered a light NP vector boson, the LDV, coupled to SM fermions. Following the EFT approach introduced in Section 3.3 we studied vector and dipole like interactions. We have shown that FCNC interactions between the LDV and SM interactions can arise after rotating to the SM Yukawa mass basis. Additionally, FCNC couplings can be generated from the couplings RGEs via running from the (flavour diagonal) high scale to the low scale.

In Chapter 6 we have systematically studied the flavour phenomenology of LDVs for two-body decays. We have restricted our analysis to scenarios where the LDV is directly linked to DM, and is either itself invisible or promptly decays to invisible particles, such that the LDV appears as missing energy. We have calculated the resulting predictions for the decay rates of mesons, baryons, and polarized leptons as a function of the LDV mass. These predictions were compared to the experimental limits on various hadronic processes and LFV transitions. The limits on the flavour-violating couplings are shown in Figures 6.2, 6.3, 6.4 and 6.5. Very stringent constraints are obtained, reaching up to $10^{12}\,\text{GeV}$ in $K \to \pi$ decays, $10^{8}\,\text{GeV}$ in B- and D-meson decays, $10^{9}\,\text{GeV}$ in $\mu \to e$ decays, and $10^{7}\,\text{GeV}$ in $\tau \to \mu/e$ decays for the vector interaction. Bounds on dipole couplings are weaker, if viewed as dimension-six operators above the EW scale, but they still probe UV scales of order $10^{6}\,\text{GeV}$ in $K \to \pi$ and $\mu \to e$ decays. Importantly, all channels will be improved by present or near-future experiments, such as NA62, Belle II, BES III, MEG-II or Mu3e. Moreover, baryon decays set the less constraining bounds, but are the only available decays in some sectors ($s \to d, c \to u$) and couplings. No direct searches for baryon decays are available (except for BES III [129] on the decay $\Sigma^+ \to p + \text{invis.}$ albeit for massless vectors), and our analysis motivates the need for direct searches via baryon decays. Finally, we have set bounds on the diagonal UV couplings from the RGE-induced flavour-violation, see Figure 6.6.

In Chapter 7 we have employed partial wave unitarity to further analyse the model. We have computed the helicity amplitudes of $2 \to 2$ processes with flavour-violation and diagonal couplings. This required calculating the scattering matrices in flavour space, which were then diagonalised to extract bounds on the couplings. Crucially, we distinguish between unitarity and perturbativity constraints: while the unitarity bounds are considerably weaker than those from two-body decays, they lack a kinematical endpoint and therefore, constrain a broader region of parameter space. Finally, we have examined the Stueckelberg mechanism and applied the GBET to deepen our understanding of the model and the associated high energy amplitudes.

PART III

Heavy New Physics and EFTs

In this part of the thesis, we study a set of UV completions of the SM corresponding to heavy NP, and the QCD corrections to four-fermion operators within the corresponding WET. In Chapter 9, we consider a BSM setup featuring scalar LQs with general couplings to SM quarks and leptons. The LQs are assumed to have masses well above the EW scale, and we analyse the $\Delta F = 2$ mixing process using the WET introduced in Section 3.2. We match the full theory onto the effective theory and compute the WCs up to $\mathcal{O}(\alpha_s)$—which amounts to a two-loop calculation in the full theory and a one-loop calculation in the WET. In Chapter 10 we examine two operators of the WET for $\Delta F = 1$ processes, focusing on the one-loop QCD corrections. We compute the corresponding ADM and amplitudes. Moreover, we introduce a computational procedure that extracts both the ADM and amplitudes, thereby avoiding the cumbersome rearrangement of Dirac structures required by traditional methods. This new approach simplifies the calculations and has the potential to speed up the evaluation of loop corrections.

Chapter 9

Next-to-Leading-Order QCD Matching for $\Delta F = 2$ Processes in Scalar Leptoquark Models

In this chapter we study $\Delta F = 2$ processes, that is, processes in which the flavour quantum number changes by two units. For example, in the B_s mixing process introduced in Section 2.5, it is the strangeness and bottomness quantum numbers that change by two units. Other relevant processes include D^0–$\bar{D}^0$, K^0–$\bar{K}^0$ and $B_{s,d}$–$\bar{B}_{s,d}$ mixing. These processes are forbidden at tree level in the SM and occur only through loop diagrams, making them sensitive probes for the flavour structure of the SM and NP models. For instance, precise measurements of the CP-violating parameter ε_K in the $K^0 - \bar{K}^0$ system tightly constrain the imaginary parts of the CKM products, while the mass differences Δm_d and Δm_s in B_d and B_s mixing predominantly determine the magnitudes of the CKM matrix $|V_{td}|$ and $|V_{ts}|$, respectively [172]. In the charm sector, D mixing—with its suppressed SM contributions and minimal expected CP violation—offers an excellent window for detecting small NP effects. Collectively, these $\Delta F = 2$ processes not only serve as rigorous tests of SM predictions but also significantly restrict the parameter space of various BSM scenarios [18, 19, 173–175]. In particular, in this chapter we consider scalar LQs, which are possible BSM particles that can arise in the context of Grand Unified Theories [27–29]. What makes them special, and defines them, are their direct couplings to SM leptons and quarks. LQs were first systematically classified in Ref. [176], where ten possible LQ representations under the SM gauge group were found, of which five are scalar fields (spin-0) and five are vector (spin-1) particles; the complete scalar LQ Lagrangian and the corresponding set of Feynman rules has been presented recently in Ref. [26]. While LQs have received varying degrees of attention in the past, they have undergone a renaissance in recent years. This can be mainly attributed to the emergence of the flavour anomalies, i.e. the deviations from the SM predictions observed in several flavour observables.

Persistent tensions include the B-physics ratios $R_{D^{(*)}}$, where $\mathcal{B}(B \to D^{(*)}\tau\nu)/\mathcal{B}(B \to D^{(*)}\ell\nu)$ exceeds SM predictions by $\sim 2\sigma$ [177], and the muon $g-2$, with a ~ 3–4σ discrepancy between Fermilab's measurement and SM theory [178]. These anomalies align with scalar or vector LQs that couple preferentially to third-generation fermions. Meanwhile, earlier $R_{K^{(*)}}$ anomalies ($b \to s\mu\mu$ deficits), once $\sim 4\sigma$ tensions, now stand at $\sim 2\sigma$ after LHCb's Run 2 updates [179], narrowing viable LQ parameter spaces. Similarly, the $B_s \to \mu^+\mu^-$ rate, initially $\sim 2\sigma$ below SM predictions, now aligns within $\sim 1\sigma$ [180], weakening scalar LQ motivations. Faded anomalies include the Kaon CP-violation parameter ε'/ε [181, 182], and the W-boson mass anomaly, mitigated by ATLAS/LHCb results favoring SM values [183]. LQs can address the $R_{K^{(*)}}$ and $R_{D^{(*)}}$ anoma-

lies via LH couplings to $b \to s\mu^+\mu^-$ and $b \to c\tau\nu$ transitions, respectively, through tree-level interactions that enhance lepton flavor universality violation [184–186]. They can also accommodate for the muon $g-2$ anomaly via chirally enhanced couplings to muons and quarks [187]. However, these models require careful tuning of Yukawa couplings (e.g., $\lambda_{b\tau} \sim \mathcal{O}(1)$ for $R_{D^{(*)}}$) and mass scales ($M_{\rm LQ} \gtrsim 1-10$ TeV) to evade constraints from B_s-mixing [188,189], electroweak precision tests, and direct LHC searches [190].

QCD corrections play a pivotal role in the EFT framework for LQ models, ensuring precision in connecting high-scale dynamics to low-energy flavour observables. These corrections govern the RGEs of WCs, which can amplify or suppress LQ contributions to processes like B_s-mixing (Δm_s) or rare decays ($B \to K^{(*)}\mu^+\mu^-$). At low energies, logarithmic enhancements from QCD loops and threshold corrections at the LQ mass scale modify matching conditions, altering predictions for anomalies such as $R_{K^{(*)}}$ or $R_{D^{(*)}}$. Precision demands rigorous control of hadronic matrix elements (e.g., via lattice QCD or sum rules) to disentangle LQ signals from SM backgrounds. Thus, incorporating QCD effects is indispensable for ensuring consistency between UV-complete LQ models, EFT interpretations, and experimental bounds while resolving the interplay of flavour anomalies and high-energy phenomenology. The QCD corrections to LQ production and decay at colliders have been known for a long time [191,192] and have been improved to include NLO parton shower [193] or a large width [194]. Such QCD corrections have also been included in recent analyses correlating the B anomalies to LHC searches [195–198]. However, the calculation for the analogous α_s corrections to flavour observables is still incomplete. So far, only the $\mathcal{O}(\alpha_s)$ corrections to semi-leptonic processes [199] and $\ell \to \ell'\gamma$ [200] have been calculated, but the analogous two-loop matching for $\Delta F = 2$ processes is still missing. Here, specially in models aiming at an explanation of $R(D^{(*)})$, but also in models accounting for $b \to s\ell^+\ell^-$ [189,201], $B_s - \bar{B}_s$ mixing provides a crucial constraint that limits the possible size of the NP contribution. In this chapter we calculate the next-to-leading order (NLO) QCD matching for $\Delta F = 2$ processes in scalar LQ models, together with the (known) two-loop QCD evolution of the corresponding effective operators [202,203], needed to reduce significantly the matching-scale uncertainty. This is particularly important in light of the increasingly tighter constraints placed by $\Delta F = 2$ processes on NP [188,204,205]. As a starting point, we consider the following generic Lagrangian governing the couplings of scalar LQs Φ of mass M to leptons ℓ (charged leptons or neutrinos) and quarks q (up or down type)

$$\mathscr{L}^{\rm LQ}_{q\ell} = \sum_a \bar{q}\left(\Gamma^{aL}_{q\ell} P_L + \Gamma^{aR}_{q\ell} P_R\right) \ell\, \Phi_a + \text{h.c.}\,, \tag{9.1}$$

with $a = 1, 2, \ldots$ running over the different LQ fields (several 'copies' of LQs belonging to the same representation also allowed). In Section 9.1 we introduce the $\Delta F = 2$ WET theory and match the full theory onto the EFT at NLO. Moreover, we discuss the calculation of the ADM and 1-loop amplitudes in the WET. In Section 9.2, we give the LO WCs, and in Section 9.3 the NLO calculation is discussed, where we renormalise the LQ theory and compute the 2-loop diagrams in the full theory. Finally, in Section 9.4 we do a phenomenological analysis and analyse the impact of the NLO corrections.

9.1. $\Delta F = 2$ Effective Field Theory and Matching

Due to the relatively low energy scale at which neutral meson mixing takes place, its physics can be described by an EFT where SM EW-scale particles (W, Z, higgs and top) as well as the LQs [1] are not dynamical DOF and are integrated out from the action. Flavour-changing transitions are

[1] We assume that the LQs are heavier than the EW scale as indicated by LHC searches [206].

then mediated by effective operators of dimension six or higher (see, e.g. Ref. [41]). The most general set of (physical) dimension six operators for $\Delta F = 2$ processes contains eight operators (for a specific flavour transition)

$$\mathscr{L}_{\text{eff}}^{\Delta F=2} = -\sum_{i=1}^{5} C_i \mathcal{O}_i - \sum_{i=1}^{3} C'_i \mathcal{O}'_i \,. \tag{9.2}$$

In the case of $B_s - \bar{B}_s$ mixing, the operators in the so-called "SUSY" basis read explicitly [41]

$$\begin{aligned}
\mathcal{O}_1 &= (\bar{s}_\alpha \gamma^\mu P_L b_\alpha)\,(\bar{s}_\beta \gamma_\mu P_L b_\beta) \;, & \mathcal{O}_5 &= (\bar{s}_\alpha P_L b_\beta)\,(\bar{s}_\beta P_R b_\alpha) \;, \\
\mathcal{O}_2 &= (\bar{s}_\alpha P_L b_\alpha)\,(\bar{s}_\beta P_L b_\beta) \;, & \mathcal{O}'_1 &= (\bar{s}_\alpha \gamma^\mu P_R b_\alpha)\,(\bar{s}_\beta \gamma_\mu P_R b_\beta) \;, \\
\mathcal{O}_3 &= (\bar{s}_\alpha P_L b_\beta)\,(\bar{s}_\beta P_L b_\alpha) \;, & \mathcal{O}'_2 &= (\bar{s}_\alpha P_R b_\alpha)\,(\bar{s}_\beta P_R b_\beta) \;, \\
\mathcal{O}_4 &= (\bar{s}_\alpha P_L b_\alpha)\,(\bar{s}_\beta P_R b_\beta) \;, & \mathcal{O}'_3 &= (\bar{s}_\alpha P_R b_\beta)\,(\bar{s}_\beta P_R b_\alpha) \;.
\end{aligned} \tag{9.3}$$

where α, β are colour indices. The corresponding expressions for $K^0 - \bar{K}^0$, $D^0 - \bar{D}^0$ and $B_d - \bar{B}_d$ mixing follow by a simple exchange of flavours. The associated WCs $C_i^{(\prime)}$ can be calculated from a given UV-complete theory by performing a matching calculation at the matching scale μ_0, which is of the order of the mass of the particles that are integrated out. The matching calculation is done by equating the full-theory and the EFT amplitudes (expanded in α_s) at the matching scale, order by order in perturbation theory. In the EFT, the amplitude reads

$$\mathcal{A}_{\text{eff}} = \sum_{i,j} C_i \left(\delta_{ij} + \hat{\alpha}_s\, r_{ij} + \mathcal{O}(\alpha_s^2)\right) \langle \mathcal{O}_j \rangle^{(0)} \,, \tag{9.4}$$

where $\langle \mathcal{O}_i \rangle^{(0)}$ are tree-level matrix elements, r_{ij} is the NLO (finite) contribution and we have defined $\hat{\alpha}_s \equiv \alpha_s/(4\pi)$. The amplitudes in the full theory at order $\mathcal{O}(\alpha_s)$ are the sum of the (one loop) LO contributions ($F_i^{(0)}$) from the diagrams in Figure 9.1 and the NLO (two loop) contributions ($F_i^{(1)}$) from the two-loop diagrams shown in Figure 9.2. It can be written as

$$\mathcal{A}_{\text{LQ}} = \sum_{i} \left(F_i^{(0)} + \hat{\alpha}_s\, F_i^{(1)} + \mathcal{O}(\alpha_s^2)\right) \langle \mathcal{O}_i \rangle^{(0)} \,, \tag{9.5}$$

again in terms of tree-level matrix elements. Requiring the equality of EFT and full-theory amplitudes at the matching scale μ_0 order-by-order in $\alpha_s(\mu_0)$, and expanding the WCs in α_s

$$C_i(\mu_0) = C_i^{(0)}(\mu_0) + C_i^{(1)}(\mu_0) + \mathcal{O}(\alpha_s(\mu_0)^2) \,, \tag{9.6}$$

yields

$$C_i^{(0)} = F_i^{(0)} \,, \tag{9.7}$$

$$C_i^{(1)} = \hat{\alpha}_s\, F_i^{(1)} - \hat{\alpha}_s \sum_j F_j^{(0)} r_{ji} \,. \tag{9.8}$$

The LO coefficients $C_i^{(0)} = F_i^{(0)}$ are given in Section 9.2, by direct computation of the corresponding 1-loop box diagrams. The NLO $C_i^{(1)}$ WCs are obtained from the evaluation of the genuine two-loop Feynman diagrams and one-loop diagrams with counterterms, to be discussed in Section 9.3. Below the matching scale, the renormalisation-scale dependence of the WCs is determined by the ADM in the EFT according to the RGE

$$\frac{dC_i}{d\log\mu} = \gamma_{ji}\, C_j = \left(\hat{\alpha}_s \gamma_{ji}^{(0)} + \hat{\alpha}_s^2 \gamma_{ji}^{(1)} + \cdots\right) C_j \,. \tag{9.9}$$

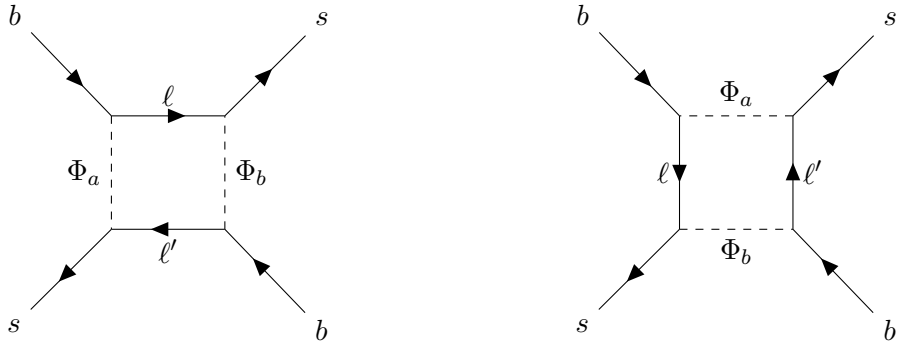

Figure 9.1.: Feynman diagrams depicting the LO scalar LQ contributions to the Wilson coefficients $C_i^{(0)}$ in B_s mixing.

In the next subsection we focus on the EFT calculation of the LO ADM $\gamma^{(0)}$ and the r_{ij}-matrix needed at NLO according to Eq. (9.8). As outlined in Section 3.2, the 1-loop ADM is found by

$$\gamma_{ij}^{(0)} = -2\left(2\delta Z_q \delta_{ij} + \delta Z'_{ij}\right) \quad \text{with} \quad \delta Z_q = -\xi C_F\,, \tag{9.10}$$

which we compute in the Feynman gauge $\xi = 1$.

9.1.1. 1-Loop EFT Calculation

In this subsection we focus on the calculation of the ADM and r-matrix at 1-loop in the EFT. The former is needed for the running of the WC according to Eq. (9.9), while the latter is needed to find the WC at NLO in α_s according to Eq. (9.8). At the quark level, the B_s mixing is given by the process $b_\alpha \bar{s}_\beta \to \bar{b}_\gamma s_\delta$. The first task corresponds to computing the tree-level matrix elements $\langle \mathcal{O}_i \rangle^{(0)}$ for the dimension-six operators of Eq. (9.3), which are given by the contact diagrams of Figure 9.3.

The tree-level matrix elements are given by $\langle \mathcal{O}_i \rangle^{(0)} = \langle \bar{b}_\gamma s_\delta | \, \mathcal{O}_i \, | b_\alpha \bar{s}_\beta \rangle$. For example, for $\mathcal{O}_1$ we find

$$\begin{aligned} \langle \mathcal{O}_1 \rangle^{(0)} &= 2i\delta_{\delta\alpha}\delta_{\gamma\beta}\left(\bar{u}_\delta \gamma_\mu P_L u_\alpha\right)\left(\bar{v}_\beta \gamma^\mu P_L v_\gamma\right) - 2i\delta_{\beta\alpha}\delta_{\gamma\delta}\left(\bar{u}_\delta \gamma_\mu P_L v_\gamma\right)\left(\bar{v}_\beta \gamma^\mu P_L u_\alpha\right) \\ &\equiv \langle \mathcal{O}_1 \rangle^{(0)}|_1 - \langle \mathcal{O}_1 \rangle^{(0)}|_2\,, \end{aligned} \tag{9.11}$$

and analogously for the other operators. Going to 1-loop in α_s we consider the QCD corrections to these amplitudes, where (some) the diagrams are depicted in Figure 9.4. The amplitudes carry a loop integral that we calculate via dimensional regularisation (DR), in which divergences take the from $1/\epsilon$. This means that we work in $d = 4 - 2\epsilon$ dimensions and accordingly the Dirac algebra is to be performed in d-dimensions. Then, one is forced to choose a γ_5 *scheme* [207], since γ_5 is strictly defined in four dimensions. In this chapter we choose naive dimensional regularisation (NDR), which assumes that the anticommutativity of the γ_5 matrix with the Dirac matrices in four dimensions also holds in d-dimensions, i.e., $\{\gamma_5, \gamma^\mu\} = 0$ [208]. In d-dimensions, the physical basis $\{\mathcal{O}_i\}$ is incomplete, because certain strings of gamma matrices cannot be reduced/projected back to the physical structures, which is needed to compute the amplitudes according to Eq. (9.4). Then, *evanescent operators* E_i are introduced [209–211], which allow to project such structures back to the physical basis $\{\mathcal{O}_i\}$. By definition, evanescent operators vanish in four dimensions, i.e. $E_i = 0$ in $d = 4$, and are thus to be understood as an artifact which arises in $d = 4 - 2\epsilon \neq 4$ calculations. We now wish to illustrate the calculation. We consider the 1-loop diagrams of Figure 9.4, which we label as D_1, D_2 and D_3 from left to right, respectively. We consider massless

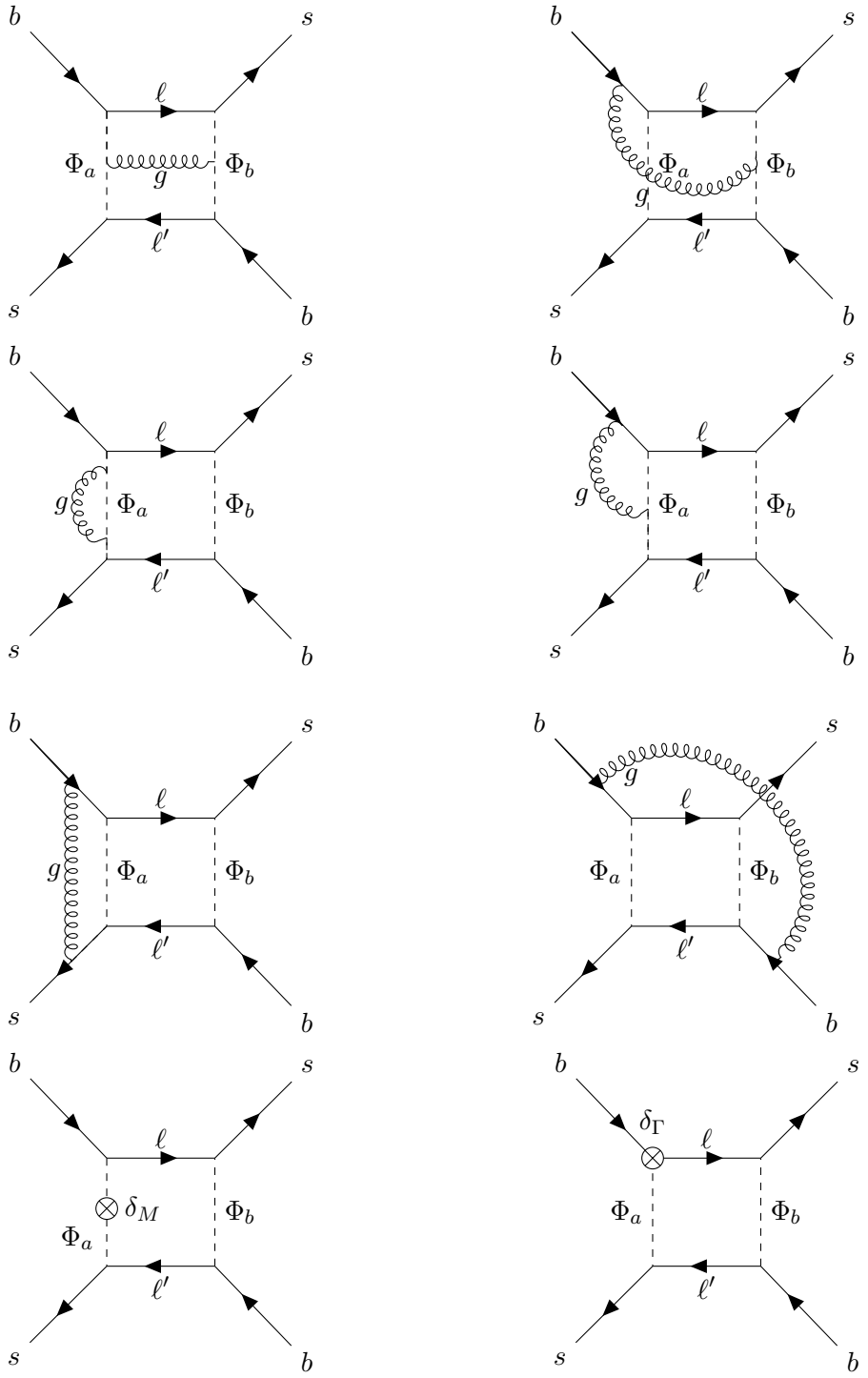

Figure 9.2.: A sample of two-loop diagrams and one-loop diagrams with counterterm insertions (indicated by the cross), contributing to the NLO QCD matching for $B_s - \bar{B}_s$ mixing.

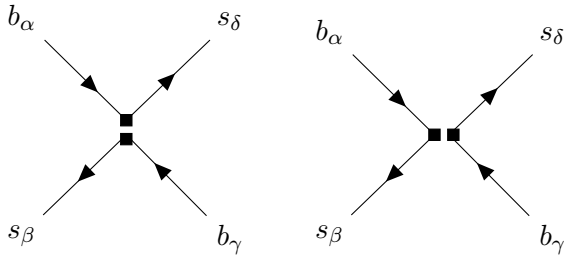

Figure 9.3.: Tree-level diagrams from the insertions of the EFT $\mathcal{O}_i$ operators in Eq. (9.3).

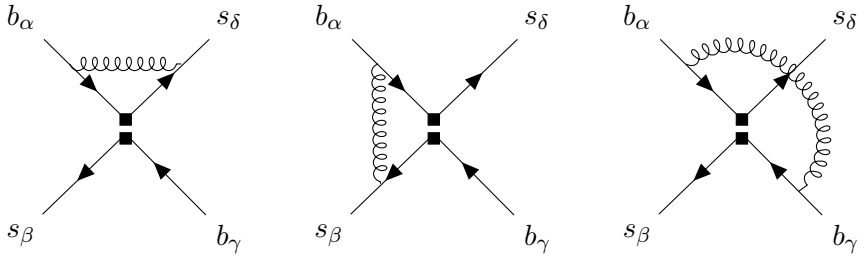

Figure 9.4.: Sample of 1-loop diagrams with QCD corrections for $\Delta F = 2$ processes from the insertions of $\mathcal{O}_i$. We name the diagrams D_1, D_2, D_3 from left to right. The other contractions, corresponding to the right diagram in Figure 9.3 can be obtained by $\bar{u}_\delta \leftrightarrow \bar{v}_\beta$.

quarks and zero external momenta, which introduces IR divergences in the soft $k \to 0$ region of the loop momenta. In order to regularise these IR divergences, we give the gluons a fictitious mass λ. Therefore, the gluon propagator in the Feynman gauge $\xi = 1$ reads

$$\Delta^{ab}_{\mu\nu} = i\frac{-g_{\mu\nu}}{k^2 - \lambda^2}\delta^{ab}\,, \tag{9.12}$$

where a, b are colour indices. In this manner, UV divergences are regularised as $1/\epsilon$ while IR divergences take the form $\log\lambda/\mu$, where μ is the renormalisation scale[1]. Moreover, we work in the $\overline{\text{MS}}$ scheme [212], for which $\mu^2 \to \mu^2 e^\gamma/4\pi$, so that γ and 4π factors are absorbed. With insertions of $\mathcal{O}_1$, the diagrams D_i of Figure 9.4 read[2]

$$\begin{aligned}
D_1 &= g_s^2 C_F \delta_{\alpha\delta}\delta_{\beta\gamma}\left(\bar{u}_\delta\gamma^\nu\gamma^\rho\gamma^\mu P_L\gamma^\tau\gamma_\nu u_\alpha\right)\left(\bar{v}_\beta\gamma_\mu P_L v_\gamma\right)\int\frac{\mu^{2\epsilon}k_\rho k_\tau}{k^4\left(k^2-\lambda^2\right)}dk\,,\\
D_2 &= g_s^2\sum_a T^a_{\delta\alpha}T^a_{\beta\gamma}\left(\bar{u}_\delta\gamma_\mu\gamma^\tau\gamma_\nu P_L u_\alpha\right)\left(\bar{v}_\beta\gamma^\nu\gamma^\rho\gamma^\mu P_L v_\gamma\right)\int\frac{\mu^{2\epsilon}k_\rho k_\tau}{k^4\left(k^2-\lambda^2\right)}dk\,,\\
D_3 &= -g_s^2\sum_a T^a_{\delta\alpha}T^a_{\beta\gamma}\left(\bar{u}_\delta\gamma_\nu\gamma^\tau\gamma_\mu P_L u_\alpha\right)\left(\bar{v}_\beta\gamma^\nu\gamma^\rho\gamma^\mu P_L v_\gamma\right)\int\frac{\mu^{2\epsilon}k_\rho k_\tau}{k^4\left(k^2-\lambda^2\right)}dk\,,
\end{aligned} \tag{9.13}$$

[1] Other regulators can be used to regularise the IR divergences, such as considering external momenta or quark masses. We will see examples with distinct regulators in Chapter 10.

[2] We define $dk \equiv dk/(2\pi)^d$.

where $\sum_a T^a_{ij}T^a_{kl} = 1/2(\delta_{il}\delta_{kj} - 1/3\delta_{ij}\delta_{kl})$ and for D_1 the colour structure has been reduced according to $\sum_a T^a_{\delta\sigma}T^a_{\sigma\alpha}\delta_{\beta\gamma} = C_F\delta_{\delta\alpha}\delta_{\beta\gamma}$ with $C_F = 4/3$. Notice that the three diagrams in Eq. (9.13) have the same loop integral. Using DR the integral yields

$$\int \frac{\mu^{2\epsilon}k_\rho k_\tau}{k^4\,(k^2-\lambda^2)}dk = i\frac{g_{\rho\tau}}{64\pi^2}\mathcal{F} \quad \text{with} \quad \mathcal{F} \equiv \frac{1}{\epsilon} - \log\frac{\lambda^2}{\mu^2} + \frac{3}{2}\,, \tag{9.14}$$

where we have used $k_\rho k_\tau \to (1/d)k^2 g_{\rho\tau}$ and the partial fraction decomposition

$$\frac{1}{k^2\,(k^2-\lambda^2)} = -\frac{1}{\lambda^2}\left(\frac{1}{k^2} - \frac{1}{k^2-\lambda^2}\right)\,. \tag{9.15}$$

The first term $(1/k^2)$ is a scaleless integral which vanishes in DR, and the second integral is solved with the usual DR formulas [213], to obtain the result of Eq. (9.14). The result contains a $1/\epsilon$ UV divergence and a IR divergence in the form $\log\lambda^2/\mu^2$, as well as a finite piece corresponding to the $3/2$ factor. The next step is rearranging the strings of gamma matrices between the spinors according to d-dimensional Clifford algebra to project back to the tree-level matrix element of $\mathcal{O}_1$ given in Eq. (9.11)

Diagram D_1

We first consider the D_1 diagram of Eq. (9.13). In order to project back to the tree-level amplitude of $\mathcal{O}_1$, the string of gamma matrices in the first bilinear $(\bar{u}_\delta\gamma^\nu\gamma^\rho\gamma^\mu P_L\gamma^\tau\gamma_\nu u_\alpha)$ is reduced according to the Clifford algebra to (the ρ,τ Lorentz indices are contracted due to the $g_{\rho\tau}$ metric coming from the loop integral in Eq. (9.14))

$$\gamma^\nu\gamma^\rho\gamma^\mu P_L\gamma_\rho\gamma_\nu = (2-d)^2\,\gamma^\mu P_L\,, \tag{9.16}$$

and the amplitude is projected back to the tree-level matrix element $\langle\mathcal{O}_1\rangle^{(0)}$ of Eq. (9.11), which yields (with $g_s^2 = 4\pi\alpha_s$)

$$D_1 = \frac{\alpha_s}{6\pi}\,(1-2\epsilon)\,\mathcal{F}\langle\mathcal{O}_1\rangle^{(0)}|_1\,. \tag{9.17}$$

Thus, the D_1 diagram is projected back to the physical basis with no problem. The corresponding 1-loop diagram with distinct contraction (found by $\bar{u}_\delta \leftrightarrow \bar{v}_\beta$ in D_1) gives the same result as D_1 up to $\langle\mathcal{O}_1\rangle^{(0)}|_1 \leftrightarrow \langle\mathcal{O}_1\rangle^{(0)}|_2$.

Diagram D_2

For the D_2 diagram of Eq. (9.13) the situation is more complicated. First and unlike D_1, which involves a single color structure, D_2 receives two distinct color contributions from $T^a_{\delta\alpha}T^a_{\beta\gamma}$. Secondly, each spinor bilinear contains a string of three gamma matrices; however, their orders differ. Specifically, the first bilinear features the sequence $\gamma^\mu\gamma^\rho\gamma^\nu$ and the second one $\gamma^\nu\gamma^\rho\gamma^\mu$. Therefore, the strings of gamma matrices must be ordered in the same manner. To do so, we use the following identity on the matrices of the second bilinear

$$\gamma^\nu\gamma^\rho\gamma^\mu = -\gamma^\mu\gamma^\rho\gamma^\nu + 2g^{\rho\nu}\gamma^\mu - 2g^{\mu\nu}\gamma^\rho + 2g^{\nu\rho}\gamma^\nu\,. \tag{9.18}$$

After using this identity and simplifying further, the amplitude reads

$$D_2 = \frac{ig_s^2}{64\pi^2}\mathcal{F}\sum_a T^a_{\delta\alpha}T^a_{\beta\gamma}\left[-\left(\gamma^\mu\gamma^\rho\gamma^\nu P_L\otimes\gamma_\mu\gamma_\rho\gamma_\nu P_L\right) + (20-12\epsilon)\left(\gamma^\mu P_L\otimes\gamma^\mu P_L\right)\right]\,, \tag{9.19}$$

where we use the notation $(A^{\mu_1\cdots\mu_n}P_L \otimes B^{\mu_1\cdots\mu_n}P_L) \equiv (\bar{u}_\delta A^{\mu_1\cdots\mu_n}P_L u_\alpha)\,(\bar{v}_\beta B^{\mu_1\cdots\mu_n}P_L v_\gamma)$. To project back to the physical basis, observe that the colour structure $\delta_{\beta\gamma}\delta_{\alpha\delta}$ with $(\gamma^\mu P_L \otimes \gamma^\mu P_L)$ can be identified with $\langle\mathcal{O}_1\rangle^{(0)}|_1$, but this is not possible for the contribution with the colour structure $\delta_{\delta\gamma}\delta_{\alpha\beta}$, because it does not have the same spinor structure as $\langle\mathcal{O}_1\rangle^{(0)}|_2$. Moreover, we also cannot project back the structures with a string of three gamma matrices. In order to be able to reduce such structures to the physical basis, we introduce the following evanescent operators [203]

$$\begin{aligned} E_1 &= (\bar{s}_\alpha\gamma_\mu P_L b_\beta)\,(\bar{s}_\beta\gamma^\mu P_L b_\alpha) - \mathcal{O}_1\,, \\ E_2 &= (\bar{s}_\alpha\gamma_\mu\gamma_\nu\gamma_\rho P_L b_\alpha)\,(\bar{s}_\beta\gamma^\mu\gamma^\nu\gamma^\rho P_L b_\beta) - (16-4\epsilon)\mathcal{O}_1\,, \\ E_3 &= (\bar{s}_\alpha\gamma_\mu\gamma_\nu\gamma_\rho P_L b_\beta)\,(\bar{s}_\beta\gamma^\mu\gamma^\nu\gamma^\rho P_L b_\alpha) - (16-4\epsilon)\mathcal{O}_1\,. \end{aligned} \tag{9.20}$$

With these new operators, the amplitude reads

$$D_2 = \frac{\alpha_s}{64\pi}\mathcal{F}\left[(20-12\epsilon)\langle E_1\rangle^{(0)}|_1 - \langle E_3\rangle^{(0)}|_1 - \frac{1}{N_c}(20-12\epsilon)\langle\mathcal{O}_1\rangle^{(0)}|_1 + \frac{1}{N_c}\langle E_2\rangle^{(0)}|_1\right]. \tag{9.21}$$

Thus, the E_i operators allow to project the amplitudes back to the physical basis, in terms of tree-level matrix elements of physical *and* evanescent operators. The corresponding 1-loop diagram with distinct contraction (found by $\bar{u}_\delta \leftrightarrow \bar{v}_\beta$ in D_2) yields the same result as D_2 up to $\langle\mathcal{O}_1\rangle^{(0)}|_1 \leftrightarrow \langle\mathcal{O}_1\rangle^{(0)}|_2$, $\langle E_i\rangle^{(0)}|_1 \leftrightarrow \langle E_i\rangle^{(0)}|_2$. A few remarks are in order regarding the evanescent operators. With the previous illustrative example at hand, we focus on the E_i of Eq. (9.20). In four dimensions, the evanescent operators must vanish, since by definition $E_i \sim \mathcal{O}(\epsilon)$. For E_2, E_3 this is the case upon using the Chisholm identity

$$\gamma_\mu\gamma_\nu\gamma_\lambda = \gamma_\mu g_{\nu\lambda} - \gamma_\nu g_{\mu\lambda} + \gamma_\lambda g_{\mu\nu} - i\gamma^\sigma\gamma_5\epsilon_{\mu\nu\lambda\sigma}\,, \tag{9.22}$$

which holds in four dimensions. Importantly, the $(16-4\epsilon)$ term in the E_2, E_3 evanescent operators can be generally written as $(16-a\epsilon)$ for any a, since the $\mathcal{O}(\epsilon)$ pieces trivially vanish in four dimensions (because then $\epsilon \to 0$). Therefore, the value of a can be understood as the scheme dependence defining the evanescent operators, while the factor 16 is precisely fixed from four dimensional Dirac algebra to guarantee the vanishing of E_i in $d = 4$. Of course, calculations might (and do) depend explicitly on a, i.e., in our calculation changing the -4ϵ factor yields distinct results. In the case of the evanescent operators of Ref. [203] employed here, the a factors are chosen/found according to the "Greek projections" [19], but other definitions (other a values) are possible [211, 214]. Regarding the "origin" of the evanescent operators, the E_2, E_3 operators arise from the fact that the strings of three gamma matrices appearing in the D_i diagrams of Eq. (9.13) cannot be reduced to the physical basis via d-dimensional Dirac algebra. Therefore, such operators are called *Dirac evanescent operators*. The E_1 operator in Eq. (9.20) also vanishes in four dimensions, but for a different reason than E_2, E_3. In four dimensions, the so called Fierz identities apply [203, 211, 214, 215], which allow to rearrange spinor contractions in products of bilinears. For example, for $\mathcal{O}_1$ we have

$$\left.\begin{aligned} \mathcal{O}_1 &= \bar{s}_\alpha\gamma^\mu P_L b_\alpha \bar{s}_\beta\gamma_\mu P_L b_\beta \\ \tilde{\mathcal{O}}_1 &= \bar{s}_\alpha\gamma^\mu P_L b_\beta \bar{s}_\beta\gamma_\mu P_L b_\alpha \end{aligned}\right\} \Rightarrow \mathcal{O}_1 = \tilde{\mathcal{O}}_1 \quad \text{in } 4d\,. \tag{9.23}$$

In d-dimensions this is not the case anymore, and therefore the *Fierz evanescent operator* E_1 is defined according to

$$E_1 = \tilde{\mathcal{O}}_1 - \mathcal{O}_1\,, \tag{9.24}$$

which automatically vanishes in four dimensions due to the corresponding Fierz identity. While the "source" of distinct evanescent operators might differ, one can understand all these operators as being needed to project back the loop amplitudes to the physical basis in d-dimensions.

Diagram D_3

For the D_3 diagram of Eq. (9.13) we also use the evanescent operators of Eq. (9.20), to find

$$D_3 = \frac{\alpha_s}{64\pi}\mathcal{F}\left[\frac{1}{N_c}\langle E_2\rangle^{(0)}|_1 - \langle E_3\rangle^{(0)}|_1\right]. \tag{9.25}$$

Again, the corresponding 1-loop diagram with distinct contraction (found by $\bar{u}_\delta \leftrightarrow \bar{v}_\beta$ in D_3) yields the same result as D_3 up to $\langle E_i\rangle^{(0)}|_1 \leftrightarrow \langle E_i\rangle^{(0)}|_2$.

ADM and matrix r

Having computed the loop amplitudes from $\mathcal{O}_1$ insertions, we extract its ADM $\gamma_{11}^{(0)}$ and r_{11}-matrix components, given by Eq. (9.10) and Eq. (9.4), respectively. We obtain $\gamma_{11}^{(0)} = 4$ and $r_{11} = -4/3\log\lambda/\mu - 5$. To determine the full ADM and r-matrix, the calculation previously outlined must be done for all the operators in Eq. (9.3). Importantly, although we introduced the evanescent operators $E_{\{1,2,3\}}$ in Eq. (9.20) for $\mathcal{O}_1$, additional evanescent operators are required when evaluating the diagrams with insertions of $\mathcal{O}_{\{2,3,4,5\}}$. The complete set of evanescent operators used in the calculation are found in Appendix A of Ref. [203], resulting in a total of eight physical and twenty evanescent operators. After doing the corresponding calculation, the full ADM and r-matrix are found to be[1]

$$\gamma^{(0)} = \begin{pmatrix} 4 & 0 & 0 & 0 & 0 \\ 0 & -28/3 & 4/3 & 0 & 0 \\ 0 & 16/3 & 32/3 & 0 & 0 \\ 0 & 0 & 0 & -16 & 0 \\ 0 & 0 & 0 & -6 & 2 \end{pmatrix}, \tag{9.26}$$

$$r = \begin{pmatrix} 4/3 & 0 & 0 & 0 & 0 \\ 0 & 44/3 & -4/3 & 0 & 0 \\ 0 & -16/3 & -16/3 & 0 & 0 \\ 0 & 0 & 0 & 64/3 & 0 \\ 0 & 0 & 0 & 6 & 10/3 \end{pmatrix} \log(\mu/\lambda) + \begin{pmatrix} -5 & 0 & 0 & 0 & 0 \\ 0 & 1/3 & -1 & 0 & 0 \\ 0 & -15/2 & -25/6 & 0 & 0 \\ 0 & 0 & 0 & 19/3 & -3 \\ 0 & 0 & 0 & -1/2 & -7/6 \end{pmatrix}, \tag{9.27}$$

for C_{1-5}, with the ADMs and r-matrix elements for C'_{1-3} equal to the ones for the C_{1-3} sector. These results are in agreement with Refs. [202,216,217]. Notice that for $\mathcal{O}_2, \mathcal{O}_3$ and $\mathcal{O}_4, \mathcal{O}_5$ there are mixing (off-diagonal) terms in the ADM and r-matrix. This is because at 1-loop the insertion of $\mathcal{O}_2(\mathcal{O}_4)$ generates $\mathcal{O}_3(\mathcal{O}_5)$ and vice-versa, i.e., there is operator mixing.

It is worth commenting on the ADM and r-matrix results of Eq. (9.26) and Eq. (9.27). The first relevant point is that the ADM at 1-loop is scheme independent, meaning independent of the γ_5 scheme and evanescent operators. This is because the ADM is obtained from the $1/\epsilon$ terms, and therefore it does not depend on the evanescent operators nor the d-dimensional Dirac algebra. To see this, note that the 1-loop diagrams schematically scale as

$$D_{\text{1-loop}} \sim \text{loop integral} \times \text{Dirac algebra} \sim \left(\frac{1}{\epsilon} + \text{finite}\right) \times (\text{finite} + \mathcal{O}(\epsilon)), \tag{9.28}$$

[1] Here and in the following all elements in the 2–3 sector will appear in gray in order to make it clear that they do not play any role when $C_{2,3} = 0$, which is our case.

and thus the resulting $1/\epsilon$ pieces can be directly extracted without the need to use evanescent operators. In other words, to find the ADM at 1-loop the Dirac algebra can be performed in four dimensions and there is no need to use evanescent operators. For the r-matrix, it turns out that the logarithmic IR piece is also scheme independent, because it comes from the finite pieces of the loop integral and Dirac algebra, but the "finite" ($\log\lambda/\mu$ independent) r-matrix piece is scheme dependent because it arises from the loop integral divergence together with $\mathcal{O}(\epsilon)$ pieces of the d-dimensional Dirac algebra. Therefore, the r-matrix is γ_5 scheme dependent and depends on the used set of evanescent operators, as well as on the IR regularisation. Therefore, when doing such calculations one must always specify the scheme that is used: the set of physical and evanescent operators ($\{E_i\}$ taken from Ref. [203]), the renormalisation scheme (e.g., $\overline{\text{MS}}$ in this case), the γ_5 scheme (we use NDR) and the IR regularisation employed (fictitious gluon mass). At this point we wish to point out that the IR (logarithmic) piece of the r-matrix in Eq. (9.27) must cancel in the matching of the $C_i^{(1)}$ at NLO as given by Eq. (9.8) with the (equivalent) IR contributions from the 2-loop full theory contained in $F_i^{(1)}$. This can be understood by recognising that the full and EFT theory must be equal in the IR (low-energy) regime, and thus must have the same IR divergences. Crucially, for this to occur one must consistently regularise IR divergences in the same manner in the full and EFT theories, i.e., introducing a gluon mass for both computations. This cancellation of IR divergences between the full and EFT theory is non-trivial and serves as a check of the calculation.

9.1.2. 2-Loop ADM

The NLO ADM $\gamma^{(1)}$ of Eq. (9.9) arises at 2-loops [202, 203]. It was derived in Ref. [203] using a different basis for physical operators (the "BMU" basis) than the "SUSY" basis of Eq. (9.3). The WCs at NLO will be scheme-dependent, and it will be important to use the same scheme for $\gamma^{(1)}$ in order to get scheme-independent observables. To obtain the 2-loop ADM in the "SUSY" basis we use a *change of basis*, and thus we do not explicitly compute the 2-loop EFT amplitudes. The "BMU" basis for physical operators reads,

$$Q = \left(Q_1^{\text{VLL}}, Q_1^{\text{SLL}}, Q_2^{\text{SLL}}, Q_1^{\text{LR}}, Q_2^{\text{LR}}, Q_1^{\text{VRR}}, Q_1^{\text{SRR}}, Q_2^{\text{SRR}}\right)^T \,, \tag{9.29}$$

where the superscripts VLL, SLL, etc denote the sector of the corresponding operator. In order to find the NLO ADM in the SUSY basis, we must rotate the BMU result in Ref. [203] to our basis. The SUSY ($\mathcal{O}$) and BMU (Q) bases are related in the following way

$$\vec{\mathcal{O}} = R\left(\vec{Q} + W\vec{E}\right) \,, \tag{9.30}$$

where the Fierz-evanescent operators $\vec{E}^T = \left(\star, E_1^{\text{SLL}}, \star, E_1^{\text{LR}}, \star\right)$ are defined in Ref. [203] and

$$R = \begin{pmatrix} 1 & 0 & 0 & 0 & 0 \\ 0 & 1 & 0 & 0 & 0 \\ 0 & -1/2 & 1/8 & 0 & 0 \\ 0 & 0 & 0 & 0 & 1 \\ 0 & 0 & 0 & -1/2 & 0 \end{pmatrix}, \quad W = \begin{pmatrix} 0 & 0 & 0 & 0 & 0 \\ 0 & 0 & 0 & 0 & 0 \\ 0 & 8 & 0 & 0 & 0 \\ 0 & 0 & 0 & -2 & 0 \\ 0 & 0 & 0 & 0 & 0 \end{pmatrix}. \tag{9.31}$$

(The corresponding results for the sector $\mathcal{O}'_{1-3}$ vs VRR/SRR are the same as the 1–3 sector above.) Due to the presence of evanescent operators ($\vec{E}$) and their mixing with the physical operators,

the transformation for $\gamma^{(1)}$ from the BMU basis to the SUSY basis corresponds to a rotation plus a change of scheme, given by (e.g. Refs. [218, 219])

$$\gamma_{\mathcal{O}}^{(1)} = R\left(\gamma_Q^{(1)} - \left[r_Q, \gamma_Q^{(0)}\right] - 2\beta_0 r_Q\right) R^{-1} + \left[r_{\mathcal{O}}, \gamma_{\mathcal{O}}^{(0)}\right] + 2\beta_0 r_{\mathcal{O}}, \tag{9.32}$$

where the matrices $r_{\mathcal{O}}$ and r_Q are defined in Eq. (9.4) in their corresponding bases. The LO ADM $\gamma^{(0)}$ is scheme-independent and thus it holds that $\gamma_{\mathcal{O}}^{(0)} = R\gamma_Q^{(0)}R^{-1}$. We compute r_Q from scratch directly in the BMU basis (along the lines of Section 9.1.1), and obtain

$$r_Q = \begin{pmatrix} 4/3 & 0 & 0 & 0 & 0 \\ 0 & 46/3 & -1/6 & 0 & 0 \\ 0 & 40 & -6 & 0 & 0 \\ 0 & 0 & 0 & 10/3 & -12 \\ 0 & 0 & 0 & 0 & 64/3 \end{pmatrix} \log(\mu/\lambda) + \begin{pmatrix} -5 & 0 & 0 & 0 & 0 \\ 0 & 5/6 & -1/8 & 0 & 0 \\ 0 & -46/3 & 1/6 & 0 & 0 \\ 0 & 0 & 0 & -7/6 & 1 \\ 0 & 0 & 0 & 3/2 & 19/3 \end{pmatrix}. \tag{9.33}$$

where again we have indicated in gray the sector that does not impact our model. Using Eq. (9.32) and taking $\gamma_Q^{(1)}$ from Ref. [203], we find

$$\gamma_{\mathcal{O}}^{(1)} = \begin{pmatrix} \frac{4f}{9} - 7 & 0 & 0 & 0 & 0 \\ 0 & \frac{220f}{27} - \frac{476}{3} & -\frac{4f}{27} - \frac{4}{3} & 0 & 0 \\ 0 & 73 + \frac{110f}{27} & \frac{359}{3} - \frac{218f}{27} & 0 & 0 \\ 0 & 0 & 0 & \frac{68f}{9} - \frac{1343}{6} & 4f - \frac{225}{2} \\ 0 & 0 & 0 & \frac{22f}{3} - 99 & \frac{71}{3} - \frac{22f}{9} \end{pmatrix}, \tag{9.34}$$

where f is the number of active quark flavours. The SLL/SRR sector (in gray) can be reproduced using the formulas given in Section C.1 of Ref. [220], leading to a result in agreement with Eq. (9.34).

9.1.3. Projections

In the previous section we have illustrated the calculation of the ADM and r-matrix to 1-loop in α_s. Upon choosing a γ_5 scheme and completing the physical basis with evanescent operators, the calculation can be carried out to obtain the corresponding ADM and r-matrix given in Eq. (9.26) and Eq. (9.27). Inevitably and despite our efforts to clarify the calculation, any attentive reader must have noticed that the calculation is cumbersome, involving numerous diagrams associated with distinct operators and tedious manipulations of the Dirac algebra. It is definitely not a trivial task to carry out such calculations, and it is therefore worth exploring the possibility of doing the calculation in a different manner. Not only might this help in the computational task, different methodologies can also shed light into distinct aspects of the problem at hand. In the previous discussion we employed what we call the "traditional" method, in which the Dirac algebra is carried out in such a way that we rearrange, order and/or reduce the strings of gamma matrices accordingly and project back to the physical basis (with the help of the evanescent operators).

Here we introduce a different methodology, in which the rearrangement of the Dirac structures is (explicitly) avoided. In the previous section we have argued that in order to compute the ADM

and r-matrix, the 1-loop amplitudes from a concrete $\mathcal{O}_i$ insertion are projected back to tree-level matrix elements of physical and evanescent operators. Consequently, after the loop integration and Dirac algebra is carried out, a generic 1-loop amplitude takes the form

$$\langle \mathcal{O}_i \rangle|_{\text{1-loop}} = \sum_i \left(a_i \langle \mathcal{O}_i \rangle^{(0)} + b_i \langle E_i \rangle^{(0)} \right) \quad \text{for} \quad \mathcal{O}_i \quad \text{insertion}\,. \tag{9.35}$$

The a_i coefficients contain the $1/\epsilon$ poles from which the ADM is found as well as the finite pieces corresponding to the r-matrix. For example, in the previous section where we computed the 1-loop amplitude for $\mathcal{O}_1$, we found $a_1 = 2/3(1-9\epsilon)\mathcal{F}$. Therefore, we wish to extract the a_i coefficients of Eq. (9.35). This can be accomplished with a *projection* P_i satisfying

$$\left.\begin{aligned} P_i \langle \mathcal{O}_j \rangle^{(0)} &= \delta_{ij} + \mathcal{O}(\epsilon^2) \\ P_i \langle E_j \rangle^{(0)} &= \mathcal{O}(\epsilon^2) \end{aligned}\right\} \Rightarrow P_i \langle \mathcal{O}_j \rangle|_{\text{1-loop}} = a_i \delta_{ij}\,. \tag{9.36}$$

Notice that we have specified that the projections must be valid up to $\mathcal{O}(\epsilon)$, with potential $\mathcal{O}(\epsilon^2)$ terms (or higher) being irrelevant because we work at 1-loop. The projector is defined according to $P_i|_S = P_i^A \otimes P_i^B$, and amounts to performing the following replacements on an amplitude

$$P_i|_S : \quad v_\alpha \bar{u}_\beta \to P_i^A S_{\alpha\beta}, \quad u_\alpha \bar{v}_\beta \to P_i^B S_{\alpha\beta}\,, \tag{9.37}$$

where $S_{\alpha\beta} = \{\delta_{\alpha\beta}, T_{\alpha\beta}\}$ are the two possible colour structures, and $P_i^{A,B}$ are composed of Dirac structures. Notice that the projection acts on the Dirac (and colour) structures, while the loop integral is to be performed as described in Section 9.1.1 with DR. Thus, the projection "replaces" the Dirac algebra operations and rearrangements of the "traditional" method. As an example, let us consider the projection on the tree-level matrix element of $\mathcal{O}_1$ as given in Eq. (9.11). We find

$$\begin{aligned} P_i|_\delta \langle \mathcal{O}_1 \rangle^{(0)} &= 2iN \text{Tr}\left(P_i^A \gamma_\mu P_L P_i^B \gamma^\mu P_L\right) - 2iN^2 \text{Tr}\left(P_i^A \gamma_\mu P_L\right) \text{Tr}\left(P_i^B \gamma^\mu P_L\right)\,, \\ P_i|_T \langle \mathcal{O}_1 \rangle^{(0)} &= 8i \text{Tr}\left(P_i^A \gamma_\mu P_L P_i^B \gamma^\mu P_L\right)\,, \end{aligned} \tag{9.38}$$

for the colour structures $\delta_{\alpha\beta}$ and $T_{\alpha\beta}$, respectively[1]. Notice that we get two types of traces, i.e., $\text{Tr}(\dots)$ and $\text{Tr}(\dots)\text{Tr}(\dots)$, coming from different contractions (spinor structures) in the amplitude. We call these terms *direct* and *crossed*, respectively. The analogous projections arise for the other physical and evanescent operators. Consequently, given a set of physical and evanescent operators we construct the projectors such that the conditions on the tree-level amplitudes of Eq. (9.36) are satisfied. The projectors are built as a linear combination of "fundamental" p_i projectors according to

$$\begin{aligned} P_i =& P_i^A \otimes P_i^B \equiv \sum_k c_{ik} p_k \quad \text{with} \\ p_k =& \{\gamma^{\mu_1} \dots \gamma^{\mu_n} P_R \otimes \gamma_{\mu_1} \dots \gamma_{\mu_n} P_R, \gamma^{\mu_1} \dots \gamma^{\mu_n} P_L \otimes \gamma_{\mu_1} \dots \gamma_{\mu_n} P_R, L \leftrightarrow R\}\,, \end{aligned} \tag{9.39}$$

where for clarity we focus on the Dirac structures and omit the colour index (structures), because the colour and Dirac structures factorise. Of course, when giving a projector we shall specify its corresponding ($\delta_{\alpha\beta}$ or $T_{\alpha\beta}$) colour structure. Here, c_{ik} are the corresponding coefficients (numbers) of each p_k structure, such that P_i are a linear combination of the fundamental p_k projections. In the case at hand of $\Delta F = 2$ processes in the WET, there are eight physical ($\mathcal{O}_i, i = 1, \dots, 8$) and twenty evanescent operators ($E_i, i = 1, \dots, 20$). Therefore, we need eight

[1] Notice that the projection with $T_{\alpha\beta}$ is recovered from the $\delta_{\alpha\beta}$ one via $N^2 \to 0, N \to 4$.

projectors $P_i, i = 1, \ldots, 8$, one for each physical operator $\mathcal{O}_i$ in Eq. (9.3). The projectors can be found perturbatively in ϵ by solving an algebraic system of equations,

$$P_i \langle Q_j \rangle^{(0)} = \sum_k c_{ik} p_k \langle Q_j \rangle^{(0)} \equiv \sum_k c_{ik} M_{kj} = \begin{cases} \delta_{ij} & j = 1, \ldots, 8 \\ 0 & j = 9, \ldots, 28 \end{cases} \tag{9.40}$$

where $Q_j = \mathcal{O}_j, j = 1, \ldots, 8; Q_j = E_{j-8}, j = 9, \ldots, 28$. The matrix M is of order $\mathcal{O}(\epsilon)$ and thus we write $M = M^0 + M^\epsilon$, while the coefficients c_{ik} are also expanded to order $\mathcal{O}(\epsilon)$, i.e., $c = c^0 + \epsilon c^\epsilon$, and thus (in matrix notation)

$$\begin{aligned} & c^0 M^0 = \delta_{Q\mathcal{O}} \,, \\ & c^0 \left(M^0 + M^\epsilon \right) + \epsilon c^\epsilon M^0 = \delta_{Q\mathcal{O}} \,, \end{aligned} \tag{9.41}$$

which are solved to find the c^0, c^ϵ coefficients for the corresponding fundamental p_k structures. The application of the projector on an amplitude according to Eq. (9.36) is implemented in a straightforward manner in packages such as FeynCalc. This is the advantage of the projectors: no (explicit) Dirac algebra nor rearrangement must be done, one simply applies the projector (P_i) to an amplitude and the desired coefficient (a_i) is outputted. But there is a source of potential issues in the NDR scheme, namely, the trace of an even number of Dirac matrices with γ_5, such as $\mathrm{Tr}(\gamma^\mu \gamma^\nu \gamma^\rho \gamma^\lambda \gamma_5)$, which are ambiguous in d-dimensions. Notice that these traces (might) appear in the crossed projections $\mathrm{Tr}(\ldots)\mathrm{Tr}(\ldots)$ of Eq. (9.38), while the direct ones $\mathrm{Tr}(\ldots)$ are free of this issue because all Lorentz indices are contracted. In order to compute such traces, one is forced to choose a scheme or prescription, such as 't Hooft–Veltman (HV) or Larin [210,221–223]. In Chapter 10 we will discuss in more detail the projections, the problematic traces with the γ_5 matrix and the different schemes. For now, we simply state the procedure we used for the $\Delta F = 2$ calculation. We carry out the calculation as follows[1]. We choose NDR and freely anticommute γ_5 to the right of the traces. For an even number of γ_5 no issue arises because $\gamma_5^2 = \mathbb{I}$ and therefore, only traces with an odd number of γ_5 yield ambiguous traces. Once this is done, the traces $\mathrm{Tr}(\gamma^{\mu_1} \ldots \gamma^{\mu_{2n}} \gamma_5), n \in \mathbb{Z}$ are dealt with via the Larin scheme, in which γ_5 is replaced according to its definition

$$\gamma_5 = -\frac{i}{4!} \epsilon_{\mu\nu\rho\sigma} \gamma^\mu \gamma^\nu \gamma^\rho \gamma^\sigma \,, \tag{9.42}$$

where $\epsilon_{\mu\nu\rho\sigma}$ is the four dimensional antisymmetric Levi–Civita tensor, with $\epsilon_{0123} = -1, \epsilon^{0123} = +1$. In the Larin scheme, contractions of Levi–Civita tensors are promoted to d-dimensions [222, 223, 226, 227]. With this procedure and solving the system of equations of Eq. (9.41), we find[2]

$$P_1 = -\frac{455i}{2304} p_1^\delta - \frac{193i}{384} p_1^T + \frac{i}{1152} p_8^\delta + \frac{323i}{12288} p_6^T + \epsilon \frac{149i}{256} p_1^\delta \,, \tag{9.43}$$

$$P_2 = -\frac{2520983i}{273888} p_2^\delta + \frac{1489i}{45648} p_7^\delta - \frac{655699i}{45648} p_2^T + \frac{10229i}{365184} p_7^T + \frac{7i}{4608} p_{10}^T \tag{9.44}$$

$$-\frac{105617i}{1095552} p_5^\delta + \epsilon \left(\frac{31272625i}{1643328} p_2^\delta + \frac{4117901i}{136944} p_2^T \right) \,, \tag{9.45}$$

$$P_3 = -\frac{1257571i}{136944} p_2^\delta + \frac{373i}{11412} p_7^\delta - \frac{655645i}{45648} p_2^T + \frac{10157i}{365184} p_7^T + \frac{7i}{4608} p_{10}^T \tag{9.46}$$

$$-\frac{51817i}{547776} p_5^\delta + \epsilon \left(\frac{15625897i}{821664} p_2^\delta + \frac{2056349i}{68472} p_2^T \right) \,, \tag{9.47}$$

[1] We stress that HV is the only (known) consistent scheme [221,223–225] in DR. It correctly reproduces chiral anomalies and avoids internal Dirac algebra contradictions, albeit counterterms must be introduced to preserve gauge invariance. Yet, one can choose a different scheme and obtain correct results, i.e., free of ambiguities. It is then crucial to cross-check the calculations to ensure their validity.

[2] The projectors $P'_{1,2,3}$ projecting into $C'_{1,2,3}$ are equal to $P_{1,2,3}$ with the replacement $P_L \leftrightarrow P_R$.

$$P_4 = -\frac{i}{16}p_3^T + \frac{i}{144}p_6^\delta + \frac{i}{16}p_4^T - \frac{i}{192}p_9^T - \frac{i}{12}p_4^\delta - \epsilon\left(\frac{3i}{16}p_4^T + \frac{i}{24}p_3^\delta\right), \tag{9.48}$$

$$P_5 = -\frac{3i}{16}p_4^T + \frac{i}{48}p_3^T - \frac{i}{36}p_3 + \frac{i}{64}p_9^T + \frac{i\epsilon}{16}p_4^T, \tag{9.49}$$

where the δ, T superscript denotes the colour structure of the corresponding fundamental projector p_i, and the list of projectors p_i reads:

$$\begin{aligned}
p_1 &= \gamma_\mu P_R \otimes \gamma^\mu P_R, & p_2 &= P_L \otimes P_L, \\
p_3 &= \gamma_\mu P_L \otimes \gamma^\mu P_R, & p_4 &= P_L \otimes P_R, \\
p_5 &= \sigma_{\mu\nu} P_L \otimes \sigma^{\mu\nu} P_L, & p_6 &= \gamma_\mu\gamma_\nu\gamma_\rho P_R \otimes \gamma^\mu\gamma^\nu\gamma^\rho P_R, \\
p_7 &= \sigma_{\mu\nu} P_L \otimes \sigma^{\mu\nu} P_R, & p_8 &= \gamma_\mu\gamma_\nu\gamma_\rho\gamma_\sigma\gamma_\lambda P_R \otimes \gamma^\mu\gamma^\nu\gamma^\rho\gamma^\sigma\gamma^\lambda P_R, \\
p_9 &= \gamma_\mu\gamma_\nu\gamma_\rho P_L \otimes \gamma^\mu\gamma^\nu\gamma^\rho P_R, & p_{10} &= \gamma_\mu\gamma_\nu\gamma_\rho\gamma_\sigma\gamma_\lambda\gamma_\delta P_L \otimes \gamma^\mu\gamma^\nu\gamma^\rho\gamma^\sigma\gamma^\lambda\gamma^\delta P_L .
\end{aligned} \tag{9.50}$$

These projectors satisfy the conditions of Eq. (9.37), and when applied to the 1-loop EFT amplitudes, the corresponding ADM and r-matrix of Eq. (9.26) and Eq. (9.27) are obtained, serving as a check of the projection method. Recall that the ADM $\gamma^{(0)}$ at 1-loop is scheme independent and can be found using four-dimensional Dirac algebra. Therefore, we have also checked that using the projectors in $d = 4$ the $\gamma^{(0)}$ is obtained. While here we have focused on the EFT calculation, the projectors can also be used in the full theory, where the amplitude must also be projected back to the tree-level matrix elements of the EFT operator basis as given by Eq. (9.5). In this case, applying the projections extracts the $F_i^{(0)}, F_i^{(1)}$ coefficients and therefore, one can fully compute the WCs at LO and NLO[1] with projections, see Eq. (9.8).

9.2. Leading Order Wilson Coefficients

We now discuss the LO $\mathcal{O}(\alpha_s^0)$ result for the WC $C_i^{(0)}$, as given by Eq. (9.8). The LO contributions originating from LQ exchange to the LO Wilson coefficients $C_i^{(0)}$ arise from the one-loop diagrams shown in Figure 9.1. These results, which are similar to the ones in the MSSM [216] or 2HDMs [228], are known [215, 229], and the non-zero WCs at the matching scale μ_0 are given by[2]

$$C_1^{(0)}(\mu_0) = \frac{1}{128\pi^2 M^2}\sum_{a,b}\Gamma_{ab}^R\Gamma_{ba}^R\,\frac{\log(x_a/x_b)}{x_a - x_b}, \tag{9.51}$$

$$C_1'^{(0)}(\mu_0) = \frac{1}{128\pi^2 M^2}\sum_{a,b}\Gamma_{ab}^L\Gamma_{ba}^L\,\frac{\log(x_a/x_b)}{x_a - x_b}, \tag{9.52}$$

$$C_4^{(0)}(\mu_0) = -\frac{1}{32\pi^2 M^2}\sum_{a,b}\Gamma_{ab}^L\Gamma_{ba}^R\,\frac{\log(x_a/x_b)}{x_a - x_b}, \tag{9.53}$$

with

$$x_a = \frac{M_a^2}{M^2}, \qquad \Gamma_{ab}^X = \sum_\ell \Gamma_{s\ell}^{aX}\Gamma_{b\ell}^{bX*}. \tag{9.54}$$

In these expressions we have introduced a generic mass M setting scale for the WCs. In the degenerate case where $M_a = M$ (for all a)

$$C_1^{(0)}(\mu_0) = \frac{1}{128\pi^2 M^2}\sum_a \Gamma_{aa}^R\Gamma_{aa}^R, \qquad C_1'^{(0)} = C_1\big|_{R\to L}, \qquad C_4^{(0)}(\mu_0) = \frac{-1}{32\pi^2 M^2}\sum_a \Gamma_{aa}^L\Gamma_{aa}^R. \tag{9.55}$$

[1] The 2-loop diagrams in the full theory have UV divergences $1/\epsilon$ and not $1/\epsilon^2$ because the LO 1-loop amplitudes are UV (and IR) finite. The projectors are found up to $\mathcal{O}(\epsilon)$ and thus can be applied in the full theory up to 2-loops.

[2] We have verified LO WCs to check our calculation.

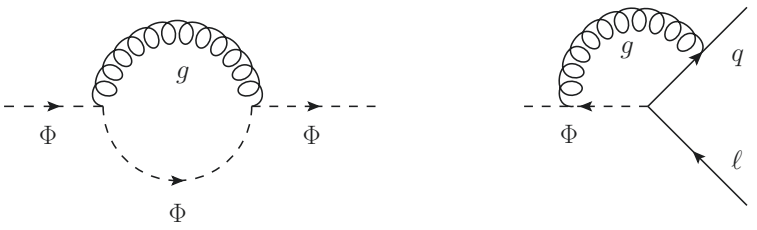

Figure 9.5.: One-loop diagrams leading to the renormalisation of the LQ mass and the LQ coupling to quarks and leptons.

Note that the $C_i^{(0)}$ do not depend explicitly on the matching scale μ_0. However, they do carry an implicit dependence through the scale dependence of the LQ masses M_a and the couplings Γ^X_{ab}. For the numerical analysis it will be reasonable to define the parameters inside $C_i^{(0)}(\mu_0)$ as the renormalised parameters at the scale μ_0, i.e. $M_a(\mu_0)$ and $\Gamma^X_{ab}(\mu_0)$. Formally, setting a different scale amounts to an α_s correction to $C_i^{(0)}$, and thus one could absorb the μ_0 dependence into $C_i^{(1)}$. However, since the renormalisation-scale dependence of M_a and Γ^X_{ab} is known prior to $C_i^{(1)}$ (which we calculate in the next section), it is reasonable to include this implicit matching scale dependence in $C_i^{(0)}$ already at LO.

9.3. Next to Leading Order

Having computed the LO WCs in the previous Section 9.2, we now discuss the calculation of the WCs $C_i^{(1)}$ at NLO in α_s for $\Delta F = 2$. In Subsection 9.3.1, we discuss the renormalisation of the theory, and give the corresponding counterterms and RGEs for the LQ mass and coupling. In Subsection 9.3.2, we discuss the computation of the 2-loop amplitudes in the full theory and finally give the expressions of the NLO WCs in Subsection 9.3.3.

9.3.1. QCD Renormalisation of the LQ Lagrangian

In the presence of NLO QCD corrections, the LQ Lagrangian must be renormalized. Thus, the couplings and fields in Eq. (9.1) are to be understood as bare (divergent) quantities. Using multiplicative renormalisation, the Lagrangian reads

$$\begin{aligned}\mathscr{L}_{\text{LQ}} \;=\;& Z_\Phi \partial^\mu \Phi^* \partial_\mu \Phi - Z_M M^2 \Phi^* \Phi \\ & - \frac{Z_G}{4} G^{A\mu\nu} G^A_{\mu\nu} + i Z_{g_s} g_s \left[\Phi^*_\alpha \partial^\mu \Phi_\beta - (\partial^\mu \Phi^*_\alpha)\Phi_\beta)\right] G^A_\mu T^A_{\alpha\beta} - Z^2_{g_s} g_s^2 \Phi^*_\alpha \Phi_\beta G^{A\mu} G^B_\mu T^A_{\alpha\sigma} T^B_{\sigma\beta} \\ & + Z_q \bar{q}_\alpha (i\partial\!\!\!/) q_\beta \delta_{\alpha\beta} + Z_{g_s} g_s \bar{q}_\alpha \mathcal{G}^A q_\beta T^A_{\alpha\beta} + \left[Z_\Gamma\, \bar{q} \left(\Gamma^{aL}_{q\ell} P_L + \Gamma^{aR}_{q\ell} P_R\right) \ell\, \Phi^*_a + \text{h.c.}\right], \end{aligned} \tag{9.56}$$

where we have considered massless quarks, only a single LQ as well as only one generation of quark and leptons. However, as QCD is flavour blind, this trivially generalizes to the case of multiple generations of quarks and leptons as well as several LQ components. The renormalisation constants $Z_i = 1 + \delta_i$ contain the counterterms δ_i. At one loop order, these counterterms are

fixed by subtracting the $1/\epsilon$ poles originating from the diagrams shown in Figure 9.5 (as well as the quark self-energy) within the $\overline{\text{MS}}$ scheme, resulting in

$$\begin{aligned} \delta_M &= -\hat{\alpha}_s C_F \frac{1}{\epsilon}\,, \qquad \delta_\Phi = \hat{\alpha}_s C_F \frac{2}{\epsilon}\,, \\ \delta_\Gamma &= -\hat{\alpha}_s C_F \frac{1}{\epsilon}\,, \qquad \delta_q = -\hat{\alpha}_s C_F \frac{1}{\epsilon}\,, \\ \delta_{g_s} &= -\hat{\alpha}_s \left(-C_F - \frac{C_A}{2}\right) \frac{1}{\epsilon}\,. \end{aligned} \tag{9.57}$$

The renormalised LQ mass and the couplings thus obey a RGE that determines their renormalisation-scale dependence:

$$\begin{aligned} \frac{dM_a}{d\log\mu} &= -3C_F\hat{\alpha}_s M_a + \mathcal{O}(\hat{\alpha}_s^2)\,, \\ \frac{d\Gamma^{aX}_{q\ell}}{d\log\mu} &= -3C_F\hat{\alpha}_s \Gamma^{aX}_{q\ell} + \mathcal{O}(\hat{\alpha}_s^2)\,, \\ \frac{d\hat{\alpha}_s}{d\log\mu} &= \mathcal{O}(\hat{\alpha}_s^2)\,, \end{aligned} \tag{9.58}$$

where $\hat{\alpha}_s \equiv \alpha_s/(4\pi)$ and $C_F = 4/3$.

9.3.2. Calculation of the 2-Loop Contributions

In order to extract the NLO functions $F_i^{(1)}$, we compute the $\mathcal{O}(\alpha_s)$ part of the (renormalised) amplitude in the full theory $\mathcal{A}(b_\alpha \bar{s}_\beta \to s_\delta \bar{b}_\gamma)$ at vanishing external momenta. We express this part of the amplitude as a sum of the two-loop Feynman diagrams ($\mathcal{D}_x$) and one-loop Feynman diagrams with counterterms ($\mathcal{C}_x$), shown in Figure 9.2,

$$i\mathcal{A}_{\text{LQ}}^{\text{NLO}} = \sum_{x\in\{\text{NLO diagrams}\}} \left(\mathcal{D}_x + \mathcal{C}_x\right)\,. \tag{9.59}$$

The counterterm diagrams have the structure of a one-loop box diagram with a $1/\epsilon$ vertex or propagator insertion, and thus the corresponding one-loop integral must be calculated up to and including terms of order ϵ. The pairs $(\mathcal{D}_x + \mathcal{C}_x)$ are UV-finite, and can be written as

$$\mathcal{D}_x + \mathcal{C}_x = \hat{\alpha}_s f_x(m_j,\lambda)(\bar{u}_{s\delta}\Gamma_x u_{b\alpha})(\bar{v}_{s\beta}\tilde{\Gamma}_x v_{b\gamma}) + \hat{\alpha}_s f'_x(m_j,\lambda)(\bar{u}_{s\delta}\Gamma'_x v_{b\gamma})(\bar{v}_{s\beta}\tilde{\Gamma}'_x u_{b\alpha})\,. \tag{9.60}$$

The parameter λ is the gluon mass that we have introduced to regularise IR divergencies in diagrams where the gluon connects the external (massless) quark legs. This is the same IR regulator appearing in the EFT r-matrix of Eq. (9.27). In order to extract the functions $F_i^{(1)}$ we must write the spinor structures in Eq. (9.60) as a linear combination of tree-level matrix elements $\langle\mathcal{O}_i\rangle^{(0)}$. We do this by applying the Dirac projectors P_i discussed in Section 9.1.3. In this way, the contribution to the function $F_i^{(1)}$ from the pair $(\mathcal{D}_x + \mathcal{C}_x)$ is given by

$$\alpha_s F_i^{(1)}\Big|_x = P_i[\mathcal{D}_x + \mathcal{C}_x]\,. \tag{9.61}$$

The advantage of this approach is that the projection can be performed before evaluating the loop integrals, transforming the integrands into scalar functions of the loop momenta. The scalar two-loop integrals can now be computed as in Ref. [216]: First, loop momenta in the numerators are reduced by expressing them in the form of the denominators; second, the denominators are

decomposed using partial fraction, after which the integral can be expressed as a sum of terms of the form

$$f(M_i,\lambda)\int\frac{d^dq_1\,d^dq_2}{(2\pi)^{2d}}\frac{1}{(q_1^2-m_1^2)^{n_1}(q_2^2-m_2^2)^{n_2}[(q_1-q_2)^2-m_3^2]^{n_3}}\,. \tag{9.62}$$

The solution of these scalar integrals is known [230]. The contributions from each pair $(\mathcal{D}_x+\mathcal{C}_x)$ to the functions $F_i^{(1)}$ are separately UV-finite, and this provides a non-trivial check of the two-loop integrals (note that the individual expressions for the scalar integrals in Eq. (9.62) contain $1/\epsilon$ and $1/\epsilon^2$ poles). The results for the functions $F_i^{(1)}$ still depend on the IR regulator λ. This dependence is cancelled in the combination $F_i^{(1)}-F_j^{(0)}r_{ji}$, and constitutes yet another check of the two-loop calculation.

All types of two-loop diagrams are shown in Figure 9.2. It is useful to classify these diagrams into finite, UV divergent and IR divergent ones. The first two diagrams are finite and thus no renormalisation is required. The following two diagrams are UV divergent, and correspond precisely to the one-loop renormalization of the LQ self-energy and vertex correction from Figure 9.5. Their corresponding counterterm diagrams are shown in the last row of Figure 9.2. The remaining diagrams, in which the gluon connects external quarks, are IR divergent. Such diagrams carry the (logarithmic) λ dependence which contributes to the function $F_i^{(1)}$, and cancels in the matching against the EFT λ dependence of the r-matrix.

9.3.3. Matching Results for the Wilson Coefficients at NLO

The final results for the (non-zero) NLO Wilson Coefficients $C_i^{(1)}$ at the matching scale are

$$\begin{aligned}
C_1^{(1)}(\mu_0) &= \frac{\alpha_s\Gamma^R_{ab}\Gamma^R_{ba}}{4608\pi^3M^2x_a^2x_b^2(x_a-x_b)^2}\\
&\times\Big[x_a^3x_b^2\left(30\mathrm{Li}_2\left(1-X_b^a\right)+\log\left(X_b^a\right)\left(54\log\left(X_b^\mu\right)+69\right)-12\log^2\left(X_b^a\right)-5\pi^2+36\right)\\
&-x_a^4x_b\left(6\mathrm{Li}_2\left(1-X_b^a\right)+3\log^2\left(X_b^a\right)+36\log\left(X_b^a\right)+\pi^2+36\right)\\
&+6x_a^5\left(6\mathrm{Li}_2\left(1-X_b^a\right)+3\log^2\left(X_b^a\right)+\pi^2\right)+a\leftrightarrow b\Big]\,,
\end{aligned} \tag{9.63}$$

$$\begin{aligned}
C_4^{(1)}(\mu_0) &= -\frac{\alpha_s\Gamma^L_{ab}\Gamma^R_{ba}}{1152\pi^3M^2x_ax_b(x_a-x_b)^2}\\
&\times\Big[x_a^2x_b\left(12\mathrm{Li}_2\left(1-X_b^a\right)+6\log\left(X_b^a\right)\left(4\log\left(X_b^a\right)-3\left(\log\left(X_a^\mu\right)+\log\left(X_b^\mu\right)\right)+10\right)+\pi^2\right)\\
&-x_b^3\left(\pi^2-6\mathrm{Li}_2\left(1-X_b^a\right)\right)+a\leftrightarrow b\Big]\,,
\end{aligned} \tag{9.64}$$

$$\begin{aligned}
C_5^{(1)}(\mu_0) &= -\frac{\alpha_s\Gamma^L_{ab}\Gamma^R_{ba}}{384\pi^3M^2x_ax_b(x_a-x_b)^2}\\
&\times\Big[x_b^3\left(\pi^2-6\mathrm{Li}_2\left(1-X_b^a\right)\right)+x_ax_b^2\left(12\mathrm{Li}_2\left(1-X_b^a\right)-12\log\left(X_b^a\right)-\pi^2\right)+a\leftrightarrow b\Big]\,,
\end{aligned} \tag{9.65}$$

with

$$X_b^a=\frac{M_a^2}{M_b^2}\,,\qquad X_a^\mu=\frac{\mu_0^2}{M_a^2}\,,\qquad x_a=\frac{M_a^2}{M^2}\,. \tag{9.66}$$

Note that the dependence on M drops out. In the equal LQ mass limit one has

$$C_1^{(1)}(\mu_0) = \alpha_s\frac{\Gamma^R_{aa}\Gamma^R_{aa}}{4608\pi^3M^2}\left(108\log\frac{\mu_0}{M}+34\pi^2-273\right)\,, \tag{9.67}$$

$$C_4^{(1)}(\mu_0) = \alpha_s\frac{\Gamma^L_{aa}\Gamma^R_{aa}}{1152\pi^3M^2}\left(72\log\frac{\mu_0}{M}+2\pi^2-105\right)\,, \tag{9.68}$$

	$K^0 - \bar{K}^0$	$D^0 - \bar{D}^0$	$B_d - \bar{B}_d$	$B_s - \bar{B}_s$
$B_P^{(1)}(\mu)$	0.506(17)	0.757(27)	0.913(86)	0.952(66)
$B_P^{(2)}(\mu)$	0.46(3)	0.65(4)	0.761(76)	0.806(59)
$B_P^{(3)}(\mu)$	0.79(5)	0.96(8)	1.07(22)	1.10(16)
$B_P^{(4)}(\mu)$	0.78(5)	0.87(6)	1.040(87)	1.022(66)
$B_P^{(5)}(\mu)$	0.47(4)	0.68(5)	0.96(10)	0.943(75)

Table 9.1.: Bag parameters calculated within lattice QCD, adapted from Refs. [231, 232]. The renormalization scale is $\mu = 3, 3, 4.18, 4.18\,\text{GeV}$ for $P = \{K^0, D^0, B_d, B_s\}$.

$$C_5^{(1)}(\mu_0) \;=\; -\alpha_s \frac{\Gamma^L_{aa}\Gamma^R_{aa}}{384\pi^3 M^2}\left(2\pi^2 + 3\right) \,. \tag{9.69}$$

The result for $C_1'^{(1)}(\mu_0)$ is equal to that of $C_1^{(1)}(\mu_0)$ with the replacement $\Gamma^R_{ab} \to \Gamma^L_{ab}$. The results derived here can be easily translated into a matching to the SMEFT above the EW scale. For the necessary formulas we refer to e.g. Ref. [205].

9.4. Phenomenological Analysis

Having computed the WCs at NLO, in Subsection 9.4.1 we compute the corresponding matrix elements in the $\Delta F = 2$ WET. Moreover, we provide the evolution matrix needed to run the WCs from the high to the low scale. In Subsection 9.4.2 we study the matching scale dependence of the WCs at NLO.

9.4.1. Numerical Results

Let us now derive simple numerical results from the analytic expressions obtained in the previous section for $K^0 - \bar{K}^0$, $D^0 - \bar{D}^0$ and $B_{s,d} - \bar{B}_{s,d}$ mixing as a function of the couplings Γ (for $\mu_0 = M$).

The relevant quantity is the matrix element of the $\Delta F = 2$ effective Hamiltonian,

$$\langle P^0|\mathcal{H}_{\text{eff}}^{\Delta F=2}|\bar{P}^0\rangle = \sum_i C_i(\mu)\langle\mathcal{O}_i(\mu)\rangle \,, \tag{9.70}$$

where $\langle\mathcal{O}_i(\mu)\rangle \equiv \langle P^0|\mathcal{O}_i(\mu)|\bar{P}^0\rangle$ can be expressed in terms of non-perturbative "bag parameters" $B_P^{(i)}$ (see e.g. Ref. [232]),

$$\langle\mathcal{O}_1^{(\prime)}(\mu)\rangle \;=\; \frac{2}{3} f_P^2 M_P^2 B_P^{(1)}(\mu) \,, \tag{9.71}$$

$$\langle\mathcal{O}_2^{(\prime)}(\mu)\rangle \;=\; -\frac{5}{12}\left(\frac{M_P}{m_h(\mu) + m_l(\mu)}\right)^2 f_P^2 M_P^2 B_P^{(2)}(\mu) \,, \tag{9.72}$$

$$\langle\mathcal{O}_3^{(\prime)}(\mu)\rangle \;=\; \frac{1}{12}\left(\frac{M_P}{m_h(\mu) + m_l(\mu)}\right)^2 f_P^2 M_P^2 B_P^{(3)}(\mu) \,, \tag{9.73}$$

$$\langle\mathcal{O}_4(\mu)\rangle \;=\; \frac{1}{2}\left[\left(\frac{M_P}{m_h(\mu) + m_l(\mu)}\right)^2 + \frac{1}{6}\right] f_P^2 M_P^2 B_P^{(4)}(\mu) \,, \tag{9.74}$$

$M_{K^0} = 497.611(13)\,\text{MeV}$ [11]	$M_{D^0} = 1.86484(5)\,\text{GeV}$ [11]
$M_{B_d} = 5.27965(12)\,\text{GeV}$ [11]	$M_{B_s} = 5.36688(14)\,\text{GeV}$ [11]
$\overline{m}_u(3\,\text{GeV}) = 2.3(2)\,\text{MeV}$ ††	$\overline{m}_d(3\,\text{GeV}) = 4.4(2)\,\text{MeV}$ ††
$\overline{m}_s(3\,\text{GeV}) = 84.4(6)\,\text{MeV}$ ††	$\overline{m}_c(3\,\text{GeV}) = 0.988(7)\,\text{GeV}$ [235]
$\overline{m}_b(\overline{m}_b) = 4.18(3)\,\text{GeV}$ [11]	
$\overline{m}_d(\overline{m}_b) = 4.1(2)\,\text{MeV}$ ††	$\overline{m}_s(\overline{m}_b) = 78.9(6)\,\text{MeV}$ ††
$f_K = 155.7(3)\,\text{MeV}$ [235]	$f_D = 212.0(7)\,\text{MeV}$ [235]
$f_{B_d} = 190.0(1.3)\,\text{MeV}$ [235]	$f_{B_s} = 230.3(1.3)\,\text{MeV}$ [235]

Table 9.2.: Set of inputs used in the numerical analysis. The inputs marked †† have been obtained from the values at the scale of 2 GeV given in Ref. [235], by running them to 3 GeV and 4.18 GeV using RunDec [236] at four loops in 4-flavour QCD.

$$\langle \mathcal{O}_5(\mu)\rangle \;=\; \frac{1}{6}\left[\left(\frac{M_P}{m_h(\mu)+m_l(\mu)}\right)^2+\frac{3}{2}\right] f_P^2 M_P^2 B_P^{(5)}(\mu)\,, \tag{9.75}$$

where $P = \{K^0, D^0, B_d, B_s\}$ and $(m_h, m_l) = \{(m_s, m_d), (m_c, m_u), (m_b, m_d), (m_b, m_s)\}$ are running $\overline{\text{MS}}$ masses. The numerical values for the bag parameters $B_P^{(i)}(\mu)$ are calculated using lattice QCD and can be found in Refs. [231,232] [1]. For convenience we list these numbers in Table 9.1 adjusted to the conventions used in Eqs. (9.71)–(9.75). The quoted results for the bag parameters are given at the renormalization scales $\mu = \{3, 3, 4.18, 4.18\}\,\text{GeV}$ for $P = \{K^0, D^0, B_d, B_s\}$, and in the renormalization scheme of Ref. [203], which is the same one used here in the calculation of the Wilson coefficients. The numerical values of the various quantities appearing in Eqs. (9.71)–(9.75) are collected in Table 9.2. The resulting numbers for the matrix elements $\langle \mathcal{O}_i(\mu)\rangle$ at the relevant renormalization scales are collected in Table 9.3.

In order to provide numerical formulas for the matrix element in Eq. (9.70) we also need the matching result $C_i(\mu_0)$ and the evolution matrix $U(\mu, \mu_0)$, defined by

$$C_i(\mu) = U(\mu, \mu_0)_{ij} C_j(\mu_0)\,. \tag{9.76}$$

The evolution matrix is calculated by solving the RGE in Eq. (9.9) numerically, using the LO and NLO ADMs in Eqs.(9.26) and (9.34). For the evolution of the strong coupling $\alpha_s(\mu)$ we use the four loop result from RunDec [236]. We find

$$U(4.18\,\text{GeV}, 1\,\text{TeV}) \;=\; \begin{pmatrix} 0.794 & 0 & 0 & 0 & 0 \\ 0 & 1.886 & -0.392 & 0 & 0 \\ 0 & -0.079 & 0.520 & 0 & 0 \\ 0 & 0 & 0 & 2.909 & 0.666 \\ 0 & 0 & 0 & 0.114 & 0.902 \end{pmatrix}, \tag{9.77}$$

[1] Other recent determinations can be found in Refs. [188, 233, 234].

	$K^0 - \bar{K}^0$	$D^0 - \bar{D}^0$	$B_d - \bar{B}_d$	$B_s - \bar{B}_s$
$\langle \mathcal{O}_1^{(\prime)}(\mu) \rangle$	0.00202(0.00007)	0.079(0.003)	0.611(0.058)	0.967(0.068)
$\langle \mathcal{O}_2^{(\prime)}(\mu) \rangle$	−0.0361(0.0024)	−0.150(0.010)	−0.508(0.051)	−0.813(0.061)
$\langle \mathcal{O}_3^{(\prime)}(\mu) \rangle$	0.0124(0.0008)	0.044(0.004)	0.142(0.030)	0.222(0.033)
$\langle \mathcal{O}_4(\mu) \rangle$	0.0739(0.0048)	0.252(0.018)	0.921(0.079)	1.367(0.092)
$\langle \mathcal{O}_5(\mu) \rangle$	0.0154(0.0013)	0.089(0.007)	0.498(0.052)	0.739(0.059)

Table 9.3.: Values for the matrix elements of $\Delta F = 2$ operators, in units of GeV^4. The renormalization scale is $\mu = \{3, 3, 4.18, 4.18\}$ GeV for $P = \{K, D, B_d, B_s\}$.

$$U(3\,\text{GeV}, 1\,\text{TeV}) = \begin{pmatrix} 0.775 & 0 & 0 & 0 & 0 \\ 0 & 2.034 & -0.445 & 0 & 0 \\ 0 & -0.089 & 0.484 & 0 & 0 \\ 0 & 0 & 0 & 3.299 & 0.798 \\ 0 & 0 & 0 & 0.148 & 0.898 \end{pmatrix} . \tag{9.78}$$

Note that the evolution for $C'_{1,2,3}$ is the same as the one for $C_{1,2,3}$. For the LQ contribution to the WCs at the matching scale $C_i(\mu_0) = C_i(1\,\text{TeV})$ we use the formulas in Eqs.(9.55) and (9.67)–(9.69) with $M = \mu_0 = 1\,\text{TeV}$ (the matching scale dependence will be discussed in the following section). We find:

$$\begin{aligned}
C_1(1\,\text{TeV}) &= 7.92 \cdot 10^{-10}\,\Gamma^R_{aa}\Gamma^R_{aa}\left[1_{\text{LO}} + 0.05_{\text{NLO}}\right]\,\text{GeV}^{-2} = 8.30 \cdot 10^{-10}\,\Gamma^R_{aa}\Gamma^R_{aa}\,\text{GeV}^{-2}\,, \\
C'_1(1\,\text{TeV}) &= 7.92 \cdot 10^{-10}\,\Gamma^L_{aa}\Gamma^L_{aa}\left[1_{\text{LO}} + 0.05_{\text{NLO}}\right]\,\text{GeV}^{-2} = 8.30 \cdot 10^{-10}\,\Gamma^L_{aa}\Gamma^L_{aa}\,\text{GeV}^{-2}\,, \\
C_4(1\,\text{TeV}) &= -3.17 \cdot 10^{-9}\,\Gamma^L_{aa}\Gamma^R_{aa}\left[1_{\text{LO}} + 0.07_{\text{NLO}}\right]\,\text{GeV}^{-2} = -3.38 \cdot 10^{-9}\,\Gamma^L_{aa}\Gamma^R_{aa}\,\text{GeV}^{-2}\,, \\
C_5(1\,\text{TeV}) &= -1.69 \cdot 10^{-10}\,\Gamma^L_{aa}\Gamma^R_{aa}\left[0_{\text{LO}} + 1_{\text{NLO}}\right]\,\text{GeV}^{-2} = -1.69 \cdot 10^{-10}\,\Gamma^L_{aa}\Gamma^R_{aa}\,\text{GeV}^{-2}\,.
\end{aligned} \tag{9.79}$$

Putting everything together, we have

$$\begin{aligned}
\langle K^0|\mathcal{H}^{\Delta F=2}_{\text{eff}}|\bar{K}^0\rangle &= \left[(0.131 \pm 0.004)(\Gamma^L_{aa}\Gamma^L_{aa} + \Gamma^R_{aa}\Gamma^R_{aa}) + (-84.5 \pm 5.5)\Gamma^L_{aa}\Gamma^R_{aa}\right] \cdot 10^{-11}\,\text{GeV}^2\,, \\
\langle D^0|\mathcal{H}^{\Delta F=2}_{\text{eff}}|\bar{D}^0\rangle &= \left[(0.051 \pm 0.002)(\Gamma^L_{aa}\Gamma^L_{aa} + \Gamma^R_{aa}\Gamma^R_{aa}) + (-2.91 \pm 0.20)\Gamma^L_{aa}\Gamma^R_{aa}\right] \cdot 10^{-9}\,\text{GeV}^2\,, \\
\langle B_d|\mathcal{H}^{\Delta F=2}_{\text{eff}}|\bar{B}_d\rangle &= \left[(0.41 \pm 0.38)(\Gamma^L_{aa}\Gamma^L_{aa} + \Gamma^R_{aa}\Gamma^R_{aa}) + (-9.41 \pm 0.81)\Gamma^L_{aa}\Gamma^R_{aa}\right] \cdot 10^{-9}\,\text{GeV}^2\,, \\
\langle B_s|\mathcal{H}^{\Delta F=2}_{\text{eff}}|\bar{B}_s\rangle &= \left[(0.64 \pm 0.04)(\Gamma^L_{aa}\Gamma^L_{aa} + \Gamma^R_{aa}\Gamma^R_{aa}) + (-13.98 \pm 0.94)\Gamma^L_{aa}\Gamma^R_{aa}\right] \cdot 10^{-9}\,\text{GeV}^2\,.
\end{aligned} \tag{9.80}$$

In a first approximation (neglecting logarithmic effects) these matrix elements scale like $1\,\text{TeV}^2/M^2$. Thus after inserting the explicit expressions for the couplings Γ, they can be easily applied to set bounds on LQ models.

9.4.2. Dependence on the Matching Scale and Importance of NLO Corrections

The renormalisation-scale dependence of the WCs is given by RGE

$$\left[\frac{\partial}{\partial\log\mu}+\frac{d\alpha_s}{d\log\mu}\frac{\partial}{\partial\alpha_s}+\frac{dM_a}{d\log\mu}\frac{\partial}{\partial M_a}+\frac{d\Gamma^{aX}_{q\ell}}{d\log\mu}\frac{\partial}{\partial\Gamma^{aX}_{q\ell}}-\gamma^T\right]\vec{C}(\mu)=0\,, \tag{9.81}$$

where a sum over the indices a, q, ℓ and $X = L, R$ is understood. It is easy to check that the matching conditions given in Eqs. (9.51)–(9.53) and (9.63)–(9.65) satisfy this RGE up to higher order $\mathcal{O}(\alpha_s^2)$ terms. More explicitly, using the beta functions in Eq. (9.58),

$$\frac{\partial C_i^{(1)}}{\partial\log\mu}=\hat{\alpha}_s\left[3C_F M_a\frac{\partial C_i^{(0)}}{\partial M_a}+3C_F\Gamma^{aX}_{q\ell}\frac{\partial C_i^{(0)}}{\partial\Gamma^{aX}_{q\ell}}+\gamma^{(0)}_{ji}C_j^{(0)}\right]. \tag{9.82}$$

As discussed already in the previous section, even though the LO Wilson coefficients $C_i^{(0)}$ do not depend explicitly on the matching scale μ_0, they do depend on it implicitly through the running masses and couplings. This means we treat $M(\mu_0)$ and $\Gamma^X_{ij}(\mu_0)$ as functions of the matching scale μ_0. Then, one can calculate the matrix element for the $\Delta F = 2$ process in question, taking into account that μ_0 is at the same time the initial scale for the renormalization-group evolution of the Wilson coefficients down to the hadronic scale. The running of the masses and couplings cancels the matching-scale dependence of physical observables order-by-order in $\alpha_s(\mu_0)$. For the evolution down to the hadronic scale we will use the NLO ADM also for the LO estimate (even though this is higher order α_s) since these results were known previously to our calculation.

In order to illustrate both the relative size of the NLO matching corrections and the reduction of the matching-scale dependence of physical observables, we focus on the case of $\bar{B}_s - B_s$ mixing and consider the quantity

$$\mathcal{R}(\mu_0)=\frac{C_i(\mu_b)\langle\mathcal{O}_i(\mu_b)\rangle}{C_i^{(0)}(\mu_b)\langle\mathcal{O}_i(\mu_b)\rangle|_{\mu_0=1\,\text{TeV}}}\,. \tag{9.83}$$

The numerator in $\mathcal{R}$ depends on the matching scale μ_0 via the starting scale of the RGE, the LQ mass $M(\mu_0)$, the LQ couplings to fermions $\Gamma^{L,R}(\mu_0)$ and the explicit μ_0 dependence of $C_i^{(1)}$, which contains a logarithm of the matching scale. In the denominator the matching scale is fixed to the reference value $\mu_0 = 1\,\text{TeV}$.

In Figure 9.6 we plot separately the contributions to $\mathcal{R}$ with $\Gamma^R\Gamma^L = 0$, $\Gamma^R\Gamma^R = \Gamma^L\Gamma^L$ and $\Gamma^R\Gamma^R = \Gamma^L\Gamma^L = 0$, which are called $\mathcal{R}_1$ and $\mathcal{R}_{4,5}$, respectively, as they are related to the corresponding Wilson coefficients. We also show separately the LO and NLO contributions to $\mathcal{R}$. The LO effect is obtained by setting $C_i = C_i^{(0)}$ in the numerator of Eq. (9.83), understanding M and $\Gamma^{L,R}$ in the expression for $C_i^{(0)}$ as running parameters at the scale μ_0 derived from their reference values $M(1\,\text{TeV}) = 1\,\text{TeV}$ and $\Gamma^{L,R}(1\,\text{TeV})$. We see that the LO result has a sizable matching scale dependence, both in the C_1 contribution (or equivalently C_1') and in the $C_{4,5}$ contribution. This scale dependence is, as expected and required, significantly reduced once the NLO matching effects are included. One can also see from Figure 9.6 that the NLO corrections lead to an additive effect of the order of 5% (8%) for the case of C_1 ($C_{4,5}$).

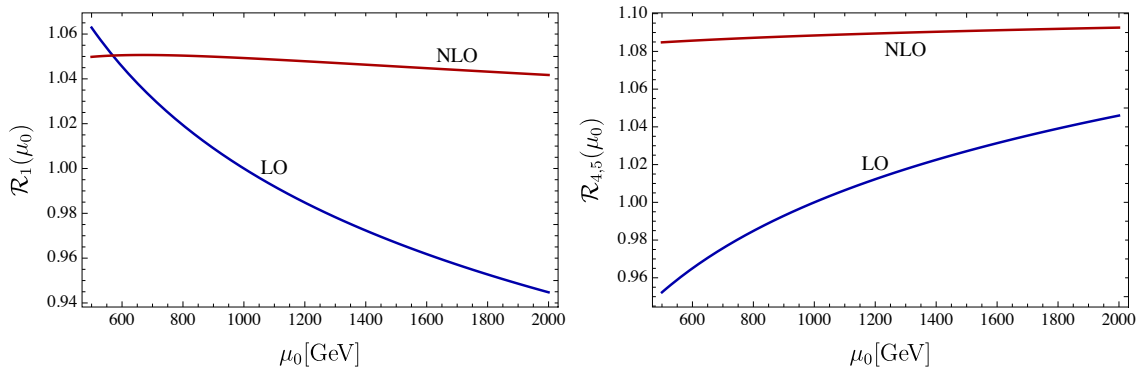

Figure 9.6.: Matching-scale dependence of the ratios $\mathcal{R}_1$ and $\mathcal{R}_{4,5}$ for $M(1\,\mathrm{TeV}) = 1\,\mathrm{TeV}$. The upper plot shows the case in which C_1 is generated (the $\Gamma^R\Gamma^R$ contribution to the mass difference), while the lower plot shows the case in which C_4 and C_5 are generated (the $\Gamma^L\Gamma^R$ contribution to the mass difference).

Chapter 10

$\Delta F = 1$ Processes and Projections

In this last chapter we study $\Delta F = 1$ processes, that is, processes in which a flavour quantum number changes by one unit. Our interests lies in studying such processes via the WET, and concretely we focus on the following $\Delta S = 1$ current–current operators [237–239]

$$Q_1 = (\bar{s}_\alpha u_\beta)_{V-A} (\bar{u}_\beta d_\alpha)_{V-A} \,, \quad Q_2 = (\bar{s}_\alpha u_\alpha)_{V-A} (\bar{u}_\beta d_\beta)_{V-A} \,, \tag{10.1}$$

where $V - A \equiv \gamma_\alpha(1 - \gamma_5)$. The aim is to study the 1-loop $\mathcal{O}(\alpha_s)$ corrections and examine the method of projections to find the ADM and r-matrix, just as we did for $\Delta F = 2$ in Section 9.1.3. In Section 10.1, we introduce the issue of ambiguous traces with the γ_5 matrix and discuss different schemes. In Section 10.2, we compute the ADM and r-matrix using the "traditional" approach, as demonstrated in Section 9.1.1 for $\Delta F = 2$ processes. Here, we do the calculation for various γ_5 schemes and IR regulators. In Section 10.3 we reproduce the calculation using projections (for different γ_5 schemes) and show that we obtain the correct ADM and r-matrices. Moreover, we focus on the dependence of the calculation on the ambiguous traces and discuss several options to speed up computations.

10.1. The Issue of γ_5

The Dirac gamma matrices obey the Clifford algebra, satisfying the anticommutation relation

$$\{\gamma^\mu, \gamma^\nu\} = 2g^{\mu\nu} \,, \tag{10.2}$$

where $g^{\mu\nu}$ is the metric tensor and $\mu, \nu \in \{0, 1, 2, 3\}$. Moreover, the γ_5 matrix is defined as

$$\gamma_5 = i\gamma^0\gamma^1\gamma^2\gamma^3 = -\frac{i}{4!}\epsilon_{\mu\nu\rho\sigma}\gamma^\mu\gamma^\nu\gamma^\rho\gamma^\sigma \,, \tag{10.3}$$

where $\epsilon_{\mu\nu\rho\sigma}$ is the antisymmetric Levi–Civita tensor with $\epsilon_{0123} = -1, \epsilon^{0123} = +1$. As defined in Eq. (10.3), the γ_5 matrix is a four-dimensional object satisfying $\gamma_5^2 = \mathbb{I}, \gamma_5^\dagger = \gamma_5$. Importantly, the following relations hold in four dimensions

$$\begin{aligned} &\{\gamma^\mu, \gamma_5\} = 0 \,, \\ &\mathrm{Tr}\,(\gamma_\mu\gamma_\nu\gamma_\rho\gamma_\sigma\gamma_5) = -4i\epsilon_{\mu\nu\rho\sigma} \,, \\ &\mathrm{Tr}\,(\Gamma_1\Gamma_2) = \mathrm{Tr}\,(\Gamma_2\Gamma_1) \,, \end{aligned} \tag{10.4}$$

where the last one is simply the cyclicity of the trace[1]. In d-dimensions it is inconsistent to require these three properties simultaneously, and one must be abandoned. To see this, let us consider the trace $d\text{Tr}\left(\gamma_\mu\gamma_\nu\gamma_\rho\gamma_\sigma\gamma_5\right)$ in d-dimensions. After using the cyclicity of the trace and anticommutation of the γ_5 matrix with the gamma matrices we find [207, 223, 240]

$$(d-4)\text{Tr}\left(\gamma_\mu\gamma_\nu\gamma_\rho\gamma_\sigma\gamma_5\right) = 0\,. \tag{10.5}$$

Therefore, either $d = 4$ or the trace vanishes, which is in contradiction with the second identity in Eq. (10.4). Hence, in $d \neq 4$ two of the equations in Eq. (10.4) are in contradiction with the third one, and to extend the algebra to d-dimensions (at least) one of the properties is abandoned. This γ_5 issue is relevant to us when using the projection method in NDR, which assumes that the anticommutativity of γ_5 and the cyclicity of the trace hold, as in Eq. (10.4), which results in $\text{Tr}\left(\gamma_\mu\gamma_\nu\gamma_\rho\gamma_\sigma\gamma_5\right)$ being ambiguous. Therefore, we must tackle this problem in our calculation.

Different *schemes/prescriptions* have been proposed [241] in order to deal with this issue, albeit the only one known to be mathematically well defined and consistent is the HV scheme [221, 224, 225]. This scheme gives up the anticommutation property of γ_5 with the gamma matrices, while preserving gauge invariance and the Ward identities (after introducing appropriate counterterms) as well as correctly reproducing the axial anomaly. Another scheme is the so called Larin scheme [222, 242, 243], which replaces any instances of the γ_5 matrix by its definition in Eq. (10.3) and has been extensively used in multi-loop QCD calculations. Meanwhile, the NDR scheme [208] assumes the anticommutativity of γ_5 with the gamma matrices to hold in d-dimensions. This scheme is a convenient choice for single Dirac lines and for Dirac traces with an even number of γ_5, because it is computationally straight forward and can lead to consistent results. But for an odd number of γ_5 an additional prescription is needed since traces like $\text{Tr}\left(\gamma_\mu\gamma_\nu\gamma_\rho\gamma_\sigma\gamma_5\right)$ (might) appear. For example, some schemes abandon the cyclicity of the trace [214, 244], introducing a "reading point" prescription. Although the HV scheme is the only known fully consistent method, it is computationally expensive and more complicated than other schemes. Therefore, using other schemes (such as NDR) might be preferable, but it is then essential to rigorously cross-check calculations to ensure the validity of computations.

10.1.1. The 't Hooft–Veltman Scheme

In the HV (also called BMHV) scheme the γ_5 matrix is defined as in Eq. (10.3), and it is therefore an intrinsically four-dimensional object. The d-dimensional space is split into four-dimensional and $d - 4 = -2\epsilon$ subspaces ($x = \bar{x} + \hat{x}$), where four-dimensional quantities are denoted with bars ($\bar{x} \in 4d$) and -2ϵ dimensional "evanescent" quantities are hatted ($\hat{x} \in -2\epsilon$). Therefore, the metric tensor and gamma matrices take the form

$$\gamma^\mu = \bar{\gamma}^\mu + \hat{\gamma}^\mu\,, \quad g^{\mu\nu} = \bar{g}^{\mu\nu} + \hat{g}^{\mu\nu}\,. \tag{10.6}$$

In this scheme, the gamma matrices in the two subspaces have distinct (anti) commutation relations, with

$$\{\gamma_5, \bar{\gamma}_\mu\} = 0\,, \quad [\gamma_5, \hat{\gamma}_\mu] = 0\,, \quad \{\gamma_\mu, \gamma_5\} = 2\hat{\gamma}_\mu\gamma_5\,, \tag{10.7}$$

while the metric acts as a projection on the $4d$ and -2ϵ sub-spaces,

$$\{\bar{\gamma}_\mu, \bar{\gamma}_\nu\} = 2\bar{g}_{\mu\nu}\,, \quad \{\hat{\gamma}_\mu, \hat{\gamma}_\nu\} = 2\hat{g}_{\mu\nu}\,, \quad \bar{g}_{\mu\rho}g^\rho_\nu = \bar{g}_{\mu\nu}\,, \quad \hat{g}_{\mu\rho}g^\rho_\nu = \hat{g}_{\mu\nu}\,, \quad \hat{g}_{\mu\rho}\bar{g}^\rho_\nu = 0\,. \tag{10.8}$$

By virtue of the Dirac algebra in the HV scheme, the chiral couplings (like the ones in Q_i of Eq. (10.1)) can be written as follows [245, 246]

$$P_R\gamma_\mu P_L = \bar{\gamma}_\mu P_L\,, \quad P_L\gamma_\mu P_R = \bar{\gamma}_\mu P_R\,. \tag{10.9}$$

It is clear that the HV is rather cumbersome due to the splitting of quantities into distinct subspaces with different Clifford algebra, and therefore, it might be desirable to use a simpler scheme.

[1] Moreover, $\text{Tr}\left(\gamma_5\right) = \text{Tr}\left(\gamma_\mu\gamma_\nu\gamma_5\right) = \text{Tr}\left(\gamma_{\mu_1}\ldots\gamma_{\mu_n}\gamma_5\right) = 0 \quad \forall n \in \text{odd}.$

10.1.2. The Larin Scheme

Larin's approach [222, 242, 243] follows the HV scheme and also defines the γ_5 matrix according to Eq. (10.3), which is a four-dimensional object. But instead of splitting quantities into the $d = 4 - 2\epsilon$ sub-spaces, it explicitly replaces any and all γ_5 matrix by its definition, which results into expressions without any explicit γ_5. Therefore, Larin's method is not really to be understood as a γ_5 scheme, but rather as a prescription on how to deal with strings of gamma matrices which also contain γ_5. In following this approach for calculations, one typically encounters contractions of the Levi–Civita tensor, which yield

$$\bar{\epsilon}^{\mu\nu\rho\sigma}\bar{\epsilon}_{\alpha\beta\gamma\delta} = -\bar{g}^{\mu}_{\alpha}\bar{g}^{\nu}_{\beta}\bar{g}^{\rho}_{\gamma}\bar{g}^{\sigma}_{\delta} \pm \dots \tag{10.10}$$

While this is a four-dimensional quantity, Larin's scheme promotes the right-hand side to d dimensions [222, 223, 226, 227], i.e. effectively without the bars.

10.1.3. Naive Dimensional Regularisation

NDR [208] promotes the γ_5 matrix as given by Eq. (10.3) to d dimensions, without introducing a decomposition into sub-spaces. Furthermore, it assumes that γ_5 anticommutes with the gamma matrices, i.e., $\{\gamma_5, \gamma_\mu\} = 0$, and that the cyclicity of the traces holds. Since γ_5 matrices can be anticommuted, for an even number of γ_5 matrices the traces pose no issue because $\gamma_5^2 = \mathbb{I}$. On the other hand, issues arise whenever there is an odd number of γ_5 matrices in a trace, because then one encounters traces such as $\mathrm{Tr}\,(\gamma_\mu\gamma_\nu\gamma_\rho\gamma_\sigma\gamma_5)$. In effect, NDR gives up the second property in Eq. (10.4), and an additional prescription is required in order to proceed if any such traces appear in the calculation at hand. Later on we use the projector methodology in the NDR scheme, together with the so called NDR-Discard prescription, which simply sets to zero the problematic traces, i.e.,

$$\mathrm{Tr}\,(\gamma_{\mu_1}\dots\gamma_{\mu_n}\gamma_5) \to 0 \quad \forall n \in \text{even}\,. \tag{10.11}$$

10.2. 1-loop QCD Amplitudes for $\Delta S = 1$

We consider the 1-loop α_s corrections to the current–current amplitudes from insertions of the following $\Delta S = 1$ four fermion operators [237]

$$Q_1 = (\bar{s}_\alpha u_\beta)_{V-A}\,(\bar{u}_\beta d_\alpha)_{V-A}\,, \quad Q_2 = (\bar{s}_\alpha u_\alpha)_{V-A}\,(\bar{u}_\beta d_\beta)_{V-A}\,, \tag{10.12}$$

with $V - A \equiv \gamma_\alpha(1 - \gamma_5)$. The corresponding 1-loop diagrams are given in Figure 10.1. The objective in this section is to compute the 1-loop ADM $\gamma^{(0)}$ as well as the r-matrix. We wish to do so in the NDR and HV γ_5 schemes, and for different IR regulators. In this section we perform the calculation in the "traditional" approach, that is, by performing the Dirac algebra as dictated by the corresponding scheme (i.e., NDR or HV) and then projecting back to the tree-level matrix elements of Q_i. Relevant references to the following discussion are Refs. [40, 40, 218, 238, 239]. As in the case of $\Delta F = 2$, the $\{Q_i\}$ operator basis of Eq. (10.12) is extended by evanescent operators, which allow to project back the loop amplitudes to the physical operators. In this case, the evanescent operators needed for the calculation are the following two [203, 247]

$$\begin{aligned} E_1 &= 4\,(\bar{s}_\alpha\gamma^\mu\gamma^\nu\gamma^\rho P_L u_\beta)\,(\bar{u}_\beta\gamma_\mu\gamma_\nu\gamma_\rho P_L d_\alpha) - (16 - 4\epsilon)Q_1\,, \\ E_2 &= 4\,(\bar{s}_\alpha\gamma^\mu\gamma^\nu\gamma^\rho P_L u_\alpha)\,(\bar{u}_\beta\gamma_\mu\gamma_\nu\gamma_\rho P_L d_\beta) - (16 - 4\epsilon)Q_2\,. \end{aligned} \tag{10.13}$$

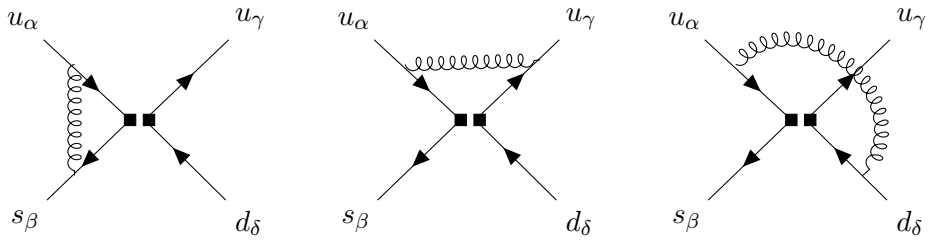

Figure 10.1.: 1-loop diagrams for $\Delta S = 1$ processes from the insertions of Q_i. We have considered the process $u_\alpha \bar{s}_\beta \to u_\gamma \bar{d}_\delta$. We name the diagrams D_1, D_2, D_3 from left to right, and each one has a multiplicity factor of two.

These are used in both the NDR and HV scheme[1], where in both cases the gamma matrices in E_i are d-dimensional. We note that in the case of the HV scheme we have (using $\gamma_\mu = \bar{\gamma}_\mu + \hat{\gamma}_\mu$)

$$\gamma^\mu\gamma^\nu\gamma^\rho = \bar{\gamma}^\mu\bar{\gamma}^\nu\bar{\gamma}^\rho + \hat{\gamma}^\mu\hat{\gamma}^\nu\hat{\gamma}^\rho + \sum_{\text{perm.}} \bar{\gamma}^\mu\bar{\gamma}^\nu\hat{\gamma}^\rho + \sum_{\text{perm.}} \bar{\gamma}^\mu\hat{\gamma}^\nu\hat{\gamma}^\rho\,, \tag{10.14}$$

where the last two terms have three terms each, compactly written as the sum indicating all possible permutations. This means that the operators E_i of Eq. (10.13) in the HV scheme schematically read (omitting fields)

$$E_i^{\text{HV}} \widetilde{=} 4\,(\bar{\gamma}^\mu\bar{\gamma}^\nu\bar{\gamma}^\rho P_L)\,(\bar{\gamma}_\mu\bar{\gamma}_\nu\bar{\gamma}_\rho P_L) - (16-4\epsilon)Q_i + \hat{\gamma}\text{ pieces}\,. \tag{10.15}$$

In four dimensions, the evanescent operators vanish by virtue of the Chisholm identity (in both NDR and HV)

$$\bar{\gamma}_\mu\bar{\gamma}_\nu\bar{\gamma}_\lambda = \bar{\gamma}_\mu\bar{g}_{\nu\lambda} - \bar{\gamma}_\nu\bar{g}_{\mu\lambda} + \bar{\gamma}_\lambda\bar{g}_{\mu\nu} - i\bar{\gamma}^\sigma\gamma_5\epsilon_{\mu\nu\lambda\sigma}\,, \tag{10.16}$$

while hatted quantities in the HV scheme are directly set to zero since they belong to the -2ϵ subspace. We now write the general form of the 1-loop diagrams[2] from Q_1 insertions, see Figure 10.1,

$$\begin{aligned}
D_1 &= -4g_s^2 T_{\beta\delta}T_{\gamma\alpha}\int \left(\bar{v}_\beta\gamma_\mu(\not{k}+\not{p}+m)\Gamma_\alpha(\not{k}+\not{p}+m)\gamma_\nu u_\alpha\right)\left(\bar{u}_\gamma\Gamma^\alpha v_\delta\right)\frac{\mu^{2\epsilon}dk}{\left((k+p)^2-m^2\right)^2}\Delta^{\mu\nu}\,,\\
D_2 &= -4g_s^2 C_F\delta_{\gamma\alpha}\delta_{\beta\delta}\int \left(\bar{v}_\beta\Gamma_\alpha(\not{k}+\not{p}+m)\gamma_\mu u_\alpha\right)\left(\bar{u}_\gamma\gamma_\nu(\not{k}+\not{p}+m)\Gamma^\alpha v_\delta\right)\frac{\mu^{2\epsilon}dk}{\left((k+p)^2-m^2\right)^2}\Delta^{\mu\nu}\,,\\
D_3 &= 4g_s^2 T_{\beta\delta}T_{\gamma\alpha}\int \left(\bar{v}_\beta\Gamma_\alpha(\not{k}+\not{p}+m)\gamma_\mu u_\alpha\right)\left(\bar{u}_\gamma\Gamma^\alpha(\not{k}+\not{p}+m)\gamma_\nu v_\delta\right)\frac{\mu^{2\epsilon}dk}{\left((k+p)^2-m^2\right)^2}\Delta^{\mu\nu}\,,
\end{aligned} \tag{10.17}$$

where $\Gamma^\alpha \equiv \gamma^\alpha P_L$. Crucially, in the HV scheme, the external momenta p is taken to be four dimensional, i.e., $\bar{p}$. Moreover, the Dirac structures from the insertion of physical operators is also four dimensional, $\Gamma^\alpha \equiv \bar{\gamma}^\alpha P_L$ in HV. Further, $\Delta^{\mu\nu}$ corresponds to the Lorentz part of the gluon propagator with a fictitious gluon mass in R_ξ gauge

$$\Delta^{\mu\nu} = i\frac{-g^{\mu\nu} + (1-\xi)\frac{k^\mu k^\nu}{k^2}}{k^2-\lambda^2}\,. \tag{10.18}$$

[1] In [203] it is stated that, in NDR, the -4ϵ term in the evanescent operators is found via the "Greek projections". If we were to use this method in the HV scheme, we would not find -4ϵ but -12ϵ. But since $\mathcal{O}(\epsilon)$ terms can be added with no issue to an evanescent operators, redefining $E_i^{HV} \to E_i^{HV} + 8\epsilon Q_i$ yields the -4ϵ factor.

[2] We work in the $\overline{\text{MS}}$ scheme, i.e., $\mu^2 \to \mu^2 e^\gamma/4\pi$ and define $dk \equiv dk/(2\pi)^d$.

In the expressions of Eq. (10.17) we have introduced the external momenta p, (identical) quark masses m and a gluon mass λ. These are three distinct IR regulators, which we shall consider independently from each other. Therefore, our analysis is divided into several cases, each isolating one of these regulators. For instance, when treating the external momentum as the sole IR regulator, we set $\lambda = m = 0$. If we instead use either the quark mass or the gluon mass, the other parameters are set to zero. This case by case approach allows us to clearly identify the individual effects of each IR regulator. Since the Q_2 operator of Eq. (10.12) only differs from Q_1 in its colour structure, the 1-loop diagrams from the insertion of Q_2 are the same as the ones in Eq. (10.17), up to the following colour structure replacements

$$\begin{aligned} D_1|_{Q_2} &= D_1|_{Q_1} \quad \text{with} \quad C_F\delta_{\beta\alpha}\delta_{\gamma\delta} \leftrightarrow T_{\beta\delta}T_{\gamma\alpha}\,, \\ D_2|_{Q_2} &= D_2|_{Q_1} \quad \text{with} \quad T_{\beta\alpha}T_{\gamma\delta} \leftrightarrow C_F\delta_{\gamma\alpha}\delta_{\beta\delta}\,, \\ D_3|_{Q_2} &= D_3|_{Q_1} \quad \text{with} \quad T_{\beta\alpha}T_{\gamma\delta} \leftrightarrow T_{\beta\delta}T_{\gamma\alpha}\,, \end{aligned} \tag{10.19}$$

while having the same Dirac and Lorentz structure as the diagrams in Eq. (10.17). Since we consider the different IR regulators independently, the loop integral in the amplitudes takes a different form in each case, while being the same integral for the three D_1, D_2, D_3 diagrams in each scenario. We now list these different cases and how to compute the corresponding loop integrals.

Fictitious gluon mass λ

The resulting loop integral reads

$$\mu^{2\epsilon}\int dk \frac{-g_{\mu\nu}+(1-\xi)\frac{k_\mu k_\nu}{k^2}}{k^2-\lambda^2}\frac{k_\sigma k_\tau}{k^4}\,, \tag{10.20}$$

which is reduced via partial fraction decomposition to a (complicated) expression containing the following massive tadpole integral

$$\int \frac{dk}{\left(k^2-\lambda^2\right)^2}\,, \tag{10.21}$$

which is solved as given in Ref. [213]

External momenta p

The resulting integral reads

$$\mu^{2\epsilon}\int dk \frac{-g_{\mu\nu}+(1-\xi)\frac{k_\mu k_\nu}{k^2}}{k^2}\frac{(k+p)_\sigma\,(k+p)_\tau}{(k+p)^4}\,. \tag{10.22}$$

The integral is simplified using partial fractioning and the resulting integrals are p-type integrals which are solved according to Ref. [248]

$$J[\alpha,\beta] = \int \frac{dk}{k^{2\alpha}\,(k-p)^{2\beta}} = \frac{(p^2)^{D/2-\alpha-\beta}}{(4\pi)^{D/2}}G(D,\alpha,\beta)\,, \tag{10.23}$$

with

$$G(D,\alpha,\beta) = \frac{\Gamma\left(D/2-\alpha\right)\Gamma\left(D/2-\beta\right)\Gamma\left(\alpha+\beta-D/2\right)}{\Gamma\left(\alpha\right)\Gamma\left(\beta\right)\Gamma\left(D-\alpha-\beta\right)}\,. \tag{10.24}$$

Quark masses m

In this case the integral does not automatically factorise out from the Dirac structures, but after simplifying the amplitude via partial fractioning the resulting integrals are massive tadpoles of the form

$$\int \frac{dk}{\left(k^2-m^2\right)^\alpha}\,, \tag{10.25}$$

which are solved according to Ref. [213].

Infrared rearrangement (IRA)

This is a different method which we did not discuss in Eq. (10.17) because it does not rely on automatically introducing an IR regulator. Instead, the starting point is the exact decomposition [39, 249, 250]

$$\frac{1}{(k+p)^2-m^2} = \frac{1}{k^2-M^2} + \frac{m^2-p^2-2kp-M^2}{k^2-M^2}\frac{1}{(k+p)^2-m^2}\,, \tag{10.26}$$

where $k(p)$ is the loop (external) momenta, m is the mass of the propagating particle and M is an auxiliary mass introduced to regularise IR divergences, taken to be the same in all the propagators and diagrams. The auxiliary mass regulates all IR divergences and the renormalisation constants and ADM can be extracted from the UV divergences of massive tadpole amplitudes. Moreover, the identity Eq. (10.26) can be applied recursively. Let us consider the case in which we have external momenta (otherwise the integral is scaleless), in which case the integral is given by

$$I = \mu^{2\epsilon}\int dk \frac{-g_{\mu\nu}+(1-\xi)\frac{k_\mu k_\nu}{k^2}}{k^2}\frac{(k+p)_\sigma\,(k+p)_\tau}{(k+p)^4}\,. \tag{10.27}$$

We apply the IRA identity of Eq. (10.26) once to every of the three propagator denominators. Keeping only the UV pieces, we find[1]

$$I = \mu^{2\epsilon}\int dk \left(-g_{\mu\nu}+(1-\xi)\frac{k_\mu k_\nu}{k^2}\right)(k+p)_\sigma\,(k+p)_\tau\left(\frac{1}{(k^2-M^2)^3}+\text{finite}\right)\,, \tag{10.28}$$

which is reduced to a massive tadpole after partial fractioning and solved according to Ref. [213]. Notice that if we had kept all terms from the IRA identity in the integral, we would obtain the same result as in the case with external momenta of Eq. (10.22). This is because the identity Eq. (10.26) is exact. The key point is that by using IRA and keeping only the UV terms, $1/\epsilon$ terms are more easily extracted as the resulting integrals are massive tadpoles instead of p-type integrals.

10.2.1. ADM and r-matrix at 1-loop

The ADM at 1-loop is found according to

$$\gamma^{(0)}_{ij} = -2\left(2\delta Z_q\delta_{ij}+\delta Z'_{ij}\right) \quad \text{with} \quad \delta Z_q = -\xi C_F\,. \tag{10.29}$$

where the $\delta Z'_{ij}$ pieces correspond to the coefficient of the UV divergences of the current–current diagrams of Figure 10.1, and δZ_q is the quark field renormalisation in R_ξ gauge. In both the NDR and HV schemes we find the 1-loop ADM to be

$$\gamma^{(0)} = \begin{pmatrix} -2 & 6 \\ 6 & -2 \end{pmatrix}\,, \tag{10.30}$$

in agreement with Refs. [237, 239]. Therefore, we conclude that the 1-loop ADM is γ_5 scheme independent. This is to be expected because the ADM is found from the $1/\epsilon$ divergences. As argued in Section 9.1.1 for $\Delta F = 2$, the ADM can be directly found by computing the Dirac algebra in four dimensions, and this is also the case here. In other words, the divergent terms are

[1] If we expanded each propagator twice or thrice recursively, the UV piece would still be the same.

unaffected by $\mathcal{O}(\epsilon)$ terms from the Dirac algebra, and the difference in the Dirac algebra between the NDR and HV schemes is precisely a $\mathcal{O}(\epsilon)$ term, i.e.

$$\text{Dirac algebra in NDR} = \text{Dirac algebra in HV} + \mathcal{O}(\epsilon)\text{terms}\,, \tag{10.31}$$

because in four dimensions they must coincide. On the other hand, the r-matrix is affected by $\mathcal{O}(\epsilon)$ terms and differs between the NDR and HV schemes. Recall that in the EFT, the amplitude reads

$$\mathcal{A}_{\text{eff}} = \sum_{i,j} C_i \left(\delta_{ij} + \hat{\alpha}_s\, r_{ij} + \mathcal{O}(\alpha_s^2)\right) \langle Q_j \rangle^{(0)}\,, \tag{10.32}$$

where $\langle Q_i \rangle^{(0)}$ are tree-level matrix elements, r_{ij} is the NLO (finite) contribution and we have defined $\hat{\alpha}_s \equiv \alpha_s/(4\pi)$. As discussed in Section 9.1.1, the inclusion of a IR regulator separates the UV and IR divergences, where the IR divergences take a logarithmic form. The general form of the r-matrix is given by

$$r = A \log \frac{\Lambda_{\text{IR}}}{\mu} + F\,, \quad \text{with} \quad \Lambda_{\text{IR}} = \{p, \lambda, m, M\}\,, \tag{10.33}$$

where A is the logarithmic prefactor, Λ_{IR} is the corresponding IR regulator and F denotes the finite piece. As in the case of the ADM, the log term (given by the matrix A) is also scheme independent, with

$$A = \begin{pmatrix} -\frac{2}{3}(8\xi + 3) & 6 \\ 6 & -\frac{2}{3}(8\xi + 3) \end{pmatrix}\,, \tag{10.34}$$

for both the NDR, HV schemes and for all IR regulators. The reason that the IR term is scheme independent is because it stems from the loop integral divergence. Schematically speaking, a 1-loop diagram scales as

$$\begin{aligned} D_{\text{1-loop}} &\sim \text{loop integral} \times \text{Dirac algebra} \sim \left(\frac{1}{\epsilon} + \log\frac{\Lambda_{\text{IR}}}{\mu} + \text{finite}_I\right) \times (\mathcal{O}(\epsilon) + \text{finite}_D) \\ &\sim \underbrace{\frac{\text{finite}_D}{\epsilon}}_{\gamma^{(0)}} + \underbrace{\text{finite}_D \log\frac{\Lambda_{\text{IR}}}{\mu}}_{A \log \Lambda_{\text{IR}}/\mu} + \underbrace{\frac{\mathcal{O}(\epsilon)}{\epsilon} + \text{finite}_I \text{finite}_D}_{F}\,, \end{aligned} \tag{10.35}$$

where the $I(D)$ index indicates that such a term comes from the integral (Dirac algebra). Therefore, we see that indeed the ADM and logarithmic IR term are scheme independent (i.e. can be found with four-dimensional Clifford algebra) while the finite pieces F are γ_5 scheme dependent. Next, we give the the F value for each IR regulator in the NDR and HV schemes.

10.2.2. r_{NDR} for Different IR Regulators

We collect the results in the NDR scheme for the piece F of the r-matrix in Eq. (10.33) for different IR regulators. We set the logarithmic piece (which takes the same value in every scheme and for all IR regulators) to zero by setting $\mu = \Lambda_{\text{IR}}$.

- With external momenta p:

$$r = \begin{pmatrix} \frac{1}{3}(15\xi + 7) & \xi - 7 \\ 2\xi - 7 & \frac{1}{3}(6\xi + 7) \end{pmatrix}\,. \tag{10.36}$$

  In the Landau gauge $\xi = 0$ we find $r_{11} = r_{22} = 7/3, r_{12} = r_{21} = -7$, which agrees with Ref. [239].

- With a gluon mass λ:

$$r = \begin{pmatrix} \frac{1}{6}(16\xi - 13) & -\frac{11}{2} \\ -\frac{11}{2} & \frac{1}{6}(16\xi - 13) \end{pmatrix} . \tag{10.37}$$

- With quark masses m:

$$r = \begin{pmatrix} -\frac{19}{6} & -\frac{5}{2} \\ -\frac{5}{2} & -\frac{19}{6} \end{pmatrix} . \tag{10.38}$$

- Via IRA:

$$r = \begin{pmatrix} -\frac{1}{3}(4\xi + 11) & -1 \\ -1 & -\frac{1}{3}(4\xi + 11) \end{pmatrix} . \tag{10.39}$$

10.2.3. r_{HV} for Different IR Regulators

We collect the results in the HV scheme for the piece F of the r-matrix in Eq. (10.33) for different IR regulators.

- With external momenta p:

$$r = \begin{pmatrix} 5\xi + 7 & \xi - 5 \\ 2\xi - 5 & \frac{1}{3}(6\xi + 21) \end{pmatrix} . \tag{10.40}$$

  In the Landau gauge $\xi = 0$ we find $r_{11} = r_{22} = 7, r_{12} = r_{21} = -5$, which agrees with Ref. [239].

- With a gluon mass λ:

$$r = \begin{pmatrix} \frac{1}{6}(16\xi + 15) & -\frac{7}{2} \\ -\frac{7}{2} & \frac{1}{6}(16\xi + 15) \end{pmatrix} . \tag{10.41}$$

- With quark masses m:

$$r = \begin{pmatrix} \frac{3}{2} & -\frac{1}{2} \\ -\frac{1}{2} & \frac{3}{2} \end{pmatrix} . \tag{10.42}$$

- Via IRA:

$$r = \begin{pmatrix} \frac{1}{3}(3 - 4\xi) & 1 \\ 1 & \frac{1}{3}(3 - 4\xi) \end{pmatrix} . \tag{10.43}$$

10.2.4. Check of Results

In the previous sections we have computed the 1-loop ADM and the r-matrices in the NDR and HV schemes with distinct IR regulators. We have checked the validity of our results for the external momenta IR regulator in the Landau gauge $\xi = 0$ comparing to the results in Ref. [239]. A check for the other r-matrices with distinct IR regulators is also possible. The check is based on the fact that the following quantity

$$\Delta r \equiv r_{\text{HV}} - r_{\text{NDR}} \,, \tag{10.44}$$

is free from gauge (ξ) and IR dependences, and therefore takes the same value for different IR regulators and any gauge. Indeed, we find

$$\Delta r = \begin{pmatrix} 14/3 & 2 \\ 2 & 14/3 \end{pmatrix} \,, \tag{10.45}$$

for every difference for the distinct IR regulators, which validates our results.

10.3. Projectors for $\Delta S = 1$

Having computed the ADM and r-matrices with the "traditional" method, we wish to find projectors which are directly applied to the loop amplitudes and "extract" the relevant coefficients to find the ADM and r-matrix. The projectors are defined and found as discussed in Section 9.1.3. Recall that projecting amounts to performing the following replacements on a given amplitude

$$v_\alpha \bar{u}_\beta \to P_A S_{\alpha\beta}, \quad u_\alpha \bar{v}_\beta \to P_B S_{\alpha\beta} \,, \tag{10.46}$$

where $S = \{\delta, T\}$ are the two possible colour structures. Thus, when applied to the tree level matrix elements of Q_1, Q_2, we find[1]

$$\begin{aligned} P\langle Q_1\rangle^{(0)}|_\delta &= 4iN\text{Tr}\left(P_B\Gamma^\alpha\right)\text{Tr}\left(P_A\Gamma_\alpha\right) \,, \\ P\langle Q_2\rangle^{(0)}|_\delta &= 4iN^2\text{Tr}\left(P_B\Gamma^\alpha\right)\text{Tr}\left(P_A\Gamma_\alpha\right) \,, \\ P\langle Q_1\rangle^{(0)}|_T &= 16i\text{Tr}\left(P_B\Gamma^\alpha\right)\text{Tr}\left(P_A\Gamma_\alpha\right) \,, \\ P\langle Q_2\rangle^{(0)}|_T &= 0 \,, \end{aligned} \tag{10.47}$$

and analogously for the evanescent operators of Eq. (10.13). Recall that $\Gamma_\alpha = \gamma_\alpha P_L$, where the gamma matrix is four dimensional if working in the HV scheme, $\Gamma_\alpha|_{\text{HV}} = \bar{\gamma}_\alpha P_L$. Then, the projectors are found by constructing them as a linear combination of "fundamental" projectors $p_k \equiv P_A \otimes P_B$

$$P_i = \sum_k c_{ik} p_k \,, \quad p_k = \{\gamma^{\mu_1}\dots\gamma^{\mu_n}P_R \otimes \gamma_{\mu_1}\dots\gamma_{\mu_n}P_R, \gamma^{\mu_1}\dots\gamma^{\mu_n}P_L \otimes \gamma_{\mu_1}\dots\gamma_{\mu_n}P_R, L \leftrightarrow R\} \,, \tag{10.48}$$

satisfying the conditions

$$\begin{aligned} P_i\langle Q_j\rangle^{(0)} &= \delta_{ij} \,, \\ P_i\langle E_j\rangle^{(0)} &= \mathcal{O}(\epsilon^2) \,, \end{aligned} \tag{10.49}$$

up to order $\mathcal{O}(\epsilon)$. Then, finding the projections is reduced to solving an algebraic system of equations. When working in NDR, we know that problematic traces with γ_5 such as $\text{Tr}(\gamma_\mu\gamma_\nu\gamma_\rho\gamma_\sigma\gamma_5)$

[1] Notice that the projections with the T structure can be found from the δ projections by replacing $N \to 4, N^2 \to 0$.

might arise, which are ambiguous. We note that in HV this is not the case, as then the Dirac algebra is well defined, no ambiguities appear and the calculation poses no issue. Therefore, we focus on the projections on the NDR scheme, as we want to study the issues that might arise from the traces with an odd number of γ_5 matrices. Of course, applying projections in the HV scheme is possible and we shall give the corresponding projectors.

Notice that already when constructing the projectors such problematic traces might (and do) appear, as one must trace according to Eq. (10.49) over the physical and evanescent Dirac structures. Then, if the projectors are found according to a certain scheme and/or prescription, this must be specified so that when applying the corresponding projectors to certain amplitudes the same scheme is employed in the calculation. In other words, the projectors are scheme dependent, i.e., they are not the same in NDR and HV, and even within NDR they differ among prescriptions that deal with the ambiguous traces in distinct ways. As previously discussed, in the HV scheme we find the projectors with no problem as the algebra is carried out without ambiguities. In the NDR scheme, traces with an even number of γ_5 pose no issue because after anticommuting we find $\gamma_5^2 = \mathbb{I}$. For an odd number of γ_5 matrices, we also anticommute γ_5 to the right, and we are therefore left with traces of the type $\mathrm{Tr}\left(\gamma_{\mu_1} \dots \gamma_{\mu_{2n}} \gamma_5\right) n \in \mathbb{Z}$. It is then that we choose a prescription for these traces, and the projectors are found accordingly by solving the system of equations satisfying Eq. (10.49). Here, we choose the Larin and NDR-Discard schemes, discussed in Section 10.1.2 and 10.1.3, respectively.

10.3.1. 't Hooft–Veltman

In the HV scheme no γ_5 issues arise, the Clifford algebra is consistent and we compute the projectors, which read

$$\begin{aligned} P_1 &= \frac{47p_1^T}{960i} - \frac{p_2^\delta}{192i} + \epsilon\frac{7p_1^T}{256i} + \frac{p_3^T}{5120i}\,, \\ P_2 &= \frac{47p_1^\delta}{2160i} - \frac{p_2^\delta}{432i} + \epsilon\left(\frac{7p_3^\delta}{147456i} - \frac{7p_1^T}{768i}\right) + \frac{p_3^\delta}{11520i} - \frac{47p_1^T}{2880i} + \frac{p_2^\delta}{576i} - \frac{p_3^T}{15360i}\,, \end{aligned} \tag{10.50}$$

with

$$p_k^S = \{\gamma^\sigma P_R \otimes \gamma_\sigma P_R, \gamma^\sigma\gamma^\rho\gamma^\nu P_R \otimes \gamma_\sigma\gamma_\rho\gamma_\nu P_R, \gamma^\sigma\gamma^\rho\gamma^\nu\gamma^\beta\gamma^\mu P_R \otimes \gamma_\sigma\gamma_\rho\gamma_\nu\gamma_\beta\gamma_\mu P_R\}, \quad S = \{\delta, T\}\,. \tag{10.51}$$

The gamma matrices in p_k are d-dimensional. These projectors are applied directly to the 1-loop amplitudes, and the ADM and r-matrices for different IR regulators given in Section 10.2.3 are found.

10.3.2. NDR-Discard

If we choose NDR-Discard, see Section 10.1.3, we simply set to zero the ambiguous traces. In this case, we obtain the following projectors

$$\begin{aligned} P_1 &= \frac{p_2^T}{384i} - \frac{p_1^T}{96i} + \epsilon\left(\frac{5p_2^T}{768i} - \frac{p_1^T}{24i}\right)\,, \\ P_2 &= \frac{p_2^\delta}{864i} - \frac{p_1^\delta}{216i} + \frac{p_1^T}{288i} - \frac{p_{11}^T}{1152i} + \epsilon\left(\frac{5p_2^T}{1728i} - \frac{p_1^\delta}{54i} + \frac{p_1^T}{72i} - \frac{5p_2^T}{2304i}\right)\,, \end{aligned} \tag{10.52}$$

with

$$p_k^S = \{\gamma^\sigma P_R \otimes \gamma_\sigma P_R, \gamma^\sigma\gamma^\rho\gamma^\nu P_R \otimes \gamma_\sigma\gamma_\rho\gamma_\nu P_R\}, \quad S = \{\delta, T\}\,. \tag{10.53}$$

Applying these projectors directly to the 1-loop EFT amplitudes in Eq. (10.17) we find the correct results for the ADM and NDR r-matrix of Section 10.2.2. We stress that NDR is an inconsistent scheme, but here we see that it correctly reproduces the desired results. Thus, despite being an algebraic inconsistent scheme these projections can be used to find the UV and finite pieces for the current–current operators. Moreover, since we are simply setting the problematic traces to zero, this prescription is very convenient to speed up and handle calculations.

10.3.3. Larin

Using the Larin scheme, discussed in Section 10.1.2, we find the following projectors[1]

$$\begin{aligned} P_1 &= \frac{p_2^T}{256i} - \frac{3p_1^T}{64i} + \epsilon\frac{15p_1^T}{128i}\,, \\ P_2 &= \frac{p_2^\delta}{576i} - \frac{p_1^\delta}{48i} + \frac{p_1^T}{64i} - \frac{p_2^T}{768i} + \epsilon\left(\frac{5p_2^\delta}{1536i} - \frac{5p_1^T}{128i}\right)\,, \end{aligned} \tag{10.54}$$

with

$$p_k^S = \{\gamma^\sigma P_R \otimes \gamma_\sigma P_R, \gamma^\sigma\gamma^\rho\gamma^\nu P_R \otimes \gamma_\sigma\gamma_\rho\gamma_\nu P_R\}, \quad S = \{\delta, T\}\,. \tag{10.55}$$

Using these projectors we obtain the corresponding NDR results for the ADM and r-matrix of Section 10.2.2. Notice how, as expected, the projectors of Eq. (10.54) in the Larin and NDR-Discard in Eq. (10.52) differ in their form, albeit providing the same results. Therefore, as we previously mentioned the projectors are scheme dependent and when given one must always specify the prescription used, as applying the projectors to certain amplitudes can result in problematic traces with γ_5.

10.3.4. Cancellation of Ambiguous Traces

We have seen that despite using two different schemes, NDR-Discard and Larin, the projectors yield the same (NDR) results for the ADM and r-matrix. Therefore, since the two schemes take different values for the $\mathrm{Tr}\,(\gamma_{\mu_1}\ldots\gamma_{\mu_{2n}}\gamma_5)\; n \in \mathbb{Z}$ traces, the result must be independent of such traces. While this might appear surprising at first, there are several ways to justify this fact:

1. We have computed the ADM and r-matrix using projections, but one can also do the calculation via the "traditional" method, as we did in Section 10.2. This procedure does not involve any traces, since the amplitudes of Eq. (10.17) do not have traces. Therefore, the computation with projections must be free of ambiguities related to γ_5 traces. This is indeed what we find.

2. The projectors can be defined as $v_\alpha\bar{v}_\beta \to P_A S_{\alpha\beta}, u_\alpha\bar{u}_\beta \to P_B S_{\alpha\beta}$, instead of using the definition of Eq. (10.46). Then, $P\langle Q_i\rangle^{(0)} \sim \mathrm{Tr}(P_A\Gamma^\alpha P_B\Gamma_\alpha)$ and analogously for E_i, which yields no problematic traces because all Lorentz indices are contracted. Again, this implies that the calculation must be independent of the ambiguous γ_5 traces, since we could have defined the projections in a manner in which no issues arise.

3. We can compute the projectors keeping the ambiguous traces undetermined, with $\mathrm{Tr}\big(\gamma_{\mu_1}\ldots\gamma_{\mu_n}\gamma_5\big) \equiv T_n$, so that the projectors[2] are a function of T_n. Such projectors fulfill the condition Eq. (10.49) for any value of $T_n, \forall n$. This indicates that the projectors are γ_5

[1] If we take the Levi-Civita contractions in four dimensions, then the projectors will be the same as the ones in the HV scheme. This is expected since the Larin scheme defines γ_5 in the same manner as HV, but then promotes the Levi-Civita contractions to d dimensions.

[2] We have these general projectors, but they have a cumbersome expression and thus we do not give them, as this is simply a check to argue the independence of the projections on the γ_5 ambiguous traces.

scheme independent, in the following sense. Once the NDR scheme is chosen, ambiguous traces appear but the projections are valid for any value of such traces because Eq. (10.49) is satisfied for any T_n.

In conclusion, our analysis indicates that the calculation is not affected by ambiguous traces in NDR. Moreover, using NDR-Discard is the optimal choice, as it significantly simplifies the calculations. Here we have computed the 1-loop ADM and amplitudes, but we wish to make the observation that the conclusions and procedure hold at any loop order, i.e., beyond $\mathcal{O}(\alpha_s)$. To argue this, we note that in QCD the gluon-fermion interactions are vector-like (with no γ_5), and thus even if beyond $\mathcal{O}(\alpha_s)$ order the current–current amplitudes have traces from fermion loops, these do not contain γ_5 and the calculation is free of ambiguities. Moreover, this also applies to QED corrections, as QED is also a vector-like theory. Of course, in going to n-loops the projectors must be valid up to $\mathcal{O}(\epsilon^n)$ order, with the corresponding evanescent operators also containing $\mathcal{O}(\epsilon^n)$ terms.

10.3.5. Avoiding Ambiguous Traces

We wish to close this discussion exploring how one might avoid ambiguous traces in a calculation, if those do actually generate a problem. In the analysis of $\Delta S = 1$ we saw that albeit problematic traces with γ_5 appear, the calculation is independent of such traces in a given scheme. This is a particular feature of the setup and calculation, and therefore such ambiguous traces might generate problems in other cases. A possibility, which also applies to the $\Delta S = 1$ discussed here, is to consider a different basis of operators. For example, if instead of working with the operators of Eq. (10.12) we consider the Fierz basis[1]

$$\tilde{Q}_1 = (\bar{s}_\alpha d_\alpha)_{V-A} (\bar{u}_\beta u_\beta)_{V-A} \,, \quad \tilde{Q}_2 = (\bar{s}_\alpha d_\beta)_{V-A} (\bar{u}_\beta u_\alpha)_{V-A} \,, \tag{10.56}$$

then the amplitudes generated by these operators have a spinor structure such that the projections of Eq. (10.46) applied to the amplitudes are

$$P\langle \tilde{\mathcal{O}}_i \rangle^{(0)} \sim \text{Tr}\left(P_B \gamma^\mu P_L P_A \gamma_\mu P_L\right) \quad \mathcal{O}_i \in \{\tilde{Q}_i, \tilde{E}_i\} \,, \tag{10.57}$$

and therefore no problematic traces arise because this is the *direct* projection and all Lorentz indices are contracted. The projectors for the Fierz basis read

$$\begin{aligned} \tilde{P}_1 &= -\frac{p_1^T}{64i} - \epsilon \frac{3p_1^T}{128i} \,, \\ \tilde{P}_2 &= \frac{p_1^T}{192i} - \frac{p_1^\delta}{144i} + \epsilon \left(\frac{p_1^T}{128i} - \frac{p_1^\delta}{96i} \right) \,, \end{aligned} \tag{10.58}$$

with

$$p_1^S = \gamma^\sigma P_R \otimes \gamma_\sigma P_R, \quad S = \{\delta, T\} \,. \tag{10.59}$$

When using a different basis, in this case the Fierz one, the results for the ADM and r-matrix in the $\tilde{Q}_i$ basis have to be transformed to the Q_i basis via a change of basis. Consider the following change of basis

$$\tilde{Q} = R\left(Q + WE\right) \,, \tag{10.60}$$

where the matrix R defines the rotation of the change of basis in four dimensions, that is, $\tilde{Q} = RQ$ in $4d$. In $d = 4 - 2\epsilon$ evanescent operators must be taken into account and thus the WE

[1] We have also computed the ADM and r-matrices in this Fierz basis. The ADM is the same as in the Q_i basis, given in Eq. (10.30). The r-matrix in the $\tilde{Q}_i, Q_i$ bases are related by $r_{\tilde{Q}} = P r_Q P$ where $P = \text{offdiag}(1, 1)$, i.e., by exchanging the diagonal and off-diagonal elements.

term is added in the basis transformation. The ADM and r-matrix change of basis is given, up to 2-loop, by [218–220, 251, 252]

$$\begin{aligned}\gamma^{(0)}_{\tilde{Q}} &= R\gamma^{(0)}_{Q}R^{-1}\,,\\ \gamma^{(1)}_{\tilde{Q}} &= R\left(\gamma^{(1)}_{Q} - \left[r_Q,\gamma^{(0)}_{Q}\right] - 2\beta_0 r_Q\right)R^{-1} + \left[r_{\tilde{Q}},\gamma^{(0)}_{\tilde{Q}}\right] + 2\beta_0 r_{\tilde{Q}}\,,\end{aligned} \tag{10.61}$$

with $\beta_0 = 11N/3 - 2f/3$. A relevant relation which also helps in such calculations is [239, 253]

$$\gamma^{(1)}_{b} = \gamma^{(1)}_{a} + \left[\Delta r,\gamma^{(0)}\right] + 2\beta_0\Delta r\,, \tag{10.62}$$

where a, b indicate a γ_5 scheme (NDR or HV), $\gamma^{(1)}$ is the ADM at 2-loops and $\Delta r = r_b - r_a$. Using this identity, one can compute quantities in the HV scheme, where no γ_5 issues appear, and then indirectly find the results in the NDR where potential γ_5 issues can appear.

Chapter 11

Conclusion

In this final third part of the thesis we have considered a heavy NP particle, the scalar LQ, which couples to SM quarks and leptons. Using the WET, we have studied $\Delta F = 2$ processes (like B_s mixing) and performed a matching calculation to extract the LO $\mathcal{O}(\alpha_s^0)$ and NLO $\mathcal{O}(\alpha_s)$ WCs, corresponding to 2-loop (1-loop) amplitudes in the full theory (EFT). This calculation allows for a consistent use of the existing 2-loop ADMs in the EFT and significantly reduces the matching scale uncertainty in the calculation of physical observables. We find that the NLO matching corrections lead to a constructive effect of the order of 5% (8%) for the case of C_1 (C_4, C_5). We have also provided easy-to-use semi-numerical formulas for the neutral meson mixing amplitudes (at the meson level).

Another focus of this part has been the computation of the ADM and amplitudes at NLO in the WET, for both $\Delta F = 2$ and $\Delta F = 1$ processes. We have introduced a projection method which extracts the desired coefficients from amplitudes, taking care of the corresponding Dirac algebra. Although the method is conceptually straightforward, problematic traces involving an odd number of gamma matrices with γ_5 typically arise. Such traces are ambiguous in d-dimensions in the NDR scheme, which keeps the anticommutativity of γ_5 and the cylicity of the trace, and one is forced to choose a scheme and/or prescription. In the case of $\Delta F = 2$, we employed the NDR scheme followed by the Larin prescription and verified that we indeed obtain the correct ADM and EFT amplitude when projecting. For $\Delta F = 1$, the calculation (without projections) has been done in the general R_ξ gauge using various infrared regulators, in both the NDR and HV schemes. Then, we have reproduced the results using the corresponding projections in each scheme, showing that in NDR the caclulation is independent of the ambiguous traces. This implies that for current–current EFT amplitudes, one can project and set the ambiguous traces to zero (NDR-Discard), which simplifies and speeds up the computation. To our knowledge, the calculation of the r-matrix in the NDR and HV schemes, in general gauge, for different IR regulators and using projections has not been done before.

Chapter 12

Final Conclusion and Outlook

In this thesis we have undertaken a comprehensive investigation of two distinct BSM scenarios using the powerful lens of flavour physics and EFTs. Our work has shown that FCNCs offer uniquely sensitive probes of NP. In Part I we have reviewed the foundations of the SM, highlighting its flavour structure and motivating FCNCs as uniquely sensitive probes of NP. By establishing the EFT framework, we laid out a systematic methodology to separate the effects of heavy and light NP: heavy DOF are integrated out, while light DOF are retained as explicit dynamical modes.

Part II has focused to the exploration of light NP in the form of LDVs, with masses at the GeV scale. We have laid out the LDV model, analysed the generation of FCNC interactions between the LDV and Standard Model fermions, and derived the corresponding phenomenological predictions from two-body decays. Our analysis—which includes both tree-level effects and renormalisation group evolution—constrains the parameter space of LDVs using data from rare meson and lepton decays. This study demonstrates that flavour factories set very tight constraints on the scale of the model, with bounds at the 10^3–10^5 TeV scale. Moreover, we have also followed a theoretical route based on the unitarity of QFTs. Here, the calculation is a complex interplay between the flavour and helicity structures of $2 \to 2$ scattering amplitudes. We have kept the calculation as general as possible, keeping massive fermions. This leads to a violation of unitarity for longitudinal LDVs, while perturbativity bounds are also part of the analysis. While the bounds from unitarity are weaker than the ones from two-body decays, no kinematical endpoint is present for $2 \to 2$ scattering and more of the parameter space can be constrained. Furthermore, the unitarity analysis has deepen our knowledge on massive vector models, highlighting the importance of the different polarisation modes and the GBET.

In Part III we turned our attention to heavy NP by focusing on scalar LQ models. Employing the WET with four-fermion operators, we computed the WCs for $\Delta F = 2$ processes at NLO in QCD. Our detailed matching procedure between the full theory and the EFT highlights the critical role of higher-order corrections in reliably translating NP effects into low-energy observables. Additionally, we have presented a novel computational strategy, which potentially simplifies and speeds up the complicated loop calculations. Moreover, we have addressed the challenge presented by the treatment of γ_5 in d dimensions and shown that despite it, the methodology is free of issues regarding ambiguous traces.

Overall, our work reinforces the importance of flavour observables as precise and powerful tools to probe NP across different energy scales. The complementary nature of the heavy (LQs) and

light (LDVs) scenarios underscores that NP might manifest in diverse forms, each leaving distinctive signatures in low-energy processes.

Looking forward, further improvements in experimental precision—from facilities such as BELLE-II and the LHC—along with advancements in precise theoretical computations, will continue to refine the constraints on BSM models. Extensions of the present analysis to additional NP scenarios, as well as the inclusion of further observables, could provide deeper insights into the underlying flavour structure of the BSM landscape. Ultimately, this thesis lays the groundwork for future research aimed at uncovering the elusive dynamics that lie beyond the SM.

PART IV

Appendices

Appendix A

Recast of Experimental Limits

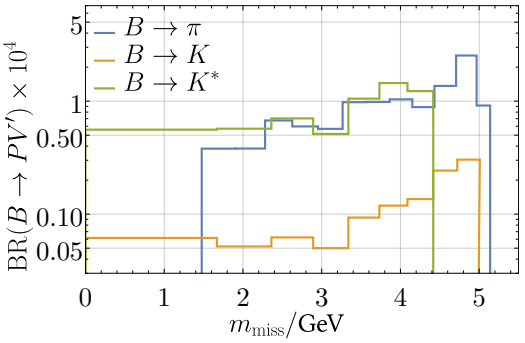

Figure A.1.: Upper 95 % $\mathrm{CL_s}$ limits on the two-body branching ratios $B \to K/K^*/\pi + V'$, as a function of the missing mass $m_{\mathrm{miss}} = \sqrt{q^2}$, obtained by recasting the experimental three-body searches at BaBar [111, 112], see text for details.

Experimental collaborations often provide only limits on the $P \to P' + \mathrm{invisible}$ branching ratios in terms of the three body decay $P \to P' \nu\overline{\nu}$, as a function of the squared invariant mass of the di-neutrino system q^2. In order to get the experimental limits on the two body decays $P \to P'V$, we use the event count n_B per q^2-bin information, if provided by the experimental collaborations. Only the BaBar experiment [111, 112] provides all information needed to perform a recast for two-body decays $B \to K/K^*/\pi + V$. For $B \to K^{(*)}$ and dark-vector masses $m_{V'} < 3\,\mathrm{GeV}$, we use the sophisticated recast of Ref. [121], otherwise we estimate upper limits on the Wilson coefficients in terms of the $\mathrm{CL_s}$ method as explained below.

For a given Wilson coefficient C, the number of signal events s in a q^2-bin i is given as

$$s = \mathrm{BR}^i_{P\to P'}(C) \times N_{\mathrm{tot}} \times \epsilon_i \,, \tag{A.1}$$

where N_{tot} is the total number of P mesons and ϵ_i the efficiency associated to bin i. Further, $\mathrm{BR}^i_{P\to P'}(C)$ denotes the branching ratio of $P \to P'$ within the q^2-bin i. The $s+b$ likelihood is then given as a Poisson distribution in the number of signal plus background events. The efficiency ϵ_i and total number of P mesons N_{tot} are included as global observables associated to auxiliary measurements. The uncertainty on the signal, assumed to be Gaussian, is given by the NP theoretical prediction and is dominated by the form-factor uncertainty. The systematic

uncertainty on the background is implemented as a Gaussian distribution. With this in mind, we denote the likelihood as $\mathcal{L}(x|C,\nu)$ with x being the outcome, i.e., the observed data, C the parameter of interest, i.e., the Wilson coefficient, and ν the nuisance parameters. As a test statistics t_C, we choose a one-sided profile likelihood. Note that the parameter of interest is actually $|C|^2$ since the branching ratio only depends on $|C|^2$ as we only consider one coupling at a time. The p-value p_C of the $s+b$ hypothesis for a given value of the Wilson coefficient C is then given by

$$p_C = \int_{t_C^{\text{obs}}}^{\infty} f(t_C|C,\hat{\hat{\nu}}(C))\,\mathrm{d}t_C\,, \tag{A.2}$$

where t_C^{obs} denotes the value of the test statistics for the observed data, f denotes the pdf of the test statistics t_C, and $\hat{\hat{\nu}}(C)$ are the values of the nuisance parameter that maximise the likelihood for a given C. The $\alpha\,\%$ CL_s limit on the Wilson coefficient is then given by the value of C such that

$$\frac{p_C}{p_0} = 1 - \frac{\alpha}{100}\,, \tag{A.3}$$

where p_0 denotes the p-value of the background only hypothesis. In order to evaluate Eq. (A.2), one needs the pdf f of the test statistics t_C for which we use the ROOT toolkit RooStats in order to sample the distribution by means of a Monte Carlo method.

Taking the $\text{BR}(P \to P'V)$ as a parameter of interest instead of the Wilson coefficient C, we can determine a model independent limit $\text{BR}_\text{exp}(P \to P'V)$ on the two body branching ratios, see Figure A.1.

Appendix B

Limits in the L/R Basis

In this appendix we present bounds on the couplings in the L/R basis $\{\mathbb{C}_{ij}^{\mathrm{DR}}, \mathbb{C}_{ij}^{\mathrm{DL}}, \mathbb{C}_{ij}^{\mathrm{VR}}, \mathbb{C}_{ij}^{\mathrm{VL}}\}$, which are obtained from the limits in the V/A basis (discussed in Section 6.2 and 6.3)) using Eq. (5.43). As the decay rates are symmetric with respect to $\mathbb{C}^{\mathrm{L}} \leftrightarrow \mathbb{C}^{\mathrm{R}}$ the bounds on both couplings are the same.

B.1. Quark Dipole Interactions

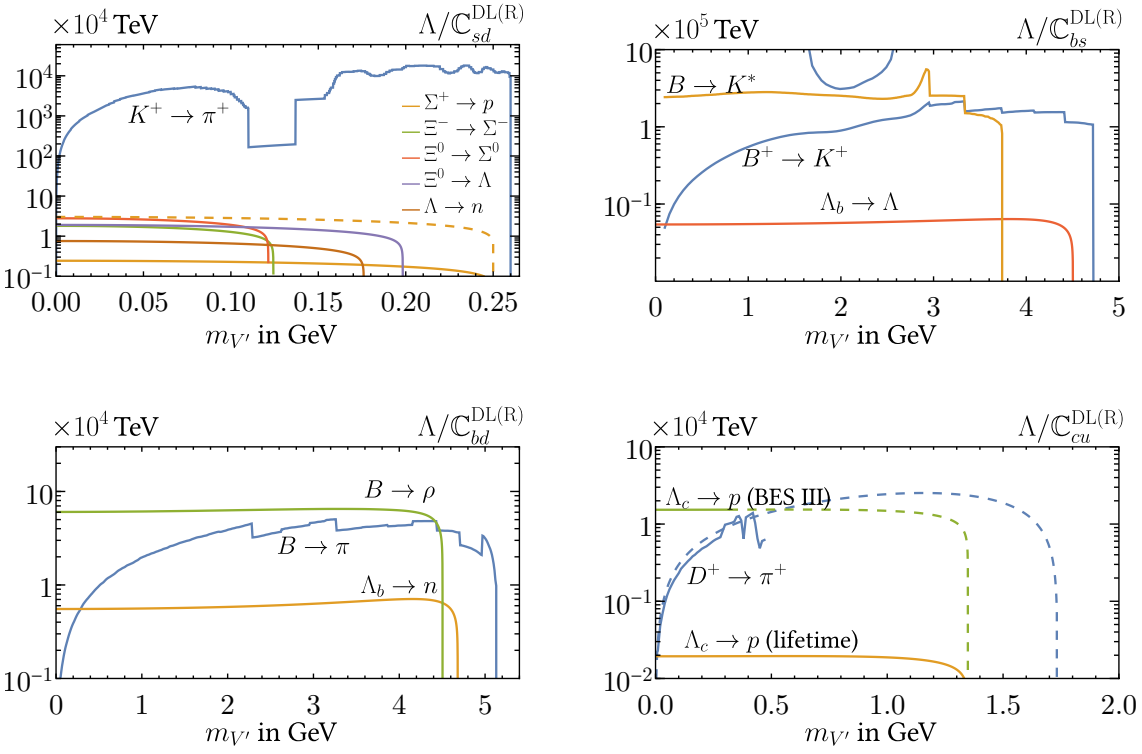

Figure B.1.: Upper limits on quark-flavour violating dipole couplings $\Lambda/|\mathbb{C}_{ij}^{\mathrm{DL}}|$, for $s \to d, b \to s, b \to d$ and $c \to u$ transitions. Bounds on $\Lambda/|\mathbb{C}_{ij}^{\mathrm{DR}}|$ are identical.

B.2. Quark Vector Interactions

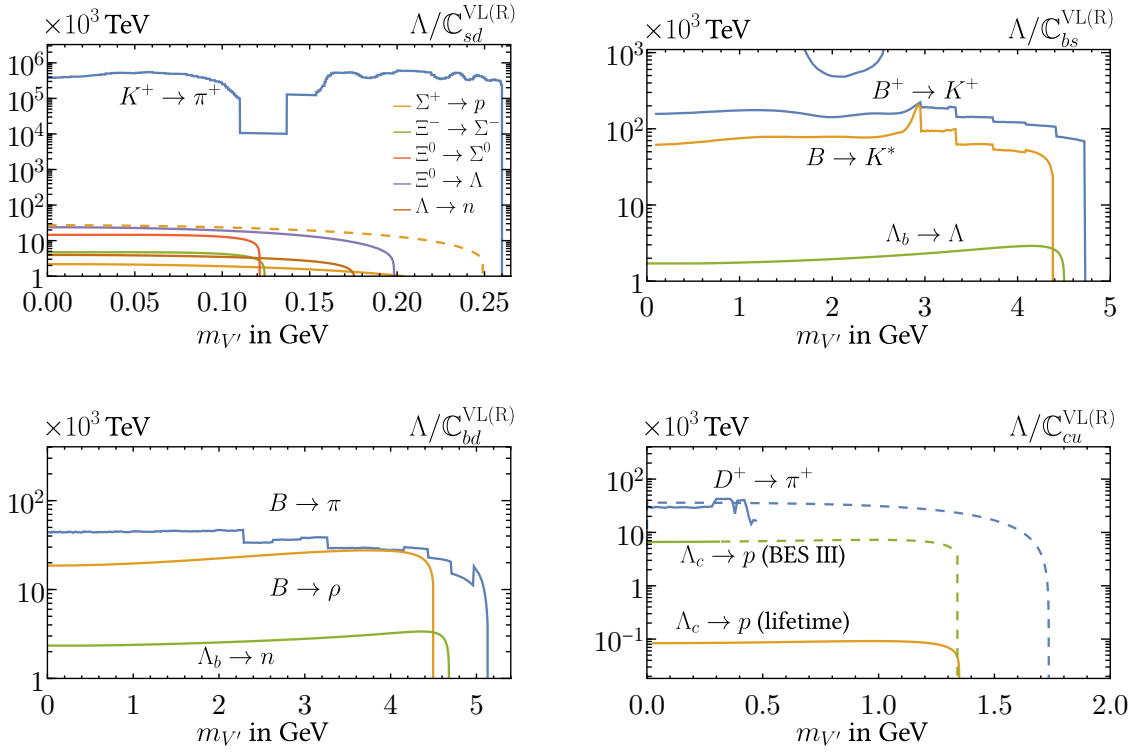

Figure B.2.: Upper limits on quark-flavour violating vector couplings $\Lambda/|\mathbb{C}_{ij}^{\mathrm{VL}}|$, for $s \to d, b \to s, b \to d$ and $c \to u$ transitions. Bounds on $\Lambda/|\mathbb{C}_{ij}^{\mathrm{VR}}|$ are identical.

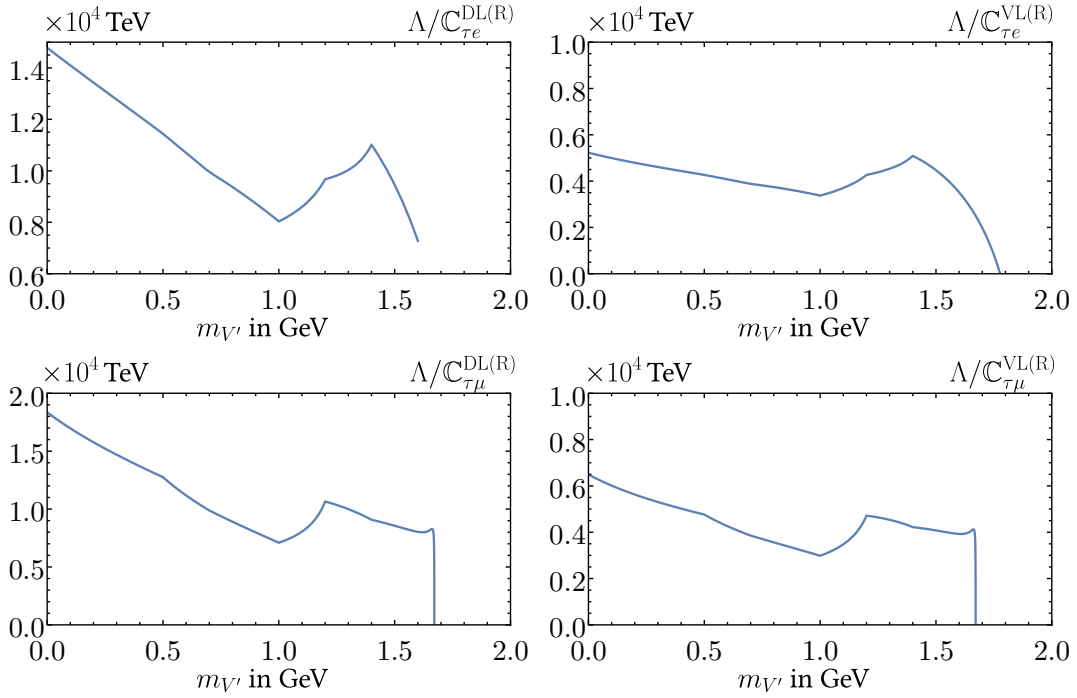

Figure B.3.: *Upper panel:* Lower limits on the dipole (left panel) and vector (right panel) couplings for $\tau \to e$ transitions $\Lambda/|\mathbb{C}_{\tau e}^{\mathrm{DL(R)}}|$, $\Lambda/|\mathbb{C}_{\tau e}^{\mathrm{VL(R)}}|$ from Belle II [114]. *Lower panel:* same for $\tau \to \mu$ transitions $\Lambda/|\mathbb{C}_{\tau \mu}^{\mathrm{DL(R)}}|$, $\Lambda/|\mathbb{C}_{\tau \mu}^{\mathrm{VL(R)}}|$.

Appendix C

Two-Body Decays to Light Dark Vectors

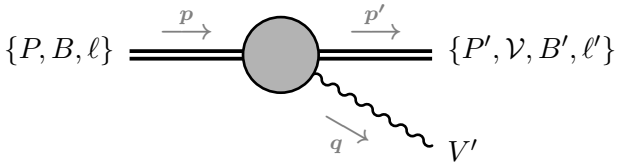

Figure C.1.: Two-body decays $\{P, B, \ell\} \to \{P', \mathcal{V}, B', \ell'\} + V'$. The blob represents the non-perturbative QCD effects for the hadronic decays.

In this appendix we present the full expressions for the two-body decays to a LDV that enter our analysis, namely

- $P \to P' + V'$: pseudoscalar meson to pseudoscalar meson and LDV,
- $P \to \mathcal{V} + V'$: pseudoscalar meson to vector meson and LDV,
- $B \to B' + V'$: baryon to baryon and LDV,
- $\ell \to \ell' V'$: lepton to lepton and LDV.

For the hadronic processes illustrative Feynman diagrams are shown in Figure 6.1, while throughout this appendix we define the two-body kinematics for all decays as in Figure C.1, namely as

$$\mathrm{SM}(p) \to \mathrm{SM}'(p') + V'(q) \tag{C.1}$$

with $q = p - p'$ and $q^2 = (p - p')^2 = m_{V'}^2$. In the next subsection we collect the parametrization of all the relevant form factors for the hadronic processes considered, and in the subsequent subsections we present the expressions for the rates. The numerical values for the form-factors are always taken from the most recent work referenced.

C.1. Form Factors

$P \to P' + V'$

For these decays the hadronic matrix elements for the vector and axial-vector currents read [130]

$$\begin{aligned} \langle P'(p')|\overline{q}'\gamma^\mu q|P(p)\rangle &= (p+p')^\mu f_+^{PP'}(q^2) + (p-p')^\mu f_-^{PP'}(q^2)\,, \\ \langle P'(p')|\overline{q}'\gamma_5\gamma^\mu q|P(p)\rangle &= 0\,. \end{aligned} \tag{C.2}$$

The corresponding matrix elements for tensor and pseudo-tensor currents read [130]

$$\begin{aligned}\langle P'(p')|\overline{q}'\sigma_{\mu\nu}q|P(p)\rangle &= \frac{2}{m_P+m_{P'}}\left(p'_\mu p_\nu - p'_\nu p_\mu\right) f_{\rm T}^{PP'}(q^2)\,,\\ \langle P'(p')|\overline{q}'\sigma^{\mu\nu}\gamma_5 q|P(p)\rangle &= \frac{2i}{m_P+m_{P'}}\epsilon^{\mu\nu\rho\sigma}p'_\rho p_\sigma f_{\rm T}^{PP'}(q^2)\,,\end{aligned} \tag{C.3}$$

where here and throughout we use the $\epsilon_{0123} = -\epsilon^{0123} = +1$ convention for the Levi-Civita tensor.

$P \to \mathcal{V} + V'$

For the pseudoscalar decays to two vectors with $\mathcal{V}$ denoting the vector-meson, the hadronic matrix element for the vector and axial-vector currents are parametrized as [130]

$$\langle \mathcal{V}(p',\lambda)|\overline{q}'\gamma^\mu\left(1\mp\gamma_5\right)q|P(p)\rangle = P_1^\mu \mathcal{V}_1(q^2) \pm P_2^\mu \mathcal{V}_2(q^2) \pm P_3^\mu \mathcal{V}_3(q^2) \pm P_P^\mu \mathcal{V}_P(q^2)\,, \tag{C.4}$$

where λ denotes the polarization of $\mathcal{V}$. The kinematic functions read

$$\begin{aligned} P_P^\mu &= i(\epsilon^*\cdot q)q^\mu\,, & P_1^\mu &= 2\epsilon^\mu{}_{\alpha\beta\gamma}\epsilon^{*\alpha}p'^\beta q^\gamma\,,\\ P_2^\mu &= i\left[\left(m_P^2-m_{\mathcal{V}}^2\right)\epsilon^{*\mu} - (\epsilon^*\cdot q)\left(p'+p\right)^\mu\right]\,, & P_3^\mu &= i(\epsilon^*\cdot q)\left[q^\mu - \frac{q^2}{m_P^2-m_{\mathcal{V}}^2}(p'+p)^\mu\right]\,,\end{aligned} \tag{C.5}$$

where $\epsilon_\mu^* = \epsilon_\mu^*(p',\lambda)$ denotes the polarization vector of the outgoing $\mathcal{V}$. The scalar form factors can be further parametrized as

$$\begin{aligned}\mathcal{V}_P(q^2) &= \frac{-2m_{\mathcal{V}}}{q^2}A_0(m_{V'}^2)\,, \qquad \mathcal{V}_1(q^2) = \frac{-V(q^2)}{m_P+m_{\mathcal{V}}}\,, \qquad \mathcal{V}_2(q^2) = \frac{-A_1(q^2)}{m_P-m_{\mathcal{V}}}\,,\\ \mathcal{V}_3(q^2) &= \frac{m_P+m_{\mathcal{V}}}{q^2}A_1(q^2) - \frac{m_P-m_{\mathcal{V}}}{q^2}A_2(q^2) \equiv \frac{2m_{\mathcal{V}}}{q^2}A_3(q^2)\,,\end{aligned} \tag{C.6}$$

with $A_3(0) = A_0(0)$, which ensures finite matrix elements at $q^2 = 0$, i.e., for massless LDV. The corresponding matrix elements for tensor and pseudo-tensor currents read [130]

$$\begin{aligned}\langle \mathcal{V}(p',\lambda)|\overline{q}'\sigma^{\mu\nu}q|P(p)\rangle &= -i\epsilon_\alpha^* T^{\alpha\mu\nu}(q^2)\,,\\ \langle \mathcal{V}(p',\lambda)|\overline{q}'\sigma_{\mu\nu}\gamma_5 q|P(p)\rangle &= \frac{1}{2}\epsilon_\alpha^*\epsilon_{\mu\nu\rho\sigma}T^{\alpha\rho\sigma}(q^2)\,,\end{aligned} \tag{C.7}$$

where

$$\begin{aligned}T^{\alpha\mu\nu}(q^2) = \epsilon^{\alpha\mu\nu\beta}&\left[\left(p_\beta + p'_\beta - q_\beta\frac{m_P^2-m_{\mathcal{V}}^2}{q^2}\right)T_1^{P\mathcal{V}}(q^2) + q_\beta\frac{m_P^2-m_{\mathcal{V}}^2}{q^2}T_2^{P\mathcal{V}}(q^2)\right]\\ &+ \frac{2p^\alpha}{q^2}\epsilon^{\mu\nu\beta\gamma}p_\beta p'_\gamma\left(T_2^{P\mathcal{V}}(q^2) - T_1^{P\mathcal{V}}(q^2) + \frac{q^2}{m_P^2-m_{\mathcal{V}}^2}T_3^{P\mathcal{V}}(q^2)\right)\,.\end{aligned} \tag{C.8}$$

For vanishing momentum transfer $q^2 = 0$, i.e., massless LDV, the scalar form-factors satisfy

$$T_1^{P\mathcal{V}}(0) = T_2^{P\mathcal{V}}(0) \equiv T\,, \tag{C.9}$$

while the contribution proportional to $T_3(0)$ vanishes.

$\boldsymbol{B \to B' + V'}$

For the baryon decays the matrix elements for vector and axial-vector currents are parametrized by [131, 133, 136]

$$\begin{aligned}\langle B'(p')|\overline{q}'\gamma_\mu q|B(p)\rangle &= \overline{u}_{B'}(p')\left(f_1(q^2)\gamma_\mu - i\frac{f_2(q^2)}{m_B}\sigma_{\mu\nu}q^\nu + \frac{f_3(q^2)}{m_B}q_\mu\right)u_B(p)\,,\\ \langle B'(p')|\overline{q}'\gamma_\mu\gamma_5 q|B(p)\rangle &= \overline{u}_{B'}(p')\left(g_1(q^2)\gamma_\mu - i\frac{g_2(q^2)}{m_B}\sigma_{\mu\nu}q^\nu + \frac{g_3(q^2)}{m_B}q_\mu\right)\gamma_5 u_B(p)\,,\end{aligned} \tag{C.10}$$

with $u_B(p)$ and $u_{B'}(p')$ the spinor functions for B and B' respectively. For Λ decays the values of the form factors are taken from [131,133,136], while for hyperon decays they are taken from [126–128].

The corresponding matrix elements for tensor and pseudo-tensor currents have the form [105, 254]

$$\begin{aligned}\langle B'(p')|\overline{q}'\sigma^{\mu\nu}q|B(p)\rangle &= g_{\rm T}^{BB'}\overline{u}_{B'}(p')\sigma^{\mu\nu}u_B(p)\,,\\ \langle B'(p')|\overline{q}'\sigma_{\mu\nu}\gamma_5 q|B(p)\rangle &= \frac{i}{2}g_{\rm T}^{BB'}\epsilon_{\mu\nu\alpha\beta}\overline{u}_{B'}(p')\sigma^{\alpha\beta}u_B(p)\,,\end{aligned} \tag{C.11}$$

which is an approximation valid for $m_{V'}^2 = 0$, which we use for the hyperon decays. For the baryon $\Lambda_b \to \Lambda$, $\Lambda_b \to n$, and $\Lambda_c \to p$ decays we use the available full parametrization, given by [131, 136]

$$\begin{aligned}\langle B'(p')|\overline{q}' i\sigma^{\mu\nu}q_\nu q|B(p)\rangle &= \overline{u}_{B'}(p')\left(\frac{f_1^{\rm TV}(q^2)}{m_B}\left(\gamma^\mu q^2 - q^\mu \not{q}\right) - f_2^{\rm TV}(q^2)i\sigma^{\mu\nu}q_\nu\right)u_B(p)\,,\\ \langle B'(p')|\overline{q}' i\sigma^{\mu\nu}q_\nu\gamma_5 q|B(p)\rangle &= \overline{u}_{B'}(p')\left(\frac{f_1^{\rm TA}(q^2)}{m_B}\left(\gamma^\mu q^2 - q^\mu \not{q}\right) - f_2^{\rm TA}(q^2)i\sigma^{\mu\nu}q_\nu\right)\gamma_5 u_B(p)\,.\end{aligned} \tag{C.12}$$

Having collected all hadronic input used in the analysis we next present the full expressions for the two-body rates. We show separately the contributions from dipole and vector interactions with the LDV, c.f. Eqs. (5.42). For brevity we drop the argument in all form factors since it is always $q^2 = m_{V'}^2$ in two-body decays. To shorten the expression we also introduce the notations

$$\kappa_x \equiv m_x^2/M^2 \qquad \text{and} \qquad \lambda_{xy} \equiv (1-\kappa_x-\kappa_y)^2 - 4\kappa_x\kappa_y\,, \tag{C.13}$$

with m_x indicating the mass of the final-state particle x and M the mass of the decaying particle.

C.2. Partial Width for $\boldsymbol{P \to P' + V'}$

The partial width for the decay $P \to P' + V'$ with an underlying $q \to q'$ flavour-changing transition is given respectively for dipole and vector interaction by

$$\Gamma(P \to P'V')\Big|_{\rm D} = \frac{\kappa_{\gamma'}m_P^3}{4\pi\Lambda^2}\frac{\lambda_{P'V'}^{3/2}}{(1+\sqrt{\kappa_{P'}})^2}|f_{\rm T}^{PP'}|^2|\mathbb{C}_{q'q}^{\rm D}|^2\,, \tag{C.14}$$

$$\Gamma(P \to P'V')\Big|_{\rm V} = \frac{m_P^3}{16\pi\Lambda^2}\lambda_{P'V'}^{3/2}|f_+^{PP'}|^2|\mathbb{C}_{q'q}^{\rm V}|^2\,, \tag{C.15}$$

Note that due to the parity conservation of strong interactions the rate is independent of the axial couplings $\mathbb{C}_{ij}^{\rm V5}$ and $\mathbb{C}_{ij}^{\rm D5}$. Therefore, $P \to P' + V'$ decays are only sensitive to the $\mathbb{C}_{ij}^{\rm V(D)}$ couplings. In the $\{{\rm L},{\rm R}\}$ basis, these decays are sensitive to both $\mathbb{C}_{ij}^{\rm DL(R)}, \mathbb{C}_{ij}^{\rm VL(R)}$ couplings.

In the limit for massless LDV, the leading in $m_{V'}$ contributions to the decay rates read

$$\lim_{m_{V'}\to 0}\Gamma(P\to P'+V')\Big|_{\mathrm{D}} = \frac{m_{V'}^2 m_P}{4\pi\Lambda^2}\left(1-\sqrt{\kappa_{P'}}\right)^3 |f_{\mathrm{T}}^{PP'}|^2 |\mathbb{C}^{\mathrm{D}}_{q'q}|^2\,, \tag{C.16}$$

$$\lim_{m_{V'}\to 0}\Gamma(P\to P'+V')\Big|_{\mathrm{V}} = \frac{m_P^3}{16\pi\Lambda^2}\left(1-\kappa_{P'}\right)^3 |f_{+}^{PP'}|^2 |\mathbb{C}^{\mathrm{V}}_{q'q}|^2\,. \tag{C.17}$$

While the rate originating from dipole interactions vanishes in the massless limit, the contribution of the vector interaction remains constant due to the linear scaling $m_{V'}/\Lambda$ introduced and discussed in Eq. (5.42).

C.3. Partial Width for $P \to \mathcal{V} + V'$

The partial width for the decay $P \to \mathcal{V} + V'$ with an underlying $q \to q'$ flavour-changing transition is given respectively for dipole and vector interaction by

$$\begin{aligned}
\Gamma(P\to \mathcal{V}+V')\Big|_{\mathrm{D}} &= \frac{m_P^3}{2\pi\Lambda^2}\lambda_{\mathcal{V}V'}^{1/2}\left(A_{\mathrm{D}}|\mathbb{C}^{\mathrm{D}}_{q'q}|^2 + A_{\mathrm{D5}}|\mathbb{C}^{\mathrm{D5}}_{q'q}|^2\right)\,,\\
\Gamma(P\to \mathcal{V}+V')\Big|_{\mathrm{V}} &= \frac{m_P^3\kappa_{\gamma'}^2}{8\pi\Lambda^2}\lambda_{\mathcal{V}V'}^{1/2}\left(A_{\mathrm{V}}|\mathbb{C}^{\mathrm{V}}_{q'q}|^2 + A_{\mathrm{V5}}|\mathbb{C}^{\mathrm{V5}}_{q'q}|^2\right)\,,
\end{aligned} \tag{C.18}$$

with the coefficients A_X given by

$$A_{\mathrm{D}} = |T_1^{P\mathcal{V}}|^2\lambda_{\mathcal{V}V'}\,, \tag{C.19}$$

$$\begin{aligned}
A_{\mathrm{D5}} &= |T_2^{P\mathcal{V}}|^2\frac{8\kappa_V\left(1-\kappa_V\right)^2+\kappa_{\gamma'}\left(1+3\kappa_V\right)^2-2\kappa_{\gamma'}^2(1+3\kappa_V)+\kappa_{\gamma'}^3}{8\kappa_V}\\
&\quad + |T_3^{P\mathcal{V}}|^2\lambda_{\mathcal{V}V'}^2\frac{\kappa_{\gamma'}}{8\kappa_V(1-\kappa_V)^2} - \mathrm{Re}(T_2^{P\mathcal{V}}T_3^{P\mathcal{V}*})\lambda_{\mathcal{V}V'}\frac{\kappa_{\gamma'}(1+3\kappa_V-\kappa_{\gamma'})}{4\kappa_V(1-\kappa_V)}\,,
\end{aligned} \tag{C.20}$$

$$A_{\mathrm{V}} = |V|^2\frac{\lambda_{\mathcal{V}V'}}{\left(1+\sqrt{\kappa_V}\right)^2}\,, \tag{C.21}$$

$$\begin{aligned}
A_{\mathrm{V5}} &= |A_1|^2\frac{\kappa_{\gamma'}^3-2\kappa_{\gamma'}^2(1+3\kappa_V)+\kappa_{\gamma'}(1+3\kappa_V)^2+8(1-\kappa_V)^2\kappa_V}{8\kappa_V\left(1-\sqrt{\kappa_V}\right)^2}\\
&\quad + |A_3|^2\frac{\lambda_{\mathcal{V}V'}^2}{2\kappa_{\gamma'}\left(1-\kappa_V\right)^2} + \mathrm{Re}(A_1A_3^*)\frac{\sqrt{1+\kappa_V}}{2\sqrt{\kappa_V}\left(1-\kappa_V\right)^2}\lambda_{\mathcal{V}V'}\left(1-\kappa_{\gamma'}+3\kappa_V\right)\,.
\end{aligned} \tag{C.22}$$

In the limit of a massless LDV, the decay rates reduce to

$$\begin{aligned}
\lim_{m_{V'}\to 0}\Gamma(P\to \mathcal{V}V')\Big|_{\mathrm{D}} &= \frac{m_P^3}{2\pi\Lambda^2}\left(1-\kappa_V\right)^3|T|^2\left(|\mathbb{C}^{\mathrm{D}}_{q'q}|^2+|\mathbb{C}^{\mathrm{D5}}_{q'q}|^2\right)\,,\\
\lim_{m_{V'}\to 0}\Gamma(P\to \mathcal{V}V')\Big|_{\mathrm{V}} &= \frac{m_P^3}{16\pi\Lambda^2}\left(1-\kappa_V\right)^3\left(|A_3|^2|\mathbb{C}^{\mathrm{V5}}_{q'q}|^2+\frac{2\kappa_{\gamma'}|V|^2}{\left(\sqrt{\kappa_V}+1\right)^2}|\mathbb{C}^{\mathrm{V}}_{q'q}|^2\right)\,,
\end{aligned} \tag{C.23}$$

which illustrates that the sensitivity to $\mathbb{C}^{\mathrm{V}}_{q'q}$ weakens for very light LDVs.

C.4. Partial Width for $B \to B' + V'$

For baryon decays $B \to B' + V'$ with an underlying $q \to q'$ transition the contribution to the partial width from the dipole and vector interaction read

$$\begin{aligned}\Gamma(B \to B'V')\Big|_{\mathrm{D}} &= \frac{m_B^3}{4\pi\Lambda^2}\lambda_{B'V'}^{1/2}\Big[\left(|f_1^{\mathrm{TV}}|^2\hat{A}_{\mathrm{D1}}^- + |f_2^{\mathrm{TV}}|^2\hat{A}_{\mathrm{D2}}^- + \hat{A}_{\mathrm{D12}}^-\mathrm{Re}(f_1^{\mathrm{TV}}f_2^{\mathrm{TV}*})\right)|\mathbb{C}_{q'q}^{\mathrm{D}}|^2 \\ &\quad + \left(|f_1^{\mathrm{TA}}|^2\hat{A}_{\mathrm{D1}}^+ + |f_2^{\mathrm{TA}}|^2\hat{A}_{\mathrm{D2}}^+ + \hat{A}_{\mathrm{D12}}^+\mathrm{Re}(f_1^{\mathrm{TA}}f_2^{\mathrm{TA}*})\right)|\mathbb{C}_{q'q}^{\mathrm{D5}}|^2\Big], \\ \Gamma(B \to B'V')\Big|_{\mathrm{V}} &= \frac{m_B^3}{16\pi\Lambda^2}\lambda_{B'V'}^{1/2}\Big[\left(|f_1|^2\hat{A}_{\mathrm{V1}}^- + |f_2|^2\hat{A}_{\mathrm{V2}}^- + \hat{A}_{\mathrm{V12}}^-\mathrm{Re}(f_1f_2^*)\right)|\mathbb{C}_{q'q}^{\mathrm{V}}|^2 \\ &\quad + \left(|g_1|^2\hat{A}_{\mathrm{V1}}^+ + |g_2|^2\hat{A}_{\mathrm{V2}}^+ + \hat{A}_{\mathrm{V12}}^+\mathrm{Re}(g_1g_2^*)\right)|\mathbb{C}_{q'q}^{\mathrm{V5}}|^2\Big],\end{aligned} \tag{C.24}$$

with the kinematic coefficients

$$\begin{aligned}\hat{A}_{\mathrm{D1}}^{\pm} &= \kappa_{\gamma'}\left(\kappa_{B'}^2 + \kappa_{B'}\left(\kappa_{\gamma'}-2\right) \pm 6\sqrt{\kappa_{B'}}\kappa_{\gamma'} - 2\kappa_{\gamma'}^2 + \kappa_{\gamma'} + 1\right), \\ \hat{A}_{\mathrm{D2}}^{\pm} &= 2\kappa_{B'}^2 - \kappa_{B'}\left(\kappa_{\gamma'}+4\right) \pm 6\sqrt{\kappa_{B'}}\kappa_{\gamma'} - \kappa_{\gamma'}^2 - \kappa_{\gamma'} + 2, \\ \hat{A}_{\mathrm{D12}}^{\pm} &= 6\kappa_{\gamma'}\left(\sqrt{\kappa_{B'}} \mp 1\right)\left(1 + \kappa_{B'} \pm 2\sqrt{\kappa_{B'}} - \kappa_{\gamma'}\right), \\ \hat{A}_{\mathrm{V1}}^{\pm} &= \left(1 + \kappa_{B'} \pm 2\sqrt{\kappa_{B'}} - \kappa_{\gamma'}\right)\left(1 + \kappa_{B'} \mp 2\sqrt{\kappa_{B'}} + 2\kappa_{\gamma'}\right), \\ \hat{A}_{\mathrm{V2}}^{\pm} &= \kappa_{\gamma'}\left(1 + \kappa_{B'} \pm 2\sqrt{\kappa_{B'}} - \kappa_{\gamma'}\right)\left(2 + 2\kappa_{B'} \mp 4\sqrt{\kappa_{B'}} + \kappa_{\gamma'}\right), \\ \hat{A}_{\mathrm{V12}}^{\pm} &= 6\kappa_{\gamma'}\left(\kappa_{B'} \pm 2\sqrt{\kappa_{B'}} - \kappa_{\gamma'} + 1\right)\left(\sqrt{\kappa_{B'}} \mp 1\right).\end{aligned} \tag{C.25}$$

In the limit of a massless LDV, the rates reduce to

$$\begin{aligned}\lim_{m_{V'}\to 0}\Gamma(B \to B'V')\Big|_{\mathrm{D}} &= \frac{m_B^3}{2\pi\Lambda^2}\left(1-\kappa_{B'}\right)^3\left[|f_2^{\mathrm{TV}}|^2|\mathbb{C}_{q'q}^{\mathrm{D}}|^2 + |f_2^{\mathrm{TA}}|^2|\mathbb{C}_{q'q}^{\mathrm{D5}}|^2\right], \\ \lim_{m_{V'}\to 0}\Gamma(B \to B'V')\Big|_{\mathrm{V}} &= \frac{m_B^3}{16\pi\Lambda^2}\left(1-\kappa_{B'}\right)^3\left(|f_1|^2|\mathbb{C}_{q'q}^{\mathrm{V}}|^2 + |g_1|^2|\mathbb{C}_{q'q}^{\mathrm{V5}}|^2\right).\end{aligned} \tag{C.26}$$

For hyperon decays we use the form factor parametrization of Eq. (C.11), valid for $m_{V'} = 0$. Nonetheless, we consider a massive LDV for the kinematics for completeness. The decay rate reads

$$\Gamma(B \to B'V')\Big|_{\mathrm{D}} = \frac{m_B^3}{4\pi\Lambda^2}\lambda_{B'V'}^{1/2}(g_{\mathrm{T}}^{BB'})^2\left(\hat{A}_{\mathrm{D}}^-|\mathbb{C}_{q'q}^{\mathrm{D}}|^2 + \hat{A}_{\mathrm{D}}^+|\mathbb{C}_{q'q}^{\mathrm{D5}}|^2\right), \tag{C.27}$$

with the kinematic coefficients

$$\hat{A}_{\mathrm{D}}^{\pm} = \left(\kappa_{B'} \pm 2\sqrt{\kappa_{B'}} - \kappa_{\gamma'} + 1\right)\left(2\kappa_{B'} \mp 4\sqrt{\kappa_{B'}} + \kappa_{\gamma'} + 2\right). \tag{C.28}$$

In the limit of a massless LDV, the rate reduces to

$$\lim_{m_{V'}\to 0}\Gamma(B \to B'V')\Big|_{\mathrm{D}} = \frac{m_B^3}{2\pi\Lambda^2}\left(1-\kappa_{B'}\right)^3|g_{\mathrm{T}}^{BB'}|^2\left(|\mathbb{C}_{q'q}^{\mathrm{D}}|^2 + |\mathbb{C}_{q'q}^{\mathrm{D5}}|^2\right). \tag{C.29}$$

For a fully polarized initial B, the differential width read

$$\begin{aligned}
\left.\frac{d\Gamma(B\to B'V')}{d\cos\theta}\right|_{\rm D} &= \frac{m_B^3}{8\pi\Lambda^2}\lambda_{B'V'}^{1/2}\Big[\\
&\quad \left(|f_1^{\rm TV}|^2\hat{A}_{\rm D1}^- + |f_2^{\rm TV}|^2\hat{A}_{\rm D2}^- + \hat{A}_{\rm D12}^-{\rm Re}(f_1^{\rm TV}f_2^{\rm TV*})\right)|\mathbb{C}_{q'q}^{\rm D}|^2 \\
&+ \left(|f_1^{\rm TA}|^2\hat{A}_{\rm D1}^+ + |f_2^{\rm TA}|^2\hat{A}_{\rm D2}^+ + \hat{A}_{\rm D12}^+{\rm Re}(f_1^{\rm TA}f_2^{\rm TA*})\right)|\mathbb{C}_{q'q}^{\rm D5}|^2 \\
&- 2\lambda_{B'V'}^{1/2}\cos\theta\left(\hat{B}_{\rm D11}{\rm Im}(f_1^{\rm TV}f_1^{\rm TA*}) + \hat{B}_{\rm D12}^-{\rm Im}(f_1^{\rm TV}f_2^{\rm TA*})\right. \\
&\qquad \left.+\hat{B}_{\rm D22}{\rm Im}(f_2^{\rm TV}f_2^{\rm TA*}) + \hat{B}_{\rm D12}^+{\rm Im}(f_2^{\rm TV}f_1^{\rm TA*})\right){\rm Re}(\mathbb{C}_{q'q}^{\rm D}\mathbb{C}_{q'q}^{\rm D5*}) \\
&- 2\lambda_{B'V'}^{1/2}\cos\theta\left(\hat{B}_{\rm D11}{\rm Re}(f_1^{\rm TV}f_1^{\rm TA*}) + \hat{B}_{\rm D12}^-{\rm Re}(f_1^{\rm TV}f_2^{\rm TA*})\right. \\
&\qquad \left.+\hat{B}_{\rm D22}{\rm Re}(f_2^{\rm TV}f_2^{\rm TA*}) + \hat{B}_{\rm D12}^+{\rm Re}(f_2^{\rm TV}f_1^{\rm TA*})\right){\rm Im}(\mathbb{C}_{q'q}^{\rm D}\mathbb{C}_{q'q}^{\rm D5*})\Big], \\
\left.\frac{d\Gamma(B\to B'V')}{d\cos\theta}\right|_{\rm V} &= \frac{m_B^3}{32\pi\Lambda^2}\lambda_{B'V'}^{1/2}\Big[\\
&\quad \left(|f_1|^2\hat{A}_{\rm V1}^- + |f_2|^2\hat{A}_{\rm V2}^- + \hat{A}_{\rm V12}^-{\rm Re}(f_1f_2^*)\right)|\mathbb{C}_{q'q}^{\rm V}|^2 \\
&+ \left(|g_1|^2\hat{A}_{\rm V1}^+ + |g_2|^2\hat{A}_{\rm V2}^+ + \hat{A}_{\rm V12}^+{\rm Re}(g_1g_2^*)\right)|\mathbb{C}_{q'q}^{\rm V5}|^2 \\
&- 2\lambda_{B'V'}^{1/2}\cos\theta\left(\hat{B}_{\rm V11}{\rm Re}(f_1g_1^*) + \hat{B}_{\rm V12}^+{\rm Re}(f_2g_1^*)\right. \\
&\qquad \left.+\hat{B}_{\rm V12}^-{\rm Re}(f_1g_2^*) + \hat{B}_{\rm V22}{\rm Re}(f_2g_2^*)\right){\rm Re}(\mathbb{C}_{q'q}^{\rm V}\mathbb{C}_{q'q}^{\rm V5*}) \\
&+ 2\lambda_{B'V'}^{1/2}\cos\theta\left(\hat{B}_{\rm V11}{\rm Im}(f_1g_1^*) + \hat{B}_{\rm V12}^+{\rm Im}(f_2g_1^*)\right. \\
&\qquad \left.+\hat{B}_{\rm V12}^-{\rm Im}(f_1g_2^*) + \hat{B}_{\rm V22}{\rm Im}(f_2g_2^*)\right){\rm Im}(\mathbb{C}_{q'q}^{\rm V}\mathbb{C}_{q'q}^{\rm V5*})\Big],
\end{aligned} \tag{C.30}$$

with the kinematic coefficients

$$\hat{B}_{\rm D11} = \kappa_{\gamma'}\left(\kappa_{B'} + 2\kappa_{\gamma'} - 1\right), \quad \hat{B}_{\rm D22} = 2\kappa_{B'} + \kappa_{\gamma'} - 2, \qquad \hat{B}_{\rm D12}^{\pm} = -\kappa_{\gamma'}\left(3\sqrt{\kappa_{B'}} \pm 1\right), \tag{C.31}$$

$$\hat{B}_{\rm V11} = \kappa_{B'} + 2\kappa_{\gamma'} - 1, \qquad \hat{B}_{\rm V22} = \kappa_{\gamma'}\left(2\kappa_{B'} + \kappa_{\gamma'} - 2\right), \quad \hat{B}_{\rm V12}^{\pm} = \kappa_{\gamma'}\left(3\sqrt{\kappa_{B'}} \pm 1\right). \tag{C.32}$$

In the limit of a massless LDV, the rate reduces to

$$\begin{aligned}
\lim_{m_{V'}\to 0}\left.\frac{d\Gamma(B\to B'V')}{d\cos\theta}\right|_{\rm D} &= \frac{m_B^3}{4\pi\Lambda^2}\left(1-\kappa_{B'}\right)^3\Big[|f_2^{\rm TV}|^2|\mathbb{C}_{q'q}^{\rm D}|^2 + |f_2^{\rm TA}|^2|\mathbb{C}_{q'q}^{\rm D5}|^2 \\
&\quad + 2\cos\theta\left({\rm Im}(f_2^{\rm TV}f_2^{\rm TA*}){\rm Re}(\mathbb{C}_{q'q}^{\rm D}\mathbb{C}_{q'q}^{\rm D5*}) + {\rm Re}(f_2^{\rm TV}f_2^{\rm TA*}){\rm Im}(\mathbb{C}_{q'q}^{\rm D}\mathbb{C}_{q'q}^{\rm D5*})\right)\Big], \\
\lim_{m_{V'}\to 0}\left.\frac{d\Gamma(B\to B'V')}{d\cos\theta}\right|_{\rm V} &= \frac{m_B^3}{32\pi\Lambda^2}\left(1-\kappa_{B'}\right)^3\Big(|f_1|^2|\mathbb{C}_{q'q}^{\rm V}|^2 + |g_1|^2|\mathbb{C}_{q'q}^{\rm V5}|^2 \\
&\quad + 2\cos\theta\left({\rm Re}(f_1g_1^*){\rm Re}(\mathbb{C}_{q'q}^{\rm V}\mathbb{C}_{q'q}^{\rm V5*}) - {\rm Im}(f_1g_1^*){\rm Im}(\mathbb{C}_{q'q}^{\rm V}\mathbb{C}_{q'q}^{\rm V5*})\right)\Big).
\end{aligned} \tag{C.33}$$

C.5. Polarized Lepton Distributions and Rates

Next we consider the decays $\ell \to \ell' + V'$ for the case in which lepton-flavour violating dipole or vector interactions with the LDV are present. In this case there is experimental sensitivity to

the polarization of the initial lepton by the measurement of the angular distribution of the angle θ, defined as the angle between the polarisation vector of ℓ and the three-momentum of ℓ'. For the different LDV interactions we find for the differential width of a fully polarised initial ℓ

$$\begin{aligned}\left.\frac{d\Gamma(\ell\to\ell' V')}{d\cos\theta}\right|_{\rm D} &= \frac{m_\ell^3}{8\pi\Lambda^2}\lambda_{\ell' V'}^{1/2}\Big[(\tilde{A}_+^{\rm D}+\tilde{A}_-^{\rm D})\left|\mathbb{C}_{\ell'\ell}^{\rm D}\right|^2+(\tilde{A}_+^{\rm D}-\tilde{A}_-^{\rm D})\left|\mathbb{C}_{\ell'\ell}^{\rm D5}\right|^2\\ &\qquad +\tilde{A}_\theta^{\rm D}\cos\theta\cdot{\rm Im}(\mathbb{C}_{\ell'\ell}^{\rm D}\mathbb{C}_{\ell'\ell}^{\rm D5*})\Big]\,,\\ \left.\frac{d\Gamma(\ell\to\ell' V')}{d\cos\theta}\right|_{\rm V} &= \frac{m_\ell^3}{32\pi\Lambda^2}\lambda_{\ell' V'}^{1/2}\Big[(\tilde{A}_+^{\rm V}+\tilde{A}_-^{\rm V})\left|\mathbb{C}_{\ell'\ell}^{\rm V}\right|^2+(\tilde{A}_+^{\rm V}-\tilde{A}_-^{\rm V})\left|\mathbb{C}_{\ell'\ell}^{\rm V5}\right|^2\\ &\qquad +\tilde{A}_\theta^{\rm V}\cos\theta\cdot{\rm Re}(\mathbb{C}_{\ell'\ell}^{\rm V}\mathbb{C}_{\ell'\ell}^{\rm V5*})\Big]\,,\end{aligned} \tag{C.34}$$

with the kinematic coefficients

$$\begin{aligned}\tilde{A}_+^{\rm D} &= 2(1-\kappa_{\ell'})^2-\kappa_{\gamma'}(1+\kappa_{\ell'})-\kappa_{\gamma'}^2\,, & \tilde{A}_+^{\rm V} &= (1-\kappa_{\ell'})^2+\kappa_{\gamma'}(1+\kappa_{\ell'})-2\kappa_{\gamma'}^2\,,\\ \tilde{A}_-^{\rm D} &= -6\sqrt{\kappa_{\ell'}}\kappa_{\gamma'}\,, & \tilde{A}_-^{\rm V} &= -6\sqrt{\kappa_{\ell'}}\kappa_{\gamma'}\,,\\ \tilde{A}_\theta^{\rm D} &= 2\lambda_{\ell' V'}^{1/2}\left(2-2\kappa_{\ell'}-\kappa_{\gamma'}\right)\,, & \tilde{A}_\theta^{\rm V} &= 2\lambda_{\ell' V'}^{1/2}\left(1-2\kappa_{\gamma'}-\kappa_{\ell'}\right)\,.\end{aligned} \tag{C.35}$$

In the limit of massless LDV, the polarised differential two-body rate reduces to

$$\begin{aligned}\lim_{m_{V'}\to 0}\left.\frac{d\Gamma(\ell\to\ell' V')}{d\cos\theta}\right|_{\rm D} &= \frac{m_\ell^3}{4\pi\Lambda^2}(1-\kappa_{\ell'})^3\left(\left|\mathbb{C}_{\ell'\ell}^{\rm D}\right|^2+\left|\mathbb{C}_{\ell'\ell}^{\rm D5}\right|^2+2\cos\theta\cdot{\rm Im}(\mathbb{C}_{\ell'\ell}^{\rm D}\mathbb{C}_{\ell'\ell}^{\rm D5*})\right)\\ \lim_{m_{V'}\to 0}\left.\frac{d\Gamma(\ell\to\ell' V')}{d\cos\theta}\right|_{\rm V} &= \frac{m_\ell^3}{32\pi\Lambda^2}(1-\kappa_{\ell'})^3\left(\left|\mathbb{C}_{\ell'\ell}^{\rm V}\right|^2+\left|\mathbb{C}_{\ell'\ell}^{\rm V5}\right|^2+2\cos\theta\cdot{\rm Re}(\mathbb{C}_{\ell'\ell}^{\rm V}\mathbb{C}_{\ell'\ell}^{\rm V5*})\right)\,.\end{aligned} \tag{C.36}$$

Finally, after integrating over θ and averaging over the initial- and final-state polarisations, the total decay rates read

$$\Gamma(\ell\to\ell' V')\Big|_{\rm D} = \frac{\lambda_{\ell' V'}^{1/2}m_\ell^3}{4\pi\Lambda^2}\left(\left|\mathbb{C}_{\ell'\ell}^{\rm D}\right|^2(\tilde{A}_+^{\rm D}+\tilde{A}_-^{\rm D})+\left|\mathbb{C}_{\ell'\ell}^{\rm D5}\right|^2(\tilde{A}_+^{\rm D}-\tilde{A}_-^{\rm D})\right)\,, \tag{C.37}$$

$$\Gamma(\ell\to\ell' V')\Big|_{\rm V} = \frac{\lambda_{\ell V'}^{1/2}m_\ell^3}{16\pi\Lambda^2}\left(\left|\mathbb{C}_{\ell'\ell}^{\rm V}\right|^2(\tilde{A}_+^{\rm V}+\tilde{A}_-^{\rm V})+\left|\mathbb{C}_{\ell'\ell}^{\rm V5}\right|^2(\tilde{A}_+^{\rm V}-\tilde{A}_-^{\rm V})\right)\,, \tag{C.38}$$

which in the limit of massless LDVs reduces to

$$\begin{aligned}\lim_{m_{V'}\to 0}\Gamma(\ell\to\ell' V')\Big|_{\rm D} &= \frac{m_\ell^3}{2\pi\Lambda^2}(1-\kappa_{\ell'})^3\left(\left|\mathbb{C}_{\ell'\ell}^{\rm D}\right|^2+\left|\mathbb{C}_{\ell'\ell}^{\rm D5}\right|^2\right)\,,\\ \lim_{m_{V'}\to 0}\Gamma(\ell\to\ell' V')\Big|_{\rm V} &= \frac{m_\ell^3}{16\pi\Lambda^2}(1-\kappa_{\ell'})^3\left(\left|\mathbb{C}_{\ell'\ell}^{\rm V}\right|^2+\left|\mathbb{C}_{\ell'\ell}^{\rm V5}\right|^2\right)\,.\end{aligned} \tag{C.39}$$

Appendix D

Kinematics of $2 \to 2$ and Polarisations

We present the kinematics of a generic $2 \to 2$ process. With the labelling $1 + 2 \to 3 + 4$, the Mandelstam variables are defined as

$$s = (p_1 + p_2)^2 = (p_3 + p_4)^2 \,, \quad t = (p_1 - p_3)^2 = (p_2 - p_4)^2 \,, \quad u = (p_1 - p_4)^2 = (p_2 - p_3)^2 \,, \tag{D.1}$$

where p_i is the four-momenta of the $i = \{1, 2, 3, 4\}$ particle. The Mandesltam variables satisfy

$$s + t + u = \sum_{i=1}^{4} m_i^2 \,, \tag{D.2}$$

where m_i is the mass of the i particle. In the center of mass frame (CM), the four momenta of the particles read

$$p_1 = (E_1, \vec{p}_I) \,, \quad p_2 = (E_2, -\vec{p}_I) \,, \quad p_3 = (E_3, \vec{p}_F) \,, \quad p_4 = (E_4, -\vec{p}_F) \,, \tag{D.3}$$

where $\vec{p}_{I(F)}$ is the inital (final) momenta, and the CM energy is given by $s = (E_1 + E_2)^2 = (E_3 + E_4)^2$. Using energy and momentum conservation along with the mass-shell conditions we find the energy of each particle to be

$$\begin{aligned} E_1 &= \frac{s + m_1^2 - m_2^2}{2\sqrt{s}} \,, \quad E_2 = \frac{s + m_2^2 - m_1^2}{2\sqrt{s}} \,, \\ E_3 &= \frac{s + m_3^2 - m_4^2}{2\sqrt{s}} \,, \quad E_4 = \frac{s + m_4^2 - m_3^2}{2\sqrt{s}} \,, \end{aligned} \tag{D.4}$$

while the magnitude of the initial and final momentum read

$$|\vec{p}_I| = \frac{1}{2\sqrt{s}} \beta^{1/2} \left(s, m_1^2, m_2^2\right) \,, \quad |\vec{p}_F| = \frac{1}{2\sqrt{s}} \beta^{1/2} \left(s, m_3^2, m_4^2\right) \,, \tag{D.5}$$

where $\beta(s, m_i^2, m_j^2)$ is the Källén function

$$\beta \left(s, m_i^2, m_j^2\right) = \left(m_i^2 - \left(\sqrt{s} + m_j\right)^2\right) \left(m_i^2 - \left(\sqrt{s} - m_j\right)^2\right) \,. \tag{D.6}$$

The scattering angle θ between particles 1 and 3 in terms of the masses and Mandelstam variables is given by the relation

$$\cos\theta = \frac{s(t-u) + \left(m_1^2 - m_2^2\right)\left(m_3^2 - m_4^2\right)}{\beta^{1/2}\left(s, m_1^2, m_2^2\right)\beta^{1/2}\left(s, m_3^2, m_4^2\right)} \,. \tag{D.7}$$

In the high energy regime, t and u read

$$t = \frac{s}{2}\left(\cos\theta - 1\right) \,, \quad u = -\frac{s}{2}\left(\cos\theta + 1\right) \,, \tag{D.8}$$

such that $s + t + u = 0$, i.e.,the masses are set to zero. Regarding the polarisation vectors, for a spin-1 particle moving in the $\hat{k}$ direction specified by polar and azimuthal angles θ, ϕ with four-momenta $k^\mu = (k^0, \vec{k})$, the polarisation vectors read

$$\begin{aligned} \epsilon^\mu\left(k, \pm 1\right) &= \frac{1}{\sqrt{2}} e^{\pm i\phi}\left(0, \mp\cos\theta\cos\phi + i\sin\phi, -i\cos\phi \mp \cos\theta\sin\phi, \pm\sin\theta\right) \,, \\ \epsilon^\mu\left(k, 0\right) &= \left(\frac{|\vec{k}|}{m_{V'}}, \frac{k^0}{m_{V'}}\hat{k}\right) \,, \end{aligned} \tag{D.9}$$

where $\epsilon\left(k, \pm 1\right)$ are the two transverse polarisations and $\epsilon^\mu\left(k, 0\right)$ the longitudinal polarisation. Since the vector boson considered in Chapter 7 is the massive LDV V'_μ, we express the longitudinal polarisation $\epsilon^\mu\left(k, 0\right)$ explicitly in terms of the LDV mass $m_{V'}$. For the polarisations of fermions, we use suitable projectors for the spinor structures [9]. For a massive spin-1/2 particle with mass m and four-momenta $p^\mu = (p^0, \vec{p})$, we define the spin vector as

$$s^\mu = \frac{2\lambda}{m}\left(|\vec{p}|, p^0\hat{p}\right) \,, \quad \text{with} \quad \lambda = \pm 1/2 \,. \tag{D.10}$$

The spin vector satisfies $s^\mu p_\mu = 0, s^\mu s_\mu = -1$, and the helicity spinors are projected according to

$$\begin{aligned} u\left(p, \lambda\right)\bar{u}\left(p, \lambda\right) &= \frac{1}{2}\left(1 + \gamma_5 \not{s}\right)\left(\not{p} + m\right) \,, \\ v\left(p, \lambda\right)\bar{v}\left(p, \lambda\right) &= \frac{1}{2}\left(1 + \gamma_5 \not{s}\right)\left(\not{p} - m\right) \,. \end{aligned} \tag{D.11}$$

Appendix E

Unitarity Constraint

We prove the unitarity constraint on the partial waves $|\mathcal{T}^j_{ii}| \leq 1$ given in Section 7.1. Introducing $S = I + i\mathcal{T}$, where $\mathcal{T}$ is the non-trivial (interacting) part of the S matrix, the unitarity condition $S^\dagger S = I$ reads

$$-i\left(\mathcal{T}_{fi} - \mathcal{T}^*_{if}\right) = \sum_k \int d\Pi_{\mathrm{L}} \mathcal{T}_{ki} \mathcal{T}^*_{kf} \,, \tag{E.1}$$

where $d\Pi_L$ is the Lorentz invariant phase space (LIPS), and the matrix elements of the scattering are defined as $\langle f | \mathcal{T} | i \rangle = (2\pi)^4 \delta\left(p_i - p_f\right) \mathcal{T}_{fi}$. If the initial and final states i, f are two-particle states, Eq. (E.1) reads (in the center of mass frame)

$$-i\left(\mathcal{T}_{fi} - \mathcal{T}^*_{if}\right) = \sum_k \frac{p_k}{16\pi^2\sqrt{s}} \int d\Omega \mathcal{T}_{ki} \mathcal{T}^*_{kf} \,. \tag{E.2}$$

Considering the same initial and final states $i = f$, and the form of the total cross section σ for a $2 \to k$ process,

$$\mathrm{Im}\mathcal{T}_{ii} = \beta^{1/2}\left(s, m_1^2, m_2^2\right) \sum_k \sigma\left(i \to k\right) \,, \tag{E.3}$$

where $\beta\left(s, m_1^2, m_2^2\right)$ is the Källén function of the two-particle initial state, defined in Eq. (D.6). The resulting Eq. (E.3) is the well known optical theorem. We wish to reproduce the equivalent of Eq. (E.3) for the partial amplitudes. Consider the expansion of the helicity amplitudes $\mathcal{T}_{fi}(s, \theta)$ in terms of partial amplitudes $\mathcal{T}^j_{fi}(s)$ [141]

$$\mathcal{T}_{fi}\left(s, \theta\right) = 16\pi\mathcal{F} \sum_j \left(2j+1\right) d^j_{\lambda_i \lambda_f}(\theta) \mathcal{T}^j_{fi}(s) \leftrightarrow \mathcal{T}^j_{fi}(s) = \frac{\mathcal{F}^{-1}}{32\pi} \int_0^\pi d\theta \sin\theta d^j_{\lambda_i \lambda_f}(\theta) \mathcal{T}_{fi}\left(s, \theta\right) \,, \tag{E.4}$$

where $\mathcal{F}$ is a (dimensionless) parameter that depends on the masses and s. The starting point is Eq. (E.2), which reads as follows with angular dependences

$$-i\left(\mathcal{T}_{fi}\left(\Omega\right) - \mathcal{T}^*_{if}\left(\Omega\right)\right) = \sum_k \frac{p_k}{16\pi^2\sqrt{s}} \int d\Omega' \mathcal{T}_{ki}\left(\Omega'\right) \mathcal{T}^*_{kf}\left(\Omega''\right) \,, \tag{E.5}$$

where Ω is the solid angle between the initial state i and final state f, Ω' is the solid angle between i and the intermediate state k, and Ω'' is the solid angle between the final state f and k. Introducing the partial waves, this expression reads[1]

$$\begin{aligned} &-i\sum_j (2j+1)\, d^j_{\lambda\lambda'}(\theta)\left(\mathcal{T}^j_{fi}-\mathcal{T}^{j*}_{if}\right) \\ &=\sum_k \frac{p_k\mathcal{F}}{\pi\sqrt{s}}\int d\Omega' \sum_{j,j'}(2j+1)\left(2j'+1\right) d^{j'}_{\lambda\lambda''}(\theta')d^j_{\lambda'\lambda''}(\theta'')\mathcal{T}^{j'}_{ki}\mathcal{T}^{j*}_{kf}\,, \end{aligned} \tag{E.6}$$

where $\lambda,\lambda',\lambda''$ are the helicities of the i,f,k states respectively (i.e., $\lambda=\lambda_1-\lambda_2$, and so on). We decompose the last d-Wigner function according to

$$d^j_{\lambda'\lambda''}(\theta'')=\sum_m d^j_{m\lambda'}(\theta)d^j_{m\lambda''}(\theta')\,, \tag{E.7}$$

and after introducing it in Eq. (E.6) we employ the following orthogonality relation

$$\int_{-1}^{j} d\cos\theta' d^j_{mm'}(\theta')d^{j'}_{mm'}(\theta')=\frac{2}{2j+1}\delta_{jj'}\,, \tag{E.8}$$

to obtain

$$-i\sum_j (2j+1)\, d^j_{\lambda\lambda'}(\theta)\left(\mathcal{T}^j_{fi}-\mathcal{T}^{j*}_{if}\right)=4\sum_k\frac{p_k\mathcal{F}}{\sqrt{s}}\sum_j (2j+1)\, d^j_{\lambda\lambda'}(\theta)\mathcal{T}^j_{ki}\mathcal{T}^{j*}_{kf}\,. \tag{E.9}$$

This equality must hold for any value of l, and thus, for *every* partial amplitude we find

$$-i\left(\mathcal{T}^j_{fi}-\mathcal{T}^{j*}_{if}\right)=2\sum_k\frac{p_k}{\sqrt{p_ip_f}}\mathcal{T}^j_{ki}\mathcal{T}^{j*}_{kf}\,. \tag{E.10}$$

In agreement with Section 7.1, we have chosen $\mathcal{F}=s/\beta_i^{1/4}\beta_f^{1/4}$. Considering $i=f$ we find

$$\mathrm{Im}\mathcal{T}^j_{ii}=\sum_k\frac{p_k}{p_i}|\mathcal{T}^j_{ki}|^2=|\mathcal{T}^j_{ii}|^2+\sum_{k\neq i}\frac{p_k}{p_i}|\mathcal{T}^j_{ki}|^2\geq|\mathcal{T}^j_{ii}|^2\,, \tag{E.11}$$

which precisely yields Eq. (7.6), from which the unitarity condition $|\mathcal{T}^j_{ii}|\leq 1$ is derived. Other approaches to find the unitarity condition are possible, see [159, 161, 257].

[1] A full treatment including the ϕ angles is also possible. For simplicity we drop such dependence in this calculation so that the $d\phi$ integration trivially yields a 2π factor; see [255, 256] for details.

Appendix F

Wigner d-function

The Wigner D-matrix is defined as the rotation operator between angular momentum eigenstates [258, 259]

$$D^j_{m'm}(\alpha,\theta,\gamma) = \langle jm'|\, e^{-i\alpha J_z} e^{-i\theta J_y} e^{-i\gamma J_z}\, |jm\rangle = e^{-im'\alpha} d^j_{m'm}(\theta) e^{-im\gamma}\,, \tag{F.1}$$

where $j = 0, 1/2, 1, 3/2, \ldots$ is the angular momentum, and m is its z component $m = -j, -j+1, \ldots, j$. J_i are the Lie algebra generators and α, θ, γ the Euler angles. The matrix elements of the Wigner (small) d-function are defined as

$$d^j_{m'm}(\theta) = \langle jm'|\, e^{-i\theta J_y}\, |jm\rangle\ . \tag{F.2}$$

The small d-Wigner function is given by[1]

$$\begin{aligned} d^j_{m'm}(\theta) =& \sqrt{(j+m')!\,(j-m')!\,(j+m)!\,(j-m)!} \\ & \sum_{k_{\min}}^{k_{\max}} (-1)^{m'-m+k}\, \frac{(\cos\theta/2)^{2j+m-m'-2k}\,(\sin\theta/2)^{m'-m+2k}}{(j+m-k)!\,(j-k-m')!\,(k-m+m')!k!}\,, \end{aligned} \tag{F.3}$$

where the sum runs from $k_{\min} = \min(0, m-m')$ to $k_{\max} = \max(0, j+m, j-m')$, running over integer values of k such that none of the arguments of the factorials in the denominator are negative. Some useful properties of the Wigner d-function are

$$\begin{aligned} d^j_{m'm}(-\theta) &= d^j_{m'm}(\theta)\,, \\ d^j_{m'm}(\theta) &= d^j_{-m,-m'}(\theta)\,, \\ d^j_{m'm}(\theta) &= (-1)^{m-m'}\, d^j_{mm'}(\theta)\,, \\ d^j_{00}(\theta) &= P_j(\cos\theta)\ , \end{aligned} \tag{F.4}$$

where $P_j(\cos\theta)$ are the Legendre polynomials. The explicit form of some d-functions with specific m, m' values can be found at [165].

[1] In `Mathematica`, the d-function is implemented with flipped m', m indices, that is, $d^j_{m'm}(\theta)$ is generated by WignerD[$\{j, m, m'\}, \theta$].

Bibliography

[1] J. F. Eguren, S. Klingel, E. Stamou, M. Tabet, and R. Ziegler, "Flavor phenomenology of light dark vectors," *JHEP* **08** (2024) 111, arXiv:2405.00108 [hep-ph].

[2] A. Crivellin, J. F. Eguren, and J. Virto, "Next-to-leading-order QCD matching for $\Delta F = 2$ processes in scalar leptoquark models," *JHEP* **03** (2022) 185, arXiv:2109.13600 [hep-ph].

[3] G. Isidori, Y. Nir, and G. Perez, "Flavor Physics Constraints for Physics Beyond the Standard Model," *Ann. Rev. Nucl. Part. Sci.* **60** (2010) 355, arXiv:1002.0900 [hep-ph].

[4] J. Zupan, "Introduction to flavour physics," *CERN Yellow Rep. School Proc.* **6** (2019) 181–212, arXiv:1903.05062 [hep-ph].

[5] Y. Nir, "Probing new physics with flavor physics (and probing flavor physics with new physics)," in *2nd Workshop on Monte Carlo Tools for Beyond the Standard Model Physics.* 8, 2007. arXiv:0708.1872 [hep-ph].

[6] J.-y. Chiu, A. Fuhrer, R. Kelley, and A. V. Manohar, "Factorization Structure of Gauge Theory Amplitudes and Application to Hard Scattering Processes at the LHC," *Phys. Rev. D* **80** (2009) 094013, arXiv:0909.0012 [hep-ph].

[7] G. Cuomo, L. Vecchi, and A. Wulzer, "Goldstone Equivalence and High Energy Electroweak Physics," *SciPost Phys.* **8** no. 5, (2020) 078, arXiv:1911.12366 [hep-ph].

[8] J. Horejsi, "Electroweak interactions and high-energy limit: An Introduction to equivalence theorem," *Czech. J. Phys.* **47** (1997) 951–977, arXiv:hep-ph/9603321.

[9] H. E. Haber, "Spin formalism and applications to new physics searches," in *21st Annual SLAC Summer Institute on Particle Physics: Spin Structure in High-energy Processes (School: 26 Jul - 3 Aug, Topical Conference: 4-6 Aug) (SSI 93)*, pp. 231–272. 4, 1994. arXiv:hep-ph/9405376.

[10] B. W. Lee, C. Quigg, and H. B. Thacker, "Weak Interactions at Very High-Energies: The Role of the Higgs Boson Mass," *Phys. Rev. D* **16** (1977) 1519.

[11] **Particle Data Group** Collaboration, P. A. Zyla *et al.*, "Review of Particle Physics," *PTEP* **2020** no. 8, (2020) 083C01.

[12] **Super-Kamiokande** Collaboration, Y. Fukuda *et al.*, "Evidence for oscillation of atmospheric neutrinos," *Phys. Rev. Lett.* **81** (1998) 1562–1567, arXiv:hep-ex/9807003.

[13] **Planck** Collaboration, N. Aghanim *et al.*, "Planck 2018 results. VI. Cosmological parameters," *Astron. Astrophys.* **641** (2020) A6, arXiv:1807.06209 [astro-ph.CO]. [Erratum: Astron.Astrophys. 652, C4 (2021)].

[14] C. A. Argüelles *et al.*, "Snowmass white paper: beyond the standard model effects on neutrino flavor: Submitted to the proceedings of the US community study on the future of particle physics (Snowmass 2021)," *Eur. Phys. J. C* **83** no. 1, (2023) 15, arXiv:2203.10811 [hep-ph].

[15] P. Hernandez, "Neutrino Physics," in *8th CERN–Latin-American School of High-Energy Physics*, pp. 85–142. 2016. arXiv:1708.01046 [hep-ph].

[16] G. Isidori, "Rare decays: Theory versus experiments," *Int. J. Mod. Phys. A* **17** (2002) 3078–3098, arXiv:hep-ph/0110255.

[17] S. L. Glashow, J. Iliopoulos, and L. Maiani, "Weak Interactions with Lepton-Hadron Symmetry," *Phys. Rev. D* **2** (1970) 1285–1292.

[18] U. Nierste, "Three Lectures on Meson Mixing and CKM phenomenology," in *Helmholz International Summer School on Heavy Quark Physics*, pp. 1–38. 3, 2009. arXiv:0904.1869 [hep-ph].

[19] A. J. Buras, "Weak Hamiltonian, CP violation and rare decays," in *Les Houches Summer School in Theoretical Physics, Session 68: Probing the Standard Model of Particle Interactions*, pp. 281–539. 6, 1998. arXiv:hep-ph/9806471.

[20] G. C. Branco, L. Lavoura, and J. P. Silva, *CP Violation*, vol. 103. 1999.

[21] T. Inami and C. S. Lim, "Effects of Superheavy Quarks and Leptons in Low-Energy Weak Processes k(L) —> mu anti-mu, K+ —> pi+ Neutrino anti-neutrino and K0 <—> anti-K0," *Prog. Theor. Phys.* **65** (1981) 297. [Erratum: Prog.Theor.Phys. 65, 1772 (1981)].

[22] M. Cirelli, A. Strumia, and J. Zupan, "Dark Matter," arXiv:2406.01705 [hep-ph].

[23] B. Holdom, "Two U(1)'s and Epsilon Charge Shifts," *Phys. Lett. B* **166** (1986) 196–198.

[24] M. Fabbrichesi, E. Gabrielli, and G. Lanfranchi, "The Dark Photon," arXiv:2005.01515 [hep-ph].

[25] G. Arcadi, Y. Mambrini, and F. Richard, "Z-portal dark matter," *JCAP* **03** (2015) 018, arXiv:1411.2985 [hep-ph].

[26] A. Crivellin and L. Schnell, "Complete Lagrangian and set of Feynman rules for scalar leptoquarks," *Comput. Phys. Commun.* **271** (2022) 108188, arXiv:2105.04844 [hep-ph].

[27] J. C. Pati and A. Salam, "Lepton Number as the Fourth Color," *Phys. Rev. D* **10** (1974) 275–289. [Erratum: Phys.Rev.D 11, 703–703 (1975)].

[28] H. Georgi and S. L. Glashow, "Unity of All Elementary Particle Forces," *Phys. Rev. Lett.* **32** (1974) 438–441.

[29] H. Georgi, H. R. Quinn, and S. Weinberg, "Hierarchy of Interactions in Unified Gauge Theories," *Phys. Rev. Lett.* **33** (1974) 451–454.

[30] D. Bečirević, S. Fajfer, N. Košnik, and O. Sumensari, "Leptoquark model to explain the B-physics anomalies, R_K and R_D," *Phys. Rev. D* **94** no. 11, (2016) 115021, arXiv:1608.08501 [hep-ph].

[31] I. Bigaran and R. R. Volkas, "Getting chirality right: Single scalar leptoquark solutions to the $(g-2)_{e,\mu}$ puzzle," *Phys. Rev. D* **102** no. 7, (2020) 075037, arXiv:2002.12544 [hep-ph].

[32] F. Feruglio, "Pieces of the Flavour Puzzle," *Eur. Phys. J. C* **75** no. 8, (2015) 373, arXiv:1503.04071 [hep-ph].

[33] M. Ardu and G. Pezzullo, "Introduction to Charged Lepton Flavor Violation," *Universe* **8** no. 6, (2022) 299, arXiv:2204.08220 [hep-ph].

[34] A. V. Manohar, "Introduction to Effective Field Theories," arXiv:1804.05863 [hep-ph].

[35] T. Mannel, "Effective Field Theories in Flavor Physics," *Springer Tracts Mod. Phys.* **203** (2004) 1–175.

[36] A. A. Petrov and A. E. Blechman, *Effective Field Theories*. WSP, 2016.

[37] T. Appelquist and J. Carazzone, "Infrared Singularities and Massive Fields," *Phys. Rev. D* **11** (1975) 2856.

[38] I. Brivio and M. Trott, "The Standard Model as an Effective Field Theory," *Phys. Rept.* **793** (2019) 1–98, arXiv:1706.08945 [hep-ph].

[39] P. Gambino, M. Gorbahn, and U. Haisch, "Anomalous dimension matrix for radiative and rare semileptonic B decays up to three loops," *Nucl. Phys. B* **673** (2003) 238–262, arXiv:hep-ph/0306079.

[40] M. Ciuchini, E. Franco, G. Martinelli, and L. Reina, "The Delta S = 1 effective Hamiltonian including next-to-leading order QCD and QED corrections," *Nucl. Phys. B* **415** (1994) 403–462, arXiv:hep-ph/9304257.

[41] J. Aebischer, M. Fael, C. Greub, and J. Virto, "B physics Beyond the Standard Model at One Loop: Complete Renormalization Group Evolution below the Electroweak Scale," *JHEP* **09** (2017) 158, arXiv:1704.06639 [hep-ph].

[42] M. Schnubel, "Flavor Probes of Axion-like Particles," Rencontres de Moriond EW 2022.

[43] S. Knapen, T. Lin, and K. M. Zurek, "Light Dark Matter: Models and Constraints," *Phys. Rev. D* **96** no. 11, (2017) 115021, arXiv:1709.07882 [hep-ph].

[44] B. A. Dobrescu, "Massless gauge bosons other than the photon," *Phys. Rev. Lett.* **94** (2005) 151802, arXiv:hep-ph/0411004.

[45] T. Hambye, M. H. G. Tytgat, J. Vandecasteele, and L. Vanderheyden, "Dark matter from dark photons: a taxonomy of dark matter production," *Phys. Rev. D* **100** no. 9, (2019) 095018, arXiv:1908.09864 [hep-ph].

[46] E. J. Chun, J.-C. Park, and S. Scopel, "Dark matter and a new gauge boson through kinetic mixing," *JHEP* **02** (2011) 100, arXiv:1011.3300 [hep-ph].

[47] B. C. Allanach, J. Davighi, and S. Melville, "An Anomaly-free Atlas: charting the space of flavour-dependent gauged $U(1)$ extensions of the Standard Model," *JHEP* **02** (2019) 082, arXiv:1812.04602 [hep-ph]. [Erratum: JHEP 08, 064 (2019)].

[48] M. Williams, C. P. Burgess, A. Maharana, and F. Quevedo, "New Constraints (and Motivations) for Abelian Gauge Bosons in the MeV-TeV Mass Range," *JHEP* **08** (2011) 106, arXiv:1103.4556 [hep-ph].

[49] A. Smolkovič, M. Tammaro, and J. Zupan, "Anomaly free Froggatt-Nielsen models of flavor," *JHEP* **10** (2019) 188, arXiv:1907.10063 [hep-ph]. [Erratum: JHEP 02, 033 (2022)].

[50] Y. Kahn, G. Krnjaic, S. Mishra-Sharma, and T. M. P. Tait, "Light Weakly Coupled Axial Forces: Models, Constraints, and Projections," *JHEP* **05** (2017) 002, arXiv:1609.09072 [hep-ph].

[51] M. Bauer, P. Foldenauer, and J. Jaeckel, "Hunting All the Hidden Photons," *JHEP* **07** (2018) 094, arXiv:1803.05466 [hep-ph].

[52] A. Greljo, P. Stangl, A. E. Thomsen, and J. Zupan, "On $(g-2)_\mu$ from gauged $U(1)_X$," *JHEP* **07** (2022) 098, arXiv:2203.13731 [hep-ph].

[53] R. Bause, H. Gisbert, G. Hiller, T. Höhne, D. F. Litim, and T. Steudtner, "U-spin-CP anomaly in charm," *Phys. Rev. D* **108** no. 3, (2023) 035005, arXiv:2210.16330 [hep-ph].

[54] J. Brod, J. Drobnak, A. L. Kagan, E. Stamou, and J. Zupan, "Stealth QCD-like strong interactions and the $t\bar{t}$ asymmetry," *Phys. Rev. D* **91** no. 9, (2015) 095009, arXiv:1407.8188 [hep-ph].

[55] J. H. Chang, R. Essig, and S. D. McDermott, "Revisiting Supernova 1987A Constraints on Dark Photons," *JHEP* **01** (2017) 107, arXiv:1611.03864 [hep-ph].

[56] T. Gherghetta, J. Kersten, K. Olive, and M. Pospelov, "Evaluating the price of tiny kinetic mixing," *Phys. Rev. D* **100** no. 9, (2019) 095001, arXiv:1909.00696 [hep-ph].

[57] S. A. Abel, M. D. Goodsell, J. Jaeckel, V. V. Khoze, and A. Ringwald, "Kinetic Mixing of the Photon with Hidden U(1)s in String Phenomenology," *JHEP* **07** (2008) 124, arXiv:0803.1449 [hep-ph].

[58] K. R. Dienes, C. F. Kolda, and J. March-Russell, "Kinetic mixing and the supersymmetric gauge hierarchy," *Nucl. Phys. B* **492** (1997) 104–118, arXiv:hep-ph/9610479.

[59] A. Hebecker, J. Jaeckel, and R. Kuespert, "Small kinetic mixing in string theory," *JHEP* **04** (2024) 116, arXiv:2311.10817 [hep-th].

[60] S. A. Abel and B. W. Schofield, "Brane anti-brane kinetic mixing, millicharged particles and SUSY breaking," *Nucl. Phys. B* **685** (2004) 150–170, arXiv:hep-th/0311051.

[61] P. Langacker, "The Physics of Heavy Z' Gauge Bosons," *Rev. Mod. Phys.* **81** (2009) 1199–1228, arXiv:0801.1345 [hep-ph].

[62] J. Jaeckel, "A force beyond the Standard Model - Status of the quest for hidden photons," *Frascati Phys. Ser.* **56** (2012) 172–192, arXiv:1303.1821 [hep-ph].

[63] K. S. Babu, C. F. Kolda, and J. March-Russell, "Implications of generalized Z - Z-prime mixing," *Phys. Rev. D* **57** (1998) 6788–6792, arXiv:hep-ph/9710441.

[64] S. Gopalakrishna, S. Jung, and J. D. Wells, "Higgs boson decays to four fermions through an abelian hidden sector," *Phys. Rev. D* **78** (2008) 055002, arXiv:0801.3456 [hep-ph].

[65] H. Ruegg and M. Ruiz-Altaba, "The Stueckelberg field," *Int. J. Mod. Phys. A* **19** (2004) 3265–3348, arXiv:hep-th/0304245.

[66] G. D. Kribs, G. Lee, and A. Martin, "Effective field theory of Stückelberg vector bosons," *Phys. Rev. D* **106** no. 5, (2022) 055020, arXiv:2204.01755 [hep-ph].

[67] C. Coriano, N. Irges, and S. Morelli, "Stuckelberg axions and the effective action of anomalous Abelian models. 1. A Unitarity analysis of the Higgs-axion mixing," *JHEP* **07** (2007) 008, arXiv:hep-ph/0701010.

[68] C. Grosse-Knetter and R. Kogerler, "Unitary gauge, Stuckelberg formalism and gauge invariant models for effective lagrangians," *Phys. Rev. D* **48** (1993) 2865–2876, arXiv:hep-ph/9212268.

[69] S. Davidson, S. Hannestad, and G. Raffelt, "Updated bounds on millicharged particles," *JHEP* **05** (2000) 003, arXiv:hep-ph/0001179.

[70] D. Feldman, Z. Liu, and P. Nath, "The Stueckelberg Z-prime Extension with Kinetic Mixing and Milli-Charged Dark Matter From the Hidden Sector," *Phys. Rev. D* **75** (2007) 115001, arXiv:hep-ph/0702123.

[71] J. Sun and Z.-P. Xing, "Dark photon effects with the kinetic and mass mixing in Z-boson decay processes," *Phys. Rev. D* **109** no. 3, (2024) 035017, arXiv:2310.06526 [hep-ph].

[72] J. M. Cornwall, D. N. Levin, and G. Tiktopoulos, "Derivation of Gauge Invariance from High-Energy Unitarity Bounds on the s Matrix," *Phys. Rev. D* **10** (1974) 1145. [Erratum: Phys.Rev.D 11, 972 (1975)].

[73] B. Kors and P. Nath, "A Stueckelberg extension of the standard model," *Phys. Lett. B* **586** (2004) 366–372, arXiv:hep-ph/0402047.

[74] B. Kors and P. Nath, "Aspects of the Stueckelberg extension," *JHEP* **07** (2005) 069, arXiv:hep-ph/0503208.

[75] J. F. Kamenik and C. Smith, "FCNC portals to the dark sector," *JHEP* **03** (2012) 090, arXiv:1111.6402 [hep-ph].

[76] A. DiFranzo, P. J. Fox, and T. M. P. Tait, "Vector Dark Matter through a Radiative Higgs Portal," *JHEP* **04** (2016) 135, arXiv:1512.06853 [hep-ph].

[77] M. Zaazoua, L. Truong, K. A. Assamagan, and F. Fassi, "Higgs Portal Vector Dark Matter Interpretation: Review of Effective Field Theory Approach and Ultraviolet Complete Models," *LHEP* **2022** (2022) 270, arXiv:2107.01252 [hep-ph].

[78] S. Baek, P. Ko, and W.-I. Park, "Addendum to "Invisible Higgs decay width versus dark matter direct detection cross section in Higgs portal dark matter models"," *Phys. Rev. D* **105** (2022) 015007, arXiv:2112.11983 [hep-ph].

[79] G. Arcadi, J. C. Criado, and A. Djouadi, "Iteration on the Higgs-portal for vector Dark Matter and its effective field theory description," arXiv:2312.14052 [hep-ph].

[80] C. D. Froggatt and H. B. Nielsen, "Hierarchy of Quark Masses, Cabibbo Angles and CP Violation," *Nucl. Phys. B* **147** (1979) 277–298.

[81] M. Leurer, Y. Nir, and N. Seiberg, "Mass matrix models," *Nucl. Phys. B* **398** (1993) 319–342, arXiv:hep-ph/9212278.

[82] L. Calibbi, Z. Lalak, S. Pokorski, and R. Ziegler, "The Messenger Sector of SUSY Flavour Models and Radiative Breaking of Flavour Universality," *JHEP* **06** (2012) 018, arXiv:1203.1489 [hep-ph].

[83] G. D'Ambrosio, G. F. Giudice, G. Isidori, and A. Strumia, "Minimal flavor violation: An Effective field theory approach," *Nucl. Phys. B* **645** (2002) 155–187, arXiv:hep-ph/0207036.

[84] E. E. Jenkins, A. V. Manohar, and M. Trott, "Renormalization Group Evolution of the Standard Model Dimension Six Operators II: Yukawa Dependence," *JHEP* **01** (2014) 035, arXiv:1310.4838 [hep-ph].

[85] J. Aebischer and J. Kumar, "Flavour violating effects of Yukawa running in SMEFT," *JHEP* **09** (2020) 187, arXiv:2005.12283 [hep-ph].

[86] J. A. Dror, R. Lasenby, and M. Pospelov, "Dark forces coupled to nonconserved currents," *Phys. Rev. D* **96** no. 7, (2017) 075036, arXiv:1707.01503 [hep-ph].

[87] A. Badin and A. A. Petrov, "Searching for light Dark Matter in heavy meson decays," *Phys. Rev. D* **82** (2010) 034005, arXiv:1005.1277 [hep-ph].

[88] E. Goudzovski *et al.*, "New physics searches at kaon and hyperon factories," *Rept. Prog. Phys.* **86** no. 1, (2023) 016201, arXiv:2201.07805 [hep-ph].

[89] L. Calibbi, D. Redigolo, R. Ziegler, and J. Zupan, "Looking forward to lepton-flavor-violating ALPs," *JHEP* **09** (2021) 173, arXiv:2006.04795 [hep-ph].

[90] Y. Jho, S. Knapen, and D. Redigolo, "Lepton-flavor violating axions at MEG II," *JHEP* **10** (2022) 029, arXiv:2203.11222 [hep-ph].

[91] S. Knapen, K. Langhoff, T. Opferkuch, and D. Redigolo, "A Robust Search for Lepton Flavour Violating Axions at Mu3e," arXiv:2311.17915 [hep-ph].

[92] R. J. Hill, R. Plestid, and J. Zupan, "Searching for new physics at $\mu \to e$ facilities with μ^+ and π^+ decays at rest," arXiv:2310.00043 [hep-ph].

[93] J. Martin Camalich, M. Pospelov, P. N. H. Vuong, R. Ziegler, and J. Zupan, "Quark Flavor Phenomenology of the QCD Axion," *Phys. Rev. D* **102** no. 1, (2020) 015023, arXiv:2002.04623 [hep-ph].

[94] J. L. Feng, T. Moroi, H. Murayama, and E. Schnapka, "Third generation familons, b factories, and neutrino cosmology," *Phys. Rev. D* **57** (1998) 5875–5892, arXiv:hep-ph/9709411.

[95] F. Björkeroth, E. J. Chun, and S. F. King, "Flavourful Axion Phenomenology," *JHEP* **08** (2018) 117, arXiv:1806.00660 [hep-ph].

[96] R. Ziegler, "Flavor Probes of Axion Dark Matter," *PoS* **DISCRETE2022** (2024) 086, arXiv:2303.13353 [hep-ph].

[97] C. Cornella, P. Paradisi, and O. Sumensari, "Hunting for ALPs with Lepton Flavor Violation," *JHEP* **01** (2020) 158, arXiv:1911.06279 [hep-ph].

[98] L. D. Landau, "On the angular momentum of a system of two photons," *Dokl. Akad. Nauk SSSR* **60** no. 2, (1948) 207–209.

[99] C.-N. Yang, "Selection Rules for the Dematerialization of a Particle Into Two Photons," *Phys. Rev.* **77** (1950) 242–245.

[100] E. Gabrielli, B. Mele, M. Raidal, and E. Venturini, "FCNC decays of standard model fermions into a dark photon," *Phys. Rev. D* **94** no. 11, (2016) 115013, arXiv:1607.05928 [hep-ph].

[101] M. Fabbrichesi, E. Gabrielli, and B. Mele, "Hunting down massless dark photons in kaon physics," *Phys. Rev. Lett.* **119** no. 3, (2017) 031801, arXiv:1705.03470 [hep-ph].

[102] J.-Y. Su and J. Tandean, "Searching for dark photons in hyperon decays," *Phys. Rev. D* **101** no. 3, (2020) 035044, arXiv:1911.13301 [hep-ph].

[103] J.-Y. Su and J. Tandean, "Kaon decays shedding light on massless dark photons," *Eur. Phys. J. C* **80** no. 9, (2020) 824, arXiv:2006.05985 [hep-ph].

[104] J.-Y. Su and J. Tandean, "Seeking massless dark photons in the decays of charmed hadrons," *Phys. Rev. D* **102** no. 11, (2020) 115029, arXiv:2005.05297 [hep-ph].

[105] J. M. Camalich, J. Terol-Calvo, L. Tolos, and R. Ziegler, "Supernova Constraints on Dark Flavored Sectors," *Phys. Rev. D* **103** no. 12, (2021) L121301, arXiv:2012.11632 [hep-ph].

[106] B.-F. Hou, X.-Q. Li, M. Shen, Y.-D. Yang, and X.-B. Yuan, "Deciphering the Belle II data on $B \to K\nu\bar{\nu}$ decay in the (dark) SMEFT with minimal flavour violation," arXiv:2402.19208 [hep-ph].

[107] J. Heeck, "Lepton flavor violation with light vector bosons," *Phys. Lett. B* **758** (2016) 101–105, arXiv:1602.03810 [hep-ph].

[108] A. Ibarra, M. Marín, and P. Roig, "Flavor violating muon decay into an electron and a light gauge boson," *Phys. Lett. B* **827** (2022) 136933, arXiv:2110.03737 [hep-ph].

[109] **NA62** Collaboration, E. Cortina Gil *et al.*, "Search for π^0 decays to invisible particles," *JHEP* **02** (2021) 201, arXiv:2010.07644 [hep-ex].

[110] **NA62** Collaboration, E. Cortina Gil *et al.*, "Measurement of the very rare $K^+ \to \pi^+\nu\bar{\nu}$ decay," *JHEP* **06** (2021) 093, arXiv:2103.15389 [hep-ex].

[111] **BaBar** Collaboration, B. Aubert *et al.*, "A search for the decay $B^+ \to K^+\nu\bar{\nu}$," *Phys. Rev. Lett.* **94** (2005) 101801, arXiv:hep-ex/0411061.

[112] **BaBar** Collaboration, J. P. Lees *et al.*, "Search for $B \to K^{(*)}\nu\bar{\nu}$ and invisible quarkonium decays," *Phys. Rev. D* **87** no. 11, (2013) 112005, arXiv:1303.7465 [hep-ex].

[113] **CLEO** Collaboration, B. I. Eisenstein *et al.*, "Precision Measurement of B(D+ —> mu+ nu) and the Pseudoscalar Decay Constant f(D+)," *Phys. Rev. D* **78** (2008) 052003, arXiv:0806.2112 [hep-ex].

[114] **Belle-II** Collaboration, I. Adachi *et al.*, "Search for lepton-flavor-violating τ decays to a lepton and an invisible boson at Belle II," arXiv:2212.03634 [hep-ex].

[115] **Belle-II** Collaboration, I. Adachi *et al.*, "Evidence for $B^+ \to K^+\nu\bar{\nu}$ Decays," arXiv:2311.14647 [hep-ex].

[116] **BESIII** Collaboration, M. Ablikim *et al.*, "Search for a massless dark photon in $\Lambda c+ \to p\gamma$' decay," *Phys. Rev. D* **106** no. 7, (2022) 072008, arXiv:2208.04496 [hep-ex].

[117] **TWIST** Collaboration, R. Bayes *et al.*, "Search for two body muon decay signals," *Phys. Rev. D* **91** no. 5, (2015) 052020, arXiv:1409.0638 [hep-ex].

[118] J. Albrecht, E. Stamou, R. Ziegler, and R. Zwicky, "Flavoured axions in the tail of $B_q \to \mu^+\mu^?$ and $B \to \gamma^*$ form factors," *JHEP* **21** (2020) 139, arXiv:1911.05018 [hep-ph].

[119] **ALEPH** Collaboration, R. Barate *et al.*, "Measurements of BR (b —> tau- anti-nu(tau) X) and BR (b —> tau- anti-nu(tau) D*+- X) and upper limits on BR (B- —> tau- anti-nu(tau)) and BR (b—> s nu anti-nu)," *Eur. Phys. J. C* **19** (2001) 213–227, arXiv:hep-ex/0010022.

[120] G. Alonso-Álvarez and M. Escudero, "The first limit on invisible decays of B_s mesons comes from LEP," arXiv:2310.13043 [hep-ph].

[121] W. Altmannshofer, A. Crivellin, H. Haigh, G. Inguglia, and J. Martin Camalich, "Light New Physics in $B \to K^{(*)}\nu\bar{\nu}$?," arXiv:2311.14629 [hep-ph].

[122] **Particle Data Group** Collaboration, R. L. Workman *et al.*, "Review of Particle Physics," *PTEP* **2022** (2022) 083C01.

[123] **BESIII** Collaboration, M. Ablikim *et al.*, "Search for the decay $D^0 \to \pi^0\nu\bar{\nu}$," *Phys. Rev. D* **105** no. 7, (2022) L071102, arXiv:2112.14236 [hep-ex].

[124] I. Baum, V. Lubicz, G. Martinelli, L. Orifici, and S. Simula, "Matrix elements of the electromagnetic operator between kaon and pion states," *Phys. Rev. D* **84** (2011) 074503, arXiv:1108.1021 [hep-lat].

[125] **ETM** Collaboration, V. Lubicz, F. Mescia, S. Simula, and C. Tarantino, "K —> pi l nu Semileptonic Form Factors from Two-Flavor Lattice QCD," *Phys. Rev. D* **80** (2009) 111502, arXiv:0906.4728 [hep-lat].

[126] T. Ledwig, J. Martin Camalich, L. S. Geng, and M. J. Vicente Vacas, "Octet-baryon axial-vector charges and SU(3)-breaking effects in the semileptonic hyperon decays," *Phys. Rev. D* **90** no. 5, (2014) 054502, arXiv:1405.5456 [hep-ph].

[127] N. Cabibbo, E. C. Swallow, and R. Winston, "Semileptonic hyperon decays," *Ann. Rev. Nucl. Part. Sci.* **53** (2003) 39–75, arXiv:hep-ph/0307298.

[128] J. M. Gaillard and G. Sauvage, "HYPERON BETA DECAYS," *Ann. Rev. Nucl. Part. Sci.* **34** (1984) 351–402.

[129] **BESIII** Collaboration, M. Ablikim *et al.*, "Search for a massless particle beyond the Standard Model in the $\Sigma^+ \to p +$ invisible decay," arXiv:2312.17063 [hep-ex].

[130] N. Gubernari, A. Kokulu, and D. van Dyk, "$B \to P$ and $B \to V$ Form Factors from B-Meson Light-Cone Sum Rules beyond Leading Twist," *JHEP* **01** (2019) 150, arXiv:1811.00983 [hep-ph].

[131] W. Detmold and S. Meinel, "$\Lambda_b \to \Lambda\ell^+\ell^-$ form factors, differential branching fraction, and angular observables from lattice QCD with relativistic b quarks," *Phys. Rev. D* **93** no. 7, (2016) 074501, arXiv:1602.01399 [hep-lat].

[132] D. Leljak, B. Melić, and D. van Dyk, "The $\overline{B} \to \pi$ form factors from QCD and their impact on $|V_{ub}|$," *JHEP* **07** (2021) 036, arXiv:2102.07233 [hep-ph].

[133] W. Detmold, C. Lehner, and S. Meinel, "$\Lambda_b \to p\ell^-\bar{\nu}_\ell$ and $\Lambda_b \to \Lambda_c\ell^-\bar{\nu}_\ell$ form factors from lattice QCD with relativistic heavy quarks," *Phys. Rev. D* **92** no. 3, (2015) 034503, arXiv:1503.01421 [hep-lat].

[134] **ETM** Collaboration, V. Lubicz, L. Riggio, G. Salerno, S. Simula, and C. Tarantino, "Tensor form factor of $D \to \pi(K)\ell\nu$ and $D \to \pi(K)\ell\ell$ decays with $N_f = 2+1+1$ twisted-mass fermions," *Phys. Rev. D* **98** no. 1, (2018) 014516, arXiv:1803.04807 [hep-lat].

[135] **ETM** Collaboration, V. Lubicz, L. Riggio, G. Salerno, S. Simula, and C. Tarantino, "Scalar and vector form factors of $D \to \pi(K)\ell\nu$ decays with $N_f = 2+1+1$ twisted fermions," *Phys. Rev. D* **96** no. 5, (2017) 054514, arXiv:1706.03017 [hep-lat]. [Erratum: Phys.Rev.D 99, 099902 (2019), Erratum: Phys.Rev.D 100, 079901 (2019)].

[136] S. Meinel, "$\Lambda_c \to N$ form factors from lattice QCD and phenomenology of $\Lambda_c \to n\ell^+\nu_\ell$ and $\Lambda_c \to p\mu^+\mu^-$ decays," *Phys. Rev. D* **97** no. 3, (2018) 034511, arXiv:1712.05783 [hep-lat].

[137] A. Jodidio *et al.*, "Search for Right-Handed Currents in Muon Decay," *Phys. Rev. D* **34** (1986) 1967. [Erratum: Phys.Rev.D 37, 237 (1988)].

[138] M. Froissart, "Asymptotic behavior and subtractions in the Mandelstam representation," *Phys. Rev.* **123** (1961) 1053–1057.

[139] A. Martin, "Unitarity and high-energy behavior of scattering amplitudes," *Phys. Rev.* **129** (1963) 1432–1436.

[140] M. Gell-Mann, M. L. Goldberger, N. M. Kroll, and F. E. Low, "Amelioration of divergence difficulties in the theory of weak interactions," *Phys. Rev.* **179** (1969) 1518–1527.

[141] M. Jacob and G. C. Wick, "On the General Theory of Collisions for Particles with Spin," *Annals Phys.* **7** (1959) 404–428.

[142] M. Luscher and P. Weisz, "Is There a Strong Interaction Sector in the Standard Lattice Higgs Model?," *Phys. Lett. B* **212** (1988) 472–478.

[143] W. J. Marciano, G. Valencia, and S. Willenbrock, "Renormalization Group Improved Unitarity Bounds on the Higgs Boson and Top Quark Masses," *Phys. Rev. D* **40** (1989) 1725.

[144] M. S. Chanowitz, M. A. Furman, and I. Hinchliffe, "Weak Interactions of Ultraheavy Fermions. 2.," *Nucl. Phys. B* **153** (1979) 402–430.

[145] A. Schuessler and D. Zeppenfeld, "Unitarity constraints on MSSM trilinear couplings," in *15th International Conference on Supersymmetry and the Unification of Fundamental Interactions (SUSY07)*, pp. 236–239. 10, 2007. arXiv:0710.5175 [hep-ph].

[146] K. Betre, S. El Hedri, and D. G. E. Walker, "Perturbative Unitarity Constraints on a Supersymmetric Higgs Portal," arXiv:1407.0395 [hep-ph].

[147] K. Betre, S. El Hedri, and D. G. E. Walker, "Perturbative Unitarity Constraints on the NMSSM Higgs Sector," *Phys. Dark Univ.* **19** (2018) 46–59, arXiv:1410.1534 [hep-ph].

[148] J. Horejsi and M. Kladiva, "Tree-unitarity bounds for THDM Higgs masses revisited," *Eur. Phys. J. C* **46** (2006) 81–91, arXiv:hep-ph/0510154.

[149] M. D. Goodsell and F. Staub, "Improved unitarity constraints in Two-Higgs-Doublet-Models," *Phys. Lett. B* **788** (2019) 206–212, arXiv:1805.07310 [hep-ph].

[150] B. Świeżewska, "Yukawa independent constraints for two-Higgs-doublet models with a 125 GeV Higgs boson," *Phys. Rev. D* **88** no. 5, (2013) 055027, arXiv:1209.5725 [hep-ph]. [Erratum: Phys.Rev.D 88, 119903 (2013)].

[151] K. Griest and M. Kamionkowski, "Unitarity Limits on the Mass and Radius of Dark Matter Particles," *Phys. Rev. Lett.* **64** (1990) 615.

[152] S. El Hedri, W. Shepherd, and D. G. E. Walker, "Perturbative Unitarity Constraints on Gauge Portals," *Phys. Dark Univ.* **18** (2017) 127–135, arXiv:1412.5660 [hep-ph].

[153] F. Kahlhoefer, K. Schmidt-Hoberg, T. Schwetz, and S. Vogl, "Implications of unitarity and gauge invariance for simplified dark matter models," *JHEP* **02** (2016) 016, arXiv:1510.02110 [hep-ph].

[154] M. Endo and Y. Yamamoto, "Unitarity Bounds on Dark Matter Effective Interactions at LHC," *JHEP* **06** (2014) 126, arXiv:1403.6610 [hep-ph].

[155] R. Capdevilla, D. Curtin, Y. Kahn, and G. Krnjaic, "No-lose theorem for discovering the new physics of (g-2)μ at muon colliders," *Phys. Rev. D* **105** no. 1, (2022) 015028, arXiv:2101.10334 [hep-ph].

[156] L. Allwicher, L. Di Luzio, M. Fedele, F. Mescia, and M. Nardecchia, "What is the scale of new physics behind the muon g-2?," *Phys. Rev. D* **104** no. 5, (2021) 055035, arXiv:2105.13981 [hep-ph].

[157] L. Di Luzio, J. F. Kamenik, and M. Nardecchia, "Implications of perturbative unitarity for scalar di-boson resonance searches at LHC," *Eur. Phys. J. C* **77** no. 1, (2017) 30, arXiv:1604.05746 [hep-ph].

[158] D. A. Dicus and H.-J. He, "Scales of fermion mass generation and electroweak symmetry breaking," *Phys. Rev. D* **71** (2005) 093009, arXiv:hep-ph/0409131.

[159] M. D. Goodsell and F. Staub, "Unitarity constraints on general scalar couplings with SARAH," *Eur. Phys. J. C* **78** no. 8, (2018) 649, arXiv:1805.07306 [hep-ph].

[160] T. Corbett, O. J. P. Éboli, and M. C. Gonzalez-Garcia, "Unitarity Constraints on Dimension-Six Operators," *Phys. Rev. D* **91** no. 3, (2015) 035014, arXiv:1411.5026 [hep-ph].

[161] M. Soldate, "Partial Wave Unitarity and Closed String Amplitudes," *Phys. Lett. B* **186** (1987) 321–327.

[162] M. Chaichian, C. Montonen, and A. Tureanu, "Tree unitarity and partial wave expansion in noncommutative quantum field theory," *Phys. Lett. B* **566** (2003) 263–270, arXiv:hep-th/0305243.

[163] C. Garcia-Garcia, M. Herrero, and R. A. Morales, "Unitarization effects in EFT predictions of WZ scattering at the LHC," *Phys. Rev. D* **100** no. 9, (2019) 096003, arXiv:1907.06668 [hep-ph].

[164] A. Hebbar, D. Karateev, and J. Penedones, "Spinning S-matrix bootstrap in 4d," *JHEP* **01** (2022) 060, arXiv:2011.11708 [hep-th].

[165] D. Barducci, M. Nardecchia, and C. Toni, "Perturbative unitarity constraints on generic vector interactions," arXiv:2306.11533 [hep-ph].

[166] L. Allwicher, P. Arnan, D. Barducci, and M. Nardecchia, "Perturbative unitarity constraints on generic Yukawa interactions," *JHEP* **10** (2021) 129, arXiv:2108.00013 [hep-ph].

[167] A. Milagre and L. Lavoura, "Unitarity constraints on large multiplets of arbitrary gauge groups," arXiv:2403.12914 [hep-ph].

[168] P. Baratella, C. Fernandez, B. von Harling, and A. Pomarol, "Anomalous Dimensions of Effective Theories from Partial Waves," *JHEP* **03** (2021) 287, arXiv:2010.13809 [hep-ph].

[169] J. Brod and M. Gorbahn, "The Z Penguin in Generic Extensions of the Standard Model," *JHEP* **09** (2019) 027, arXiv:1903.05116 [hep-ph].

[170] J. C. Criado and M. Pérez-Victoria, "Field redefinitions in effective theories at higher orders," *JHEP* **03** (2019) 038, arXiv:1811.09413 [hep-ph].

[171] H. Georgi, "On-shell effective field theory," *Nucl. Phys. B* **361** (1991) 339–350.

[172] M. A. Shifman, A. I. Vainshtein, and V. I. Zakharov, "QCD and Resonance Physics. Theoretical Foundations," *Nucl. Phys. B* **147** (1979) 385–447.

[173] A. Lenz, U. Nierste, J. Charles, S. Descotes-Genon, A. Jantsch, C. Kaufhold, H. Lacker, S. Monteil, V. Niess, and S. T'Jampens, "Anatomy of New Physics in $B - \bar{B}$ mixing," *Phys. Rev. D* **83** (2011) 036004, arXiv:1008.1593 [hep-ph].

[174] A. Lenz and U. Nierste, "Theoretical update of $B_s - \bar{B}_s$ mixing," *JHEP* **06** (2007) 072, arXiv:hep-ph/0612167.

[175] A. J. Buras and J. Girrbach, "Towards the Identification of New Physics through Quark Flavour Violating Processes," *Rept. Prog. Phys.* **77** (2014) 086201, arXiv:1306.3775 [hep-ph].

[176] W. Buchmuller, R. Ruckl, and D. Wyler, "Leptoquarks in Lepton - Quark Collisions," *Phys. Lett. B* **191** (1987) 442–448. [Erratum: Phys.Lett.B 448, 320–320 (1999)].

[177] **ATLAS** Collaboration, G. Aad *et al.*, "CP Properties of Higgs Boson Interactions with Top Quarks in the $t\bar{t}H$ and tH Processes Using $H \to \gamma\gamma$ with the ATLAS Detector," *Phys. Rev. Lett.* **125** no. 6, (2020) 061802, arXiv:2004.04545 [hep-ex].

[178] **Muon g-2** Collaboration, T. Albahri *et al.*, "Measurement of the anomalous precession frequency of the muon in the Fermilab Muon $g - 2$ Experiment," *Phys. Rev. D* **103** no. 7, (2021) 072002, arXiv:2104.03247 [hep-ex].

[179] **LHCb** Collaboration, R. Aaij *et al.*, "Test of lepton universality in beauty-quark decays," *Nature Phys.* **18** no. 3, (2022) 277–282, arXiv:2103.11769 [hep-ex]. [Addendum: Nature Phys. 19, (2023)].

[180] X. Ji, Y. Liu, and Y. Su, "Threshold resummation for computing large-x parton distribution through large-momentum effective theory," *JHEP* **08** (2023) 037, arXiv:2305.04416 [hep-ph].

[181] V. Cirigliano, H. Gisbert, A. Pich, and A. Rodríguez-Sánchez, "A complete update of ε'/ε in the Standard Model," *PoS* **EPS-HEP2019** (2020) 238, arXiv:1911.06554 [hep-ph].

[182] H. Gisbert and A. Pich, "Direct CP violation in $K^0 \to \pi\pi$: Standard Model Status," *Rept. Prog. Phys.* **81** no. 7, (2018) 076201, arXiv:1712.06147 [hep-ph].

[183] **ATLAS** Collaboration, G. Aad *et al.*, "Measurement of the CP properties of Higgs boson interactions with τ-leptons with the ATLAS detector," *Eur. Phys. J. C* **83** no. 7, (2023) 563, arXiv:2212.05833 [hep-ex].

[184] D. Buttazzo, A. Greljo, G. Isidori, and D. Marzocca, "B-physics anomalies: a guide to combined explanations," *JHEP* **11** (2017) 044, arXiv:1706.07808 [hep-ph].

[185] A. Crivellin, D. Müller, A. Signer, and Y. Ulrich, "Correlating lepton flavor universality violation in B decays with $\mu \to e\gamma$ using leptoquarks," *Phys. Rev. D* **97** no. 1, (2018) 015019, arXiv:1706.08511 [hep-ph].

[186] L. Di Luzio, A. Greljo, and M. Nardecchia, "Gauge leptoquark as the origin of B-physics anomalies," *Phys. Rev. D* **96** no. 11, (2017) 115011, arXiv:1708.08450 [hep-ph].

[187] M. Bauer and M. Neubert, "Minimal Leptoquark Explanation for the $R_{D^{(*)}}$, R_K , and $(g-2)_\mu$ Anomalies," *Phys. Rev. Lett.* **116** no. 14, (2016) 141802, arXiv:1511.01900 [hep-ph].

[188] L. Di Luzio, M. Kirk, A. Lenz, and T. Rauh, "ΔM_s theory precision confronts flavour anomalies," *JHEP* **12** (2019) 009, arXiv:1909.11087 [hep-ph].

[189] L. Di Luzio, M. Kirk, and A. Lenz, "Updated B_s-mixing constraints on new physics models for $b \to s\ell^+\ell^-$ anomalies," *Phys. Rev. D* **97** no. 9, (2018) 095035, arXiv:1712.06572 [hep-ph].

[190] **ATLAS** Collaboration, G. Aad *et al.*, "Search for leptoquarks decaying into the bτ final state in pp collisions at $\sqrt{s}$ = 13 TeV with the ATLAS detector," *JHEP* **10** (2023) 001, arXiv:2305.15962 [hep-ex].

[191] M. Kramer, T. Plehn, M. Spira, and P. M. Zerwas, "Pair production of scalar leptoquarks at the Tevatron," *Phys. Rev. Lett.* **79** (1997) 341–344, arXiv:hep-ph/9704322.

[192] M. Kramer, T. Plehn, M. Spira, and P. M. Zerwas, "Pair production of scalar leptoquarks at the CERN LHC," *Phys. Rev. D* **71** (2005) 057503, arXiv:hep-ph/0411038.

[193] T. Mandal, S. Mitra, and S. Seth, "Pair Production of Scalar Leptoquarks at the LHC to NLO Parton Shower Accuracy," *Phys. Rev. D* **93** no. 3, (2016) 035018, arXiv:1506.07369 [hep-ph].

[194] J. B. Hammett and D. A. Ross, "NLO Leptoquark Production and Decay: The Narrow-Width Approximation and Beyond," *JHEP* **07** (2015) 148, arXiv:1501.06719 [hep-ph].

[195] D. A. Faroughy, A. Greljo, and J. F. Kamenik, "Confronting lepton flavor universality violation in B decays with high-p_T tau lepton searches at LHC," *Phys. Lett. B* **764** (2017) 126–134, arXiv:1609.07138 [hep-ph].

[196] G. Hiller, D. Loose, and I. Nišandžić, "Flavorful leptoquarks at hadron colliders," *Phys. Rev. D* **97** no. 7, (2018) 075004, arXiv:1801.09399 [hep-ph].

[197] A. Monteux and A. Rajaraman, "B Anomalies and Leptoquarks at the LHC: Beyond the Lepton-Quark Final State," *Phys. Rev. D* **98** no. 11, (2018) 115032, arXiv:1803.05962 [hep-ph].

[198] M. Schmaltz and Y.-M. Zhong, "The leptoquark Hunter's guide: large coupling," *JHEP* **01** (2019) 132, arXiv:1810.10017 [hep-ph].

[199] J. Aebischer, A. Crivellin, and C. Greub, "QCD improved matching for semileptonic B decays with leptoquarks," *Phys. Rev. D* **99** no. 5, (2019) 055002, arXiv:1811.08907 [hep-ph].

[200] L. Delle Rose, C. Marzo, and L. Marzola, "Simplified leptoquark models for precision $l_i \to l_f\gamma$ experiments: two-loop structure of $O(\alpha_S Y^2)$ corrections," *Phys. Rev. D* **102** no. 11, (2020) 115020, arXiv:2005.12389 [hep-ph].

[201] A. Crivellin, D. Müller, and F. Saturnino, "Flavor Phenomenology of the Leptoquark Singlet-Triplet Model," *JHEP* **06** (2020) 020, arXiv:1912.04224 [hep-ph].

[202] M. Ciuchini, E. Franco, V. Lubicz, G. Martinelli, I. Scimemi, and L. Silvestrini, "Next-to-leading order QCD corrections to Delta F = 2 effective Hamiltonians," *Nucl. Phys. B* **523** (1998) 501–525, arXiv:hep-ph/9711402.

[203] A. J. Buras, M. Misiak, and J. Urban, "Two loop QCD anomalous dimensions of flavor changing four quark operators within and beyond the standard model," *Nucl. Phys. B* **586** (2000) 397–426, arXiv:hep-ph/0005183.

[204] **UTfit** Collaboration, M. Bona *et al.*, "Model-independent constraints on $\Delta F = 2$ operators and the scale of new physics," *JHEP* **03** (2008) 049, arXiv:0707.0636 [hep-ph].

[205] J. Aebischer, C. Bobeth, A. J. Buras, and J. Kumar, "SMEFT ATLAS of ΔF = 2 transitions," *JHEP* **12** (2020) 187, arXiv:2009.07276 [hep-ph].

[206] **CMS** Collaboration, A. Hayrapetyan *et al.*, "Search for pair production of scalar and vector leptoquarks decaying to muons and bottom quarks in proton-proton collisions at s=13 TeV," *Phys. Rev. D* **109** no. 11, (2024) 112003, arXiv:2402.08668 [hep-ex].

[207] F. Jegerlehner, "Facts of life with gamma(5)," *Eur. Phys. J. C* **18** (2001) 673–679, arXiv:hep-th/0005255.

[208] M. S. Chanowitz, M. Furman, and I. Hinchliffe, "The Axial Current in Dimensional Regularization," *Nucl. Phys. B* **159** (1979) 225–243.

[209] M. J. Dugan and B. Grinstein, "On the vanishing of evanescent operators," *Phys. Lett. B* **256** (1991) 239–244.

[210] A. J. Buras and P. H. Weisz, "QCD Nonleading Corrections to Weak Decays in Dimensional Regularization and 't Hooft-Veltman Schemes," *Nucl. Phys. B* **333** (1990) 66–99.

[211] S. Herrlich and U. Nierste, "Evanescent operators, scheme dependences and double insertions," *Nucl. Phys. B* **455** (1995) 39–58, arXiv:hep-ph/9412375.

[212] W. A. Bardeen, A. J. Buras, D. W. Duke, and T. Muta, "Deep Inelastic Scattering Beyond the Leading Order in Asymptotically Free Gauge Theories," *Phys. Rev. D* **18** (1978) 3998.

[213] C. Bobeth, M. Misiak, and J. Urban, "Photonic penguins at two loops and m_t dependence of $BR[B \to X_s l^+ l^-]$," *Nucl. Phys. B* **574** (2000) 291–330, arXiv:hep-ph/9910220.

[214] J. Fuentes-Martín, M. König, J. Pagès, A. E. Thomsen, and F. Wilsch, "Evanescent operators in one-loop matching computations," *JHEP* **02** (2023) 031, arXiv:2211.09144 [hep-ph].

[215] P. Arnan, A. Crivellin, M. Fedele, and F. Mescia, "Generic Loop Effects of New Scalars and Fermions in $b \to s\ell^+\ell^-$, $(g-2)_\mu$ and a Vector-like 4^{th} Generation," *JHEP* **06** (2019) 118, arXiv:1904.05890 [hep-ph].

[216] J. Virto, "Exact NLO strong interaction corrections to the Delta F=2 effective Hamiltonian in the MSSM," *JHEP* **11** (2009) 055, arXiv:0907.5376 [hep-ph].

[217] M. Ciuchini, E. Franco, D. Guadagnoli, V. Lubicz, V. Porretti, and L. Silvestrini, "Next-to-leading order strong interaction corrections to the Delta F = 2 effective Hamiltonian in the MSSM," *JHEP* **09** (2006) 013, arXiv:hep-ph/0606197.

[218] K. G. Chetyrkin, M. Misiak, and M. Munz, "$|\Delta F| = 1$ nonleptonic effective Hamiltonian in a simpler scheme," *Nucl. Phys. B* **520** (1998) 279–297, arXiv:hep-ph/9711280.

[219] M. Gorbahn and U. Haisch, "Effective Hamiltonian for non-leptonic $|\Delta F| = 1$ decays at NNLO in QCD," *Nucl. Phys. B* **713** (2005) 291–332, arXiv:hep-ph/0411071.

[220] M. Gorbahn, S. Jager, U. Nierste, and S. Trine, "The supersymmetric Higgs sector and $B - \bar{B}$ mixing for large tan β," *Phys. Rev. D* **84** (2011) 034030, arXiv:0901.2065 [hep-ph].

[221] G. 't Hooft and M. J. G. Veltman, "Regularization and Renormalization of Gauge Fields," *Nucl. Phys. B* **44** (1972) 189–213.

[222] S. A. Larin, "The Renormalization of the axial anomaly in dimensional regularization," *Phys. Lett. B* **303** (1993) 113–118, arXiv:hep-ph/9302240.

[223] H. Bélusca-Maïto, A. Ilakovac, P. Kühler, M. Mađor-Božinović, D. Stöckinger, and M. Weißwange, "Introduction to Renormalization Theory and Chiral Gauge Theories in Dimensional Regularization with Non-Anticommuting γ_5," *Symmetry* **15** no. 3, (2023) 622, arXiv:2303.09120 [hep-ph].

[224] P. Breitenlohner and D. Maison, "Dimensional Renormalization and the Action Principle," *Commun. Math. Phys.* **52** (1977) 11–38.

[225] P. Breitenlohner and D. Maison, "Dimensionally Renormalized Green's Functions for Theories with Massless Particles. 1.," *Commun. Math. Phys.* **52** (1977) 39.

[226] M. F. Zoller, "Top-Yukawa effects on the β-function of the strong coupling in the SM at four-loop level," *JHEP* **02** (2016) 095, arXiv:1508.03624 [hep-ph].

[227] S. Moch, J. A. M. Vermaseren, and A. Vogt, "On $\gamma 5$ in higher-order QCD calculations and the NNLO evolution of the polarized valence distribution," *Phys. Lett. B* **748** (2015) 432–438, arXiv:1506.04517 [hep-ph].

[228] A. Crivellin, A. Kokulu, and C. Greub, "Flavor-phenomenology of two-Higgs-doublet models with generic Yukawa structure," *Phys. Rev. D* **87** no. 9, (2013) 094031, arXiv:1303.5877 [hep-ph].

[229] P. Arnan, L. Hofer, F. Mescia, and A. Crivellin, "Loop effects of heavy new scalars and fermions in $b \to s\mu^+\mu^-$," *JHEP* **04** (2017) 043, arXiv:1608.07832 [hep-ph].

[230] A. I. Davydychev and J. B. Tausk, "Two loop selfenergy diagrams with different masses and the momentum expansion," *Nucl. Phys. B* **397** (1993) 123–142.

[231] **ETM** Collaboration, N. Carrasco, P. Dimopoulos, R. Frezzotti, V. Lubicz, G. C. Rossi, S. Simula, and C. Tarantino, "ΔS=2 and ΔC=2 bag parameters in the standard model and beyond from N_f=2+1+1 twisted-mass lattice QCD," *Phys. Rev. D* **92** no. 3, (2015) 034516, arXiv:1505.06639 [hep-lat].

[232] **Fermilab Lattice, MILC** Collaboration, A. Bazavov *et al.*, "$B^0_{(s)}$-mixing matrix elements from lattice QCD for the Standard Model and beyond," *Phys. Rev. D* **93** no. 11, (2016) 113016, arXiv:1602.03560 [hep-lat].

[233] A. Bazavov *et al.*, "Short-distance matrix elements for D^0-meson mixing for $N_f = 2 + 1$ lattice QCD," *Phys. Rev. D* **97** no. 3, (2018) 034513, arXiv:1706.04622 [hep-lat].

[234] R. J. Dowdall, C. T. H. Davies, R. R. Horgan, G. P. Lepage, C. J. Monahan, J. Shigemitsu, and M. Wingate, "Neutral B-meson mixing from full lattice QCD at the physical point," *Phys. Rev. D* **100** no. 9, (2019) 094508, arXiv:1907.01025 [hep-lat].

[235] **Flavour Lattice Averaging Group** Collaboration, S. Aoki *et al.*, "FLAG Review 2019: Flavour Lattice Averaging Group (FLAG)," *Eur. Phys. J. C* **80** no. 2, (2020) 113, arXiv:1902.08191 [hep-lat].

[236] K. G. Chetyrkin, J. H. Kuhn, and M. Steinhauser, "RunDec: A Mathematica package for running and decoupling of the strong coupling and quark masses," *Comput. Phys. Commun.* **133** (2000) 43–65, arXiv:hep-ph/0004189.

[237] A. J. Buras, M. Jamin, M. E. Lautenbacher, and P. H. Weisz, "Two loop anomalous dimension matrix for $\Delta S = 1$ weak nonleptonic decays I: $\mathcal{O}(\alpha_s^2)$," *Nucl. Phys. B* **400** (1993) 37–74, arXiv:hep-ph/9211304.

[238] A. J. Buras, M. Jamin, and M. E. Lautenbacher, "Two loop anomalous dimension matrix for Delta S = 1 weak nonleptonic decays. 2. O(alpha-alpha-s)," *Nucl. Phys. B* **400** (1993) 75–102, arXiv:hep-ph/9211321.

[239] A. J. Buras, M. Jamin, M. E. Lautenbacher, and P. H. Weisz, "Effective Hamiltonians for $\Delta S = 1$ and $\Delta B = 1$ nonleptonic decays beyond the leading logarithmic approximation," *Nucl. Phys. B* **370** (1992) 69–104. [Addendum: Nucl.Phys.B 375, 501 (1992)].

[240] D. Kreimer, "The Role of gamma(5) in dimensional regularization," arXiv:hep-ph/9401354.

[241] P. Kühler, D. Stöckinger, and M. Weißwange, "Advances at the γ_5-Frontier," *PoS* **LL2024** (2024) 022, arXiv:2407.07247 [hep-ph].

[242] S. A. Larin and J. A. M. Vermaseren, "The α_s^3 corrections to the Bjorken sum rule for polarized electroproduction and to the Gross-Llewellyn Smith sum rule," *Phys. Lett. B* **259** (1991) 345–352.

[243] E. B. Zijlstra and W. L. van Neerven, "Order-α_s^2 corrections to the polarized structure function $g_1(x, Q^2)$," *Nucl. Phys. B* **417** (1994) 61–100. [Erratum: Nucl.Phys.B 426, 245 (1994), Erratum: Nucl.Phys.B 773, 105–106 (2007), Erratum: Nucl.Phys.B 501, 599–599 (1997)].

[244] J. G. Korner, D. Kreimer, and K. Schilcher, "A Practicable gamma(5) scheme in dimensional regularization," *Z. Phys. C* **54** (1992) 503–512.

[245] L. Naterop and P. Stoffer, "Low-energy effective field theory below the electroweak scale: one-loop renormalization in the 't Hooft-Veltman scheme," *JHEP* **02** (2024) 068, arXiv:2310.13051 [hep-ph].

[246] O. L. Crosas, C. J. Monahan, M. D. Rizik, A. Shindler, and P. Stoffer, "One-loop matching of the CP-odd three-gluon operator to the gradient flow," *Phys. Lett. B* **847** (2023) 138301, arXiv:2308.16221 [hep-lat].

[247] P. Morell and J. Virto, "On the two-loop penguin contributions to the Anomalous Dimensions of four-quark operators," *JHEP* **04** (2024) 105, arXiv:2402.00249 [hep-ph].

[248] A. V. Kotikov and S. Teber, "Multi-loop techniques for massless Feynman diagram calculations," *Phys. Part. Nucl.* **50** no. 1, (2019) 1–41, arXiv:1805.05109 [hep-th].

[249] K. G. Chetyrkin, M. Misiak, and M. Munz, "Beta functions and anomalous dimensions up to three loops," *Nucl. Phys. B* **518** (1998) 473–494, arXiv:hep-ph/9711266.

[250] M. Misiak and M. Munz, "Two loop mixing of dimension five flavor changing operators," *Phys. Lett. B* **344** (1995) 308–318, arXiv:hep-ph/9409454.

[251] M. Egner, M. Fael, K. Schönwald, and M. Steinhauser, "Nonleptonic B-meson decays to next-to-next-to-leading order," *JHEP* **10** (2024) 144, arXiv:2406.19456 [hep-ph].

[252] M. Jamin and A. Pich, "QCD corrections to inclusive Delta S = 1,2 transitions at the next-to-leading order," *Nucl. Phys. B* **425** (1994) 15–38, arXiv:hep-ph/9402363.

[253] A. J. Buras, M. E. Lautenbacher, M. Misiak, and M. Munz, "Direct CP violation in K(L) —> pi0 e+ e- beyond leading logarithms," *Nucl. Phys. B* **423** (1994) 349–383, arXiv:hep-ph/9402347.

[254] R. Gupta, B. Yoon, T. Bhattacharya, V. Cirigliano, Y.-C. Jang, and H.-W. Lin, "Flavor diagonal tensor charges of the nucleon from (2+1+1)-flavor lattice QCD," *Phys. Rev. D* **98** no. 9, (2018) 091501, arXiv:1808.07597 [hep-lat].

[255] H. M. Pilkuhn, *Relativistic particle physics*. Springer Science & Business Media, 2013.

[256] A. D. Martin and T. D. Spearman, "Elementary particle theory.,".

[257] R. G. Newton, *SCATTERING THEORY OF WAVES AND PARTICLES*. 1982.

[258] N. Tajima, "Analytical formula for numerical evaluations of the Wigner rotation matrices at high spins," *Phys. Rev. C* **91** no. 1, (2015) 014320, arXiv:1501.06347 [nucl-th].

[259] J. J. Sakurai and J. Napolitano, *Modern quantum mechanics*. Cambridge University Press, 2020.